Dissertation
submitted to the
Combined Faculties for the Natural Sciences and for Mathematics
of the Ruperto–Carola University of Heidelberg, Germany
for the degree of
Doctor of Natural Sciences

presented by

Diplom–Physicist:	Katja Klein
born in:	Ludwigshafen am Rhein

Oral examination: 22.7.2002

A Search for Sleptons with Intermediate Lifetimes in e^+e^- Collisions at $\sqrt{s} = 189 - 209\,\mathrm{GeV}$

Referees: Prof. Dr. Jürgen von Krogh
Prof. Dr. Michael G. Schmidt

Suche nach Sleptonen mit mittlerer Lebensdauer in e^+e^- Ereignissen bei $\sqrt{s} = 189 - 209\,\mathrm{GeV}$

In dieser Arbeit wird eine Suche nach Sleptonen mit mittlerer Lebensdauer ($\approx 10^{-11} - 10^{-9}\,\mathrm{s}$) mit dem OPAL–Detektor am LEP–Speicherring vorgestellt für den Fall, daß das Slepton das NLSP (next–to–lightest supersymmetric particle) ist. Sleptonen mit mittlerer Lebensdauer werden im Rahmen des Minimal Gauge Mediated Supersymmetry Breaking (GMSB) Modells vorhergesagt und zerfallen jeweils in ein Lepton und ein Gravitino. Für die Suche wurde die charakteristische Topologie von Spuren mit großen Stoßparametern und fehlender Energie ausgenutzt. Alle bei LEP 2 erlaubten Produktionskanäle (direkte sowie indirekte Produktion über Paar–Erzeugung von Neutralinos, Charginos und, im Falle des Staus, Selektronen und Smyonen) wurden berücksichtigt. In dem untersuchten Datensatz bei $\sqrt{s} = 189 - 209\,\mathrm{GeV}$ mit einer integrierten Luminosität von etwa $600\,\mathrm{pb}^{-1}$ wurde keine Evidenz für die Existenz von Sleptonen mit mittlerer Lebensdauer gefunden. Die Ergebnisse wurden daher mit Resultaten von Suchen für prompt zerfallende, langlebige und stabile Sleptonen kombiniert und für alle Kanäle wurden obere Grenzen für die Wirkungsquerschnitte ermittelt. Hieraus wurden lebensdauerunabhängige untere Slepton–Massengrenzen von $m_{\tilde{e}_R} > 60.1\,\mathrm{GeV}/c^2$, $m_{\tilde{\mu}_R} > 93.7\,\mathrm{GeV}/c^2$ und $m_{\tilde{\tau}_1} > 87.4\,\mathrm{GeV}/c^2$ mit 95 % Konfidenz abgeleitet. Die Kombination dieser Resultate mit Suchen nach Topologien, bei denen das Neutralino als NLSP fungiert, ermöglicht eine Eingrenzung des GMSB–Parameterraumes und führt zu einer unteren Grenze für die SUSY Massenskala Λ von $15\,\mathrm{TeV}/c^2$ für einen Messenger–Index $N \leq 5$, unabhängig von der Lebensdauer des NLSP.

A Search for Sleptons with Intermediate Lifetimes in e^+e^- Collisions at $\sqrt{s} = 189 - 209\,\mathrm{GeV}$

Searches were performed for sleptons with intermediate lifetimes ($\approx 10^{-11} - 10^{-9}\,\mathrm{s}$) in the framework of the Minimal Gauge Mediated Supersymmetry Breaking (GMSB) model, for the case that the slepton is the NLSP (next–to–lightest supersymmetric particle). The data recorded with the OPAL detector at LEP at center–of–mass energies of $\sqrt{s} = 189 - 209\,\mathrm{GeV}$, corresponding to an integrated luminosity of $600\,\mathrm{pb}^{-1}$, were investigated. The topology of tracks with large impact parameters and missing energy, caused by the decay of the slepton to a lepton and a gravitino, was exploited. All production channels possible at LEP 2 were considered; i.e. direct pair–production and indirect production via pair–production of neutralinos and charginos, and – for the case that the stau is the NLSP – of selectrons and smuons. Since no evidence for sleptons with intermediate lifetimes was found, the results were combined with searches for promptly decaying, long–lived and stable sleptons, and for all channels upper limits on the production cross–sections were obtained. From these, lifetime–independent lower limits on the slepton masses at 95 % confidence level of $m_{\tilde{e}_R} > 60.1\,\mathrm{GeV}/c^2$, $m_{\tilde{\mu}_R} > 93.7\,\mathrm{GeV}/c^2$ and $m_{\tilde{\tau}_1} > 87.4\,\mathrm{GeV}/c^2$ were derived. The combination with searches for neutralino NLSP signatures allows for constraints on the GMSB parameter space and leads to a lower limit of $15\,\mathrm{TeV}/c^2$ on the mass scale Λ of the SUSY particles for a messenger index $N \leq 5$, independent of the NLSP lifetime.

Contents

1 Introduction **1**

2 The Minimal GMSB Model **5**
2.1 A Few Basic Facts about Supersymmetry 5
2.2 Supersymmetry Breaking 6
2.2.1 SUSY Breaking via Gravity Mediation 7
2.2.2 SUSY Breaking via Gauge Mediation 8
2.3 GMSB Phenomenology 8

3 The LEP Collider and the OPAL Detector **15**
3.1 The LEP Accelerator 15
3.2 The OPAL Detector 15
3.2.1 The Tracking System 16
3.2.2 The Outer Detector 18

4 Monte Carlo Simulation **21**
4.1 SUSY Signal Event Simulation 21
4.1.1 The SUSYGEN Event Generator 21
4.1.2 Modifications in GEANT and GOPAL 21
4.2 Background Event Simulation 24

5 Search for the Large Impact Parameter Topology **27**
5.1 The Signal: Channels and Topologies 27
5.2 Data Set and Integrated Luminosities 31
5.3 Preselection 31
5.4 Background Composition and Checks 32
5.5 The Event Selections 35
5.5.1 Selectron and Smuon Pair–Production in the Slepton co–NLSP Scenario: 2–Lepton Selection 35
5.5.2 Stau Pair–Production: 2–Tau Selection 41
5.5.3 Neutralino Pair–Production: 4–Lepton Selection 44
5.5.4 Slepton Pair–Production in the Stau NLSP Scenario: 6–Lepton Selection 49
5.5.5 Chargino Pair–Production 51

6 Determination of the Signal Efficiency **53**

7 The GMSB Scan Database **57**
7.1 The Minimal Expected Cross–Section 58

8 Systematic Uncertainties **63**

9 Results and Interpretations **67**
9.1 The Slepton as the NLSP . . . 67
9.1.1 Combination of Slepton NLSP Searches . . . 67
9.1.2 Cross–Section Limits for Slepton Pair–Production . . . 70
9.1.3 Constraints on the Slepton Masses . . . 74
9.1.4 Cross–Section Limits for Neutralino Pair–Production . . . 77
9.1.5 Cross–Section Limits for Selectron and Smuon Pair–Production in the Stau NLSP Scenario . . . 82
9.1.6 Cross–Section Limits for Chargino Pair–Production . . . 86
9.2 The Neutralino as the NLSP . . . 89
9.2.1 Cross–Section and Mass Limits for Neutralino Pair–Production . . . 95
9.2.2 Cross–Section Limits for Slepton Pair–Production . . . 98
9.2.3 Cross–Section Limits for Chargino Pair–Production . . . 98
9.3 Interpretations in the Framework of the GMSB Model . . . 106
9.3.1 Exlusions within the GMSB Parameter Space . . . 106
9.3.2 Constraints on the SUSY Particle Mass Scale Λ . . . 116

10 Summary and Discussion **119**

A The OPAL Track Parameters **123**

B The Signal Monte Carlo Grid **125**

Chapter 1

Introduction

During the last century our knowledge of the elementary particles and the three fundamental forces governing them, the strong and weak forces and electro–magnetism, has increased enormously, culminating in what is called the Standard Model of elementary particles. In this model all our present knowledge of the micro–world is summarized. We have identified the constituents of matter, up and down quarks and electrons, and the neutrino, a particle produced in weak decays. It has been found that for the quarks and the electron two unstable heavier "brothers" can be produced in the laboratory, e. g. with particle colliders, and that all particles can be arranged in multiplets, of which hence three generations exist. For all particles there are anti–particles with opposite additive quantum–numbers such as charge but with exactly the same mass and lifetime. The particles that are responsible for transmitting the forces have been identified: the massless photon for electro–magnetism, the massive $W^{\pm}$ and Z^0 bosons for the weak force and the massless gluon for the strong force. In addition, the graviton is associated with the fourth force, gravitation, which describes the interaction of massive objects and is negligible in the world of elementary particles. The Standard Model has proven to be tremendously successful in explaining the phenomena of elementary particle physics. It has been validated in laboratories all over the world, especially at CERN by the four experiments at the former LEP (Large Electron Positron) collider, and no clear evidence for its failure has been found.

Nevertheless, the Standard Model leaves several questions unanswered. Why are there three generations of leptons and quarks, with only the lightest generation being stable? How do particles acquire their masses and what determines these masses, with, e.g., the tau lepton being about 3500 times as heavy as the electron? Why do the electron and proton apparently have exactly the same electrical charge? Are the particles we know fundamental or are they composed of even smaller constituents? Is it possible to unify the strong with the electro–weak force, as the weak force was unified with electro–magnetism 35 years ago, and does this help us to calculate at least some of the more than 19 free parameters in the Standard Model? Is there a quantum field theory for gravitation? All these questions need to be answered to provide us with a better understanding not only of the world of elementary particles but also of the development of our universe, and a great variety of models has been proposed by theorists to answer at least some of these questions.

To solve the problem of the generation of mass, the Higgs mechanism (as part of the Standard Model) has been proposed. Particles would receive their masses by interaction with a scalar field, the Higgs field. The massive particle associated with this field, the Higgs boson, is not yet discovered but is searched for extensively. If the Higgs boson exists, this would give rise to another, more technical problem, known as the fine–tuning problem. The mass of the Higgs boson itself receives contributions from radiative corrections, which are diverging. Although fermions and bosons contribute with opposite signs, their contributions cancel only partially, and the correction to the Higgs mass is many orders of magnitude larger than the Higgs mass itself. In the Standard Model, this is fixed by renormalization theory,

Particle	Spin	Sparticle	Spin
lepton ℓ	1/2	slepton $\tilde{\ell}$	0
neutrino ν	1/2	sneutrino $\tilde{\nu}$	0
quark q	1/2	squark $\tilde{\mathrm{q}}$	0
photon γ	1	photino $\tilde{\gamma}$	1/2
W	1	wino $\tilde{\mathrm{W}}$	1/2
Z	1	zino $\tilde{\mathrm{Z}}$	1/2
gluon g	1	gluino $\tilde{\mathrm{g}}$	1/2
Higgs boson H	0	higgsino $\tilde{\mathrm{H}}$	1/2
graviton G	2	gravitino $\tilde{\mathrm{G}}$	3/2

Table 1.1: *Standard Model particles (left) and their supersymmetric partners (right).*

assuming a "bare" Higgs mass that is tuned to cancel these contributions from radiative corrections and thus to arrive at the physical value for the Higgs mass. For this fine–tuning no theoretical motivation is given in the Standard Model.

An elegant solution to this fine–tuning problem is, however, provided by supersymmetry. In supersymmetry (SUSY) [1, 2, 3], for each Standard Model particle a supersymmetric partner is postulated, differing in spin by half a unit. Thus fermions have bosons as super–partners, while the supersymmetric partners of bosons are fermions. A summary of the particles expected in supersymmetry is given in Table 1.1. The scalar partners of the fermions are called sleptons, sneutrinos and squarks, while the partners of the gauge bosons have $S = 1/2$ and are called gluino, wino, zino and photino [1]. Instead of one Higgs boson five (charged and neutral) Higgs bosons are postulated, whose superpartners are called higgsinos. The electro–weak gauginos and the higgsinos mix to form four neutral and two charged physical mass eigenstates, the charginos and neutralinos. If supersymmetry exists, the Higgs boson mass receives diverging contributions not only from Standard Model particles but also from their super–partners. Since there are equal numbers of fermions and bosons with equal couplings, the contributions from the supersymmetric particles cancel those from their Standard Model partners, if the condition $|m_B^2 - m_F^2| \lesssim 1\,\mathrm{TeV}^2$ for the boson masses m_B and fermion masses m_F is fulfilled [2].

Supersymmetry has more advantages than just solving the fine–tuning problem. If R–parity, a quantum number distinguishing between SUSY and Standard Model particles, is conserved, SUSY particles can be produced only in pairs, and the lightest supersymmetric particle (LSP) cannot decay further but remains stable. This particle, if light, neutral and only weakly interacting, is an excellent candidate for the non–baryonic dark matter, which is known to contribute significantly to the total matter of the universe. Furthermore supersymmetry provides the possibility to unify the electro–weak and the strong force. Extrapolation of the inverse of the three associated coupling constants to energies as high as $10^{16}\,\mathrm{GeV}$ under the assumption of the existence of supersymmetry yields a common intersection point (Fig. 1.1) [3]. Without supersymmetry, this is not the case.

How – if at all – supersymmetry might be realized in nature is unknown. The model with the minimal number of new particles is called the minimal supersymmetric extension of the Standard Model (MSSM). In this model apart from the SUSY partners of the SM particles and two Higgs doublets no new particles are introduced. Unfortunately, this model has 124 free parameters, including the free parameters of the Standard Model. In general, some basic assumptions are made to reduce the number of free parameters. From the fact that up to now no supersymmetric particles have been discovered it can be deduced that SUSY cannot be an exact symmetry but has to be broken. Depending on how this is

[1] The zino and the photino are in fact mixtures of the SUSY–partners of the B^0 (the bino) and the W^0.

accomplished different classes of models can be distinguished, including minimal supergravity (mSUGRA) models [4], in which SUSY breaking is mediated by gravity, the Gauge Mediated Supersymmetry Breaking (GMSB) models [5, 6, 7] and, more recently proposed, the Anomaly Mediated Supersymmetry Breaking (AMSB) models [8]. Since we have no knowledge of which of these might be realized, it is crucial to search for all of them in the existing data to be sure not to miss any hint for supersymmetry.

In this work a search for sleptons with intermediate lifetimes, in the framework of the GMSB model, is presented. In GMSB the next–to–lightest supersymmetric particle (NLSP) is either the lightest slepton or the lightest neutralino, and the lifetime of the NLSP can have any value. In this analysis the event topology of tracks with large impact parameters, which is expected if sleptons have lifetimes in the range of $10^{-11} - 10^{-9}$ s, is exploited. This lifetime region has not been investigated in OPAL before, thus previously obtained slepton mass limits were not valid for all slepton lifetimes but assumed either promptly decaying or stable sleptons. All theoretically allowed production and decay channels for sleptons at LEP 2 energies are covered, in some channels for the first time at LEP. The results are combined with the results of previous searches for sleptons with shorter and longer lifetimes to account for the whole lifetime range. Constraints on the production cross–sections are presented for all channels, and lifetime–independent lower limits on the slepton masses are derived. By further combining these results with searches that assume the NLSP to be the neutralino, most topologies predicted within the framework of GMSB are covered. This allows for the exclusion of considerable regions in the GMSB parameter space.

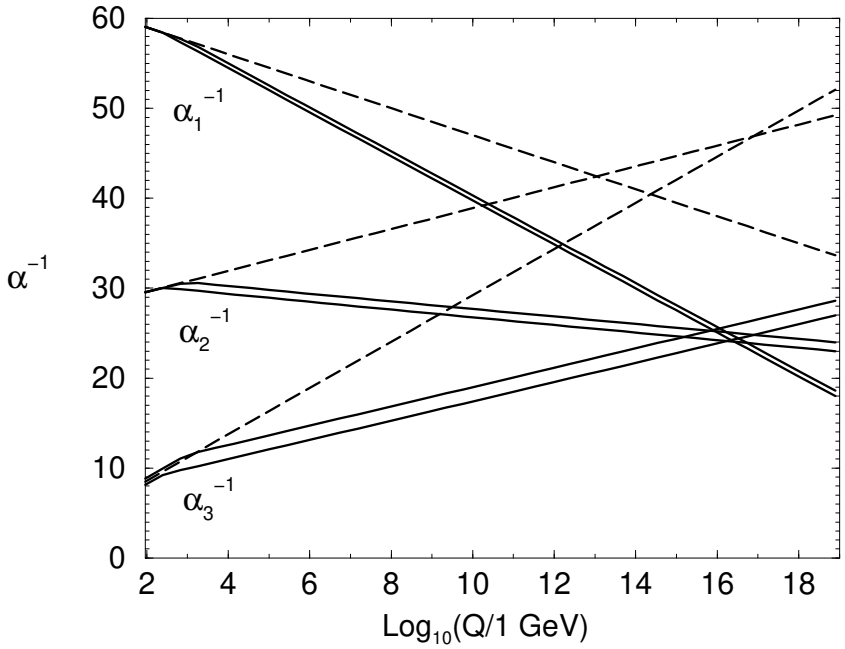


Figure 1.1: *The running of the inverse of the three gauge coupling constants in the Standard Model (dashed lines) and in the MSSM (solid lines; the widths represent the theoretical uncertainties) including two loop effects [3]. In supersymmetry a unification of the gauge coupling constants at around 10^{16} GeV is possible.*

Chapter 2

The Minimal GMSB Model

Supersymmetry (SUSY) is an extension of the Standard Model (SM) that proposes supersymmetric partners, differing in spin by half a unit, for all Standard Model particles, in order to cancel contributions to the Higgs boson mass from SM particle loops that otherwise lead to divergences and would require an amount of fine–tuning that is considered theoretically undesirable.

A comprehensive overview of supersymmetry can be found in [1, 2, 3]. Here only a few of the building blocks of SUSY are mentioned (Sect. 2.1), following mostly the conventions from [3]. In Sect. 2.2 some aspects of SUSY breaking are discussed. The phenomenology of the GMSB model is described in Sect. 2.3 with emphasis on the aspects relevant for this work.

2.1 A Few Basic Facts about Supersymmetry

The SUSY generators Q^i_α are fermionic; i.e., they carry spin $S = 1/2$ and change a bosonic state into a fermionic state and vice versa. Here $\alpha = 1, 2$ is the spinor index (i.e. the fields are described by two–dimensional Weyl spinors) and $i = 1, ..., K$, where K is the number of such generators. Usually $K = 1$ with only one generator Q_α is assumed. In this case, the generators Q_α and the hermetian conjugates $Q^\dagger_{\dot\alpha}$ (with spinor indices $\dot\alpha$) obey the algebra

$$\{Q_\alpha, Q_\beta\} = \{Q^\dagger_{\dot\alpha}, Q^\dagger_{\dot\beta}\} = 0\,, \tag{2.1}$$

$$\{Q_\alpha, Q^\dagger_{\dot\beta}\} = 2\,\sigma^\mu_{\alpha\dot\beta} P_\mu\,, \tag{2.2}$$

where the σ^μ are the Pauli matrices and P_μ is the four–momentum operator.

In the model with minimal field content, called the minimal extension of the Standard Model (MSSM), there are SUSY partners for all SM particles plus two Higgs doublets, which are discussed in more detail later. In this model SUSY is a global symmetry and gravity is not included. In general, however, SUSY is assumed to be a local symmetry, since this is the only way to include gravity [3]. Then it is possible to unify the spacetime symmetries of general relativity with local supersymmetric transformations. Local supersymmetry is referred to as supergravity or SUGRA and is often embedded in a wider framework such as string theories. In SUGRA the supermultiplets used to describe matter and Higgs bosons, gauge fields and gravity, are (the numbers correspond to the spins of the particles):

$$\text{matter}: \begin{pmatrix} \frac{1}{2} \\ 0 \end{pmatrix} \qquad \text{gauge}: \begin{pmatrix} 1 \\ \frac{1}{2} \end{pmatrix} \qquad \text{gravity}: \begin{pmatrix} 2 \\ \frac{3}{2} \end{pmatrix}. \tag{2.3}$$

In the MSSM with boson fields ϕ_i and fermion fields ψ_i, where the index i runs over all gauge and flavour degrees of freedom, the most general Lagrangian has the form

$$\mathcal{L} = -\partial^\mu \phi^{*i} \partial_\mu \phi_i - i\psi^{\dagger i} \bar\sigma^\mu \partial_\mu \psi_i + F^{*i} F_i + \left(\frac{\delta W}{\delta \phi_i} F_i - \frac{1}{2} \frac{\delta^2 W}{\delta \phi_i \delta \phi_j} \psi_i \psi_j + c.c. \right).$$

The stars denote the complex conjugates. The first two terms describe free bosons and fermions with $\overline{\sigma}_0 = \sigma_0$ and $\overline{\sigma}_i = -\sigma_i$ for $i = 1, 2, 3$. The last two terms describe the interactions. W is the superpotential describing all matter interactions:

$$W = \frac{1}{2} M^{ij} \phi_i \phi_j + \frac{1}{6} y^{ijk} \phi_i \phi_j \phi_k$$

with the fermion mass matrix M and coupling constants y^{ijk}. The F_i are auxiliary fields without a physical meaning and can be eliminated by the equations of motion, $F_i = -W_i^*$ with $W_i = \frac{\delta W}{\delta \phi_i}$.

The supersymmetric partners of the SM particles are summarised in Table 1.1. In the following the Higgs sector of the MSSM will be described in more detail. In SUSY two complex Higgs doublets H_1, H_2 are required:

$$H_1 = \begin{pmatrix} H_1^0 \\ H_1^- \end{pmatrix}, \qquad\qquad H_2 = \begin{pmatrix} H_2^+ \\ H_2^0 \end{pmatrix}.$$

The ratio of their vacuum expectation values is described by the parameter $\tan\beta$:

$$\tan\beta = \frac{< 0|H_2|0 >}{< 0|H_1|0 >}.$$

From the eight degrees of freedom of the two complex doublets three are absorbed via the Higgs mechanism to give mass to the $W^{\pm}$ and Z^0 bosons, leaving five physical states: two CP–even neutral states h^0 and H^0, the CP–odd neutral state A^0 and two charged states, $H^{\pm}$. The superpotential contains the interactions of the Higgs doublets with SM particles described by Yukawa couplings and a term $\mu H_1 H_2$, describing the interaction of the two Higgs doublets. The parameter μ is called the Higgs sector mixing parameter.

The superpartners of the electroweak gauge bosons, the photino $\tilde{\gamma}$, zino $\tilde{Z}^0$ and the wino $\tilde{W}^{\pm}$, are called gauginos, the superpartners of the Higgs bosons are called higgsinos. The gauginos and higgsinos mix to form two charged states, the charginos $\chi_i^{\pm}$ $(i = 1, 2)$, and four neutral states, the neutralinos χ_i^0 $(i = 1, ..., 4)$. The convention is such that the smaller the index the lighter the particle.

2.2 Supersymmetry Breaking

From the fact that no supersymmetric particles have been observed so far, it can be deduced that the SUSY particles must be heavier than most of the Standard Model particles (with the exception of the top quark). Since exact supersymmetry leads to mass degeneracy in a supermultiplet, supersymmetry must be a broken symmetry.

Supersymmetry breaking can be accomplished either explicitly, by SUSY breaking terms in the Lagrangian, or spontaneously. Only for spontaneous SUSY breaking can a cancellation of divergencies in the Higgs mass be achieved, and therefore we focus on this possibility.

SUSY is broken spontaneously if the groundstate of the SUSY potential is positive, i.e. if

$$E_0 = \langle 0|\mathcal{H}|0\rangle > 0\,.$$

Since

$$\begin{aligned} \sum_{\alpha=1,2} \{Q_\alpha, Q_{\dot{\alpha}}^\dagger\} &= Q_1 Q_1^\dagger + Q_1^\dagger Q_1 + Q_2 Q_2^\dagger + Q_2^\dagger Q_2 \\ &= 2\,(\sigma_{11}^\mu P_\mu + \sigma_{22}^\mu P_\mu) \\ &= 2\,Tr(\sigma^\mu P_\mu) = 4P_0 \end{aligned}$$

the Hamiltonian is related to the SUSY generators by

$$\mathcal{H} = P_0 = \frac{1}{4} \sum_{\alpha=1,2} \{Q_\alpha, Q^\dagger_{\dot{\alpha}}\} \,.$$

The groundstate E_0 is then given by

$$\begin{aligned} \langle 0|\mathcal{H}|0\rangle &= \frac{1}{4} \sum_{\alpha=1,2} < 0\,|\{Q_\alpha, Q^\dagger_{\dot{\alpha}}\}|0 > \\ &= \frac{1}{4} \left(|\, Q_1|0 >|^2 + \left|\, Q_1^\dagger|0 >\right|^2 + |\, Q_2|0 >|^2 + \left|\, Q_2^\dagger|0 >\right|^2 \right) > 0 \,. \end{aligned}$$

Thus a non–zero groundstate is equivalent to the vacuum not being invariant under the supersymmetric generator Q_α:

$$Q_\alpha|0 > \neq 0 \,.$$

As in electro–weak symmetry breaking this is achieved by introducing a field with a non–zero vacuum expectation value (VEV). However, as it turns out, introducing SM fields with non–zero VEV's is not possible without also breaking the $SU(3)$ or $U(1)$ gauge invariance. Therefore extra sources of spontaneous SUSY breaking must exist.

The most common scenario for SUSY breaking is that there are two particle sectors: the visible sector containing the usual matter, i.e. conventional particles and their SUSY partners as given in the MSSM or SUGRA, and a "hidden sector" at a very high mass scale, containing fields that carry no $SU(3) \times SU(2) \times U(1)$ quantum numbers and do not have any renormalizable interactions with the visible sector. These fields are responsible for SUSY breaking. The sectors interact with each other via so–called messenger fields with scale M that mediate SUSY breaking from the hidden sector to the visible sector. Depending on the nature of the messenger fields different kinds of spontaneous SUSY breaking are distinguished. The two most important ones are gravity mediation and gauge mediation.

Spontaneous SUSY breaking implies the existence of a massless Goldstone fermion, the goldstino with S=1/2. If SUSY is a global symmetry the goldstino is a physical particle and, since it is massless, is the lightest supersymmetric particle. However, in most viable models SUSY is assumed to be a local symmetry. For unbroken local SUSY the graviton and the gravitino are both massless and have two spin polarization states. The two polarization states of the Goldstino are absorbed by the gravitino to make it massive and to provide the longitudinal (helicity $\pm 1/2$) components of the four polarization states of a massive particle with spin 3/2. Since the graviton and the gravitino then have different masses, this breaks local supersymmetry. This mechanism is known as the super–Higgs mechanism. The longitudinal components of the gravitino then inherit the non–gravitational interactions of the goldstino it has absorbed, while the tranverse components (helicity $\pm 3/2$) have only gravitational interactions and can be ignored in collider physics.

2.2.1 SUSY Breaking via Gravity Mediation

In this scenario the hidden and visible sector interact only via gravitational interactions.

Gravity mediation requires the messenger mass scale M to be near the Planck scale. The energy scale below which SUSY is broken is called the SUSY–breaking scale, $\sqrt{F}$. It is of the order $10^{11}\,\mathrm{GeV}$. Since the gravitino mass is proportional to F/M_P with $M_P = 2.4 \cdot 10^{18}\,\mathrm{GeV}/c^2$ being the reduced Planck mass, in this model the gravitino is expected to be rather heavy and thus the gravitino is not of phenomenological interest.

2.2.2 SUSY Breaking via Gauge Mediation

In the Gauge Mediated Supersymmetry Breaking Model (GMSB), SUSY breaking is transmitted to the visible sector via the gauge interactions. To accomplish this, new chiral supermultiplets are introduced that couple via gravitational interaction to the hidden sector and through ordinary $SU(3)_C \times SU(2)_L \times U(1)_Y$ gauge interactions to the (s)quarks, (s)leptons, Higgs bosons, gauginos and higgsinos of the visible sector. In this case the mass scale M can be anywhere between the electroweak and the Planck scale, leading to the possibility of $\sqrt{F}$ being as low as $100\,\mathrm{TeV}/c^2$. Detailed descriptions of GMSB Models can be found in [5, 6, 7].

One advantage of GMSB with respect to gravity mediated models is the absence of excessive flavour–changing neutral currents (FCNC). These are not present in GMSB due to the flavour–invariance of the gauge interactions, while gravity couples to the particles mass. In gravity mediated models, FCNC lead to rates for processes like $\mu \to \mathrm{e}\gamma$ that are just at the edge of present experimental bounds.

In the minimal GMSB model there are only six free parameters. In addition to the above mentioned parameters M and $\sqrt{F}$, these are the ratio of the vacuum expectation values of the two Higgs doublets, $\tan\beta$, the sign of the Higgs sector mixing parameter, $sign(\mu)$ [1], the number of generations of messenger particles, N, and the mass scale of the SUSY particles, Λ.

2.3 GMSB Phenomenology

Not much is known about the content of the hidden and the messenger sector. The particles in the hidden sector can be described by a superfield X which aquires a vacuum expectation value $< 0|X|0 >$. In the simplest case X is the Goldstino field. The messenger superfields couple to the Goldstino at tree level and this coupling creates a mass of order M for the messenger fields. They are chiral superfields Φ_i and $\bar{\Phi}_i$ with $i = 1, ..., N$, where N is the number of flavours of these messenger fields. The interaction between the Goldstino and the messenger fields is given by the superpotential term W:

$$W = \lambda_{ij} \bar{\Phi}_i X \Phi_j \,,$$

where the parameters λ_{ij} are the coupling constants.

In spite of the incomplete knowledge we have about the hidden and messenger sector, the minimal GMSB model is very predictive with respect to the observable sector of SM particles and their superpartners. The masses of the ordinary supermultiplets are degenerate at tree level, but mass splittings arise due to gauge interactions between ordinary and messenger fields at the quantum level. Gaugino masses are generated at one loop, squark and slepton masses at two loop level.

The gaugino masses at the messenger scale are given (in leading order and for $F \ll M^2$) by [7]

$$m_{\lambda_i}(M) = \frac{\alpha_i(M)}{4\pi} \Lambda N \,,$$

where λ_i are the gaugino fields of gauge group i and the α_i are the GUT normalised coupling constants of these gauge groups (i.e. $\alpha_1 = \alpha_2 = \alpha_3$ at the unification scale). The mass scale Λ can be written as $\Lambda = F/M \cdot \lambda$.

The scalar masses have been calculated from the formula [7]

$$m^2(M) = 2N\Lambda^2 \sum_{i=1}^{3} k_i \left(\frac{\alpha_i(M)}{4\pi} \right)^2 ,$$

where the sum runs over the gauge groups $SU(3)_C \times SU(2)_L \times U(1)_Y$ with $k_1 = 3/5(Y/2)^2$ (Y is the hypercharge) for $U(1)_Y$, $k_2 = 3/4$ for $SU(2)_L$ doublets and 0 for singlets, and

[1] $|\mu|$ can be calculated by imposing electroweak symmetry breaking.

$k_3 = 4/3$ for $SU(3)_C$ triplets and 0 for singlets. A more complete discussion, including next–to–leading order effects and the case $F \approx M^2$, can be found in [5].

Using these formulae and taking into account that the squarks form a $SU(3)_C$ triplet, the left–handed sleptons a $SU(2)_L$ doublet and that the right–handed sleptons have hypercharge $Y = 2$, the gaugino masses of the three gauge groups follow the relation $m_1 : m_2 : m_3 \simeq \alpha_1 : \alpha_2 : \alpha_3$, and the scalar (squared) masses obey the relation $m^2_{\tilde{q}} : m^2_{\tilde{\ell}_L} : m^2_{\tilde{\ell}_R} \simeq \frac{4}{3}\alpha_3^2 : \frac{3}{4}\alpha_2^2 : \frac{3}{5}\alpha_1^2$. If the messenger scale is well below the unification scale, then $\alpha_3 \gg \alpha_2 > \alpha_1$. Therefore in GMSB models, the squarks and gluinos are usually too heavy to have an impact on the phenomenology at LEP energies, and the right–handed sleptons are in general lighter than the left–handed ones. Fig 2.1 shows the particle mass spectrum at the messenger scale for different values of this scale (for $\tan\beta = 3$, $N = 1$ and a bino mass of $m_{\tilde{\mathrm{B}}}(M) = 115\,\mathrm{GeV}/c^2$). There it can be seen that for a low messenger scale the typical features of a GMSB particle spectrum described above are realised, while for very large messenger mass scales the typical mass spectrum of models with gravity mediation is found.

To get the physical mass spectrum at the electroweak scale, the parameters at the messenger scale have to be run down by renormalization group evolution. This introduces (positive and negative) mass shifts of the order of $10\,\mathrm{GeV}/c^2$ with respect to the masses at the messenger scale [7].

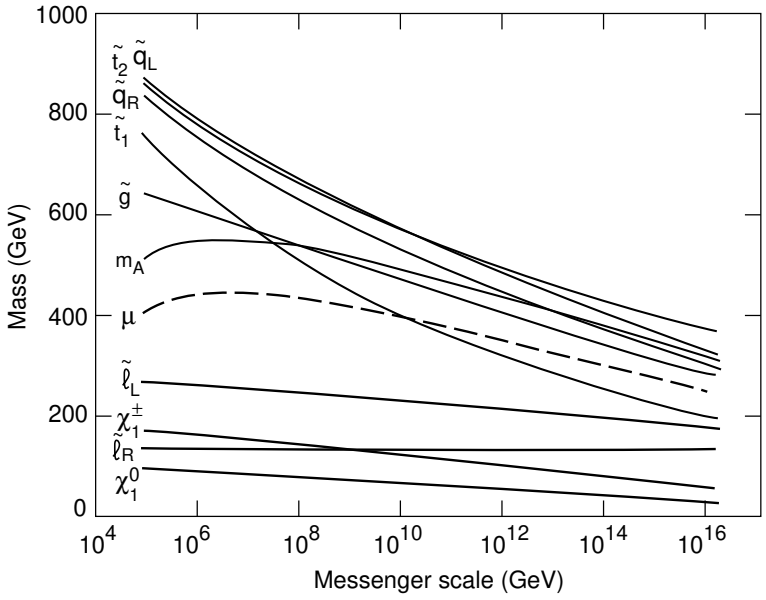


Figure 2.1: *Messenger scale dependence of some sparticle masses, including neutralinos and charginos, right– and left–handed sleptons and light squarks and the mass eigenstates of the stop, $\tilde{t}_1$ and $\tilde{t}_2$, for $N = 1$, $\tan\beta = 3$ and a messenger scale bino mass of 115 GeV/c^2 [7].*

The masses of the right–handed sleptons are increased, but are still smaller than the masses of left–handed sleptons. In addition to the positive mass shift for selectrons and smuons, the staus, due to their larger Yukawa coupling, receive a negative mass shift. The right– and left–handed staus mix to form the mass eigenstates $\tilde{\tau}_1$ and $\tilde{\tau}_2$. For large $\tan\beta$ ($> \mathcal{O}(5)$), the lightest stau, which is in general assumed to be the right–handed one, is the lightest slepton.

From an experimental point of view, the most important features of a supersymmetric model are the nature of the particles that can be produced, and their decay channels. As has been mentioned already, the gravitino acquires a mass by absorbing the degrees of freedom of the goldstino via the super–Higgs mechanism. The gravitino mass, assuming a vanishing

cosmological constant, is given by

$$m_{\tilde{G}} = \frac{F}{k\sqrt{3}M_P} = \frac{1}{k}\left(\frac{\sqrt{F}}{100\,\mathrm{TeV/c^2}}\right)^2 \cdot 2.4\,\mathrm{eV/c^2}\,. \tag{2.4}$$

Here k is a model–dependent parameter describing how SUSY breaking is communicated to the messenger sector, with $k < 1$ and possibly $k \ll 1$. For all viable GMSB models, the gravitino $\tilde{G}$ is the lightest SUSY particle, the LSP.

R–parity is a quantum number that is -1 for SUSY and $+1$ for SM particles. It is related to the baryon number B, the lepton number L and the spin S: $R = (-1)^{3B+L+2S}$. If R–parity is conserved, as will be assumed throughout this work, all SUSY particles have to be produced in pairs and decay chains have to terminate with the LSP and SM particles. In GMSB, following from what has been said before, the next–to–lightest SUSY particle, the NLSP, can either be the lightest neutralino, or the right–handed sleptons. The first case is called the *neutralino NLSP scenario*, while in the latter case two scenarios have to be distinguished (which, in the following, will often be summarised as the slepton NLSP scenario). If all sleptons are degenerate in mass, as is the case for low $\tan\beta$, sleptons of all flavours form the NLSP. This is referred to as the *slepton co–NLSP scenario*. On the other hand, for larger $\tan\beta$, when the stau is significantly lighter than the selectron and the smuon, the stau is the sole NLSP. This is called the *stau NLSP scenario*.

In this work a search for sleptons in the slepton co–NLSP and the stau NLSP scenario was developed, and therefore in the following only production and decay channels relevant for these cases will be discussed. All three dominant production channels were considered: direct slepton pair–production and indirect production via neutralino pair–production and chargino pair–production. Slepton pair–production, shown [2] in Fig. 2.2, proceeds via the s–channel, but for selectrons also t–channel production with neutralino exchange is possible. As shown in Fig. 2.3, neutralinos can be produced via s–channel and t–channel with a selectron exchange. Finally, charginos are produced in the s–channel and t–channel with selectron–sneutrino exchange, as illustrated in Fig. 2.4. While slepton pair–production is kinematically favoured in the slepton NLSP scenario, neutralino and chargino pair–production may have larger cross–sections, if kinematically allowed.

Sleptons, if they are the NLSP, decay directly to their SM partner and the $\tilde{\mathrm{G}}$, as is shown in Fig. 2.5 by the left Feynman diagram. If the stau is the sole NLSP, selectrons and smuons decay, via neutralinos, to $\ell\tilde{\tau}_1\tau$. This is shown in the graph on the right hand–side of Fig. 2.5.

Neutralinos, assuming they are not the NLSP, decay to $\tilde{\ell}_R\ell$, as shown in Fig. 2.6. Depending on the slepton mass splittings, the branching ratios (BR) for the different flavours can be 1/3 or $\mathrm{BR}\,(\tilde{\chi}_1^0 \to \tilde{\tau}_1\tau) = 100\,\%$.

Charginos decay in the slepton NLSP case to $\tilde{\ell}_R\nu_\ell$, as shown in Fig. 2.7. Here again the branching ratio for the different flavours depend on the mass relations between the sleptons.

In GMSB models, the decay length L of the NLSP depends in the laboratory frame on its mass m and energy E, and on the SUSY breaking scale $\sqrt{F}$:

$$L = \frac{1}{\kappa_\gamma}\left(\frac{100\,\mathrm{GeV/c^2}}{m}\right)^5\left(\frac{\sqrt{F/k}}{100\,\mathrm{TeV/c^2}}\right)^4\sqrt{\frac{E^2}{m^2}-1}\times 10^{-2}\mathrm{cm}\,. \tag{2.5}$$

The factor κ_γ is only relevant if the neutralino is the NLSP, as it measures its photino content, and is 1 for sleptons. So, depending on the SUSY breaking scale, the decay length of the NLSP can vary between microscopical and astronomical distances. This can be seen from Fig. 2.8, where the mean slepton decay length in the laboratory, calculated from

[2] In the literature various conventions are used for Feynman diagrams including SUSY particles. Here the conventions of [9] are adopted.

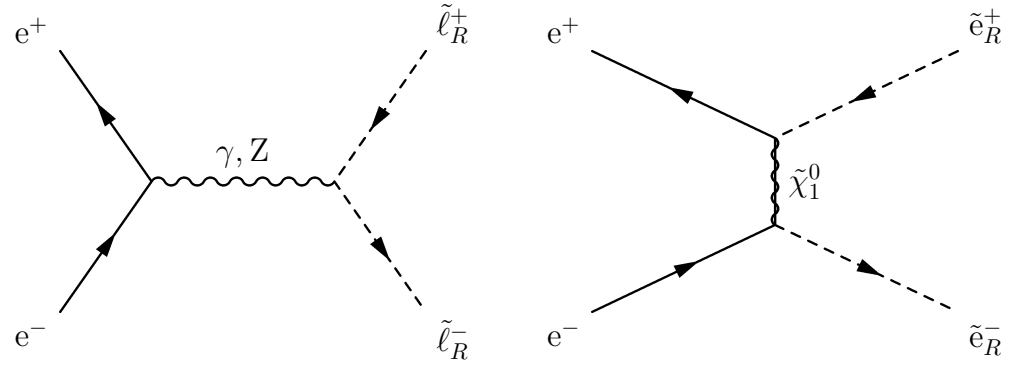


Figure 2.2: *Slepton pair–production. The t–channel production is possible for selectrons only.*

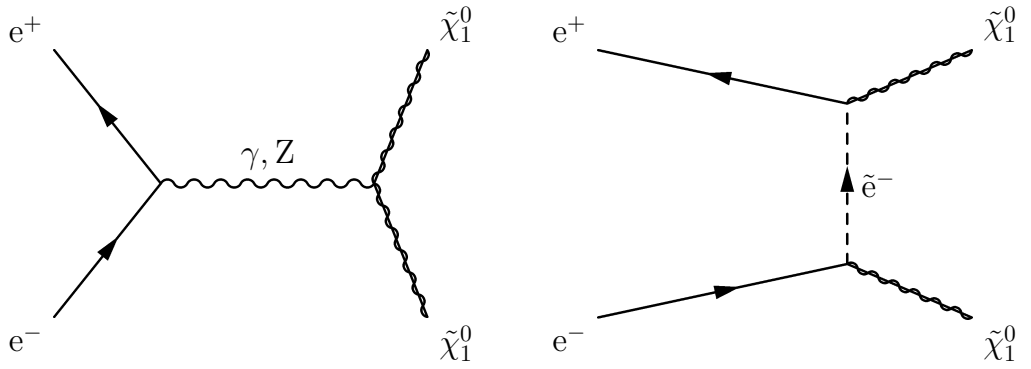


Figure 2.3: *Neutralino pair–production.*

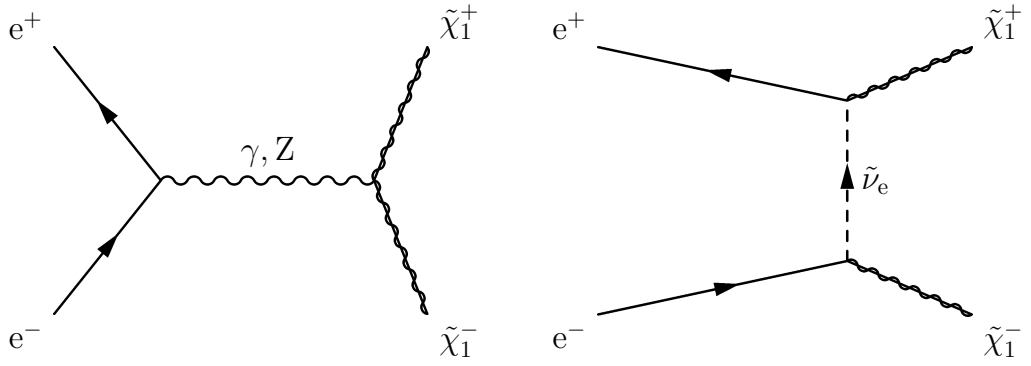


Figure 2.4: *Chargino pair–production.*

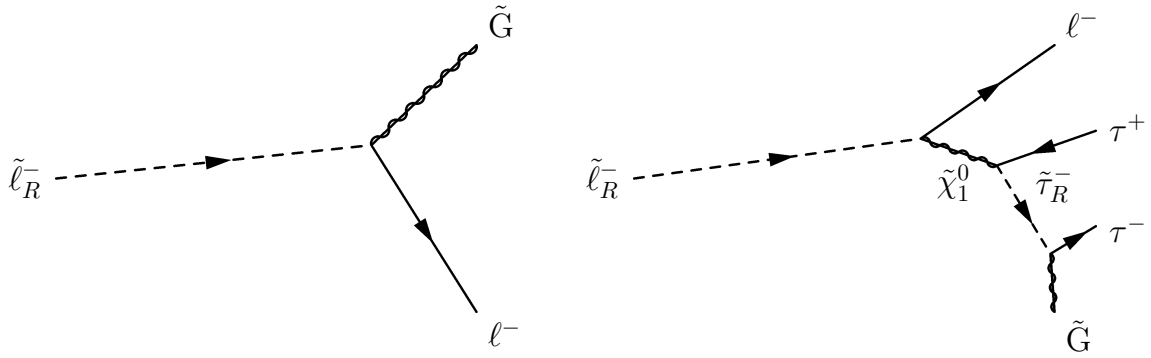


Figure 2.5: *Slepton decay in GMSB in the slepton co–NLSP (left, $\tilde{\ell}_R = \tilde{e}_R$, $\tilde{\mu}_R$, $\tilde{\tau}_1$; $\ell =$ e, μ, τ) and the stau NLSP (right, $\tilde{\ell}_R = \tilde{e}_R$, $\tilde{\mu}_R$; $\ell =$ e, μ) scenario.*

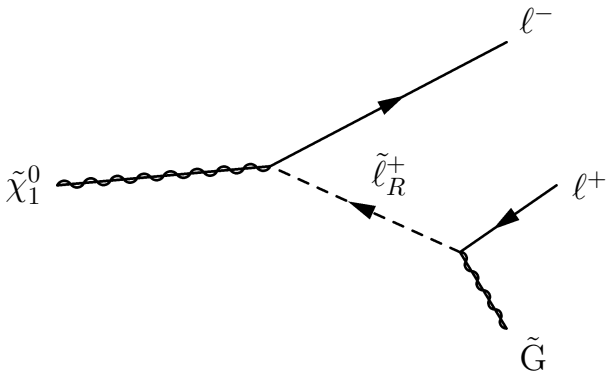


Figure 2.6: *Neutralino decay in GMSB in the slepton NLSP scenario ($\tilde{\ell}_R = \tilde{e}_R$, $\tilde{\mu}_R$, $\tilde{\tau}_1$; $\ell =$ e, μ, τ).*

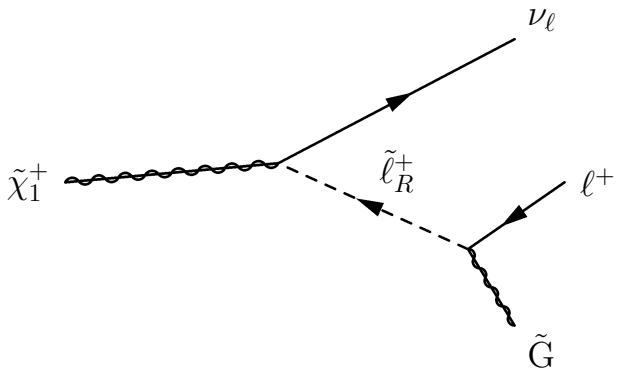


Figure 2.7: *Chargino decay in GMSB in the slepton NLSP scenario ($\tilde{\ell}_R = \tilde{e}_R$, $\tilde{\mu}_R$, $\tilde{\tau}_1$; $\ell =$ e, μ, τ).*

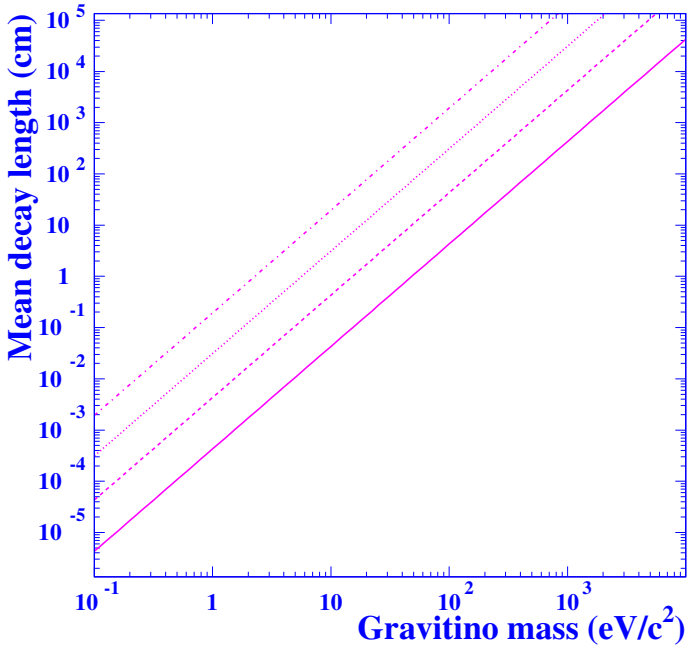


Figure 2.8: *The mean slepton decay length in the laboratory as function of the gravitino mass, for pair–produced sleptons with masses of 100 GeV/c^2 (solid line), 80 GeV/c^2 (dashed line), 60 GeV/c^2 (dotted line) and 45 GeV/c^2 (dashed–dotted line).*

formula (2.4) and (2.5) [3], is plotted for gravitino masses between 0.1 eV and 10 MeV for pair–produced sleptons with different masses. For a slepton with a mass of 100 GeV/c^2 the decay length is negligible ($\lesssim 0.01$ mm) for $M_{\tilde{\mathrm{G}}} \lesssim 10$ eV, i.e. in this case most sleptons decay promptly. For $M_{\tilde{\mathrm{G}}} \lesssim 1$ MeV the decay length exceeds the detector dimensions and quasi–stable NLSP's have to be searched for. For intermediate lifetimes, delayed decays of the NLSP within the detector volume are expected, leading to topologies with tracks with large impact parameters (sensitivity for decay lengths of 0.01 cm $\lesssim L \lesssim$ 10 cm) and tracks with kinks (sensitivity for decay lengths of 10 cm $\lesssim L \lesssim$ 1 m). Lighter particles have a longer mean decay length compared to heavier particles for the same gravitino mass. This is true even for the proper decay length due to the factor $(1/m)^5$ in (2.5).

To cover the whole theoretically allowed range for the gravitino mass or, equivalently, the SUSY breaking scale, it is crucial to search for all possible topologies. In this work a search for the large impact parameter topology is presented, including a combination of this analysis with other analyses undertaken at OPAL that are sensitive to shorter and longer decay lengths. Such a combination is the only way to obtain constraints on the cross–sections, particle masses and model parameters that are valid for all NLSP lifetimes respectively all values of the SUSY breaking scale.

[3] For $\kappa_\gamma = 1$. The model dependent parameter k is eliminated since both $m_{\tilde{G}}$ and L are functions of $\sqrt{F/k}$.

Chapter 3

The LEP Collider and the OPAL Detector

3.1 The LEP Accelerator

The Large Electron Positron (LEP) Collider at the European Organization for Nuclear Research (CERN) was[1] a ring accelerator with a circumference of 27 km, built about 100 m underground. Electrons and positrons were accelerated in opposite directions to energies up to about 104 GeV and brought into collision at four interaction points, which were surrounded by the ALEPH, DELPHI, L3 and OPAL detectors. Figure 3.1 gives a view of LEP with the four experiments.

In the first phase, called LEP 1, the accelerator was operating at centre–of–mass energies around 91 GeV, the energy where the Z^0 boson is produced resonantly. Between 1989 and 1995 more than 4 millions of Z^0 boson decays were recorded per experiment.

In 1996 LEP entered its second phase, LEP 2, where it was operating above the W^+W^- production threshold. The centre–of–mass energy was increased in steps from 161 GeV in 1996 to a mean energy of about 206 GeV in 2000, reaching a centre–of–mass energy of 209 GeV for a short time period, the highest energy ever achieved in an e^+e^- collider.

3.2 The OPAL Detector

The OPAL[2] detector, described in detail in [10] and sketched in Figure 3.2, was constructed by an international collaboration of physicists to record e^+e^- collisions, classify all types of interactions that occur in these collisions, and measure the energy, momentum and charge of the produced particles and their decay products. OPAL was a multi–purpose detector with a length, width and height of about 12 m×12 m×12 m. The cylindrical detector provided almost full solid angle coverage and consisted of a number of individual components, which formed layers around the interaction point.

The momenta and directions of charged particles were measured by a tracking system, which formed the inner part of the detector and consisted of, from inside to outside, the silicon microvertex detector, the vertex chamber, the central jet chamber and the z–chambers. The tracking devices, with exception of the silicon microvertex detector, were located inside a pressure vessel, which maintained a pressure of 4 bar, and a solenoid, which provided a uniform axial magnetic field of 0.435 T.

The part outside the pressure vessel is called the outer detector. The first layer was formed by a scintillation counter array, measuring the time–of–flight of passing charged particles. An electromagnetic calorimeter measured, together with preshower detectors, the energy and

[1] LEP was disassembled at the end of 2000 to install the Large Hadron Collider LHC, which is scheduled to collide protons at a center–of–mass energy of 14 TeV in 2007.

[2] Omni–Purpose Apparatus at LEP

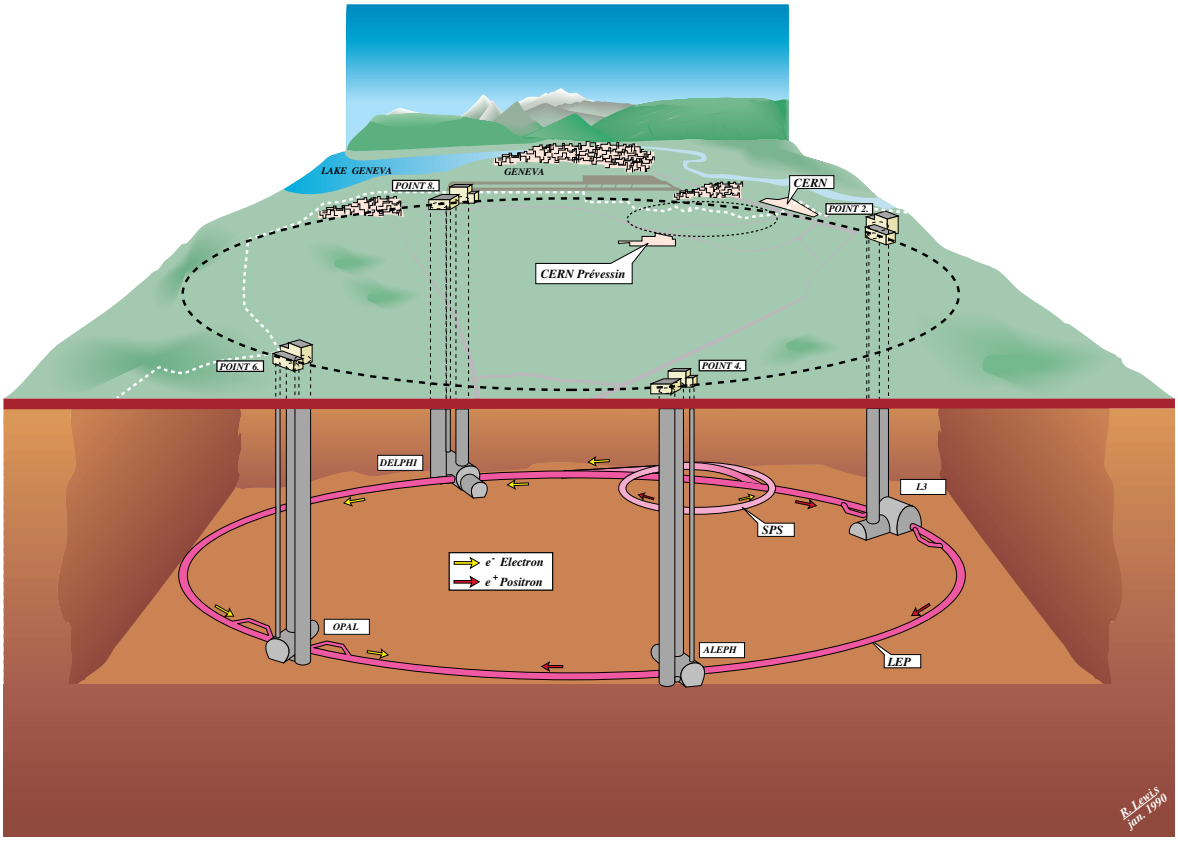


Figure 3.1: *The LEP accelerator complex at CERN.*

direction of showering particles. Then followed the iron return yoke of the magnet, which was instrumented with streamer tubes and multiwire chambers serving as a hadronic calorimeter to determine the energy and direction of hadronically interacting particles. Muon chambers formed the outside layer, identifying muons which penetrated all other detector components without interaction. Calorimeter systems on both sides of the interaction point, and close to the beam axes, measured the luminosity via small angle Bhabha scattering.

For this work the tracking detectors are most relevant and are described in detail in the next section. In Sect. 3.2.2 a short overview of the components of the outer detector is given.

3.2.1 The Tracking System

The Silicon Microvertex Detector

The version of the silicon microvertex detector (SI) used when collecting data for this work was installed in 1995 and is described in detail in [11]. The cylindrical two–layered silicon detector with an outer radius of 8 cm and a length of 30 cm was located just outside the beam pipe. The inner and outer layers were made up of 12 and 15 ladders, respectively. A ladder was formed by five back–to–back mounted pairs of silicon wafers with ϕ and z readout [3], arranged in a row. The wafers were 250 μm thick and had an area of $60 \times 33\,\mathrm{mm}^2$.

The single hit resolution from the silicon microvertex detector is 10 μm perpendicular to and 15 μm along the beam direction.

[3] A right–handed coordinate system is adopted, where the x–axis points towards the centre of the LEP ring and the z–axis points in the direction of the electron beam. The polar angle θ and the azimuthal angle ϕ are defined w.r.t. z and x, respectively.

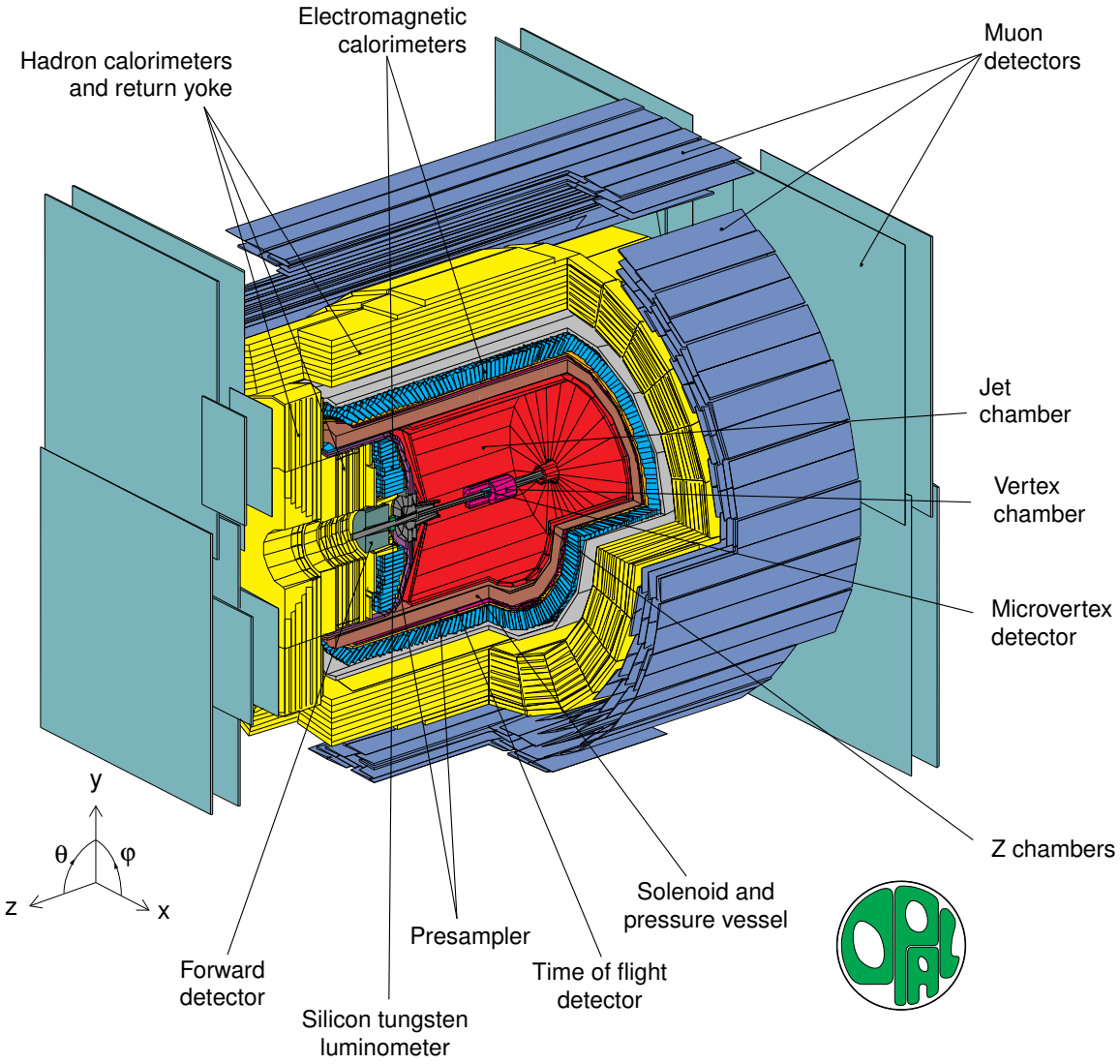


Figure 3.2: *General layout of the OPAL detector. The main detector components are labeled.*

The Vertex Chamber

The vertex chamber (CV) was located between the silicon microvertex detector and the jet chamber inside the 4 bar pressure vessel. It was a cylindrical drift chamber with a length of 1 m and a diametre of 47 cm. The chamber consisted of two layers with 36 cells in ϕ each. Each cell of the inner layer contained 12 axial anode wires with a radial spacing of 5.3 mm, and each cell of the outer layer contained six anode wires with a radial spacing of 5.0 mm and inclined by a stereo angle of 4° with respect to the axial wires.

The aim of the vertex chamber was to improve the measurement of secondary vertices of short–lived particles and, by combining axial and stereo cell information, to provide a precise measurement of the $z-$coordinate near the interaction region.

The Central Jet Chamber

The central jet chamber (CJ), a cylindrical drift chamber with a length of about 4 m, an inner radius of 24.5 cm and an outer radius of 185 cm, surrounded the vertex detector. It consisted of 24 sectors in ϕ, which were separated by the cathode wire planes. In the centre plane of each sector were 159 anode or sense wires with a radial spacing of 1 cm, alternating with 160 potential wires. All wires were stretched parallel to the beam direction. The anode wires were at ground potential and were staggered by $\pm 100\,\mu$m with respect to the potential

wire plane to resolve left–right ambiguities. The chamber was filled with a gas mixture of 88.2 % argon, 9.8 % methane and 2.0 % isobutane at a nominal pressure of 4 bar.

A maximum of 159 hits could be measured for tracks with $|\cos\theta| < 0.73$, and at least eight hits could be measured within a solid angle covering 98 % of 4π. For each hit, the $r-$ and $\phi-$coordinates were determined from the wire position and the drift time, and the $z-$coordinate was calculated by charge division. The specific energy loss $\mathrm{d}E/\mathrm{d}x$ along the drift path provided a tool for particle identification with a resolution $\sigma_{\mathrm{dE/dx}}/\mathrm{dE/dx}$ of approximately 3 %. Particle momenta in the plane transverse to the beam direction were calculated from the track curvature in the magnetic field.

Averaged over all drift distances, single hit resolutions of 135 μm in $r-\phi$ and 4.5 cm in z for muon–pairs (6 cm for multi–hadronic events) were achieved. The double hit resolution in $r-\phi$, for a separation efficiency of 80 %, was 2.5 mm. The track reconstruction efficiency in a high–multiplicity environment was 97.9 % for $p > 100\,\mathrm{MeV}/c$ and $|\cos\theta| < 0.95$.

The z–Chambers

The $z-$chambers formed a barrel outside the jet chamber. Their purpose was to provide a precise measurement of the $z-$coordinate of charged particles when leaving the jet chamber, and thus to improve the polar angle measurement and the invariant mass resolution. The $z-$chambers consisted of 24 drift chambers with the drift parallel to the z axis, each 4 m long, 50 cm wide and 5 cm thick. Each panel was split into eight cells of $50 \times 50\,\mathrm{cm}^2$. In each cell six anode wires with increasing radii were stretched perpendicularly to the $z-$axis.

In these chambers the $z-$coordinate was determined from the drift time measurement with a resolution better than 300 μm.

Tracking Performance

The impact parameter and momentum resolutions of the jet chamber alone, obtained from muon–pair and Bhabha events, are typically $\sigma(d_0) = 110\,\mu\mathrm{m}$ and $\sigma(p)/p^2 = 1.9 \cdot 10^{-3}\,(\mathrm{GeV}/c)^{-1}$ for LEP2 data. Combining CJ and CV information, the corresponding numbers are $\sigma(d_0) = 46\,\mu\mathrm{m}$ and $\sigma(p)/p^2 = 1.67 \cdot 10^{-3}\,(\mathrm{GeV}/c)^{-1}$. Including available SI information as well, the numbers improve further and are $\sigma(d_0) = 21\,\mu\mathrm{m}$ and $\sigma(p)/p^2 = 1.59 \cdot 10^{-3}\,(\mathrm{GeV}/c)^{-1}$, respectively [12].

3.2.2 The Outer Detector

The Time–of–Flight System

The purpose of the time–of–flight (TOF) system was to provide fast trigger signals and, by measuring the time–of–flight from the primary interaction point, allow for the identification of charged particles and rejection of cosmic ray events.

The TOF barrel detector (TB), covering the region with $|\cos\theta| < 0.82$, consisted of 160 scintillation counters. The produced scintillation light was collected at both ends of the counters via plexiglass light guides and then measured with phototubes. The timing resolution for muon pairs is better than 0.5 ns.

In 1996 additional time–of–flight detectors were installed in the endcaps between the presamplers and the electromagnetic calorimeters. They were made out of scintillating tiles and used mainly to enhance the trigger performance in the forward region.

The Presampler and Electromagnetic Calorimeter

The electromagnetic calorimeter measured energies and directions of electrons and photons with momenta ranging from tens of MeV/c up to about $100\,\mathrm{GeV}/c$, and provided discrimination between neutral pions and photons as well as electrons and hadrons. It was built of lead

glass blocks and split up into a barrel part ($|\cos\theta| < 0.82$) with about 24.6 radiation lengths and two endcap detectors ($0.81 < |\cos\theta| < 0.98$), each with about 22 radiation lengths.

The barrel calorimeter was a cylindrical array of 9440 lead glass blocks, 59 blocks in the z direction and 160 blocks forming a ring in the azimuthal angle. The blocks were mounted in a quasi–pointing geometry, meaning that they were pointing towards the interaction region but tilted slightly to prevent neutral particles from escaping undetected through the gaps between the blocks. Each block had a cross–section of about $10 \times 10\,\mathrm{cm}^2$ and a depth of 37 cm. If a photon or electron enters a lead glass block an electromagnetic shower is produced via pair–production and Bremsstrahlung. The electrons emerging from this shower give rise to Čerenkov light, and the amount of Čerenkov light produced from all electrons of the shower is proportional to the energy of the original particle. The Čerenkov light was measured with phototubes.

The two endcap detectors each consisted of 1132 lead glass blocks, arranged coaxially with the beam directions. Due to the full axial magnetic field present in the endcaps vacuum photo triodes were used to measure the Čerenkov light.

The intrinsic energy resolution σ_E/E of the electromagnetic calorimeter for electrons and photons combined is $1\,\% + 21\,\%/\sqrt{E\,[\mathrm{GeV}]}$ in the barrel and $5\,\% + 12\,\%/\sqrt{E\,[\mathrm{GeV}]}$ in the endcaps [13].

Due to the material in front of the electromagnetic calorimeter (about two radiation lengths) showering started in front of the lead glass. Therefore presampler detectors were installed in front of the lead glass both in the barrel and the endcap region to measure the position and sample the energy of these showers. The barrel presampler was a cylinder–shaped array of 16 chambers with each chamber consisting of two drift tubes operating in limited streamer mode. In the endcap region each presampler was built out of 32 thin multiwire proportional chambers.

The Hadron Calorimeter

The hadron calorimeter was divided into three parts, the barrel ($|\cos\theta| < 0.81$), the endcaps ($0.81 < |\cos\theta| < 0.91$), and the pole tips ($0.91 < |\cos\theta| < 0.99$). The barrel hadron calorimeter consisted of nine active layers instrumented with plastic limited streamer tubes, alternating with passive layers of iron slabs, provided by the segmented magnet return yoke. The doughnut–shaped endcaps consisted of eight layers of streamer tubes. In the hadron poletip detectors the active layers were instrumented with thin multiwire chambers.

With four or more hadronic interaction lengths of material, most hadrons were absorbed in the hadron calorimeter, while most muons left a clean track and reached the muon chambers. The energy resolution is $120\,\%/\sqrt{E\,[\mathrm{GeV}]}$.

The Muon Chambers

The muon barrel detector consisted of 110 drift chambers, each 1.2 m wide, 1.5 cm thick and between 6 m and 10.4 m long. They were arranged in four layers around the interaction point. The transverse and longitudinal coordinates were measured with a precision of 1.5 mm and 2 mm, respectively.

The muon endcap detector consisted of four layers of limited streamer tubes arranged perpendicularly to the beam axes.

The efficiency to detect isolated muons with a momentum greater than $3\,\mathrm{GeV}/c$ within the geometrical acceptance (93 % of the solid angle) of the muon detector is close to 100 %.

The Luminosity Counters

Two detector systems were used mainly to measure the Bhabha scattering cross–section in the very forward and backward direction: an electromagnetic calorimeter system called the forward detector and silicon–tungsten calorimeters covering the very small polar angle

region. Both detectors were split up symmetrically between the two sides of the interaction point.

Each forward detector consisted of four separate components, three lead–scintillator sandwich detectors and one drift tube array.

The silicon–tungsten calorimeters consisted of 19 layers of silicon detectors and tungsten plates each. They were installed in 1993 and are described in detail in [14].

Chapter 4

Monte Carlo Simulation

The event simulation at OPAL is done in two stages. First, the reaction of interest is simulated with a Monte Carlo generator, i.e. the particles and their four–momenta (E, $\vec{p}$), defining the event kinematics, are generated. Then these events are passed through the OPAL detector simulation program GOPAL [15] to properly treat effects such as energy loss in the detector material or the curvature of the trajectories of charged particles in the magnetic field. The geometrical detector parameters are introduced through the CERN GEANT3 [16] package, which tracks the particles through the detector material, including all necessary processes like scattering, hadronic interaction, pair–production and Bremsstrahlung as well as decays of some long–lived particles. Within GOPAL the event reconstruction is done with the OPAL reconstruction program ROPE [17], in the same way as for the recorded data.

4.1 SUSY Signal Event Simulation

For the simulation of the signal (i.e. slepton, neutralino and chargino production and decay), the SUSYGEN generator was used. This generator is described in the next section. To properly treat supersymmetric particles with delayed decays, significant modifications of the GOPAL and GEANT code were necessary. A summary of these modifications is given in Sect. 4.1.2.

4.1.1 The SUSYGEN Event Generator

SUSYGEN is a standard Monte Carlo generator for the production and decay of supersymmetric particles at tree–level, using the precise lowest order matrix elements. From version 2.2 [18] onwards it includes also GMSB processes. For slepton pair–production in the slepton co–NLSP scenario and neutralino pair–production the version 2.2 was used, other processes were simulated with the more recent version 3.0 [19].

SUSYGEN provides an interface to JETSET 7.4 [20] for hadronisation according to the Lund parton shower model. It includes initial state radiation using the structure–function method [21]. Final state radiation is implemented up to $\mathcal{O}(\alpha^2)$ using the PHOTOS [22] library. From version 3.0 onwards, helicity correlations in the initial and final states are taken into account.

SUSYGEN can be used not only for SUSY particle production (four–vectors), but also for SUSY parameter scans, where it calculates the mass spectrum, production cross–sections and branching ratios for each parameter setting. This mode was used for the interpretation, discussed in Chapter 9.

4.1.2 Modifications in GEANT and GOPAL

For several reasons, discussed below, the standard GOPAL and GEANT code is not suited to handle supersymmetric particles with long lifetimes. Therefore a program was developed

for this analysis that includes modifications to a number of GEANT and GOPAL routines and runs in the standard OPAL Monte Carlo production environment. It was used not only for the channels covered here, but also for the simulation of neutralino NLSP channels and even for non–GMSB processes such as pair–production of doubly charged Higgs bosons and MSSM chargino pair–production with a small mass difference between the chargino and the neutralino.

In the following, the shortcomings of the standard code along with the implemented modifications are listed:

- Supersymmetric particles are not tracked by GEANT. Instead, it is assumed that they decay promptly. Thus, to pass also supersymmetric particles to GEANT to allow for their tracking, the particles and their properties (including the lifetime) had to be defined in GEANT with calls to the routine GSPART.

- The same applies to the τ lepton, which, due to its lifetime of $(290.6 \pm 1.1) \cdot 10^{-15}$ s, is assumed to decay in the beam pipe. Here, however, the tau can be the decay product of a long–lived sparticle, so that tau decays within the detector volume had to be simulated.

- The GEANT particle codes 51 – 60 were used for the newly defined supersymmetric particles and the tau lepton, since these numbers are not used in the standard GEANT.

- The charges of the SUSY particles had to be defined in the GOPAL routine PDGCHG.

- In contrast to SM particles, the masses of SUSY particles are not known. Therefore usually a whole grid of masses is simulated. To allow for the treatment of four–vectors with different masses within one job, the GOPAL routine GOKINE was modified in a way that the masses are read–in from a four–vector file.

- To pass a particle to GEANT, its "end flag" has to indicate that the particle is still alive but has not yet decayed in the generator. Therefore the end flag of supersymmetric particles as well as the tau was changed in the GOPAL routine GOLIFE.

- After choosing a certain lifetime for the supersymmetric particle, its decay length is calculated using a random number generator. The decay products of this particle, however, have to be attached to the end point of the parent particles trajectory. Therefore the decay products first were "removed", i.e. their start point was set to a large number (specific for each decay vertex). This was done in the routine GOLIFE.

- After a supersymmetric particle has decayed in GEANT, the decay particles have to be moved to their parents end point. To do this a new routine GUDCAY (a dummy routine is provided by GEANT) was written, in which the decay particles are found and their start points set to their parents end point. However, it has to be taken into account that the parent particle might have lost energy due to interaction with the detector material (like the gas in the jet chamber) and that, due to the magnetic field, the trajectory of the parent particle is a helix and therefore the direction of flight of the decay particles will have changed. The correction of the four–momenta of the decay particles was done in the following way. In the routine KIDISK, which is the routine to apply changes to the KINE tree [1], the decay particles were boosted into the rest frame of the parent. Both the momenta of the decay particles and the parent particles were transformed to spherical coordinates (p, ϕ, θ) to separate the direction information from the absolute momentum. Then p and the quantities $\delta\phi = \phi_{\text{parent}} - \phi_{\text{daughter}}$ and $\delta\theta = \theta_{\text{parent}} - \theta_{\text{daughter}}$ were stored in the tree for the decay particles. In the

[1] Two trees have to be distinguished: the KINE tree, in which only particles from the generator are included, and the full tree, in which also particles created by GEANT are present.

routine GUDCAY the parent momentum at the time of its decay is known. This was transformed to spherical coordinates as well. Then the new values for ϕ and θ – corrected for the effect of the magnetic field – of the decay particles were calculated by subtracting $\delta\phi$ and $\delta\theta$ from the parent values at the time of decay. The momenta of the decay particles were transformed back to cartesian coordinates and finally boosted back to the laboratory frame with the parent's momentum at the time of decay. This method assures that the decay angle distributions $\cos(\theta^*)$ are maintained by the correction. The decay angle distributions on generator and corrected detector level are shown in the upper plots of Fig. 4.1 and Fig. 4.2 for the stau decay products and the leptonic tau decay products, respectively. For a perfect detector correction the distributions on generator and corrected detector level should be identical, and indeed a difference is barely visible. Their ratios, $\cos(\theta^*)_{\text{Generator}}/\cos(\theta^*)_{\text{GEANT}}$, are shown in the lower left plots. There it can be seen that the difference is below 4 per mille in most bins. The event–by–event deviations in θ^* are shown in the bottom right plots.

In addition, for the tau decay products, a correction had to be applied to account for a slight ($\mathcal{O}(20\,\text{MeV})$) energy non–conservation, which, due to rounding errors induced by the trigonometrical calculations, appeared in a small fraction of events.

- In the routine KIDISK also the KINE tree was "cleaned up" to take care of the fact that hadrons from tau decays, that had already decayed in the generator, and their daughters now are put into GEANT. Some hadrons like the ρ^+ and the K^{*+} are not known to GEANT, thus they were removed from the tree and only their decay particles are kept. On the other hand the decay of hadrons that are known to GEANT, like the π^0, the K_s^0 and the η, is handled by GEANT. Therefore in this case their decay particles were removed from the KINE tree.

- The routine GOKING handles the storage of newly created particles, e.g. from pair–production, as well as from the decays of the sparticles and the tau. It decides if the particle will be stored at all (e.g. shower electrons with very low energies and particles with $r < 23.5\,\text{cm}$ but $z > 50\,\text{cm}$ are not stored in the tree). A work around was introduced to store the decay particles from the sparticle and the tau decay in any case, independently from their position in the detector. For particles newly created by GEANT itself or, as in this case, passed to GEANT by the user via the routine GUDCAY, the number of tree entries is increased by one. This has to be avoided, as in this case the decay particles are not created by GEANT, but were already present in the four–vectors.

- The kinematics and the vertex number of the new particle is stored in the KINE tree by the GEANT routine GSKINE (called from GOKING). A new routine, similar to GSKINE, was created. It stores the properties of the decay particle in the KINE bank without increasing the number of tree particles.

- The GEANT tree banks also have to be updated with the new particles. This is done by the routine GOTRUP (called from GOKING). Again it has to be avoided that the number of tree particles is increased. Also the number of decay products of the primary particle has to be kept, as it is already correct. The endpoints of the neutrinos from the tau decay were calculated in such a way that the largest coordinate $\xi_{\text{end}} = 7\,\text{m}$ and that the others are scaled by their momentum: $\eta_{\text{end}} = \eta_{\text{start}} + (7\,\text{m} - \xi_{\text{start}}) \cdot \mathrm{p}_\eta/\mathrm{p}_\xi$.

- Finally in USOUT the end flag of particles that have not decayed inside the detector volume due to their long lifetime were set to "still alive", and the start and end point of the in this case unused decay particles were set to the end point of the parent particle to flag but keep them.

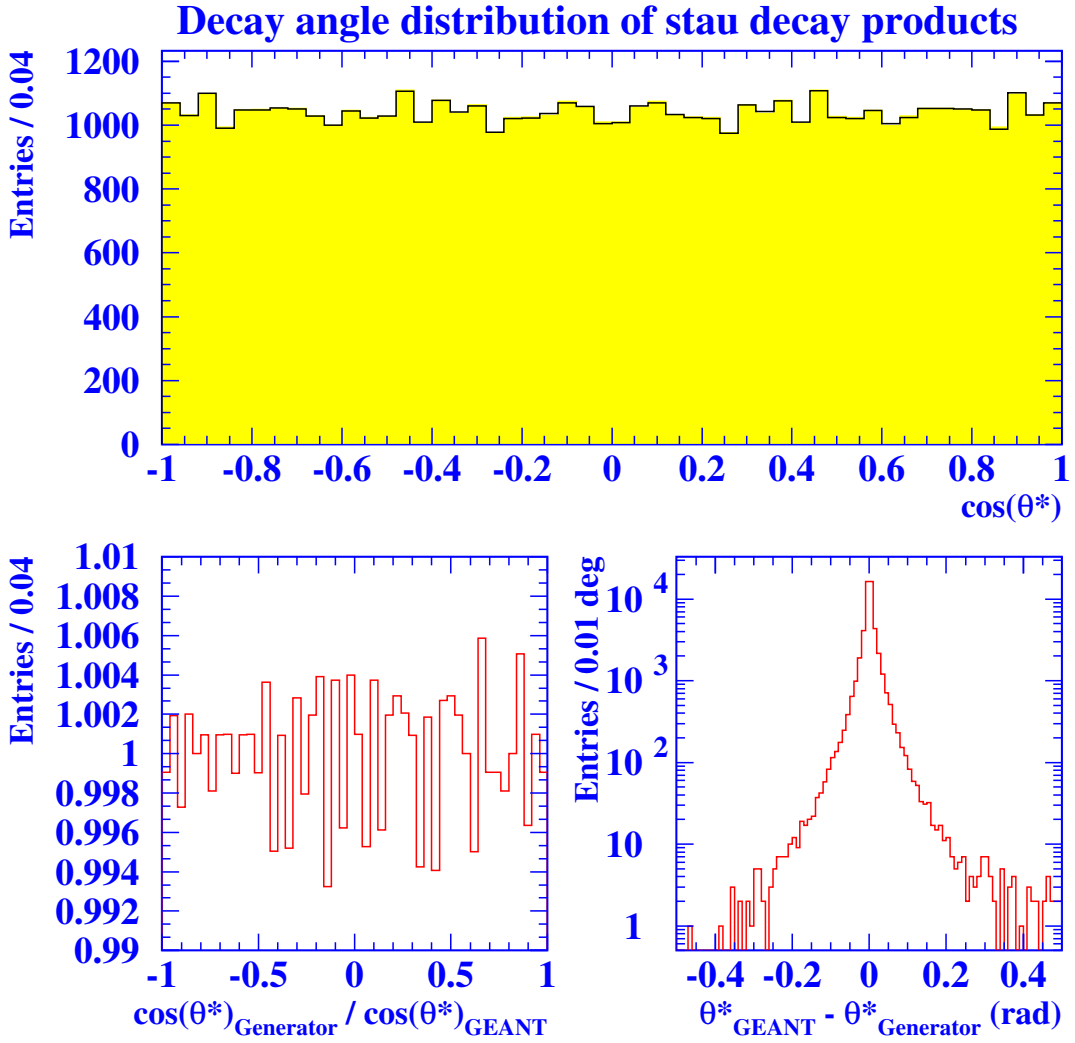


Figure 4.1: *The upper plot shows the decay angle distribution* $\cos(\theta^*)$ *of the stau decay products (i.e. the tau and the gravitino) on generator level (yellow histogram) and after detector simulation, with the modifications described in the text (solid line). The difference is barely visible. The ratio of the two distributions is shown in the lower left plot. The lower right plot shows the event–by–event deviations in* θ^* *between generator and detector level.*

Signal events were generated for ten different NLSP lifetimes: $\tau = 10^{-12}$, 10^{-11}, 10^{-10}, $5 \cdot 10^{-10}$, 10^{-9}, $5 \cdot 10^{-9}$, 10^{-8}, $5 \cdot 10^{-8}$, 10^{-7}, 10^{-6} s. The generated mass grid for the various channels is described in detail in Appendix B.

4.2 Background Event Simulation

As possible sources of background for this analysis all Standard Model processes were considered. They are described in detail in Sect. 5.4. Here the processes and the Monte Carlo generators used to simulate them are listed only briefly. In all cases the generators that are standard in OPAL were used.

One of the most relevant background sources for this analysis is two–photon production, where photons radiated by both the beam electron and positron scatter and produce hadronic or leptonic final states: $e^+e^- \rightarrow e^+e^-X$. Hadronic two–photon events ($X = q\bar{q}$) with two quasi–real photons ($Q_1^2 < 4.5\,\mathrm{GeV}/c^2$, $Q_2^2 < 4.5\,\mathrm{GeV}/c^2$, Q_1^2 and Q_2^2 being the negative squared four–momenta of the two photons) were simulated with the PHOJET [23] program, and processes with one virtual photon ($Q_1^2 > 4.5\,\mathrm{GeV}/c^2$, $Q_2^2 < 4.5\,\mathrm{GeV}/c^2$) with

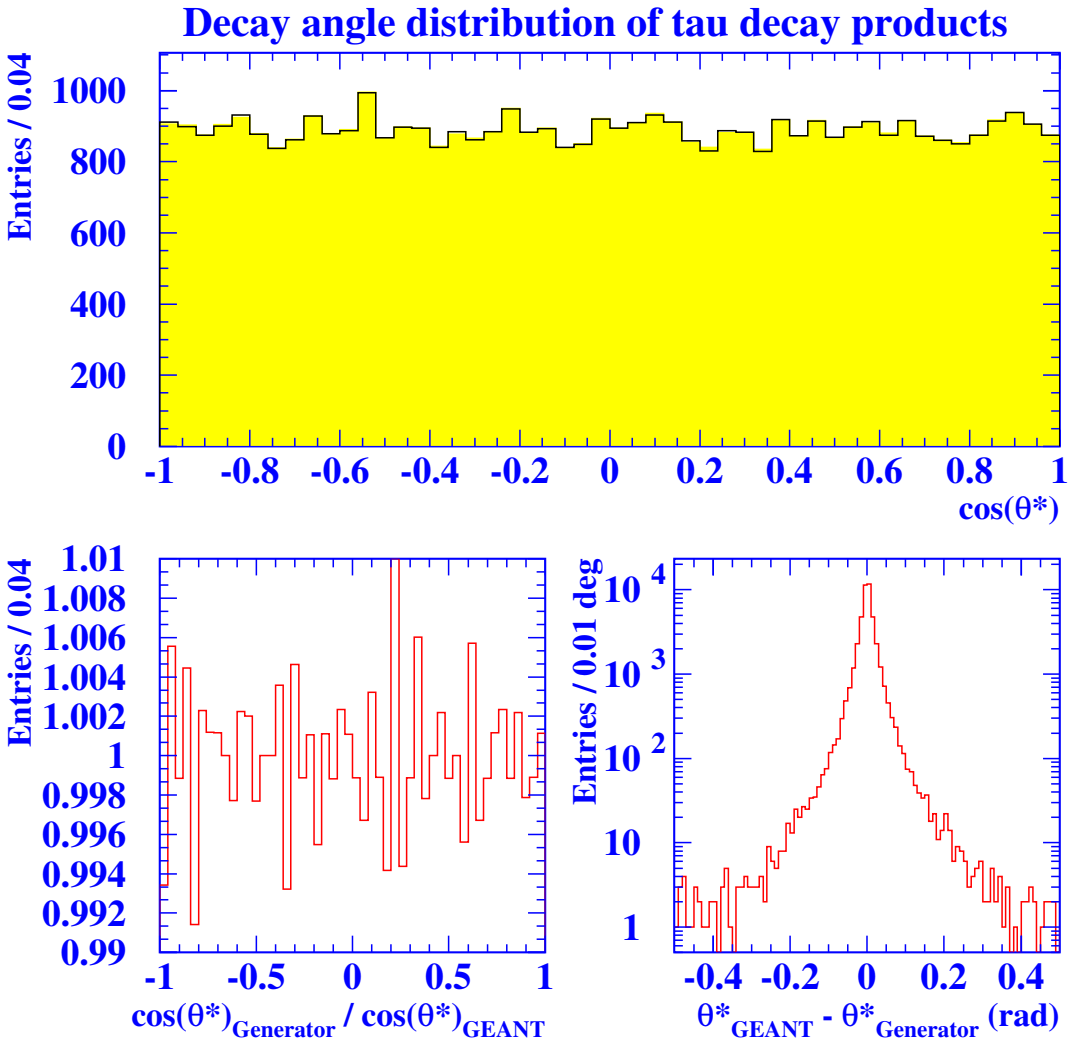


Figure 4.2: *The upper plot shows the decay angle distribution* $\cos(\theta^*)$ *of the leptonic tau decay products on generator level (yellow histogram) and after detector simulation, with the modifications described in the text (solid line). The difference is barely visible. The ratio of the two distributions is shown in the lower left plot. The lower right plot shows the event–by–event deviations in* θ^* *between generator and detector level.*

the HERWIG [24] program. Since the differential production cross–section diverges for low invariant masses W of the hadronic system, only events down to a certain lower limit of W ($5\,\mathrm{GeV}/c^2$ for PHOJET, $1.73\,\mathrm{GeV}/c^2$ for HERWIG) were simulated. The PHOJET program includes $\mathrm{c\bar{c}}$ production, but does not cover the $\mathrm{b\bar{b}}$ final state. For $\mathrm{e^+e^-} \to \mathrm{e^+e^-e^+e^-}$ events the Vermaseren generator [25] was used, while $\mathrm{e^+e^-} \to \mathrm{e^+e^-}\mu^+\mu^-(\gamma)$ events and $\mathrm{e^+e^-} \to \mathrm{e^+e^-}\tau^+\tau^-(\gamma)$ events were simulated with the BDK [26] program, which, in contrast to Vermaseren, includes radiative corrections.

RADCOR [27] served to simulate $\mathrm{e^+e^-}$ annihilation into multi–photon final states $\mathrm{e^+e^-} \to \gamma\gamma(\gamma)$.

Muon– and tau–pairs as well as $\mathrm{q\bar{q}}(\gamma)$ events were simulated with the KK2f [28] generator. KK2f uses PYTHIA 6.125 [29] for fragmentation and hadronisation and TAUOLA [30] for tau decays.

Wide–angle ($12.5^\circ < \theta < 167.5^\circ$) Bhabha scattering events, $\mathrm{e^+e^-} \to \mathrm{e^+e^-}(\gamma)$, were simulated with the BHWIDE [31] program, radiative Bhabha events with one or both electrons scattering with an azimuthal angle smaller than 12.5° (t–channel production) with the TEEGG [32] generator.

Neutrino pairs with up to three initial state photons, $\mathrm{e^+e^-} \to \nu\bar{\nu}\gamma(\gamma\gamma)$ were simulated

using the NUNUGPV [33] program.

To simulate four–fermion processes with electrons, the grc4f [34] program, which provides only collinear initial state radiation (ISR), was used. Final states without electrons were simulated with the KoralW [35] generator, which internally uses grc4f matrix elements, but simulates ISR according to a p_T spectrum using the PHOTOS package. Both generators use JETSET for hadronisation and TAUOLA for the simulation of tau decays.

Chapter 5

Search for the Large Impact Parameter Topology

5.1 The Signal: Channels and Topologies

In Gauge Mediated Supersymmetry Breaking models with a slepton NLSP the experimental topology depends strongly on the mean lifetime of the sleptons. For negligible lifetimes ($\tau \lesssim 10^{-11}$ s) most sleptons decay promptly and the decay products, the lepton and the invisible gravitino, originate within the experimental resolution from the primary vertex. For lifetimes [1] of the order of $10^{-11} - 10^{-9}$ s the sleptons decay with high probability inside the beam pipe, the silicon microvertex detector or the vertex chamber. In this case, as at least ten hits in the OPAL jet chamber are required to reconstruct a track, the slepton is invisible and the decay lepton will not originate from the primary vertex but will have a large impact parameter (for the definition of the impact parameter see Appendix A). If the slepton lifetime is of the order of 10^{-8} s the sleptons reach the jet chamber and, if they leave enough hits to allow for the reconstruction of the track, the slepton as well as the decay lepton are visible and they will form a kinked track. Finally, if the sleptons are so long–lived that they decay outside the jet chamber, or if they are stable, they can be identified by their anomalously high or low specific energy loss $\mathrm{d}E/\mathrm{d}x$ due to their high mass.

In the present investigation, an analysis was developed to efficiently select events which contain tracks with large impact parameters. It covers the slepton lifetime range around $10^{-11} - 10^{-9}$ s, in the following referred to as short lifetime, and is later combined with three other analyses that cover very short (referred to as zero lifetime) and longer (referred to as medium and long lifetime) lifetimes.

In addition to the slepton lifetime the event topology depends also on the production channel. All production channels that are allowed in GMSB models within the slepton co–NLSP scenario and the stau NLSP scenario at LEP 2 energies were studied. In order to assure good performance for the different channels four distinct selections were developed. The efficiency and the level of remaining Standard Model background vary considerably among these selections.

The following channels were studied:

- *Selectron and smuon pair–production in the slepton co–NLSP scenario:*
  In the slepton co–NLSP scenario selectrons and smuons are produced in pairs, $\mathrm{e}^+\,\mathrm{e}^- \to \tilde{\ell}_R^+\,\tilde{\ell}_R^-$, and decay as $\tilde{\ell}_R^\pm \to \ell^\pm\,\tilde{\mathrm{G}}$. For short lifetimes, no primary tracks but at least two tracks with large impact parameters are expected. The selection developed for this channel, in the following referred to as the *2–lepton channel*, is described in Sect. 5.5.1.

[1] The experimental topology depends in fact on the decay length in the laboratory, $L = \beta\gamma c\tau = (p/m)c\tau$, rather than the lifetime, thus for very heavy particles close to the kinematic limit these numbers shift towards longer lifetimes.

Since the track multiplicity and the amount of visible and missing energy depend on the flavour of the sleptons, staus were treated separately (see next paragraph).

As an example Fig. 5.1 shows a Monte Carlo smuon pair–production event, where both smuons decay inside the vertex chamber and thus the muon tracks have impact parameters around 10 cm. This event was simulated at $\sqrt{s} = 208.1\,\mathrm{GeV}$ with a smuon lifetime of $10^{-9}\,\mathrm{s}$ and a smuon mass of $100\,\mathrm{GeV}/c^2$.

- *Stau pair–production in the slepton co–NLSP and the stau NLSP scenario:*
  Stau pair–production, $\mathrm{e}^+\,\mathrm{e}^- \to \tilde{\tau}_1^+\,\tilde{\tau}_1^-$, followed by the decay $\tilde{\tau}_1^\pm \to \tau^\pm\,\tilde{\mathrm{G}}$, is possible both in the stau NLSP scenario and in the slepton co–NLSP scenario. The topology is similar to the previous one, but with a higher track multiplicity and less visible energy present in the event. The selection developed for this channel, in the following referred to as the *2–tau channel*, is described in Sect. 5.5.2.

- *Neutralino pair–production in the slepton co–NLSP and the stau NLSP scenario:*
  Neutralino pair–production, $\mathrm{e}^+\,\mathrm{e}^- \to \tilde{\chi}_1^0\,\tilde{\chi}_1^0$, is possible both in the slepton co–NLSP scenario and the stau NLSP scenario. In the first case the neutralinos decay as $\tilde{\chi}_1^0 \to \tilde{\ell}_R^\pm\,\ell^\mp$, with equal branching fractions for all flavours. Thus in the slepton co–NLSP scenario there are six possible flavour combinations. In the stau NLSP scenario the neutralino decays purely to $\tilde{\tau}_1^\pm\,\tau^\mp$. In both cases the sleptons decay to lepton gravitino. Depending on the slepton lifetime, two of the four leptons in the final state might have large impact parameters. These large impact parameter leptons can be of different flavour and they can have equal or opposite charges (since the neutralino is a Majorana particle). The selection developed for this channel, in the following referred to as the *4–lepton channel*, is described in Sect. 5.5.3.

  Fig. 5.2 shows an example for such an event from Monte Carlo, where one of the neutralinos decays to $\tilde{\mathrm{e}}_R^+\mathrm{e}^-$ and the other one to $\tilde{\tau}_1^-\,\tau^+$. This event was simulated at $\sqrt{s} = 206\,\mathrm{GeV}$ with a lifetime of $5 \cdot 10^{-10}\,\mathrm{s}$, a neutralino mass of $102\,\mathrm{GeV}/c^2$ and a slepton mass of $85\,\mathrm{GeV}/c^2$. The primary tau decays to $\bar{\nu}_\tau\,\pi^+\,\pi^+\,\pi^-$, the secondary tau from the stau decay decays to $\nu_\tau\,\pi^-$. The secondary positron and the pion originating from the stau decay have impact parameters of the order of 1 cm, while the other tracks originate from the primary event vertex.

- *Selectron or smuon pair–production in the stau NLSP scenario:*
  In the stau NLSP scenario there can be selectron or smuon pair–production, $\mathrm{e}^+\,\mathrm{e}^- \to \tilde{\ell}_R^+\,\tilde{\ell}_R^-$ with $\tilde{\ell}_R^\pm = \tilde{e}_R^\pm$ or $\tilde{\mu}_R^\pm$, followed by decays $\tilde{\ell}_R^+ \to \tilde{\chi}_1^0\ell^+ \to \tilde{\tau}_1^\pm\,\tau^\mp\ell^+$. The staus then undergo their usual decay to $\tau\tilde{\mathrm{G}}$. In this channel there will thus be six leptons in the final state: two electrons or muons originating from the primary vertex, two primary taus and finally the two secondary taus respectively their decay products from the stau decays, which, depending on the lifetime, might have large impact parameters. The selection developed for this channel, in the following referred to as the *6–lepton channel*, is described in Sect. 5.5.4.

- *Chargino pair–production in the slepton co–NLSP and the stau NLSP scenario:*
  Chargino pair–production, $\mathrm{e}^+\,\mathrm{e}^- \to \tilde{\chi}_1^+\,\tilde{\chi}_1^-$, is possible both in the slepton co–NLSP scenario and the stau NLSP scenario. In the first case, the charginos decay as $\tilde{\chi}_1^+ \to \tilde{\ell}_R^+\,\nu_\ell$, with equal branching fractions for all flavours. In the stau NLSP scenario the charginos decay solely to $\tilde{\tau}_1^+\,\nu_\tau$. This channel is important in a restricted part of the GMSB parameter space only [36]. The experimental topology is similar to the direct pair–production with the difference that now an additional neutral particle carries away energy. Thus no dedicated selection was developed for this channel, and good sensitivity is reached with the 2–lepton selection for selectron and smuon pair–production in the slepton co–NLSP scenario and with the 2–tau selection for stau pair–production in the stau NLSP scenario. The results are summarised in Sect. 5.5.5.

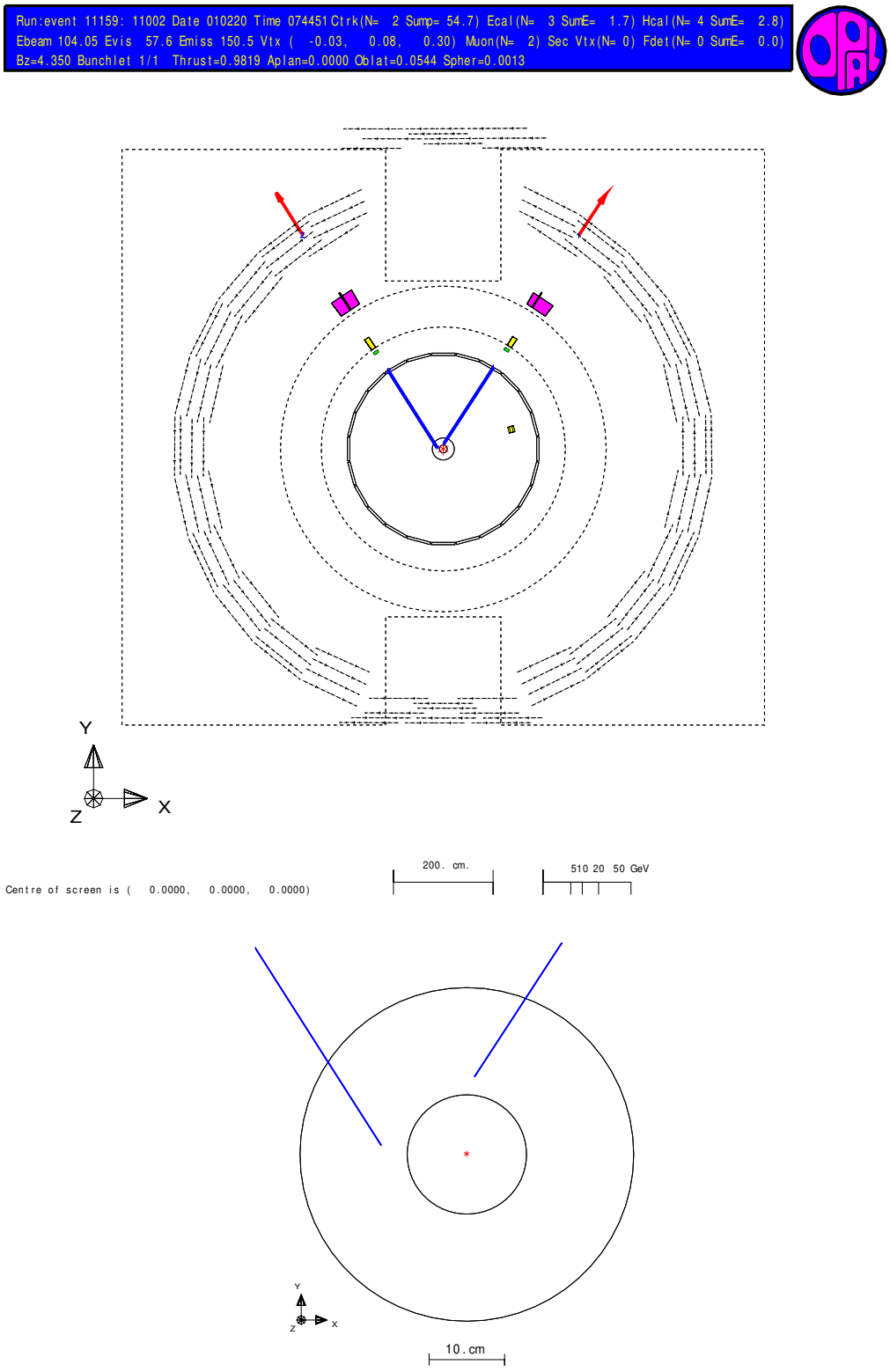


Figure 5.1: *A simulated* $e^+\,e^- \to \tilde{\mu}_R^+\,\tilde{\mu}_R^-$ *event, shown in the* $r-\phi$ *plane (top). The blue lines indicate the smuon tracks and the red arrows the signal in the muon chambers. The green, yellow and pink boxes symbolise signals in the presampler, electromagnetic calorimeter and hadronic calorimeter, respectively, with the radial length of these boxes being logarithmically proportional to the energy deposit in the respective detector component. In the bottom plot the region close to the interaction point (symbolised by a red star) is shown. Both tracks start in the vertex chamber and have impact parameters of the order of 10 cm. The event was simulated at* $\sqrt{s}$ *=208.1 GeV with a smuon lifetime of* 10^{-9} *s and a smuon mass of* $100\,GeV/c^2$.

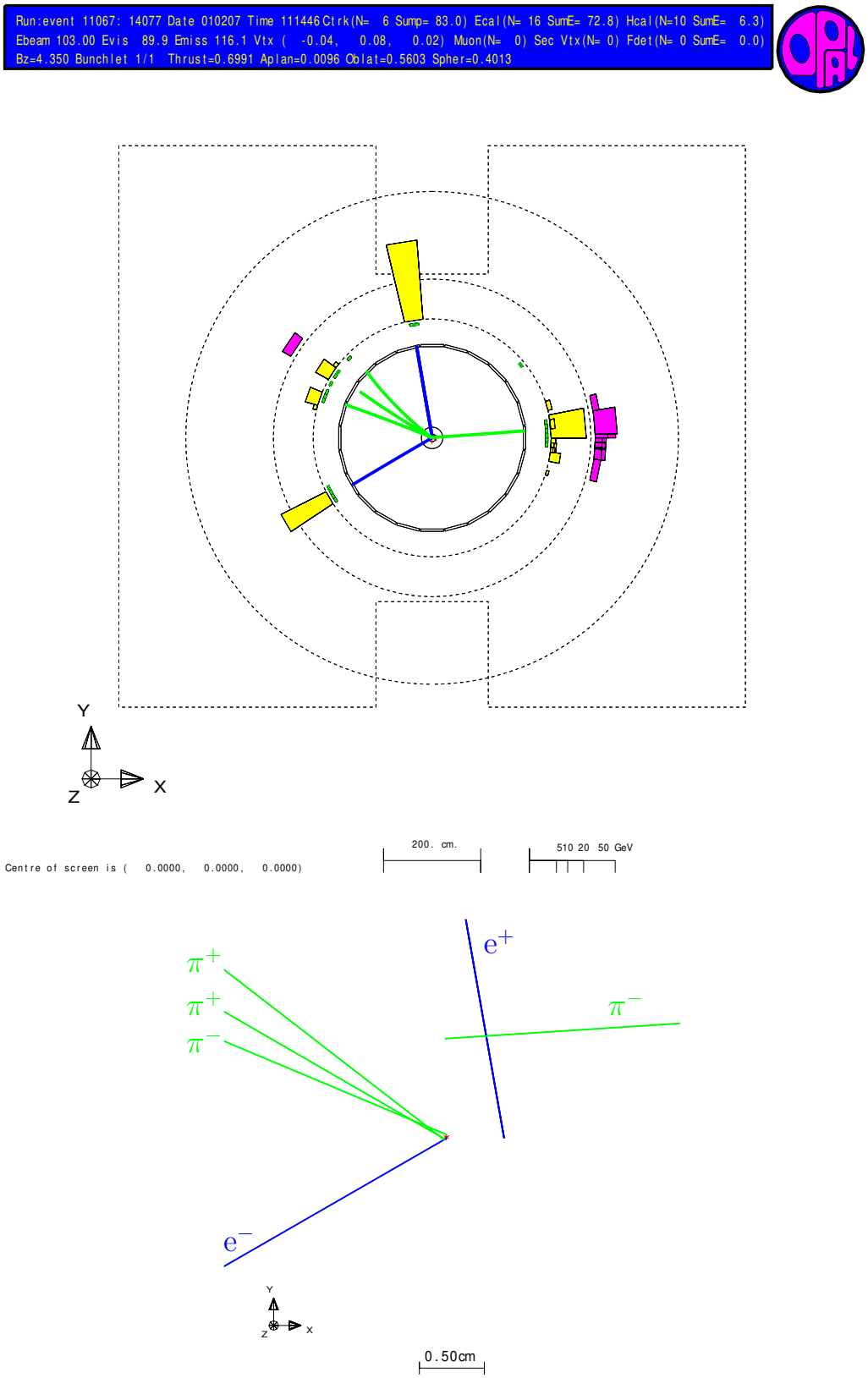


Figure 5.2: *A simulated* $e^+\,e^- \to \tilde{\chi}^0_1\,\tilde{\chi}^0_1 \to \tilde{e}^+_R\,e^-\tilde{\tau}^-_1\,\tau^+ \to e^+\tilde{G}e^-\,\tau^-\tilde{G}\tau^+$ *event, shown in the* $r-\phi$ *plane (top). The* τ^+ *decays to* $\bar{\nu}_\tau\,\pi^+\,\pi^+\,\pi^-$*, while the* τ^- *decays to* $\nu_\tau\,\pi^-$*. The tracks from the electrons and the tau decay products are coloured in blue and green, respectively. In the bottom plot the region close to the interaction point (symbolised by a red star) is shown. The positron and one of the pions have impact parameters of the order of 1 cm. The event was simulated at* $\sqrt{s}$ *=206 GeV with a slepton lifetime of* $5{\cdot}10^{-10}$ *s, a neutralino mass of* $102\,GeV/c^2$*, and a slepton mass of* $85\,GeV/c^2$*.*

Year	$\sqrt{s}$ [GeV]	$\int \mathcal{L}$ [pb^{-1}]
1998	189	166.73
1999	192	29.51
	196	75.06
	200	78.06
	202	36.71
2000	204–206	74.15
	206–207	121.66
	> 207	8.30
1998–2000	189–209	590.18

Table 5.1: *The integrated luminosities used for this analysis, split up into the individual years and centre–of–mass energies and in total.*

5.2 Data Set and Integrated Luminosities

For this analysis the data recorded in the years 1998, 1999 and 2000 were used. In the year 2000, data were taken at centre–of–mass energies between 200 GeV and 209 GeV [2]. Following a LEP wide agreement for SUSY searches, the data of the year 2000 were split into three energy bins: $204\,\text{GeV} \leq \sqrt{s} < 206\,\text{GeV}$, $206\,\text{GeV} \leq \sqrt{s} < 207\,\text{GeV}$ and $\sqrt{s} \geq 207\,\text{GeV}$, with luminosity–weighted centre–of–mass energies of 205.255 GeV, 206.500 GeV and 208.094 GeV, respectively. For this calculation the integrated luminosity was determined for (non–centered) energy bins of one GeV width. A small amount of data (8.3 pb^{-1}) with $\sqrt{s} < 204\,\text{GeV}$ from the year 2000 was not used. The integrated luminosities and the centre–of–mass energies reached in the years 1998, 1999 and 2000 are summarised in Table 5.1. Overall, the data set consists of 590.18 pb^{-1} with $189\,\text{GeV} \leq \sqrt{s} \leq 209\,\text{GeV}$.

The integrated luminosities were determined with the ROCROS program [37], which uses Bhabha events with low scattering angles, where t–channel production dominates and the cross–section can be calculated from electrodynamics. The Bhabha events were recorded with the silicon–tungsten calorimeters, or, in case these were not fully operational, with the forward detector.

5.3 Preselection

A common preselection was applied to the four channels studied.

It was required that the sub–detectors that are most crucial for the analysis (the silicon microvertex detector, the vertex chamber, the jet chamber and the time–of–flight barrel detector) as well as at least one of the sub–detectors that are used to determine the integrated luminosity (the silicon–tungsten luminosity calorimeter and the forward detector) were fully operational during data taking.

The above requirements were applied also to the luminosity events, to ensure that the luminosity is calculated for the data taking period used for the analysis.

Only events passing the standard OPAL selection for various kinds of physics events (the so–called FYZ1 selection) were considered for the analysis.

[2] In the year 2000 the maximum centre–of–mass energy was squeezed out of the accelerator by so–called mini–ramps, short (seconds to minutes) acceleration periods during which the centre–of–mass energy was increased. Events taken during these periods were not used for this analysis.

The track parameters were calculated including the full information of the silicon microvertex detector. Both impact parameters $d_0^{\text{uncorr.}}$ and $z_0^{\text{uncorr.}}$ were calculated with respect to the origin of the coordinate system and therefore have to be corrected for the actual interaction point of the electron and positron beam $(x_{\text{BX}}, y_{\text{BX}}, z_{\text{BX}})$ (obtained from the routine CXBPOS) by the following formula:

$$\begin{aligned} d_0 &= d_0^{\text{uncorr.}} + x_{\text{BX}} \sin\phi_0 - y_{\text{BX}} \cos\phi_0 \\ z_0 &= z_0^{\text{uncorr.}} - z_{\text{BX}} \,, \end{aligned}$$

where ϕ_0 is defined in Appendix A.

Furthermore, tracks without hits in the $z-$chambers are constrained to the primary vertex in the z direction by the OPAL reconstruction software [38] in order to improve the precision of the z coordinate, assuming that they originate from the primary vertex. This constraint had to be removed, as in this analysis secondary tracks are part of the signal topology. The removal of this constraint changes the track parameters z_0 and $\tan\lambda$ (for a detailed description of the track parameters see Appendix A) along with their errors as well as several other variables (e.g. p_z) which are calculated from these parameters.

Furthermore the following set of track quality cuts was applied:

- A track must have at least 20 hits in the central jet chamber. This corresponds to a maximum allowed polar angle of $|\cos\theta| = 0.963$.
- The transverse track momentum must satisfy $p_T \geq 50\,\text{MeV}/c$.
- The total track momentum must satisfy $p \leq 250\,\text{GeV}/c$.
- The χ^2/ndf of the track fits in the r–ϕ and the $s-z$ plane, where s is the path integral along the track in r–ϕ, have to be smaller than 999 (the requirement in the standard OPAL selection for good tracks).

Selected events have to contain at most ten good tracks and at least two tracks with an impact parameter $|d_0| \geq 0.035\,\text{cm}$ and $|p| > 1\,\text{GeV}/c$. Later on a tighter cut on $|d_0|$ is applied. At this stage the cut on $|d_0|$ is made to reduce the amount of data that has to be handled. In the following event selection all (not only good) tracks are used.

After this preselection, 1122863 data events are left, while 24120 events are expected from Standard Model sources. The number of events before and after the preselection separately for each year is given in Table 5.2. The cut on the impact parameter d_0 is the main reason for the disagreement between data and Monte Carlo after the preselection. This disagreement will be discussed in the next section.

5.4 Background Composition and Checks

The background for events containing tracks with large impact parameters can be divided into three classes: background sources that are well described in the Standard Model Monte Carlo programs ("well modeled" background), background that is known to be not well simulated ("poorly modeled" background) and background that is not contained in these simulations at all ("unmodeled" background). In the following these classes are described in more detail.

"Well Modeled" Background

All known Standard Model processes were considered for the evaluation of the level of remaining modeled background. The most relevant ones are listed below:

- Two–photon scattering ($e^+e^- \to e^+e^- X$) is the most important background source after the preselection. It can be reduced drastically, as will be described in the next sections. Nevertheless, due to the large cross–section of e.g. $\approx 11870\,\mathrm{pb}$ for untagged [3] hadronic events with an invariant hadronic mass $W > 5\,\mathrm{GeV}/c^2$, and negative squared four–momenta of the photons Q_1^2 and $Q_2^2 < 4.5\,\mathrm{GeV}/c$ (for $\sqrt{s} = 206.0\,\mathrm{GeV}$), each selected Monte Carlo event receives a large weight, when the integrated luminosity of the data is taken into account. Thus it contributes significantly to the remaining number of background events. For stau pair–production the leptonic two–photon events are important, while for the 4–lepton and 6–lepton channels the hadronic (untagged and single–tagged) two–photon events contribute most. All selections are described in the next section.

- Bhabha scattering events ($e^+e^- \to e^+e^-$) have a large cross–section, and give the second most important contribution to the background after the preseletion. Nevertheless, with the cuts described in the following sections, an efficient suppression of this background is achieved. Bhabha events are selected because tracks with large impact parameters can be produced in conversions of ISR photons and conversions of photons produced in the electro–magnetic shower in the material ($\gamma(Z) \to e^+e^-(Z)$).

- Quark–antiquark pairs, $e^+e^- \to q\bar{q}(g)$, with a moderate cross–section of $(79.461 \pm 0.055)\,\mathrm{pb}$ for $\sqrt{s} = 206.0\,\mathrm{GeV}$, give a significant contribution to the background in the 4–lepton and especially the 6–lepton channel. The tracks identified as secondary tracks can be electrons from conversions of ISR photons or photons from π^0 decays, particles from decays of long–lived hadrons such as the K_s^0 with a proper decay length of $c\tau \approx 3\,\mathrm{cm}$ ($\tau = 0.89 \cdot 10^{-10}\,\mathrm{s}$ [39]) and various other particles produced in the hadronic shower, including particles that are produced by interactions with the detector material.

- The background from processes that lead to final states with four fermions (e.g. $e^+e^- \to eeee$, $e^+e^- \to eeqq$, $e^+e^- \to qqqq$, $e^+e^- \to \mu\mu\nu\nu$), and are not from two–photon processes, is summarized under the term four–fermion background. These final states are produced by W and Z pair–production, single W production ($e^+e^- \to W\,e\,\nu$) and single Z production in compton scattering of quasi–real photons ($e^+e^- \to e^+e^-\,Z/\gamma^*$). The cross–sections are, in general, relatively small ($< 50\,\mathrm{pb}$). Therefore, although high–multiplicity events with missing energy like $W\,W \to \tau\nu\,\tau\nu$ or $W\,W \to \tau\nu\,q\bar{q}$ are selected by the 4–lepton and 6–lepton selections, they give a minor contribution to the total number of expected background events, taking into account the integrated luminosity of the data .

- Tau–pairs with hadronic decays are a considerable background source for the 4–lepton and especially the 6–lepton channel due to their relatively high track–multiplicity, although the small cross–section of $(6.881 \pm 0.008)\,\mathrm{pb}$ for $\sqrt{s} = 206.0\,\mathrm{GeV}$ gives a low weight to this process when the integrated luminosity of the data is taken into account.

"Poorly Modeled" Background

- Events with tracks that are not reconstructed properly are not very well simulated in the Monte Carlo. Examples for such misreconstructions are: tracks where the matching of the jet chamber hits with the corresponding hits in the silicon microvertex detector or the vertex chamber fails, unresolved double tracks (e.g. from photon conversions) and tracks that are reconstructed on the wrong side of the anode wire plane in the jet chamber. Especially the last effect often fakes tracks with large impact parameters.

[3] In *untagged* two–photon events both photons are quasi–real, and both beam electrons escape through the beam pipe. In *single–tagged* two–photon events only one of the scattered photons is quasi–real, and one of the scattered beam electrons is observed in the detector.

- Primary particles can interact hadronically with the detector material or the particles of the detector gas before reaching the tracking chamber, producing secondary particles in these collisions. Such hadronic interactions are not properly simulated in the Monte Carlo, as has been shown in [40] for the jet chamber.

Unmodeled Background

- Hadronic two–photon background with an invariant hadronic mass below $5\,\mathrm{GeV}/c^2$ for untagged and $1.73\,\mathrm{GeV}/c^2$ for single–tagged events is not simulated at all in the Monte Carlo, due to the rapid increase of the cross–section in these kinematic regions. In general it can be said that details of the two–photon background are not simulated very accurately and that the hadronic two–photon cross–section is uncertain within 10–20% [41].

- Muons created by interactions of cosmic particles in the atmosphere are passing through the earth and therefore also the OPAL detector. These cosmic muon events are one of the main sources of background after the preselection, as the muons are in general quite energetic and the tracks do not originate from the primary event vertex but have large impact parameters. Cosmic muons can also be present in standard physics events when they pass through the detector in random coincidence with the beam–crossing.

- Off–momentum beam electrons or positrons are mainly produced by scattering of beam particles with remaining gas molecules in the beam pipe. They are deflected out of the beamline by the focussing magnets and eventually produce secondary particles by interaction with other gas molecules in the beam pipe or with the beam pipe itself. All these particles can end up in the detector, but they do not originate from the primary interaction point and therefore often have large impact parameters. Such beam gas and beam wall events are very relevant as a source of background, after the preselection.

In Fig. 5.3 the specific energy loss of 200000 tracks from events with $\sqrt{s} = 204 - 208\,\mathrm{GeV}$, together with the expectation from the Bethe–Bloch formula [39], is shown. In this plot tracks from events with at least two tracks with $|d_0| \geq 0.05\,\mathrm{cm}$ and $\delta d_0/|d_0| < 0.1$ (these cuts are later used in the selections) are included. The events must pass the preselection cuts; however, the preselection cut on the momentum of the large impact parameter tracks was removed to include also the low momentum tracks where the various particle species can be distinguished most easily. In this plot different event classes are visible. Cosmic muons and electrons from beam–gas or beam–wall events show up in the large–momentum region ($p > 2\,\mathrm{GeV}/c$). The proton band is strongly populated mainly due to hadronic interactions with the material, where, to a lesser extent, also deuterons are produced. In the very low momentum region there are mainly pions and electrons from two–photon collisions.

In Fig. 5.4 the invariant mass of all pairs of unlike–charged secondary tracks ($|d_0| > 0.05\,\mathrm{cm}$), assuming them to be pions, is shown. For this figure only events with less than five secondary tracks were considered, and the tracks were required to have $|d_0| < 5\,\mathrm{cm}$ and $|z_0| < 10\,\mathrm{cm}$. No cut on the number of primary tracks was applied. The peak from $\mathrm{K}^0_\mathrm{s} \to \pi^+\pi^-$ is clearly visible in data and Monte Carlo and shows good agreement, proving that the disagreement in the number of events in data and Monte Carlo, after the preselection, is due to the selection cuts and not to a general normalisation problem. For this plot a correction of the kaon mass peak in the PHOJET Monte Carlo for the underestimation of the inclusive K^0_s production cross–section in the PHOJET Monte Carlo generator by a factor of approximately 0.65 [42] was applied. For this correction in the PHOJET Monte Carlo samples, the background [4] was subtracted in the range between $440\,\mathrm{MeV}/c^2$ and $536\,\mathrm{MeV}/c^2$ and

[4] It was found that the background to the K^0_s peak in the PHOJET Monte Carlo can be approximated by a constant. The K^0_s peak can be described by a Gaussian.

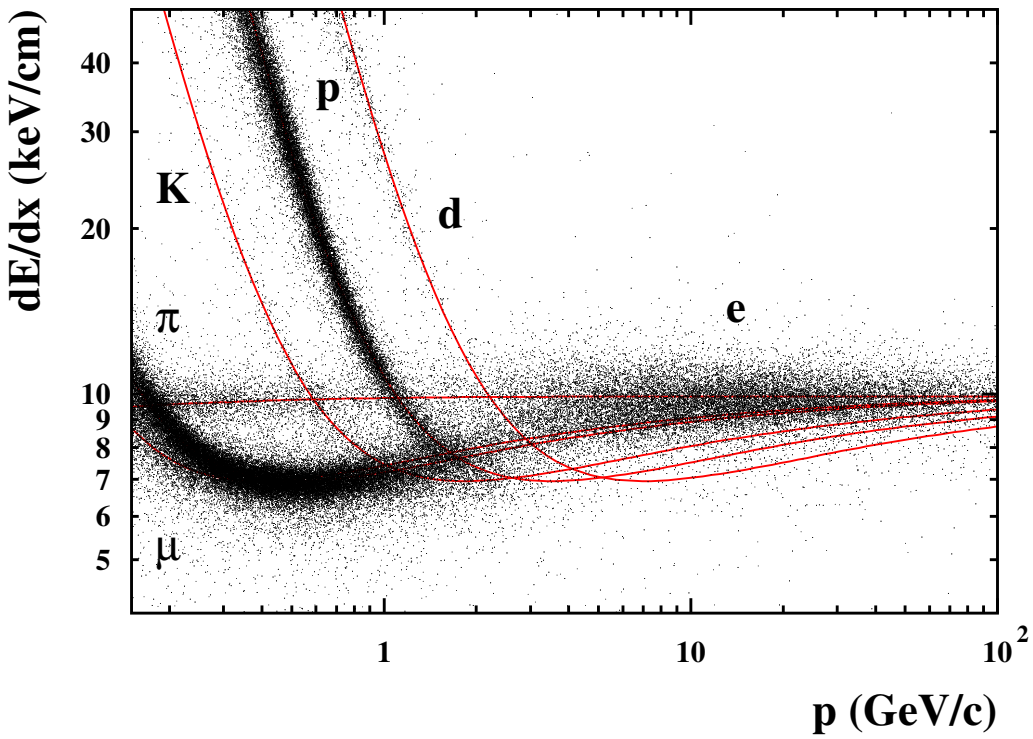


Figure 5.3: *The specific energy loss (dE/dx) for tracks with $|d_0| \geq 0.05$ cm and $\delta d_0/|d_0| < 0.1$ after the preselection. Shown is the dE/dx of 200000 tracks (points) from events with $\sqrt{s} = 204 - 208$ GeV together with the expectations from the Bethe–Bloch formula (solid lines). Different event classes are distinguishable. For further details see Sect. 5.4. To include also the low–momentum region where the different particle species can be distinguished most easily, the preselection cut on the momentum was removed. No cut on the number of primary tracks was applied. Both positive and negative tracks are included.*

the remaining signal was multiplied by a factor of 1.5. A fit to the data points with a Gaussian and a third order Chebyshev polynomial results in a kaon mass of $(497.9 \pm 2.8)\,\mathrm{MeV}/c^2$ with a χ^2/ndf of 3.4, in agreement with the PDG value of $(497.672 \pm 0.031)\,\mathrm{MeV}/c^2$.

5.5 The Event Selections

In this section, the four event selections are described in detail. For each of them the cuts are explained and the results and the efficiency are discussed.

5.5.1 Selectron and Smuon Pair–Production in the Slepton co–NLSP Scenario: 2–Lepton Selection

The topology for selectron or smuon pair–production, $\mathrm{e^+\,e^-} \to \tilde{\mathrm{e}}_R^+\,\tilde{\mathrm{e}}_R^-$ and $\mathrm{e^+\,e^-} \to \tilde{\mu}_R^+\,\tilde{\mu}_R^-$, followed by decays $\tilde{\mathrm{e}}_R^\pm \to \mathrm{e}^\pm\,\tilde{\mathrm{G}}$ and $\tilde{\mu}_R^\pm \to \mu^\pm\,\tilde{\mathrm{G}}$, respectively, is two tracks with large impact parameters ("secondary tracks") and no tracks from the collision point ("primary tracks"). The selection described in this section, in the following referred to as the *2–lepton selection*, yields similar efficiencies for selectron and smuon pair–production. Staus, however, were treated separately (see Sect. 5.5.2) to account for their higher decay multiplicity and their lower track momenta.

Secondary tracks are required to have

- a significant amount of momentum transverse to the z axis: $p_T > 1.5\,\mathrm{GeV}/c$,
- a large impact parameter: $|d_0| \geq 0.05\,\mathrm{cm}$,

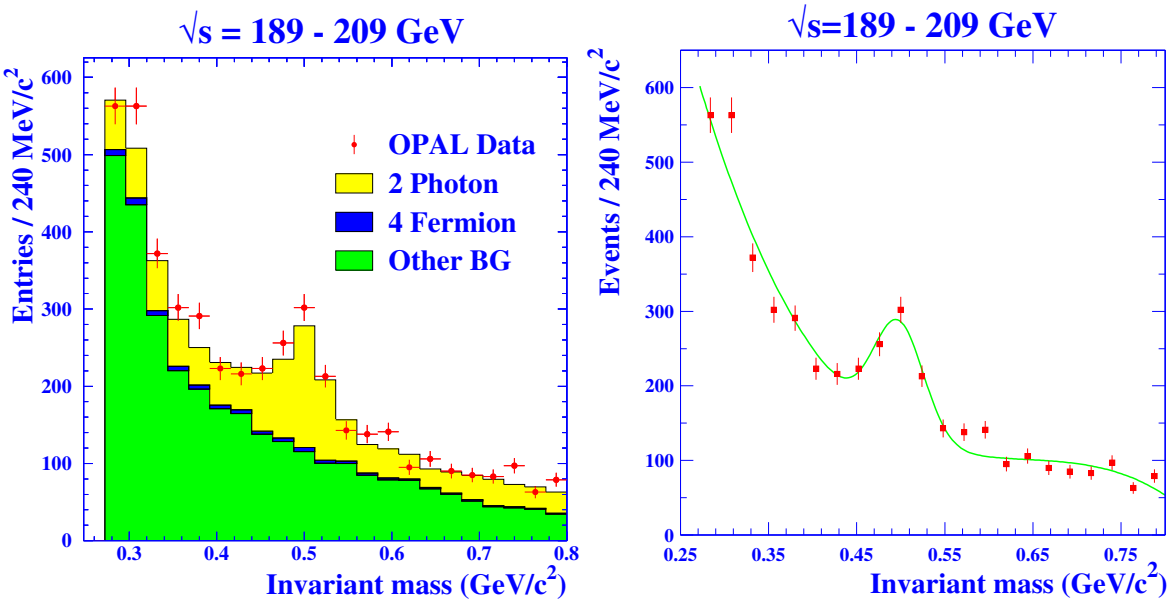


Figure 5.4: *The invariant mass of all pairs of unlike–charged secondary tracks ($|d_0| > 0.05$ cm) in events with less than five secondary tracks. For this figure only secondary tracks with $|d_0| < 5$ cm and $|z_0| < 10$ cm are considered. In the plot on the left hand–side the data with $\sqrt{s} = 189 - 209$ GeV are shown as filled circles with error bars, the expected two–photon background is shown in yellow, the expected four–fermion background in blue and all other Standard Model background in green. The green curve on the right hand–side shows the fit to the data points, resulting in a kaon mass of (497.9 ± 2.8) MeV/c^2. The χ^2/ndf of the fit is 3.4.*

- a high impact parameter precision: $\delta d_0/|d_0| < 0.1$.

Tracks with $|d_0| < 0.05$ cm are regarded as *primary tracks*, while all tracks which do not fall in one of these two categories form are third class of not very well measured secondary tracks and are, in the following, referred to as *additional tracks*. The classification of tracks into these three categories is common for all four channels. For all channels it is then required that at least two secondary tracks are found. After this part of the selection, in the following referred to as the *topological selection*, the Standard Model background is reduced drastically by a factor of about 24, with only 987 events being left, as visible from Table 5.2. On the other hand the total background is reduced by only about 17 % to 930100 events, implying that most of the unmodeled events actually contain tracks with large impact parameters. Therefore at this stage the disagreement between data and Monte Carlo is further increased.

Furthermore it is required that exactly two secondary tracks, no primary tracks and not more than three additional tracks are found.

The remaining sample of events was then subjected to the following set of cuts (see Table 5.2 for the remaining number of events after each cut):

(1) To reduce combinatorial background, charge conservation has to be fulfilled, i.e. the two secondary tracks must have different charges.

(2) To reject cosmic events the barrel time–of–flight detector (ToF) is used: if a track is contained within the geometrical acceptance region of the ToF ($|\cos\theta| < 0.82$), a ToF hit associated to this track is required. Since the efficiency of this detector is almost 100 %, tracks which have no corresponding hit are either stopped in the material on their way to the ToF or – in case of cosmic events – are outside the time window in which the readout of the detector is active. If the time–of–flight has actually been measured,

	Year 1998		Year 1999		Year 2000		Years 1998–2000	
After	Data	MC Bkg.	Data	MC Bkg.	Data	MC Bkg.	Data	MC Bkg.
-	12461200	1799240	16285760	2391640	16441800	2294610	45188760	6485490
Preselection	331327	7267.7	331405	8694.9	460131	8157.5	1122863	24120.1
Topological selection	278801	277.2	273197	365.4	378102	344.5	930100	987.1
2 secondary tracks	97007	265.2	94102	349.6	131374	330.7	322483	945.5
No primary tracks	95362	59.6	92347	80.0	129335	69.1	317044	208.7
# add. tracks < 4	92873	33.5	89657	41.2	124861	41.3	307391	116.0
Cut (1)	58711	23.4	57365	25.9	79454	26.6	195530	75.9
Cut (2)	1019	20.5	840	21.6	1224	21.9	3083	64.0
Cut (3)	1010	20.5	834	21.6	1214	21.9	3058	64.0
Cut (4)	331	17.2	256	18.2	387	19.7	974	55.1
Cut (5)	95	16.7	109	17.8	133	19.3	337	53.8
Cut (6)	4	6.1	6	6.5	6	6.9	16	19.5
Cut (7)	1	0.07	0	0.12	1	0.03	2	0.22
Cut (8)	0	0.05	0	0.02	0	0.02	0	0.09

Table 5.2: *The remaining number of events after each cut (see Section 5.5.1) for simulated background and data for the years 1998, 1999 and 2000 and in total in the 2–lepton channel.*

it is required to be consistent with the time that a relativistic particle needs to travel from the interaction point to the time–of–flight detector to veto against events which did not occur at the collision time: $5\,\mathrm{ns} < t < 20\,\mathrm{ns}$. These cuts reduce the number of data events drastically from 195530 events to 3083 events, while the number of simulated background events is almost unaffected, illustrating that indeed most of the events selected in data are unmodeled background.

(3) To reject cosmic events which pass the detector outside the geometrical acceptance region of the ToF, the following cut is applied: if an event contains more than 50 hits in the muon chambers, the selected tracks must have at least 30 hits in the central tracking chamber. This requirement makes use of the fact that for cosmic events, which are not in time with the beam crossing, tracks are often reconstructed as many individual small track segments.

(4) Interactions of beam electrons with particles of the beam gas or with the wall of the beam pipe can happen at z coordinates far away from the primary vertex. Therefore beam gas and beam wall events usually contain tracks coming from an interaction point that is shifted by a large amount in z w.r.t. the main vertex. Thus, to reduce this background, the z coordinate of the point of closest approach, z_0, of the two tracks must not be in the same z hemisphere, if both tracks have a $|z_0|$ of at least 6 cm [5].

(5) The remaining unmodeled background can be drastically reduced by requiring $|z_0| < 40\,\mathrm{cm}$ for the secondary tracks. After this cut there are 337 events left in the data, with about 54 events expected from the SM Monte Carlo. As visible from Table 5.2, with cuts (2) – (5) a reduction of the data by a factor of 580 was achieved, while these cuts, designed to reduce unmodeled background, have indeed only a minor impact on the expected SM background, which changes from 76 events to 54 events.

(6) The acoplanarity angle $\alpha = 180^\circ - \varphi$, where φ is the angle between the two tracks in the r–ϕ plane, must satisfy: $5^\circ < \alpha < 175^\circ$. This cut helps to reject further background containing back–to–back tracks, especially Bhabha events and muon pairs. Also neutrino pair events with a converted ISR photon are removed by this cut, as the tracks from the conversion electron and positron are close to each other due to their boost in the forward direction. In addition, the remaining unmodeled background is further reduced, as beam gas interactions tend to have high acoplanarity angles while cosmic events with one track misreconstructed as two tracks usually have small acoplanarity angles. After this cut there is good agreement between the number of data and background events (16 versus 19.5).

(7) To further reduce the remaining background, mainly from two–photon collisions, each secondary track is required to have a total momentum $p > 10\,\mathrm{GeV}/c$. The distribution of the total momentum after cut (6) for the whole data set and the simulated background is shown in Figure 5.5 (a), where it can be seen that the qualitative agreement between the data and the MC background is reasonable. The two–photon background dominates and the distribution peaks in the very low momentum region. This has to be compared with the signal expectation shown in Fig. 5.5 (b), where the momentum distributions for, as examples, selectrons with masses of $50\,\mathrm{GeV}/c^2$ and $100\,\mathrm{GeV}/c^2$ are shown. Especially for the most interesting high mass events only a small fraction of events are reconstructed in the momentum region below $10\,\mathrm{GeV}/c$. After this cut the remaining background is reduced to much less than one expected event.

(8) As already mentioned, two–photon events with an invariant hadronic mass W smaller than $5\,\mathrm{GeV}/c^2$ are not included in the PHOJET Monte Carlo simulation. To reject

[5] This last requirement takes care of the coarse z resolution of the OPAL jet chamber: 4.5 cm for muon pair events and 6 cm for multi–hadronic events.

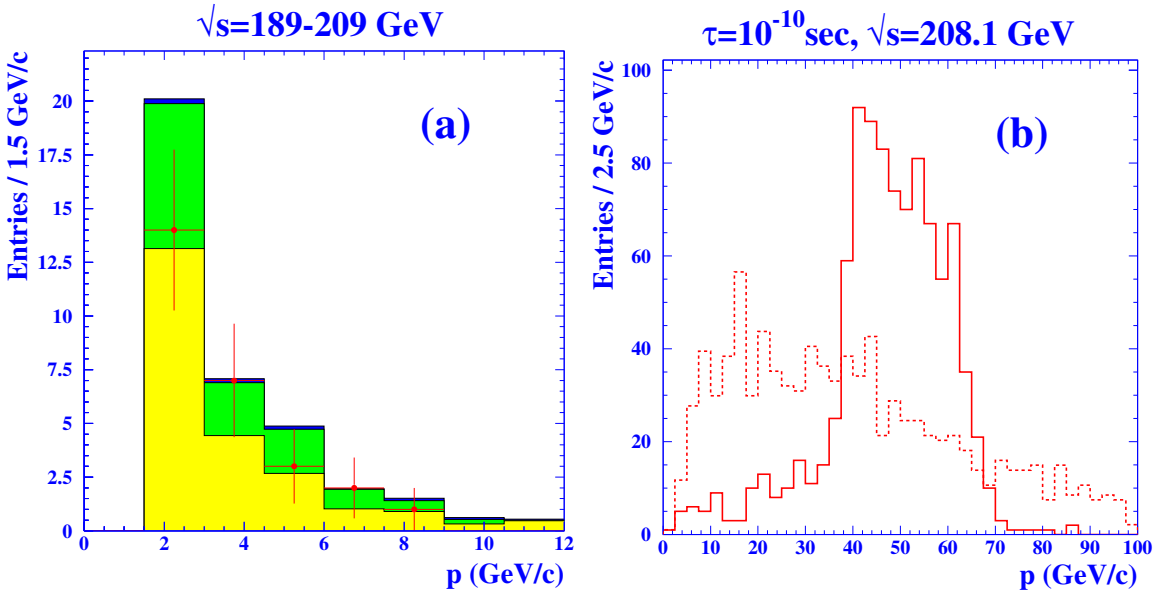


Figure 5.5: *The distribution of the total momentum p of each secondary track in the 2–lepton channel (see Section 5.5.1), plotted directly before the cut on p is applied. In (a) the data taken in the years 1998–2000 at $\sqrt{s} = 189 - 209$ GeV are shown as filled circles with error bars, the expected two–photon background is shown in yellow, the expected four–fermion background in blue and all other Standard Model background in green. There are two entries per event. In (b) the total momentum is shown for pair–production of selectrons with masses of 50 GeV/c^2 (dashed line) and 100 GeV/c^2 (solid line). The selectrons were simulated with a lifetime of 10^{-10} s at $\sqrt{s} = 208.1$ GeV. The normalisation in (b) is arbitrary.*

this unmodeled background the invariant mass W of the two selected tracks must satisfy $W > 5\,\mathrm{GeV}/c^2$. Throughout this work for the calculation of the variable W the tracks are treated as pions. The distribution of W for the data and the simulated Standard Model background after cut (7), for the whole data set, is shown in Figure 5.6 (a). In Fig. 5.6 (b) the W distribution is shown for selectrons with the parameters as described above. For the signal the distributions peak around $70\,\mathrm{GeV}/c^2$.

In the whole data set no event is finally selected, in perfect agreement with the 0.09 events that are expected from the Standard Model Monte Carlo. Table 5.4 gives a summary of the number of selected and expected events in each channel for different centre–of–mass energies and in total after all cuts. In the 2–lepton channel, shown in the second column, at four centre–of–mass energies no event remains in the background. Conservatively for the limit calculation (see Sect. 9.1.2) in these cases the number of expected background events was set to 0.01.

As examples the efficiencies after each cut for selectrons and smuons with masses of $100\,\mathrm{GeV}/c^2$ and lifetimes of 10^{-9} s are shown in Tab 5.3. After all cuts, efficiencies [6] of about $30-65\,\%$ for selectrons and about $60-70\,\%$ for smuons, depending on the mass, are reached. The reason for the smaller efficiency for selectrons is that, for small selectron masses, the t–channel distribution dominates. This leads to a strong production in the forward direction and therefore, since a large fraction of particles are lost in the beam pipe, to a smaller

[6] Here and in the following, efficiencies are quoted for the lifetime where the efficiency has its maximum ($\tau = 10^{-10} - 10^{-9}$ s, depending on the mass of the particle). Of course the efficiency drops rapidly for lifetimes for which no tracks with large impact parameters are produced, since in this case the analysis has no sensitivity.

efficiency. This, however, is not a problem, because for small masses the expected cross–section is large. In combination with the extremely low level of remaining background these high efficiencies assure an excellent sensitivity for smuon and selectron pair–production.

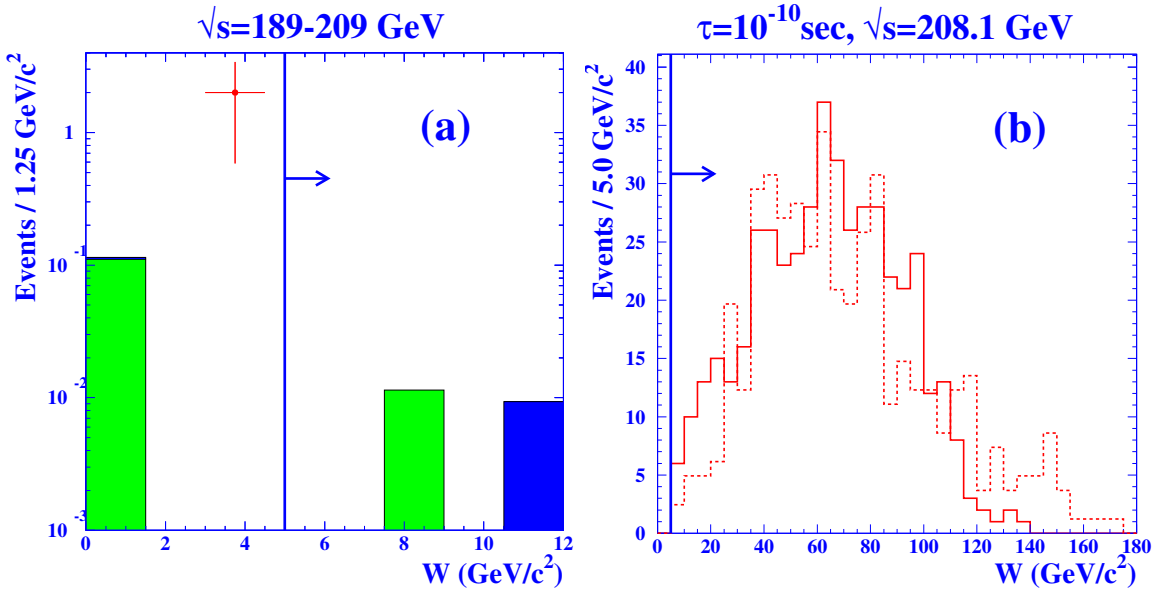


Figure 5.6: *The distribution of the invariant mass W in the 2–lepton channel (see Sect. 5.5.1), plotted directly before the cut on W is applied. In (a) the data taken in the years 1998–2000 at* $\sqrt{s} = 189 - 209$ *GeV are shown as filled circles with error bars, the expected two–photon background is shown in yellow, the expected four–fermion background in blue and all other Standard Model background in green. The arrow indicates the accepted region. In (b) the invariant mass is shown for pair–production of selectrons with masses of 50* GeV/c^2 *(dashed line) and 100* GeV/c^2 *(solid line). The selectrons were simulated with a lifetime of* 10^{-10} *s at* $\sqrt{s} = 208.1$ *GeV. The normalisation in (b) is arbitrary.*

After	Efficiency [%] $e^+e^- \to \tilde{e}_R\tilde{e}_R$	Efficiency [%] $e^+e^- \to \tilde{\mu}_R\tilde{\mu}_R$
-	100.0	100.0
Preselection	86.6	89.0
Topological selection	84.0	86.7
2 secondary tracks	82.5	86.7
No primary tracks	82.1	86.2
# add. tracks < 4	81.1	86.0
Cut (1)	80.1	85.6
Cut (2)	75.0	78.1
Cut (3)	75.0	78.1
Cut (4)	73.2	76.1
Cut (5)	71.7	75.4
Cut (6)	68.1	71.0
Cut (7)	66.1	71.0
Cut (8)	66.1	71.0

Table 5.3: *The efficiencies for selectron and smuon pair–production, simulated at* $\sqrt{s} = 208.1$ *GeV with a slepton mass of 100* GeV/c^2 *and a slepton lifetime of* 10^{-9} *s, after each cut.*

	2–Lepton channel		2–Tau channel		4–Lepton channel		6–Lepton channel	
$\sqrt{s}$ [GeV]	Data	MC Bkg.	Data	MC Bkg.	Data	MC Bkg.	Data	MC Bkg.
189	0	0.05	2	0.93	1	1.20	4	3.68
192	0	< 0.01	0	0.11	1	0.23	1	0.64
196	0	< 0.01	1	0.25	0	0.57	1	1.00
200	0	0.02	0	0.49	0	1.25	2	1.91
202	0	< 0.01	0	0.18	1	0.23	2	0.62
204–206	0	< 0.01	0	0.56	0	0.91	1	2.23
206–207	0	0.01	1	1.13	1	1.24	2	3.42
> 207	0	0.01	0	0.14	0	0.08	0	0.22
189–209	0	< 0.13	4	3.79	4	5.71	13	13.72

Table 5.4: *The remaining number of data events and events expected from Standard Model background after all cuts at the different centre–of–mass energies.*

5.5.2 Stau Pair–Production: 2–Tau Selection

For stau pair–production, $e^+ e^- \to \tilde{\tau}_1^+ \tilde{\tau}_1^-$, followed by decays $\tilde{\tau}_1^\pm \to \tau^\pm \tilde{G}$, the topology is two or more secondary tracks, depending on the tau decays, and no tracks from the primary event vertex. The topology is thus similar to the one for selectron and smuon pair–production, but with a higher track multiplicity and less visible energy present in the events. This selection is in the following referred to as the *2–tau selection*.

The topological selection is identical to Sect. 5.5.1. For the further event selection the aim was to keep the cuts of the 2–lepton selection wherever possible. In the case when exactly two secondary tracks are reconstructed, the cuts from Sect. 5.5.1 are used, with slight modifications to take into account that in the case of staus the visible energy is reduced due to the neutrinos. However, when at least one of the taus decays hadronically with more than one charged tracks in the final state (the branching ratio for "three prong" decays is 15.18 %), more than two secondary tracks will in general be present. In this case the secondary tracks are clustered to objects, which can be considered as "tau candidates". These tau candidates are then treated like single particles and cuts analogous to the cuts of Section 5.5.1 are applied.

For the reconstruction of the tau candidates the following method is used: two secondary tracks i and j are clustered together, if either

- $\left| |d_0^i| - |d_0^j| \right| < 0.1\,\text{cm}$

or

- $(\left| |d_0^i| - |d_0^j| \right|)/d_0^{ij} < 15\,\%$, with $d_0^{ij} = (|d_0^i| + |d_0^j|)/2\,.$

For lifetimes of $10^{-10} - 10^{-9}$ s in about 53 % of all events the tracks of both taus are correctly identified and assigned to tau candidates. Events in which all tracks are assigned to the same tau candidate are rejected. If more than two tau candidates are formed the scalar momenta of the n tracks assigned to a tau candidate are summed up and the two tau candidates with the highest total momenta p^{tau_1} and p^{tau_2}, with $p^{\text{tau}_\text{i}} = \sum_{k=1}^{n_i} |\vec{p}^{\,k}|$ are used in the event selection below. For each tau candidate the following variables are calculated from the n tracks that are associated with it:

- the momentum $\vec{p}^{\,\text{tau}} = (p_x^{\text{tau}}, p_y^{\text{tau}}, p_z^{\text{tau}})$, with $p_x^{\text{tau}} = \sum_{k=1}^{n} p_x^k\,,\ p_y^{\text{tau}} = \sum_{k=1}^{n} p_y^k\,,\ p_z^{\text{tau}} = \sum_{k=1}^{n} p_z^k\,,$

- the transverse momentum $p_T^{\mathrm{tau}} = \sqrt{(p_x^{\mathrm{tau}})^2 + (p_y^{\mathrm{tau}})^2}$,
- the average longitudinal impact parameter $z_0^{\mathrm{tau}} = \frac{1}{n}\sum_{k=1}^{n} z_0^k$,
- the average time–of–flight relative to the beam crossing $t^{\mathrm{tau}} = \frac{1}{n'}\sum_{k=1}^{n'} t^k$ from the n' tracks which have a ToF hit associated to them.

The (pseudo) tau momenta are then used to calculate the acoplanarity angle $\alpha^{\mathrm{tau}} = 180^\circ - \varphi^{\mathrm{tau}}$, φ^{tau} being the angle between the momenta of the tau candidates in the transverse plane, as well as the invariant mass W^{tau} of the two tau candidates.

As in Section 5.5.1, events with more than three additional tracks are rejected. The number of data and simulated background events after each cut for the different years can be found in Table 5.5. At this point there is again a large discrepancy between the number of data events and the events expected from Standard Model sources: 551019 versus 118 events. This discrepancy is reduced with the following set of cuts:

(1) The tau candidates are required to satisfy $p_T^{\mathrm{tau}} \geq 1.5\,\mathrm{GeV}/c$.

(2) If the number of secondary tracks is exactly two, these must have different charges.

(3) The momentum p^{tau} of each tau candidate must not be larger than the beam energy to reduce combinatorial background.

(4) If exactly two secondary tracks are found: tracks contained within the geometrical acceptance region of the ToF ($|\cos\theta| < 0.82$) must have a ToF hit associated with them, and the time–of–flight must satisfy: $5\,\mathrm{ns} < t < 20\,\mathrm{ns}$ (cut (2) of Sect. 5.5.1, see there for details and motivation). If more than two secondary tracks are found, all of them must be associated to hits in the ToF and for each tau candidate the variable t^{tau} is required to fulfill $5\,\mathrm{ns} < t^{\mathrm{tau}} < 20\,\mathrm{ns}$.

(5) If an event contains more than 50 hits in the muon chambers, all selected secondary tracks must have at least 30 hits in the central tracking chamber.

(6) If exactly two secondary tracks are found: The z_0 of the two tracks must not be in the same z hemisphere, if both tracks have a $|z_0|$ of at least 6 cm (cut (4) of Sect. 5.5.1). If more than two secondary tracks are found, for each tau candidate the same requirement must be fulfilled for the average z_0^{tau}.

(7) For all secondary tracks the longitudinal impact parameter $|z_0|$ must be at most 40 cm.

(8) If exactly two secondary tracks are found: the acoplanarity angle must satisfy: $5^\circ < \alpha < 175^\circ$ (cut (6) of Sect. 5.5.1). If more than two secondary tracks are found the acoplanarity α^{tau} must fulfill $10^\circ \leq \alpha^{\mathrm{tau}} \leq 175^\circ$. As can be seen from Table 5.5, after this cut there is good agreement between the number of data events (22) and the number of expected Standard Model events (19.8).

(9) At least one of the secondary tracks or the tau candidates must have a momentum $p \geq 5\,\mathrm{GeV}/c$ or $p^{\mathrm{tau}} \geq 5\,\mathrm{GeV}/c$, respectively. In Fig. 5.7 (b) this variable is shown for stau pair–production signal events simulated with a lifetime of $10^{-10}\,\mathrm{s}$ and stau masses of $50\,\mathrm{GeV}/c^2$ and $100\,\mathrm{GeV}/c^2$. Compared with the distributions for smuon pair–production shown in Fig. 5.5 (b), the peaks of the distributions are shifted to much smaller values for both slepton masses, illustrating the effect of the neutrinos carrying away additional energy. The same distribution for the data and the simulated Standard Model background after cut (8) is shown in Fig. 5.7 (a). Again the largest fraction of remaining background is two–photon background. Data and background agree well.

	Year 1998		Year 1999		Year 2000		Years 1998–2000	
After	Data	MC Bkg.	Data	MC Bkg.	Data	MC Bkg.	Data	MC Bkg.
-	12461200	1799240	16285760	2391640	16441800	2294610	45188760	6485490
Preselection	331327	7267.7	331405	8694.9	460131	8157.5	1122863	24120.1
Topological selection	278801	277.2	273197	365.4	378102	344.5	930100	987.1
0 primary tracks	276835	60.9	271088	81.2	375663	69.7	923586	211.8
# vertices > 1	169133	60.9	166178	81.1	228071	69.6	563382	211.6
# add. tracks < 4	165851	34.3	162705	41.8	222463	41.7	551019	117.8
Cut (1)	152667	34.3	149610	41.8	204539	41.7	506816	117.8
Cut (2)	118505	24.2	117318	26.5	159132	27.0	394955	77.7
Cut (3)	99219	24.2	99278	26.5	136695	27.0	335192	77.7
Cut (4)	1718	21.1	1526	21.9	2064	22.2	5308	65.2
Cut (5)	1709	21.1	1519	21.9	2054	22.2	5282	65.2
Cut (6)	514	17.7	434	18.6	620	20.0	1568	56.3
Cut (7)	204	17.1	228	18.0	267	19.7	699	54.8
Cut (8)	5	6.2	9	6.5	8	7.1	22	19.8
Cut (9)	2	2.1	5	2.8	4	2.4	11	7.3
Cut (10)	2	0.9	1	1.0	1	1.9	4	3.8

Table 5.5: *The remaining number of events after each cut (see Section 5.5.2) for simulated background and data for the years 1998, 1999 and 2000 and in total in the 2–tau channel.*

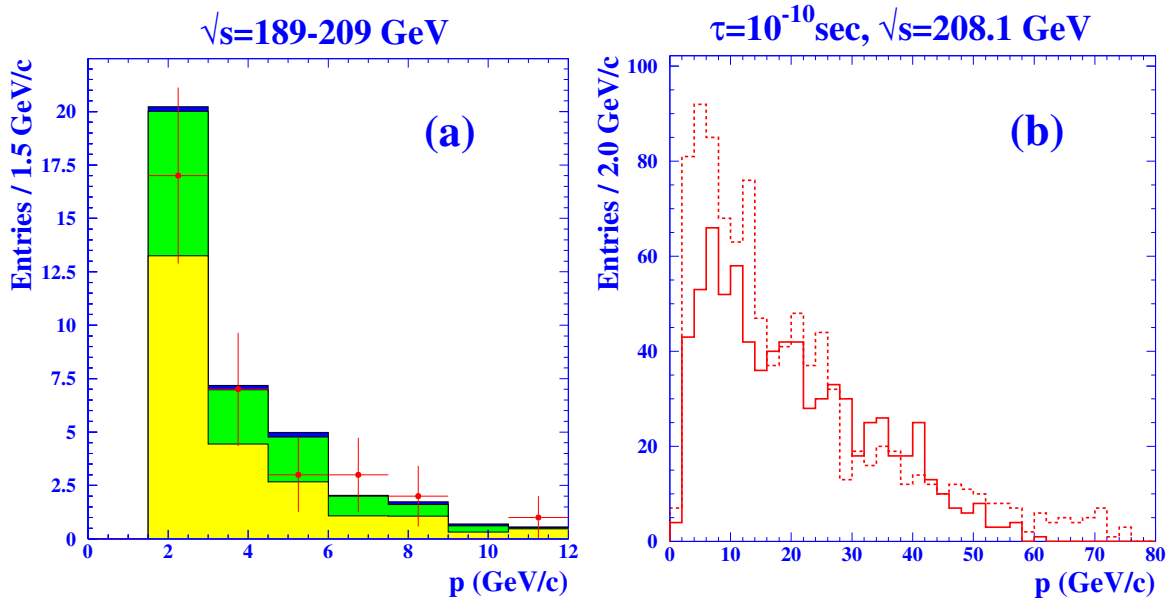


Figure 5.7: *The distribution of the total momentum p of each secondary track in the 2–tau channel (see Section 5.5.2), plotted directly before the cut on p is applied. In (a) the data taken in the years 1998–2000 at $\sqrt{s} = 189 - 209$ GeV are shown as filled circles with error bars, the expected two–photon background is shown in yellow, the expected four–fermion background in blue and all other Standard Model background in green. There are two entries per event. In (b) the total momentum is shown for pair–production of staus with masses of 50 GeV/c^2 (dashed line) and 100 GeV/c^2 (solid line). The staus were simulated with a lifetime of 10^{-10} s at $\sqrt{s} = 208.1$ GeV. The normalisation in (b) is arbitrary.*

(10) The invariant mass of the two secondary tracks respectively the two tau candidates is required to be at least 3 GeV/c^2. The invariant mass for signals with the parameters described above are shown in Fig. 5.8 (b), exhibiting again the effect of smaller visible energy compared to Fig. 5.6 (b). The distributions for the data and the simulated Standard Model background after cut (9) are shown in Fig. 5.8 (a).

After all cuts there are four events left in the data, with 3.8 events expected from simulated Standard Model sources. The results for the different centre–of–mass energies are summarised in the third column of Table 5.4 (page 41).

The efficiency after each cut for stau pair–production events simulated with a lifetime of 10^{-9} s and a mass of 100 GeV/c^2 is shown in Table 5.6. It can be seen that the loss of efficiency, compared to the 2–lepton selection, is happening before cut (1), due to the multiplicity cuts. After all cuts the efficiency is still around 45–52 %, depending on the stau mass.

5.5.3 Neutralino Pair–Production: 4–Lepton Selection

In this section a selection for a production of neutralino pairs, $e^+ e^- \to \tilde{\chi}_1^0 \tilde{\chi}_1^0$, followed by decays $\tilde{\chi}_1^0 \to \tilde{\ell}_R^\pm \ell^\mp$, is presented. In this channel there are four leptons in the final state, of which two, depending on the slepton lifetime, might have large impact parameters. Thus the topology is at least two tracks with large impact parameters and at least two tracks from the primary interaction point. The multiplicity depends on the flavour composition. Two cases were studied: in the slepton co–NLSP scenario the neutralino decays to sleptons of all flavours with equal branching fractions, while in the stau NLSP scenario it decays with 100 % branching fraction to $\tilde{\tau}_1 \tau$. The selection described here, referred to as the *4–lepton selection*, was used in both cases.

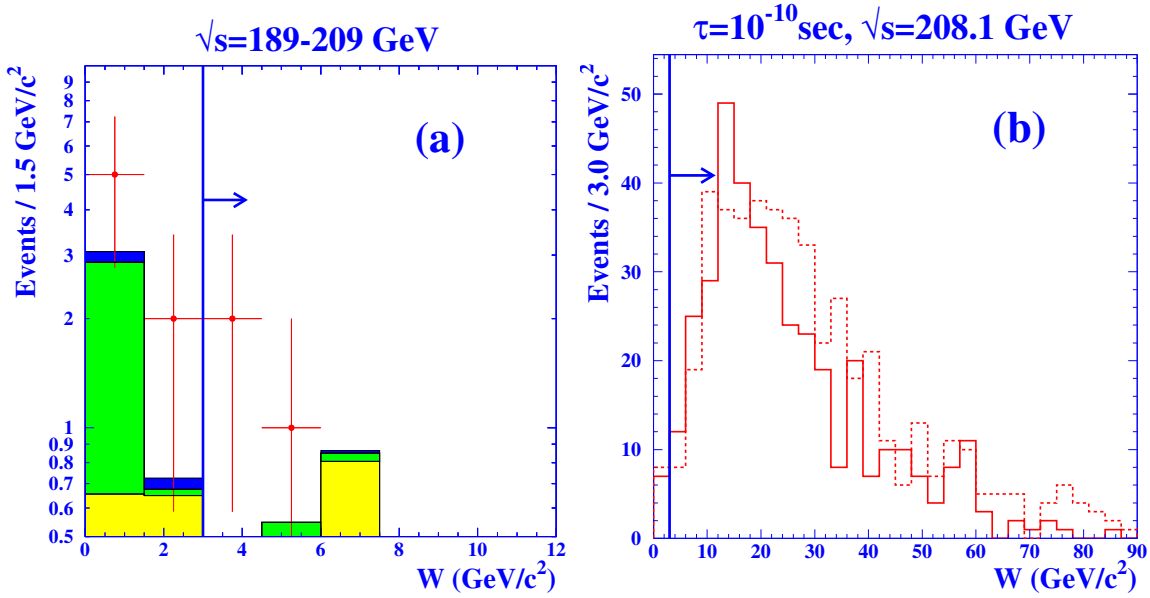


Figure 5.8: *The distribution of the invariant mass W of the secondary tracks in the 2–tau channel (see Section 5.5.2), plotted directly before the cut on W is applied. In (a) the data taken in the years 1998–2000 at $\sqrt{s} = 189 - 209$ GeV are shown as filled circles with error bars, the expected two–photon background is shown in yellow, the expected four–fermion background in blue and all other Standard Model background in green. The arrow indicates the accepted region. In (b) the invariant mass is shown for pair–production of staus with masses of 50 GeV/c^2 (dashed line) and 100 GeV/c^2 (solid line). The staus were simulated with a lifetime of 10^{-10} s at $\sqrt{s} = 208.1$ GeV. The normalisation in (b) is arbitrary.*

After	Efficiency [%]
-	100.0
Preselection	83.8
Topological selection	78.3
0 primary tracks	75.6
# vertices > 1	73.3
# add. tracks < 4	68.0
Cut (1)	68.0
Cut (2)	67.3
Cut (3)	67.3
Cut (4)	60.8
Cut (5)	60.8
Cut (6)	58.7
Cut (7)	57.8
Cut (8)	53.2
Cut (9)	52.9
Cut (10)	52.1

Table 5.6: *The efficiency for stau pair–production, simulated at $\sqrt{s} = 208.1$ GeV with a stau mass of 100 GeV/c^2 and a stau lifetime of 10^{-9} s, after each cut.*

After the topological selection, described in Section 5.5.1, it is required that at least two primary tracks are found. As visible from Table 5.7, this leads to a drastic reduction of the number of data events by a factor of about 280 (from 930100 to 3290 events). In contrast, the Monte Carlo background is suppressed by approximately a factor of only two. This is explained by the fact that in most of the unmodeled background sources tracks from the primary vertex are not present. No cut on the number of additional tracks is imposed. The following cuts are applied to the remaining number of events:

(1) All secondary tracks are required to have $|z_0| \leq 40\,\mathrm{cm}$.

(2) At least two of the primary tracks must have a transverse momentum larger than $1\,\mathrm{GeV}/c$. The transverse momenta of the primary tracks for the data and the Monte Carlo background after cut (1) are plotted in Fig. 5.9 (a). Apart from the poorly modeled very low–momentum region good agreement is found. Fig 5.9 (b) shows this variable for signal events in the slepton co–NLSP scenario simulated at $\sqrt{s} = 206.0\,\mathrm{GeV}$ with a lifetime of $5 \cdot 10^{-10}\,\mathrm{s}$. As examples, the cases ($M_{\tilde{\chi}_1^0} = 50\,\mathrm{GeV}/c^2$, $M_{\tilde{\ell}_R} = 45\,\mathrm{GeV}/c^2$) and ($M_{\tilde{\chi}_1^0} = 102\,\mathrm{GeV}/c^2$, $M_{\tilde{\ell}_R} = 100\,\mathrm{GeV}/c^2$) are shown. Close to the kinematic limit small transverse momenta are expected.

(3) Hits in the silicon microvertex detector and the vertex chamber must exist for at least two of the primary tracks.

(4) For Bhabha events the two primary tracks are usually back–to–back. To reject this

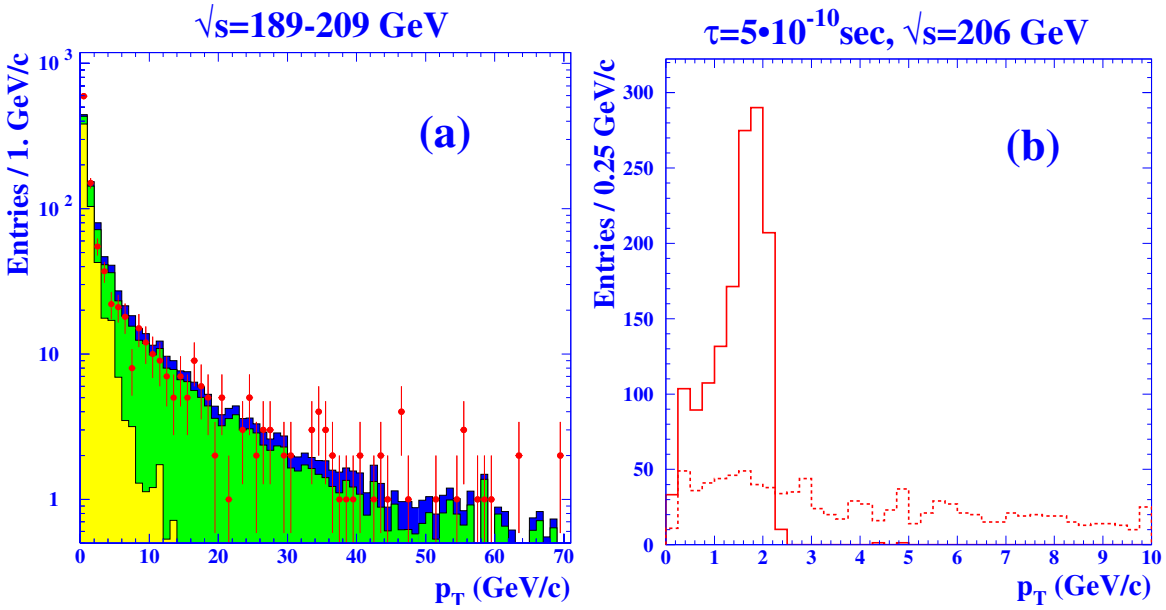


Figure 5.9: *The distribution of the transverse momentum p_T of each primary track in the 4–lepton channel (see Sect. 5.5.3), plotted directly before the cut on p_T is applied. In (a) the data taken in the years 1998–2000 at $\sqrt{s} = 189 - 209\,GeV$ are shown as filled circles with error bars, the expected two–photon background is shown in yellow, the expected four–fermion background in blue and all other Standard Model background in green. There are at least two entries per event. In (b) the transverse momentum of each primary track is shown for neutralino pair–production in the slepton co–NLSP scenario. Two cases are plotted: $M_{\tilde{\chi}_1^0} = 50\,GeV/c^2$ and $M_{\tilde{\ell}_R} = 45\,GeV/c^2$ (dashed line) and $M_{\tilde{\chi}_1^0} = 102\,GeV/c^2$ and $M_{\tilde{\ell}_R} = 100\,GeV/c^2$ (solid line). The events were simulated with a slepton lifetime of $5 \cdot 10^{-10}$ s at $\sqrt{s} = 206.0\,GeV$. The normalisation in (b) is arbitrary.*

background, the opening angle ξ in the $r-\phi$ plane, between each two primary tracks, must satisfy $\xi \leq 176°$.

(5) The invariant mass of all m secondary tracks

$$W = \sqrt{\left(\sum_{i=1}^{m} E^i\right)^2 - \left(\sum_{i=1}^{m} p_x^i\right)^2 - \left(\sum_{i=1}^{m} p_y^i\right)^2 - \left(\sum_{i=1}^{m} p_z^i\right)^2}$$

must fulfill $W > 5\,\mathrm{GeV}/c^2$. The distributions of the invariant mass after cut (6) for the data and the simulated background are shown in Fig. 5.10 (a). Good agreement is found. In Fig 5.10 (b) the corresponding signal distributions for the parameters described above are plotted. It can be seen, that, in contrast to cut (2), only a small fraction of signal events fail this cut.

(6) Secondary particles can also be produced in photon conversions. In this case their tracks often start in the middle of the jet chamber and have, due to the boost in the forward direction, relatively small but not negligible impact parameters. For the signal secondary particles arise from the decay of heavy particles, resulting in a much smaller boost. Thus to produce equally small impact parameters the flight lengths of the primary particles must be much shorter than for photons, and the secondary tracks start, in general, at radii smaller than those of the jet chamber. To veto such tracks from photon conversions the following cut is applied: for tracks with an impact parameter $|d_0| < 2\,\mathrm{cm}$ the first hit in the jet chamber must be measured at a radial distance to the primary interaction point of less than 40 cm.

(7) The transverse momentum of all secondary tracks, $\sqrt{\left(\sum_{i=1}^{m} p_x^i\right)^2 + \left(\sum_{i=1}^{m} p_y^i\right)^2}$, must exceed $3\,\mathrm{GeV}/c$.

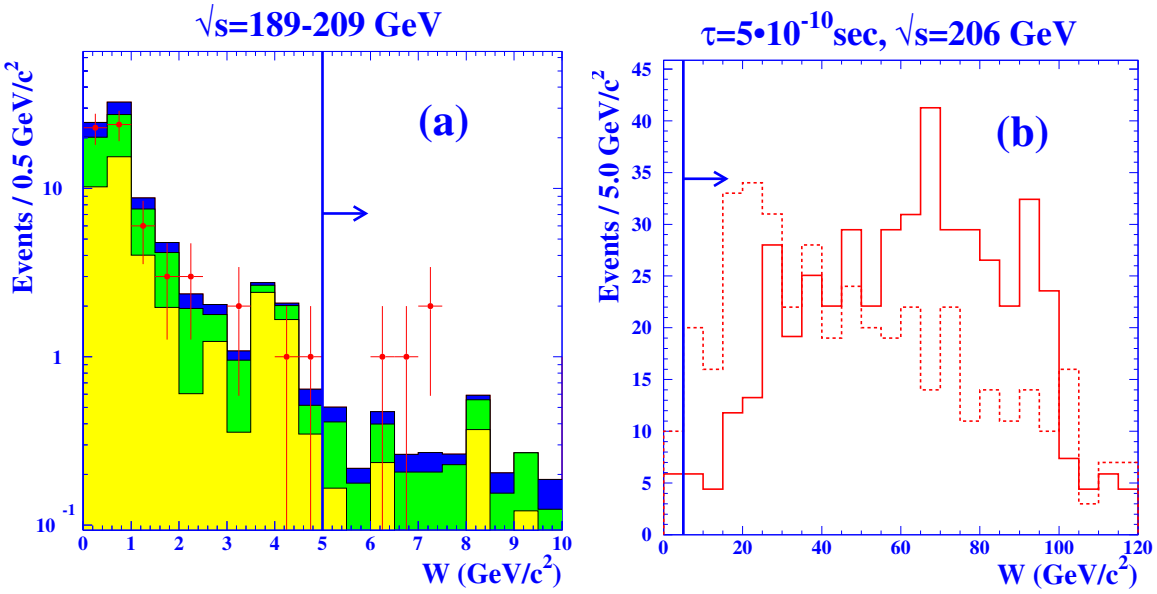


Figure 5.10: *The distributions of the invariant mass W of all secondary tracks in the 4–lepton channel, plotted directly before the cut on W is applied. In (a) the data taken in the years 1998–2000 at $\sqrt{s} = 189 - 209$ GeV are shown as filled circles with error bars, the expected two–photon background is shown in yellow, the expected four–fermion background in blue and all other Standard Model background in green. The arrow indicates the accepted region. In (b) the invariant mass is shown for neutralino pair–production in the slepton co–NLSP scenario. Two cases are plotted: $M_{\tilde{\chi}_1^0} = 50\ GeV/c^2$ and $M_{\tilde{\ell}_R} = 45\ GeV/c^2$ (dashed line) and $M_{\tilde{\chi}_1^0} = 102\ GeV/c^2$ and $M_{\tilde{\ell}_R} = 100\ GeV/c^2$ (solid line). The events were simulated with a slepton lifetime of $5 \cdot 10^{-10}$ s at $\sqrt{s} = 206.0$ GeV. The normalisation in (b) is arbitrary.*

After	Year 1998		Year 1999		Year 2000		Years 1998–2000	
	Data	MC Bkg.	Data	MC Bkg.	Data	MC Bkg.	Data	MC Bkg.
-	12461200	1799240	16285760	2391640	12461200	2294610	45188760	6485490
Preselection	331328	7267.7	331405	8694.9	460131	8157.5	1122863	24120.1
Topological selection	278801	277.2	273197	365.4	378102	344.5	930100	987.1
# primary tracks > 1	983	142.8	1113	182.4	1194	181.5	3290	506.7
Cut (1)	112	93.4	133	123.4	135	112.8	380	329.6
Cut (2)	37	53.6	60	67.0	61	65.8	158	186.4
Cut (3)	30	47.8	51	58.4	53	56.8	134	163.0
Cut (4)	15	25.1	29	31.6	31	31.1	75	87.8
Cut (5)	2	2.3	8	3.5	2	3.2	12	9.0
Cut (6)	1	1.8	4	3.0	2	2.7	7	7.5
Cut (7)	1	1.2	2	2.3	1	2.2	4	5.7

Table 5.7: *The remaining number of events after each cut (see Section 5.5.3) for simulated background and data for the years 1998, 1999 and 2000 and in total in the 4–lepton channel.*

After	Year 1998		Year 1999		Year 2000		Years 1998–2000	
	Data	MC Bkg.	Data	MC Bkg.	Data	MC Bkg.	Data	MC Bkg.
-	12461200	1799240	16285760	2391640	16441800	2294610	45188760	6485490
Preselection	331328	7267.7	331405	8694.9	460131	8157.5	1122863	24120.1
Topological selection	278801	277.2	273197	365.4	378102	344.5	930100	987.1
# primary tracks > 2	385	74.5	493	87.3	530	97.5	1408	259.3
Cut (1)	54	48.4	60	62.6	61	63.1	175	174.1
Cut (2)	30	36.4	43	49.1	44	52.5	117	138.0
Cut (3)	5	4.4	11	5.3	3	6.7	19	16.4
Cut (4)	4	3.7	6	4.2	3	5.9	13	13.7

Table 5.8: *The remaining number of events after each cut (see section 5.5.4) for simulated background and data for the years 1998, 1999 and 2000 and in total in the 6–lepton channel.*

In the fourth column of Table 5.4 (page 41) the number of data and background events remaining after all cuts is given, for the individual centre–of–mass energies. In total four events are left in the data in good agreement with the 5.7 events expected from simulated Standard Model background sources.

In Table 5.9 the efficiency is shown after each cut for a slepton lifetime of 10^{-9} s, a neutralino mass of 95 GeV/c^2 and a slepton mass of 85 GeV/c^2 in the slepton co–NLSP scenario and the stau NLSP scenario. The efficiency is reduced mainly by the cut on the transverse momentum of the primary tracks. After all cuts, efficiencies around 50 % are obtained in the slepton co–NLSP scenario. Due to the non–negligible tau mass the efficiency in the stau NLSP scenario depends crucially on the mass difference between the neutralino and the stau, ΔM. For large ΔM the highest efficiencies are about 35 %, while for $\Delta M <$ 2 GeV/c^2 the efficiencies drop to only a few percent.

After	Efficiency [%] $\tilde{\ell}$ co–NLSP	Efficiency [%] $\tilde{\tau}$ NLSP
-	100.0	100.0
Preselection	85.2	76.9
Topological selection	81.5	72.0
# primary tracks > 1	70.5	57.6
Cut (1)	66.8	55.3
Cut (2)	60.4	39.3
Cut (3)	56.9	37.7
Cut (4)	55.0	36.3
Cut (5)	53.3	33.4
Cut (6)	52.5	32.3
Cut (7)	52.1	31.5

Table 5.9: *The efficiencies after each cut for neutralino pair–production signals simulated at $\sqrt{s}$ = 206 GeV with a neutralino mass of 95 GeV/c^2 and a slepton mass of 85 GeV/c^2 for a slepton lifetime of 10^{-9} s in the slepton co–NLSP scenario (BR$(\tilde{\chi}_1^0 \to \tilde{\tau}_1\tau) = 1/3$) and the stau NLSP scenario (BR$(\tilde{\chi}_1^0 \to \tilde{\tau}_1\tau) = 100$ %).*

5.5.4 Slepton Pair–Production in the Stau NLSP Scenario: 6–Lepton Selection

In the stau NLSP scenario staus can be produced indirectly via selectron or smuon pair–production, $e^+e^- \to \tilde{\ell}_R^+\tilde{\ell}_R^-$ with $\tilde{\ell}_R^\pm = \tilde{e}_R^\pm$ or $\tilde{\mu}_R^\pm$, followed by decays $\tilde{\ell}_R^+ \to \tilde{\chi}_1^0\ell^+ \to \tilde{\tau}_1^\pm\tau^\mp\ell^+$. In this channel there are six leptons in the final state: two electrons or muons originating from the primary vertex, two primary taus and finally the two secondary taus respectively their decay products from the stau decays, which, depending on the lifetime, might have large impact parameters. Thus the topology in this channel is at least two tracks with large impact parameters and at least four primary tracks. This selection, in the following referred to as the *6–lepton selection*, is very similar to the selection described in Section 5.5.3. It was used both for selectron and smuon pair–production, for which it yields similar efficiencies.

First the topological selection described in Sect. 5.5.1 is applied. All events with less than three primary tracks are rejected, while no cut on the number of additional tracks is applied. The remaining 1408 data and 259.3 MC events are subjected to the following cuts:

(1) All secondary tracks are required to have $|z_0| \leq 40$ cm (cut (1) of Sect. 5.5.3). After this cut there are 175 events left in the data, while about 174 events are expected from the simulated Standard Model background.

(2) At least one of the primary tracks must have a transverse momentum larger than $1\,\mathrm{GeV}/c$. The transverse momenta of the primary tracks for the data and the Monte Carlo background after cut (1) are plotted in Fig. 5.11 (a) and show very good agreement. Fig 5.11 (b) shows this variable for smuon pair–production signal events simulated at $\sqrt{s} = 206.0\,\mathrm{GeV}$ with a stau lifetime of $10^{-10}\,\mathrm{s}$. As examples the cases ($M_{\tilde{\mu}_R} = 60\,\mathrm{GeV}/c^2$, $M_{\tilde{\chi}_1^0} = 58\,\mathrm{GeV}/c^2$, $M_{\tilde{\tau}_1} = 56\,\mathrm{GeV}/c^2$) and ($M_{\tilde{\mu}_R} = 102.5\,\mathrm{GeV}/c^2$, $M_{\tilde{\chi}_1^0} = 99.9\,\mathrm{GeV}/c^2$, $M_{\tilde{\tau}_1} = 98\,\mathrm{GeV}/c^2$) are shown.

(3) The invariant mass of all secondary tracks must fulfill $W > 5\,\mathrm{GeV}/c^2$ (cut (5) of Sect. 5.5.3). The distributions of the invariant mass after cut (4) for the data and the simulated background are shown in Fig. 5.12 (a). Again good agreement is found. In Fig 5.12 (b) the corresponding signal distributions for the parameters described above are plotted. Compared with the 4–lepton channel the invariant mass peaks at much smaller values due to fact that in the 6–lepton channel in addition to the gravitino two neutrinos carry away energy.

(4) For tracks with an impact parameter $|d_0| < 2\,\mathrm{cm}$ the first hit in the jet chamber must be measured at a radial distance to the primary interaction point of less than 40 cm (cut (6) of Sect. 5.5.3).

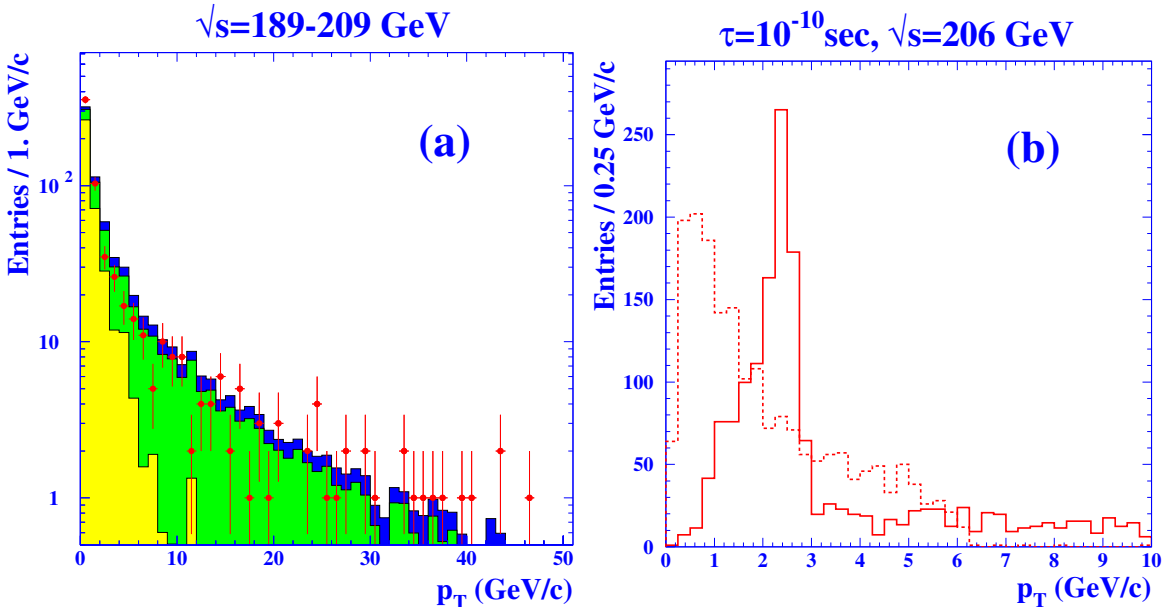


Figure 5.11: *The distributions of the transverse momentum p_T of each primary track in the 6–lepton channel (see Section 5.5.4), plotted directly before the cut on p_T is applied. In (a) the data taken in the years 1998–2000 at $\sqrt{s} = 189 - 209$ GeV are shown as filled circles with error bars, the expected two–photon background is shown in yellow, the expected four–fermion background in blue and all other Standard Model background in green. There are at least two entries per event. In (b) the transverse momentum is shown for smuon pair–production in the stau NLSP scenario. Two cases are plotted: $M_{\tilde{\mu}_R} = 60$ GeV/c^2, $M_{\tilde{\chi}_1^0} = 58$ GeV/c^2, $M_{\tilde{\tau}_1} = 56$ GeV/c^2 (dashed line) and $M_{\tilde{\mu}_R} = 102.5$ GeV/c^2, $M_{\tilde{\chi}_1^0} = 99.9$ GeV/c^2, $M_{\tilde{\tau}_1} = 98$ GeV/c^2 (solid line). The events were simulated with a stau lifetime of 10^{-10} s at $\sqrt{s} = 206.0$ GeV. The normalisation in (b) is arbitrary.*

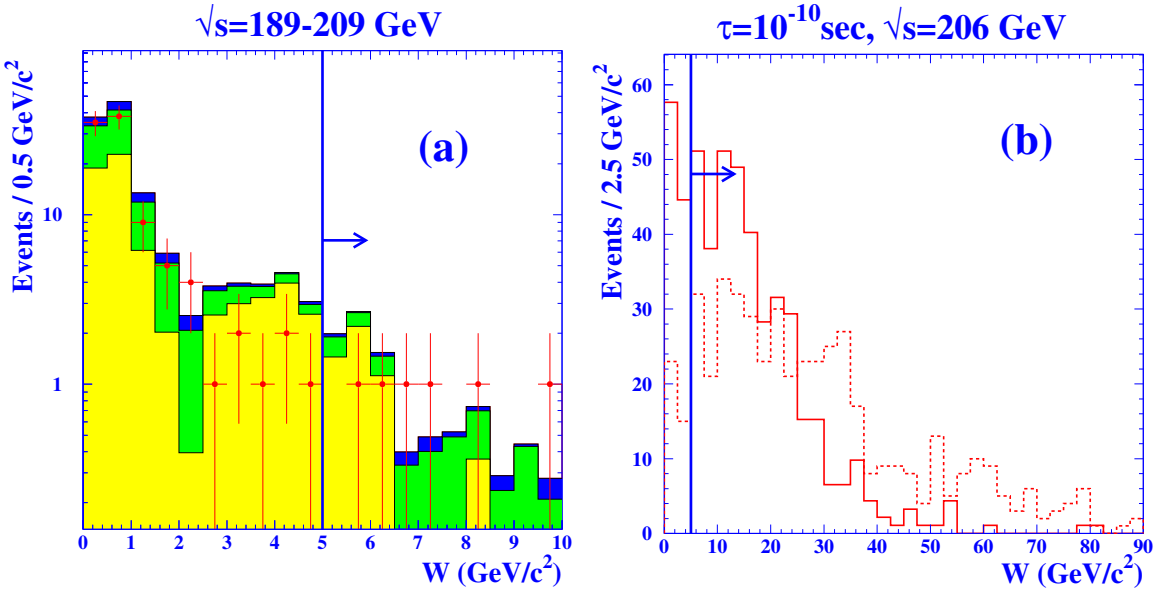


Figure 5.12: *The distributions of the invariant mass W of all secondary tracks in the 6l–channel (see Section 5.5.4), plotted directly before the cut on W is applied. In (a) the data taken in the years 1998–2000 at* $\sqrt{s} = 189 - 209$ *GeV are shown as filled circles with error bars, the expected two–photon background is shown in yellow, the expected four–fermion background in blue and all other Standard Model background in green. There are two entries per event. The arrow indicates the accepted region. In (b) the invariant mass is shown for smuon pair–production in the stau NLSP scenario. Two cases are plotted:* $M_{\tilde{\ell}} = 60$ *GeV*$/c^2$, $M_{\tilde{\chi}^0_1} = 58$ *GeV*$/c^2$, $M_{\tilde{\tau}} = 56$ *GeV*$/c^2$ *(dashed line) and* $M_{\tilde{\ell}} = 102.5$ *GeV*$/c^2$, $M_{\tilde{\chi}^0_1} = 99.9$ *GeV*$/c^2$, $M_{\tilde{\tau}} = 98$ *GeV*$/c^2$ *(solid line). The events were simulated with a stau lifetime of* 10^{-10} *s at* $\sqrt{s} = 206.0$ *GeV. The normalisation in (b) is arbitrary.*

The number of data and background events remaining after all cuts for the individual centre–of–mass energies are given in the last column of Table 5.4 (page 41). In total 13 data events survive the selection in good agreement with the 13.7 events that are expected from Standard Model background sources. The efficiencies after each cut for a selectron and smuon pair–production signal simulated at $\sqrt{s} = 206\,\text{GeV}$ with a stau lifetime of $10^{-10}\,\text{s}$, a selectron or smuon mass of $100\,\text{GeV}/c^2$, a neutralino mass of $98\,\text{GeV}/c^2$ and a stau mass of $90\,\text{GeV}/c^2$ are given in Table 5.10. A reduction in efficiency is introduced already at the preselection level due to the multiplicity requirement. After all cuts efficiencies of 45–50% for selectron and 40–45% for smuon pair–production are reached.

5.5.5 Chargino Pair–Production

For chargino pair–production, $e^+ e^- \to \tilde{\chi}^+_1 \tilde{\chi}^-_1$, two cases were studied: in the slepton co–NLSP scenario the chargino decays as $\tilde{\chi}^+_1 \to \tilde{\ell}^+_R \nu_\ell$, with equal branching fractions for sleptons of all flavours. In the stau NLSP scenario the chargino decays with 100 % branching fraction to $\tilde{\tau}_1 \nu_\tau$. The experimental topology is similar to slepton pair–production in the slepton co–NLSP and stau NLSP scenarios (Sect. 5.5.1 and 5.5.2), with the difference that now an additional neutral particle, the neutrino, carries away energy. For the slepton co–NLSP case the selection from Sect. 5.5.1 was used, while for the stau NLSP case the selection for stau pair–production described in Sect. 5.5.2 was applied.

For the slepton co–NLSP scenario efficiencies of about 35–43 % are reached. No events are selected in the total data set with 0.09 events expected from SM background sources (see Sect. 5.5.1 for details).

After	Efficiency [%] $\tilde{\ell}$ co–NLSP	Efficiency [%] $\tilde{\tau}$ NLSP
-	100.0	100.0
Preselection	68.2	66.1
Topological selection	61.9	59.8
# primary tracks > 2	55.5	53.6
Cut (1)	53.9	52.2
Cut (2)	53.6	51.9
Cut (3)	49.1	46.1
Cut (4)	47.2	44.1

Table 5.10: *The efficiencies after each cut for slepton pair–production with a stau NLSP. The efficiencies for selectron and smuon pair production simulated at $\sqrt{s} = 206$ GeV with a smuon/selectron mass of 100 GeV/c^2, a neutralino mass of 98 GeV/c^2 and a stau mass of 90 GeV/c^2 for a stau lifetime of 10^{-9} s are shown.*

For the stau NLSP scenario the efficiencies are slightly higher and reach 38–48 %. However, with 3.8 events expected from Standard Model background sources, the sensitivity is lower than in the slepton co–NLSP case. Four events are selected in the total data set (see Sect. 5.5.2 for details).

Chapter 6

Determination of the Signal Efficiency

In SUSY, the masses and (for GMSB models) lifetimes of the supersymmetric particles are unknown. Searches have to be performed for all values, but Signal Monte Carlo samples can only be generated for a finite number of sparticle masses and NLSP lifetimes. To determine efficiencies for arbitrary masses and lifetimes, an interpolation has to be performed between the generated points. For this purpose an efficiency function, based on the kinematics of the production and decay of the particles, is used to describe the efficiencies as a function of the centre–of–mass energy, the lifetime and $\beta\gamma$ of the particles. This method was originally developed at OPAL for the search for tracks with kinks and later generalised to be appropriate for all GMSB searches. It is described in detail in [40] and [43]. Here only the basic ideas of this method will be discussed. A list of the generated Monte Carlo points that were used as input for the fit can be found in Appendix B.

Several simplifications and assumptions [1] are made for the calculation of the efficiency function:

- The decay of the particle with lifetime τ follows an exponential decay law.
- The detector geometry is approximated by the shell of a sphere.
- The efficiency is assumed to be constant within the inner and outer radius of this shell. These radii do not correspond to any physical radii of the detector, but depend on the selection.
- Initial and final state radiation are neglected in the calculation of the event kinematics.

The search for tracks with large impact parameters is only efficient if both sleptons decay within a certain fiducial volume of the detector. The efficiency for selecting a single sparticle ϵ_{single} is proportional to the probability that the particle has decayed within this fiducial volume, i.e. between its inner and outer radius, R_{start} and R_{stop}:

$$\epsilon_{\text{single}} \sim \int_{R_{\text{start}}}^{R_{\text{stop}}} P(l)dl\,,$$

where l is the decay length in the lab frame. The decay probability $P(l)$ is given by

$$P(l) = \frac{1}{\lambda}\exp\left(-\frac{l}{\lambda}\right)\,.$$

[1] It has to be stressed that these assumptions are made for the efficiency functions only. The signal Monte Carlo is generated with the correct geometry and includes initial and final state radiation.

The parameter λ is the mean decay length of the particle in the lab frame and is given by

$$\lambda = \beta\gamma c\tau\,.$$

Integration yields

$$\epsilon_{\text{single}} = \epsilon_0 \left[\exp\left(-\frac{\mathrm{R}_{\text{start}}}{\lambda}\right) - \exp\left(-\frac{\mathrm{R}_{\text{stop}}}{\lambda}\right)\right].$$

The factor ϵ_0 is introduced to take into account that not all particles decaying in the fiducial volume will be selected. For the case of pair–produced long–lived particles with mass m, momentum $\vec{p}$ and energy $E = \sqrt{s}/2$ (both in the lab frame), $\beta\gamma$ is given by

$$\beta\gamma = \frac{|\vec{p}|}{m} = \sqrt{\frac{s}{4m^2} - 1}\,.$$

Then the mean decay length can be expressed as

$$\lambda = c\tau\sqrt{\frac{s}{4m^2} - 1}\,.$$

In this analysis both particles are required to decay in the detector. The total event selection efficiency is therefore given by

$$\epsilon(m, s, \tau) = \epsilon^2_{\text{single}}(m, s, \tau)\,.$$

For long–lived particles that are not pair–produced directly but are decay products of pair–produced particles, as in the 4–lepton and 6–lepton channels, $\beta\gamma$ has to be calculated differently. For a two–body decay A→B+C the momentum of the long–lived particle B in the rest frame (denoted with superscript *) of the parent particle A can be calculated from basic kinematics and is given by:

$$|\vec{p}^{\,*}_{\mathrm{B}}| = \frac{\sqrt{\left[m^2_{\mathrm{A}} - (m_{\mathrm{B}} + m_{\mathrm{C}})^2\right]\left[m^2_{\mathrm{A}} - (m_{\mathrm{B}} - m_{\mathrm{C}})^2\right]}}{2m_{\mathrm{A}}}\,. \tag{6.1}$$

It can be decomposed into its components parallel and perpendicular to the parent momentum:

$$\begin{aligned} p^*_{\mathrm{B}_\perp} &= |\vec{p}^{\,*}_{\mathrm{B}}| \sin\theta^* \\ p^*_{\mathrm{B}_\parallel} &= |\vec{p}^{\,*}_{\mathrm{B}}| \cos\theta^*\,. \end{aligned} \tag{6.2}$$

For the decay angle in the rest frame of the parent, θ^*, a value of $\pi/2$ is used. Then $\beta\gamma$ of the secondary particle can be calculated by

$$\beta_{\mathrm{B}}\gamma_{\mathrm{B}} = \frac{|\vec{p}_{\mathrm{B}}|}{m_{\mathrm{B}}} = \frac{\sqrt{p^2_{\mathrm{B}_\perp} + p^2_{\mathrm{B}_\parallel}}}{m_{\mathrm{B}}}\,.$$

The momentum components in the lab frame are calculated from the components in the rest frame of particle A by

$$\begin{aligned} p_{\mathrm{B}_\perp} &= p^*_{\mathrm{B}_\perp} \\ p_{\mathrm{B}_\parallel} &= \beta_{\mathrm{A}}\gamma_{\mathrm{A}} E^* + \gamma_{\mathrm{A}} p^*_{\mathrm{B}_\parallel} \end{aligned} \tag{6.3}$$

with

$$\beta_{\mathrm{A}}\gamma_{\mathrm{A}} = \frac{|\vec{p}_{\mathrm{A}}|}{m_{\mathrm{A}}}\,.$$

With the described functions a fit is performed to the efficiency points, determined at a given $\sqrt{s}$, lifetime and mass, separately for each channel and slepton flavour. The free parameters are the efficiency scale, ϵ_0, and the inner and outer radius of the fiducial detector volume, R_{start} and R_{stop}. The parameters are then fixed and the resulting efficiency function is used to calculate the efficiency for all centre–of–mass energies and arbitrary sparticle masses and lifetimes.

Chapter 7

The GMSB Scan Database

Interpreting the experimental results in terms of the GMSB model requires that they be compared with the theoretical expectations within the framework of this model. To exclude a certain point in the parameter space of the minimal GMSB model, one has to compare the experimental upper limit on the cross–section with the expected cross–section σ, taking into account the branching ratio BR ($\sigma \times \mathrm{BR}^2$ for pair–produced particles decaying to the same final state), for the processes kinematically allowed at this point.

A scan in the parameter space was performed in order to calculate the complete mass spectrum, the production cross–sections and the branching ratios for different SUSY particles at each point considered. For this scan the framework and formulae of [7] were used and generalised to include a full mass treatment for all three generations. The calculations are embedded in the SUSYGEN generator. A detailed description of the method can be found in [44].

The model parameters as well as the range and step size considered for them in the scan are summarised in Table 7.1. The messenger scale is arbitrary in the minimal model, but, as the mass m_b of the messenger bosons is given by $m_b = M\sqrt{1 \pm \Lambda/M}$, the relation $M > \Lambda$ has to be fulfilled in order to obtain a positive messenger boson mass. Both models with $M \sim \Lambda$ and $M \gg \Lambda$ do exist. Therefore three scenarios for the messenger scale were studied: M very close to Λ ($M = 1.01 \cdot \Lambda$), $M = 250\,\mathrm{TeV}/c^2$ and M very large ($10^6\,\mathrm{TeV}/c^2$). For the integer parameter N values up to five were considered. This is adequate, since perturbativity of the gauge interactions up to the grand unification scale, M_{GUT}, implies [5]

$$N \lesssim 150 \,/\, \ln \tfrac{M_{\mathrm{GUT}}}{M} \,.$$

Thus, for a messenger mass scale $M = 100\,\mathrm{TeV}/c^2$, $N \leq 5$ is required, and even for a very high M of $10^{10}\,\mathrm{TeV}/c^2$, $N > 10$ is disfavoured from a theoretical point of view. For the parameter μ both signs were studied. For each of the 30 combinations of N, M and sign(μ), a scan in Λ and $\tan\beta$ was performed. The upper and lower limits for this scan were chosen for the following reasons: for $\Lambda > 150\,\mathrm{TeV}/c^2$ the sparticles are already very heavy and no exclusion is possible at LEP. For $\tan\beta < 2.0$ the calculations are unstable (small values of $\tan\beta$ are disfavoured by searches for Higgs bosons [45]). Both the regions with $\tan\beta > 50.0$ and $\Lambda < 5\,\mathrm{TeV}/c^2$ are theoretically forbidden. The exact shape of the theoretically inaccesible region in the $\Lambda - \tan\beta$ plane depends on the other parameters.

A top mass of $175\,\mathrm{GeV}/c^2$ was used (the most recent PDG value is $174.3 \pm 5.1\,\mathrm{GeV}/c^2$), and at one centre–of–mass energy a full scan was performed for systematic studies with the top mass varied by two standard deviations. This is discussed in Chapter 8.

The scan information was saved in a database for comparison with the experimental results. Overall, 270 such data sets were produced: 30 for each centre–of–mass energy, for nine different energy points [1].

[1] The center–of–mass energies for the scan were 182.7, 188.7, 191.6, 195.5, 199.5, 201.6, 205.1, 206.7 and 208.1 GeV. They closely match the luminosity–weighted center–of–mass energies of the data, which are slightly different due to various cuts as for example the detector status cuts.

For the gravitino mass a value of $2\,\mathrm{eV}/c^2$, corresponding to a SUSY breaking scale of $\sqrt{F} \approx 100\,\mathrm{TeV}/c^2$, was chosen. This is motivated by the requirement that the branching ratio of the next–to–NLSP to the gravitino is small and only the NLSP decays to the gravitino. As long as this is fulfilled, the cross–sections and branching ratios do not depend on the gravitino mass. This makes it possible to decouple the issue of NLSP lifetime, which depends on $\sqrt{F}$, completely from the scan.

Parameter	Scan points	Step size
Λ	$5 - 150\,\mathrm{TeV}/c^2$	$1\,\mathrm{TeV}/c^2$
$\tan\beta$	2.0 – 50.0	0.2
M	$1.01 \cdot \Lambda$, $250\,\mathrm{TeV}/c^2$, $10^6\,\mathrm{TeV}/c^2$	
N	1, 2, 3, 4, 5	
sign(μ)	+1, −1	

Table 7.1: *Scanned points in the GMSB parameter space. The parameter Λ sets the overall mass scale of the SUSY particles,* $\tan\beta$ *is the ratio of the vacuum expectation values of the two Higgs doublets, M is the messenger scale, N the messenger index, and sign(μ) is the sign of the Higgs sector mixing parameter.*

7.1 The Minimal Expected Cross–Section

For the combination of the data with different centre–of–mass energies as well as for the calculation of NLSP mass limits, the theoretically expected cross–sections times the branching ratio squared (for pair–produced particles) within the model have to be known. Naturally these vary strongly within the model, depending on the chosen parameter set. To obtain values which are conservative and valid for each of the considered parameter sets, the following minimisation procedure was applied.

First, for each of the 30 parameter combinations, a scan over the parameters Λ and $\tan\beta$ was performed to obtain for each NLSP mass the minimum $\sigma \cdot \mathrm{BR}^2$ within this special parameter set. The $\sigma \cdot \mathrm{BR}^2$ distributions for the 30 points at $\sqrt{s} = 208.1\,\mathrm{GeV}$ are shown in Fig. 7.1 for selectrons and Fig. 7.2 for neutralinos [2]. The strong variation of $\sigma \cdot \mathrm{BR}^2$ between the various parameter sets can clearly be seen. For smuons and staus the cross–sections are much more uniform due to the fact that for these only s–channel production is allowed. Thus for these particles the cross–section is a function of the kinematics (slepton mass and $\sqrt{s}$) rather than the details of the model.

Then for each NLSP mass the minimum of $\sigma \cdot \mathrm{BR}^2$ within these 30 scenarios was calculated. The resulting minimal $\sigma \cdot \mathrm{BR}^2$ is shown in Fig. 7.3 for selectrons (left) and neutralinos (right). In both cases "steps" are present, which occur if the minimum jumps from one combination of the parameters (M, N, $sign(\mu)$) to another. In Fig. 7.4 the minimal $\sigma \cdot \mathrm{BR}^2$ is shown for smuons (left) and staus (right) in the slepton co– and the stau NLSP scenario. These are all smooth functions, because the minimum is found in the same parameter combination for all slepton masses.

For the minimisation it was required that either the neutralino NLSP scenario or the slepton co–NLSP scenario (for selectron, smuon and stau pair–production) or, for stau pair–production only, the stau NLSP scenario was realised. Otherwise, for each mass parameter points can be found where the cross–section vanishes, and the minimal cross–section will be

[2] Minimal $\sigma \cdot \mathrm{BR}^2$ were calculated not only for slepton pair–production but also for neutralino pair–production in the neutralino NLSP scenario (decays to $\gamma\tilde{\mathrm{G}}$). This channel was used for the interpretations, as discussed in Section 9.2.

zero. For the different scenarios the following conditions, taken from [6] and modified to include a proper treatment of the masses of all leptons, have to be fulfilled:

- Slepton co–NLSP scenario ($\tilde{\ell}, \tilde{\ell}' = \tilde{\mathrm{e}}_\mathrm{R}, \tilde{\mu}_\mathrm{R}, \tilde{\tau}_1$; $\ell = \mathrm{e}, \mu, \tau$):

$$\begin{aligned} M_{\tilde{\ell}} &< M_{\tilde{\chi}_1^0} - M_\ell \,, \\ M_{\tilde{\ell}} &< M_{\tilde{\ell}'} + M_\tau \,. \end{aligned}$$

- Stau NLSP scenario ($\tilde{\ell} = \tilde{\mathrm{e}}_\mathrm{R}, \tilde{\mu}_\mathrm{R}$; $\ell = \mathrm{e}, \mu$):

$$\begin{aligned} M_{\tilde{\tau}_1} &< M_{\tilde{\ell}_R} - M_\tau - M_\ell \,, \\ M_{\tilde{\tau}_1} &< M_{\tilde{\chi}_1^0} - M_\tau \,. \end{aligned}$$

- Neutralino NLSP scenario:

$$M_{\tilde{\chi}_1^0} < M_{\tilde{\tau}_1} - M_\tau \,.$$

The regions in the parameter space where the slepton co–NLSP scenario or the neutralino NLSP scenario is realised are shaded in Fig. 7.1 and Fig. 7.2, respectively.

This minimisation method was not used for the 4–lepton, 6–lepton and chargino channel. These are important in restricted parts of the GMSB parameter space only, and therefore a minimisation in the whole GMSB parameter space yields a marginal cross–section. No mass limits were calculated for these channels, and the theoretical cross–section enters only into the combination of different center–of–mass energies. For simplicity, for spin 1/2 sparticles a β/s dependence of the cross–section was assumed, while for scalars a β^3/s dependence was used. These assumptions are strictly true only for the photon propagator [18] and are approximations, especially for processes with a dominant $t-$channel.

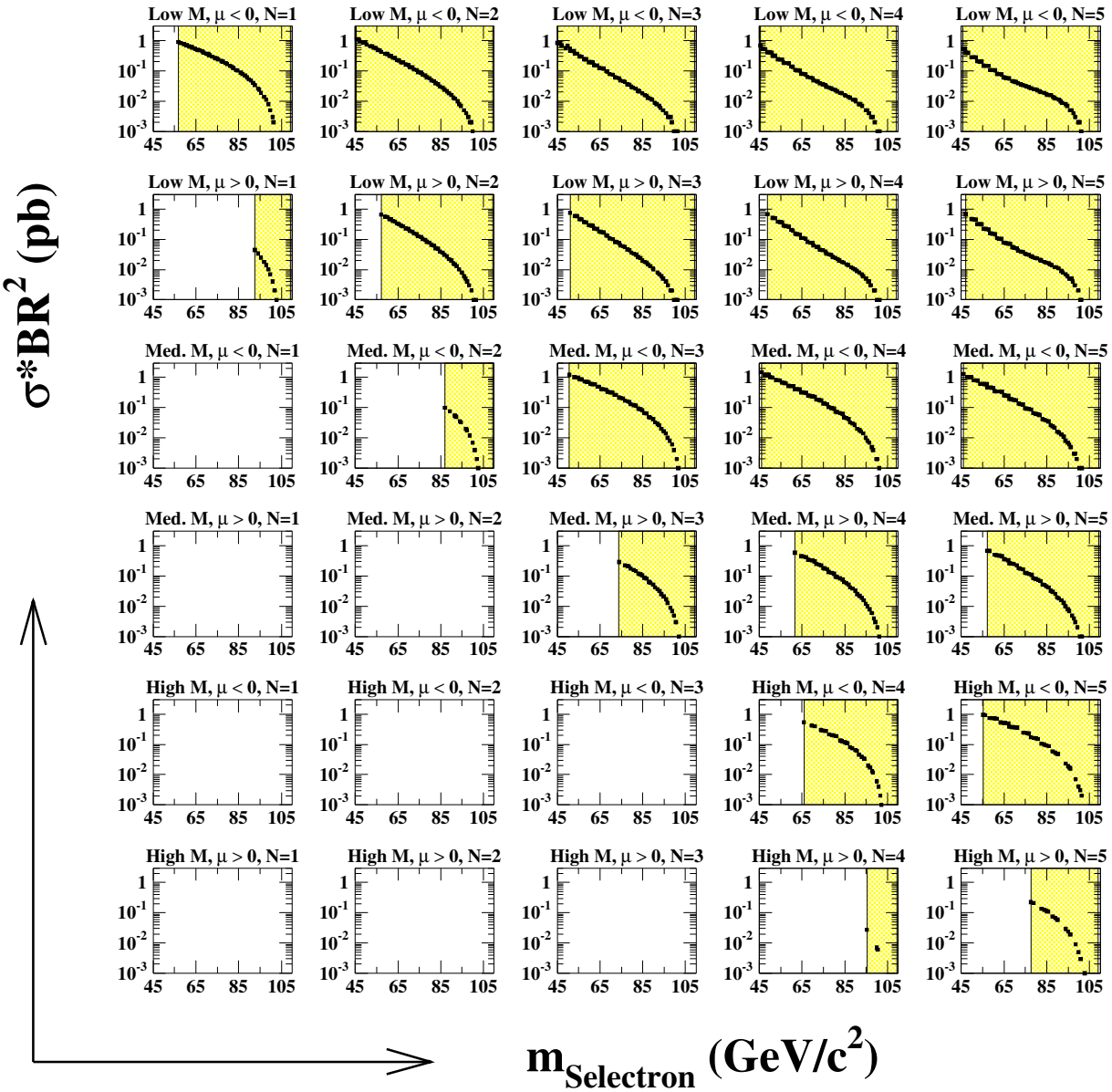


Figure 7.1: *Minimal cross–section for selectron pair–production times the branching ratio squared for $e\tilde{G}$ in the slepton co–NLSP scenario at $\sqrt{s}$ =208.1 GeV, in the different parameter sets considered in the scan. The plots show $\sigma \cdot \mathrm{BR}^2$ as a function of the selectron mass, for, from top to bottom, low, medium and high M for both signs of μ, and, from left to right, for N from one to five. A minimisation in the parameters Λ and $\tan\beta$ was already performed. In the shaded regions the conditions for the slepton co–NLSP scenario described in the text are fulfilled. In the white regions, the NLSP is either the neutralino or the stau.*

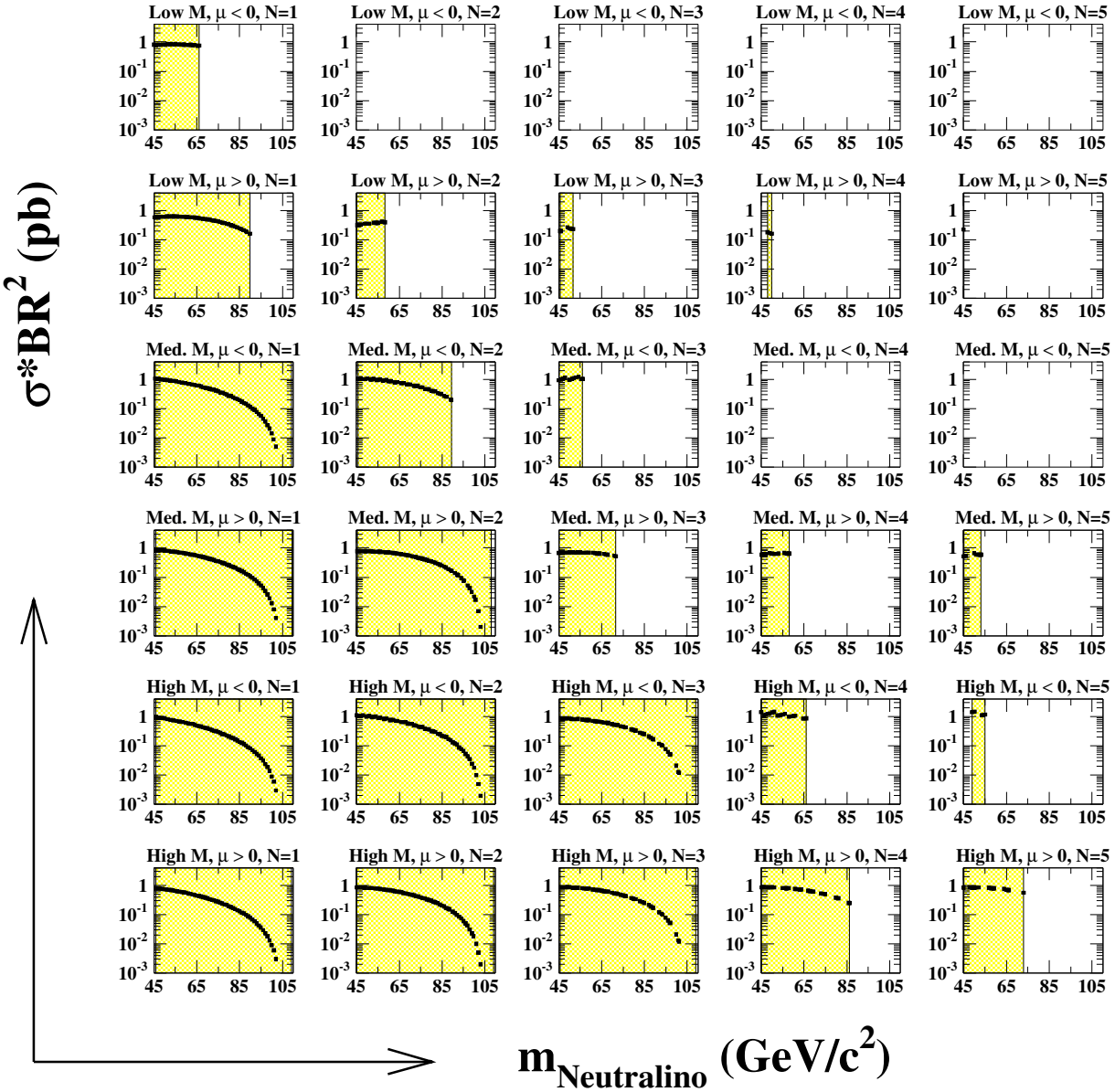


Figure 7.2: *Minimal cross–section for neutralino pair–production times the branching ratio squared for $\gamma\tilde{G}$ in the neutralino NLSP scenario at $\sqrt{s}$ =208.1 GeV, in the 30 different parameter sets considered in the scan. The plots show $\sigma \cdot \mathrm{BR}^2$ as a function of the neutralino mass, for, from top to bottom, low, medium and high M for both signs of μ, and, from left to right, for N from one to five. In the shaded regions the condition for the neutralino NLSP scenario described in the text is fulfilled. In the white regions, the NLSP is the lightest slepton.*

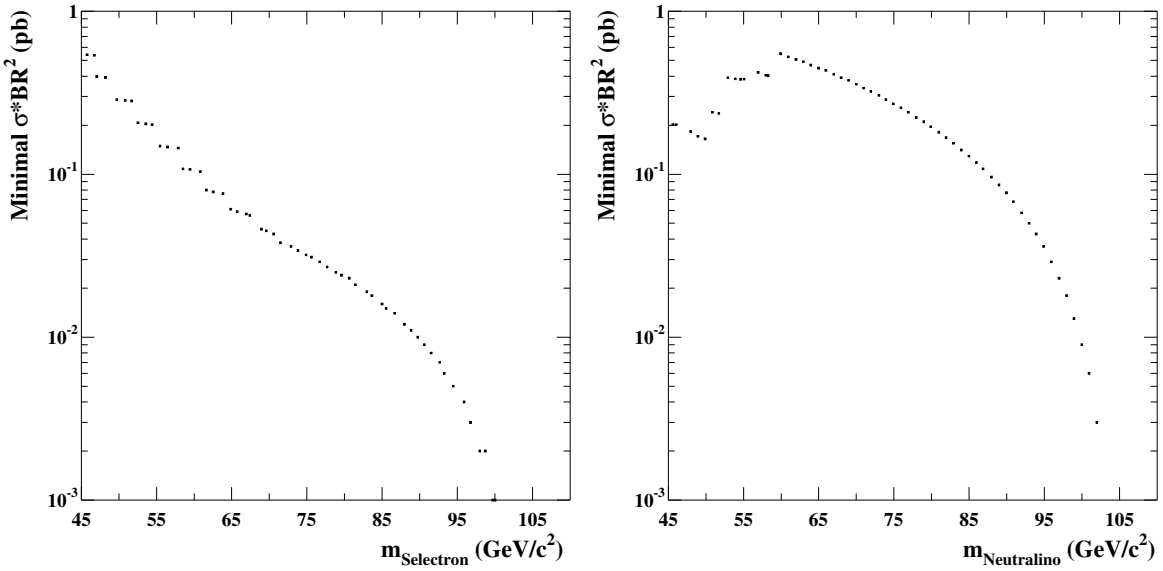


Figure 7.3: *Minimal cross–section for selectron pair–production times the branching ratio squared for $e\tilde{G}$ (left), and for neutralino pair–production times the branching ratio squared for $\gamma\tilde{G}$ (right), at $\sqrt{s}$ =208.1 GeV. The minimisation procedure is described in the text.*

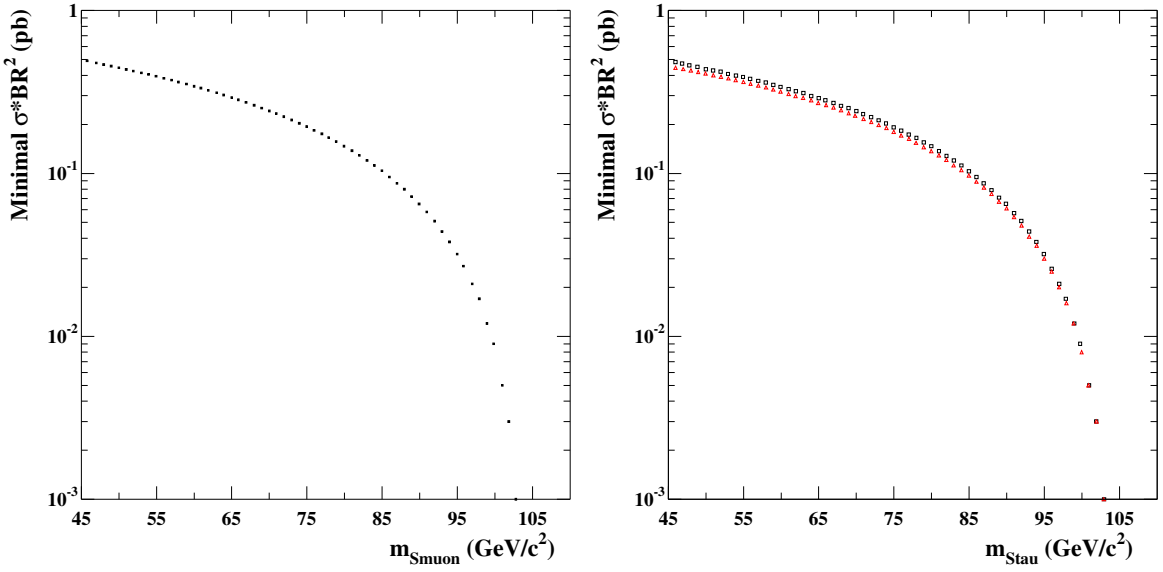


Figure 7.4: *Minimal cross–section for smuon pair–production times the branching ratio squared for $\mu\tilde{G}$ (left) and for stau pair–production times the branching ratio squared for $\tau\tilde{G}$ in the slepton co–NLSP scenario (right, black squares) and the stau NLSP scenario (right, red triangles) at $\sqrt{s}$ =208.1 GeV. The minimisation procedure is described in the text.*

Chapter 8

Systematic Uncertainties

The number of expected signal events S and the number of background events B expected from Standard Model processes are calculated by the formula

$$\begin{aligned} S &= \mathcal{L}^{\text{int}}\,\epsilon_S\,\sigma_S \\ B &= \mathcal{L}^{\text{int}}\sum\nolimits_i \epsilon_i\,\sigma_i \end{aligned}$$

from the integrated luminosity $\mathcal{L}^{\text{int}}$, the signal efficiency ϵ_S (Chapter 6), the signal cross–section σ_S (Section 7.1), and the selection efficiency and cross–section for the various Standard Model processes taken into account, ϵ_i and σ_i. In this chapter the different contributions considered for the determination of the uncertainties on the number of expected background and signal events will be discussed.

Uncertainty on the Integrated Luminosity

The relative statistical, systematic and total uncertainty on the luminosity $\delta\mathcal{L}/\mathcal{L}$ ($= \delta\mathcal{L}^{\text{int}}/\mathcal{L}^{\text{int}}$) is given in Table 8.1. Contributions to the systematic uncertainty are e.g. the uncertainty on the beam energy, irreducible background to Bhabha scattering and the uncertainty on the trigger efficiency. The numbers used for this analysis are taken from the documents listed under [46], where also more details about the determination of the systematic uncertainty on the luminosity can be found. The total relative uncertainty on the (also integrated) luminosity is $0.2 - 0.3\,\%$.

$\sqrt{s}$ [GeV]	189	192	196	200	202	204–209
$\delta\mathcal{L}/\mathcal{L}$ (statistical) [%]	0.09	0.203	0.131	0.132	0.187	0.079
$\delta\mathcal{L}/\mathcal{L}$ (systematic) [%]	0.20	0.240	0.217	0.229	0.230	0.223
$\delta\mathcal{L}/\mathcal{L}$ (total) [%]	0.21	0.314	0.253	0.264	0.296	0.237

Table 8.1: *Statistical, systematic and total relative uncertainties in percent on the luminosities measured with ROCROS (see Section 5.2) for different years and centre–of–mass energies.*

Uncertainty on the Cross–Sections

The statistical uncertainties on the cross–sections for the various background processes from the generators are in general small ($< 1\%$) and were neglected.

The top mass is measured with an experimental error of $2.9\,\%$. To determine the uncertainty on the signal cross–sections due to this error a scan was performed at $\sqrt{s} = 200\,\text{GeV}$

with a top mass of $165\,\mathrm{GeV}/c^2$ in addition to the default value of $175\,\mathrm{GeV}/c^2$. The minimal cross–section times BR^2 at 200 GeV for selectron, smuon, stau and neutralino pair–production were re–evaluated and compared with the values obtained with the default top mass. For selectron, smuon and stau pair–production the effect is small and a conservative uncertainty of $\delta_\sigma = 1\,\%$ independent of the slepton mass is assigned to the cross–sections due to this variation. For neutralino pair–production, however, the effect can be large depending on the neutralino mass. For small neutralino masses changes are of the order of 50 %, while for masses larger than $\approx 65\,\mathrm{GeV}/c^2$ the uncertainty drops to a few percent. This effect was fully taken into account by using a mass–dependent uncertainty $\delta_\sigma(M_{\tilde{\chi}_1^0})$ in the limit calculation at all energies.

Statistical Uncertainties

The statistical uncertainty on the signal efficiency can be calculated from the formula

$$\delta\epsilon_S^{\mathrm{stat}} \quad = \quad \sqrt{\epsilon_S(1-\epsilon_S)/N} \tag{8.1}$$

with N being the number of generated events in the Monte Carlo sample. With 1000 events per mass point, $\delta\epsilon_S^{\mathrm{stat}}/\epsilon_S$ is typically $3-4\,\%$ for the peak efficiencies.

The statistical uncertainty on the number of background events due to the necessarily limited Monte Carlo statistics is given by

$$\delta B_{\mathrm{stat}} \quad = \quad \mathcal{L}^{\mathrm{int}} \cdot \sqrt{\sum\nolimits_i \left(\sigma_i\,\delta\epsilon_i^{\mathrm{stat}}\right)^2}$$

where the $\delta\epsilon_i$ are calculated analogously to (8.1). The uncertainties due to the Monte Carlo statistics thus depend on the squareroot of the number of selected simulated events and are summarised in Table 8.2 for the four channels and all centre–of–mass energies. It was found that these uncertainties can be quite sizable and, due to the small number of selected background events, the relative uncertainty can easily reach 50 %.

	2–Lepton channel	2–Tau channel	4–Lepton channel	6–Lepton channel
$\sqrt{s}$ [GeV]	δB_{stat}	δB_{stat}	δB_{stat}	δB_{stat}
189	0.02	0.34	0.24	0.97
192	0.0	0.05	0.04	0.17
196	0.0	0.13	0.30	0.31
200	0.01	0.20	0.89	0.90
202	0.0	0.07	0.05	0.16
204–206	0.0	0.20	0.31	0.54
206–207	0.01	0.35	0.52	0.89
> 207	0.01	0.04	0.04	0.06

Table 8.2: *Uncertainties on the number of background events expected from Standard Model processes due to the limited Monte Carlo statistics.*

Uncertainties due to the Tracking Performance

Most cuts applied in this analysis deal with the tracking of the particles. If the resolution of the track parameters in the detector simulation is better than in the recorded data this can lead to an overestimation of the selection efficiencies and an underestimation of the background. Therefore, to obtain a conservative estimation of the size of this effect, the resolution of the track parameters was degraded ("smeared") substantially and new efficiencies and background numbers were determined with these smeared track parameters. Comparing

the experimental resolution from muon pairs and Bhabha events with the Monte Carlo simulation [48] it was found that smearing the track parameters in the $r-\phi$ plane by 10 % and in the $s-z$ plane by 40 % gives a conservative estimation of the systematic uncertainty due to this effect. Technical details about this track smearing can be found in [47]. The number of background events expected after this smearing can be found in Table 8.3. Indeed in most – but not all – cases the number of background events is increased, in some cases substantially, e.g. in the 2–lepton channel for 206 GeV$< \sqrt{s} \leq$ 207 GeV from 0.01 events to 0.74 events. The (absolute) differences to the background numbers without smearing are taken as the systematic uncertainties due to this effect. The smearing also leads, in most cases, to a slight decrease of the signal efficiency. Performing detailed studies of the smeared efficiencies in all channels, it was found that a relative uncertainty of 4 % is fairly conservative and is therefore used for all channels and lifetimes.

	2–Lepton channel	2–Tau channel	4–Lepton channel	6–Lepton channel
$\sqrt{s}$ [GeV]	MC Bkg.	MC Bkg.	MC Bkg.	MC Bkg.
189	0.07	1.38	1.43	4.15
192	< 0.01	0.14	0.29	0.73
196	< 0.01	0.26	0.64	1.20
200	0.02	0.79	1.35	2.08
202	0.004	0.45	0.22	0.62
204–206	< 0.01	0.70	0.91	1.98
206–207	0.74	2.09	1.35	2.94
> 207	0.01	0.15	0.09	0.20

Table 8.3: *Expected number of events from Standard Model sources after all cuts in the four selections after smearing the track parameters as described in the text.*

Uncertainty due to Cosmic Background

To suppress the background from cosmic ray events a cut on the time–of–flight t in the barrel time–of–flight detector is applied (see Section 5.5.1): 5 ns $\leq$ t $\leq$ 20 ns. However, cosmic events cross the detector at random times and thus can also fall in this time window. The contamination with cosmics due to this effect cannot be studied directly, since physics events from Standard Model processes are in this window as well and cannot be distinguished easily from cosmic events. To get an estimation of the remaining background due to cosmic events thus the time–of–flight region outside the window was studied and, assuming an approximately flat time–of–flight distribution, used to calculate the number of expected cosmic events inside the window.

The following study was performed for the 2–lepton channel, which is the channel with most unmodelled background. All tracks are required to have a meaningful time–of–flight information unless they are flagged as being not in the fiducial volume of the barrel time–of–flight detector.

To evaluate the number of cosmic events outside the time window a time–of–flight range of $\Delta t = 435$ ns from -300 ns up to 5 ns and from 20 ns up to 150 ns was chosen. The number of tracks expected inside the time window N_{in} is calculated from the number outside the window N_{out}:

$$N_{\text{in}} = N_{\text{out}} \frac{15\,\text{ns}}{\Delta t}\,.$$

The probability of a single track being inside the time window is thus

$$P_{\text{track}} = \frac{N_{\text{in}}}{N_{\text{track}}} = \frac{N_{\text{in}}}{N_{\text{in}} + N_{\text{out}}}\,,$$

where N_{track} is the total number of tracks. In the main analysis an event is selected if both tracks are inside the time window, thus the probability is $P_{\text{event}} = P^2_{\text{track}}$. Multiplication with the total number of events N_{event} gives an estimation of the expected remaining cosmic background: $N_{\text{cosmics}} = N_{\text{event}} P_{\text{event}}$. N_{event} includes also events with tracks that passed through one of the endcaps, i.e. outside the geometrical acceptance region of the barrel time–of–flight detector. Such events are treated the same way as events with barrel tracks only, assuming that the probability for cosmic events in the endcap region is the same as in the barrel region. This is an extremely conservative assumption.

The number of events expected after the various cuts are listed in Table 8.4, including the whole data set. No remaining cosmic events are expected after the cut (7), thus no systematic uncertainty was assigned to the number of background events due to this effect.

After	N_{cosmics}
Cut (2)	28.15
Cut (3)	28.12
Cut (4)	5.19
Cut (5)	4.68
Cut (6)	0.13
Cut (7)	0.003
Cut (8)	0.002

Table 8.4: *Expected number of remaining cosmic ray events inside the time–of–flight window considered for the analysis, after the last seven cuts as explained in Sect. 5.5.1 and for* $\sqrt{s} = 189 - 206$ *GeV.*

Total Uncertainties

The total uncertainty on the number of signal events is calculated by adding the various contributions discussed in quadrature:

$$\begin{aligned} \delta S_{\text{tot}} &= S \cdot \sqrt{\left(\frac{\delta\mathcal{L}}{\mathcal{L}}\right)^2 + \left(\frac{\delta\epsilon_S}{\epsilon_S}\right)^2} \\ &= S \cdot \sqrt{\left(\frac{\delta\mathcal{L}}{\mathcal{L}}\right)^2 + \left(\frac{\delta\epsilon_S^{\text{stat}}}{\epsilon_S}\right)^2 + \left(\frac{\delta\epsilon_S^{\text{syst}}}{\epsilon_S}\right)^2 + \left(\frac{\delta_\sigma}{\sigma}\right)} \end{aligned}$$

and is typically $4 - 5\%$.

Analogously the total uncertainty on the number of background events is calculated:

$$\begin{aligned} \delta B_{\text{tot}} &= B \cdot \sqrt{\left(\frac{\delta\mathcal{L}}{\mathcal{L}}\right)^2 + \left(\frac{\delta B_{\text{stat}}}{B}\right)^2 + \left(\frac{\delta B_{\text{sys}}}{B}\right)^2} \\ &= \sqrt{\left(B \cdot \frac{\delta\mathcal{L}}{\mathcal{L}}\right)^2 + \mathcal{L}^2 \sum \left(\delta\epsilon_i^{\text{stat}}\,\sigma_i\right)^2 + \delta B^2_{\text{smear}}}\,. \end{aligned}$$

The uncertainties δB_{tot} and δS_{tot} are taken into account for the calculation of the cross–section and mass limits as described in [49], using the method from [50]. The limit calculation is described in Chapter 9.

Chapter 9

Results and Interpretations

9.1 The Slepton as the NLSP

The analysis presented in this thesis covers NLSP lifetimes roughly between 10^{-11} s and 10^{-9} s (**short lifetime**), corresponding to a proper decay length of $0.3 - 30$ cm. According to formulae (2.4) and (2.5), this corresponds, for pair–production of a slepton with a mass of $100\,\mathrm{GeV}/c^2$, to a $\sqrt{F/k}$ range of $234 - 740\,\mathrm{TeV}/c^2$, where $\sqrt{F}$ is the SUSY breaking scale and k a model–dependent parameter ($k < 1$), or a gravitino mass between 13.1 eV and 131 eV. To cover all possible values for $\sqrt{F}$, however, shorter and longer lifetimes should be included as well. For this reason the analysis presented was combined with complementary analyses performed at OPAL. This allows upper limits on the production cross–sections as a function of the lifetime to be calculated. Furthermore, lifetime–independent limits on the slepton masses were obtained for slepton pair–production in the slepton co–NLSP scenario and staus in the stau NLSP scenario.

The analyses used for the combination and the combination procedure are briefly outlined in Sect. 9.1.1. The combined cross–section limits for slepton pair–production in the slepton co–NLSP scenario and staus in the stau NLSP scenario are discussed in Sect. 9.1.2. In Sect. 9.1.3 the determination of the slepton mass limits is described. In Sections 9.1.4–9.1.6 cross–section limits are presented for the three indirect production channels.

9.1.1 Combination of Slepton NLSP Searches

The other analyses used for the combination are described only briefly. Details can be found in the references given below.

Zero Lifetime

- *Search for acoplanar leptons:*
  If sleptons are pair–produced and decay promptly to a lepton and a gravitino each (2–lepton and 2–tau channel), only the lepton tracks are visible in the detector, along with a significant amount of missing energy and missing transverse momentum due to the invisible gravitinos. An OPAL analysis, developed for MSSM signatures, is sensitive to this topology. Since this topology suffers from irreducible background from fully leptonic $\mathrm{W^+W^-}$ decays, $\mathrm{W^+W^-} \to \ell^+\nu\ell^-\bar{\nu}$, it gives the lowest slepton mass constraints, thus limiting the "all lifetime" mass limits. Details of this analysis can be found in [51].

- *Search for events with ≥ 4 leptons plus missing energy:*
  This analysis is used for the 4–lepton and 6–lepton channels, where, for promptly decaying sleptons, the topology is four or more primary tracks and missing energy. Although this analysis has several applications, it was originally developed for GMSB

searches. The same basic selection is used for the 4– and 6–lepton channel, with only one cut omitted for the latter. Details of this analysis are described in [52].

Medium Lifetime

- *Search for tracks with kinks:*
  For lifetimes of the order of $10^{-9} - 10^{-8}$ s, the primary charged particle will, in general, reach the jet chamber and there produce enough hits (at least ten hits are required by the track reconstruction software) to allow for the reconstruction of its track. The decay of the primary particle to a charged and a neutral particle leads to the topology of a track with a measurable kink. An OPAL analysis searching for such tracks was developed for the GMSB topologies described in this work. This analysis was optimised separately for the 2–lepton/2–tau, 4–lepton and 6–lepton topology. Details about these three selections can be found in [40].

Quasi–Infinite Lifetime

- *Search for pair–produced heavy stable charged particles:*
  If the pair–produced sleptons are stable or decay outside the detector, two back–to–back tracks will be visible in the detector. Due to their large masses the sleptons are highly ionising and their tracks will distinguish themself from "ordinary" tracks by their anomalous specific energy loss $\mathrm{d}E/\mathrm{d}x$. A highly efficient OPAL search exists for this almost background–free topology. It is described in [53].

  A more generalised search for heavy stable charged particles, with sensitivity also to final states where the tracks with anomalous $\mathrm{d}E/\mathrm{d}x$ are not back–to–back, is presently in preparation at OPAL. The results are not available yet and hence cannot be used in the combination.

In Table 9.1 a summary of the analysis methods used for the different channels and lifetime ranges is given. The second part of this table refers to channels in the neutralino NLSP scenario. These channels are discussed in Sect. 9.2.

All results from previous OPAL searches used in the combination are preliminary.

	NLSP Lifetime			
Channel	zero l.t.	short l.t.	medium l.t.	quasi–infinite l.t.
$\tilde{\ell}^+_R\tilde{\ell}^-_R$ (2–lepton)	acoplanar leptons	large d_0	kinks	heavy stable particles
$\tilde{\chi}^0_1\tilde{\chi}^0_1$ (4–lepton)	≥ 4 leptons + $\not\!\!E$	large d_0	kinks	–
$\tilde{\ell}^+_R\tilde{\ell}^-_R$ (6–lepton)	≥ 4 leptons + $\not\!\!E$	large d_0	kinks	–
$\tilde{\chi}^+_1\tilde{\chi}^-_1$	acoplanar leptons	large d_0	kinks	–
$\tilde{\chi}^0_1\tilde{\chi}^0_1$	single and acoplanar photons			–
$\tilde{\chi}^+_1\tilde{\chi}^-_1$	photons+leptons/jets+$\not\!\!E$		acoplanar leptons / MSSM $\tilde{\chi}^+_1$ searches	
$\tilde{\ell}^+_R\tilde{\ell}^-_R$	photons+leptons/jets+$\not\!\!E$		acoplanar leptons	

Table 9.1: *Summary of the analysis methods used for the different channels and NLSP lifetimes. The channels in the slepton NLSP case are listed in the upper four lines, while in the lower three lines channels in the neutralino NLSP scenario are listed (see Sect. 9.2). All analyses are briefly described in the text.*

For all channels the results from several analyses were combined. Although the different analyses are sensitive to distinct topologies, some overlap between them is expected. To properly treat the overlaps between the various analyses, all analyses use the same signal Monte Carlo samples. This allows, via an event–by–event comparison of the selected signal, for the determination of the signal overlaps between all combinations of the analyses used in each channel. The efficiencies were described by empirically determined functions of the lifetime, $\sqrt{s}$ and $\beta\gamma$, as discussed in Chapt. 6. The selection efficiencies were split in "exclusive selection efficiencies" and "overlap efficiencies". The efficiency for events that are selected by only *one* analysis are denoted as exclusive selection efficiencies. Events that are selected by two (or even three) analyses are described by overlap efficiencies. For example, for the case of three analyses, there are, in total, three exclusive selection efficiencies and four overlap efficiencies (three for the overlaps between each two analyses and one for the overlap among all three analyses). An overlap was only considered if its efficiency exceeded 0.1 %. All efficiencies, i.e. exclusive selection efficiencies and "significant" overlap efficiencies, were determined with the method explained in Chapt. 6. The various "overlap selections" were treated as separate channels in the limit calculation. The overlaps between the different analyses was carefully investigated for data as well as background events, but no overlap was found for the candidates. The overlap for the background was found to be negligible (< 0.01 events) in all slepton NLSP channels (for the neutralino NLSP channels there is one exception; see Sect. 9.2). In the cases where a tiny overlap of the background events was found, this is mentioned in the respective sections.

A likelihood ratio method [49] was used for the calculation of all limits. In this method, the likelihood ratio is used as estimator X for the computation of the confidence level CL_s, defined as

$$\mathrm{CL}_s = \frac{\mathrm{CL}_{s+b}}{\mathrm{CL}_b} \,. \tag{9.1}$$

CL_{s+b} is the probability that the experimental outcome is compatible with the signal–and–background hypothesis and CL_b is the probability that the experimental outcome is compatible with the background–only hypothesis. The estimator is a function that separates "signal–like" experimental outcomes from "background–like" ones. The likelihood ratio for a channel i is defined as

$$X_i = \frac{e^{-(s_i+b_i)}(s_i+b_i)^{n_i}}{n_i!} \Big/ \frac{e^{-(b_i)}b_i^{n_i}}{n_i!} \,, \tag{9.2}$$

where s_i is the number of signal events expected for channel i, b_i is the estimated background and n_i is the number of candidates in this channel. The estimator for a set of N channels is the product of the individual estimators:

$$X = \prod_{i=1}^{N} X_i \,. \tag{9.3}$$

A point in the parameter plane studied (e.g. the slepton mass – lifetime plane) is excluded at 95 % confidence level (C.L.), if it gives a $\mathrm{CL}_s < 0.05$, while points with $\mathrm{CL}_s > 0.05$ are allowed. The point with $\mathrm{CL}_s = 0.05$ determines the mass limit.

9.1.2 Cross–Section Limits for Slepton Pair–Production

To obtain constraints on the production cross–sections for slepton pair–production in the slepton co–NLSP scenario and stau pair–production in the stau NLSP scenario the following four analyses were combined: the search for acoplanar leptons, the search for tracks with large impact parameters described in this work, the search for tracks with kinks and the search for heavy stable charged particles. A significant overlap was found between the acoplanar lepton and large impact parameter search (maximal overlap efficiency $\epsilon \approx 40\,\%$), between the acoplanar lepton and kink search ($\epsilon \approx 4\,\%$), between the large impact parameter and kink search ($\epsilon \approx 7\,\%$), and between the kink and heavy stable charged particle search ($\epsilon \approx 20\,\%$). The efficiencies for staus at some mass points, as examples, are shown in Fig. 9.1. The overlap between the data and background events of the four analyses was checked and no overlap was found for the data, while for the background an overlap of ≈ 0.01 events was found between the large impact parameter and acoplanar lepton searches in the selectron channel at $\sqrt{s} = 189\,\mathrm{GeV}$ and the stau channel at $\sqrt{s} = 189$ and $205\,\mathrm{GeV}$.

The efficiency of the search for heavy stable charged particles are, in general, smallest for masses around $60\,\mathrm{GeV}/c^2$. This effect is due to the fact that in this selection tracks with anomalous $\mathrm{d}E/\mathrm{d}x$ are searched for. The $\mathrm{d}E/\mathrm{d}x$ curve for a given slepton mass crosses the $\mathrm{d}E/\mathrm{d}x$ band of the Standard Model particles for certain momenta, or equivalently, since the particles are pair–produced, certain center–of–mass energies. This means that for the center–of–mass energy where this happens discrimination power is lost, while for other $\sqrt{s}$ the $\mathrm{d}E/\mathrm{d}x$ can still be outside the Standard Model band. Therefore the sensitivity for the affected masses can be enhanced by using data at different center–of–mass energies. For this reason the data at $\sqrt{s} = 183\,\mathrm{GeV}$ ($\int\mathcal{L} = 56.3\,\mathrm{pb}^{-1}$), $\sqrt{s} = 171\,\mathrm{GeV}$ ($\int\mathcal{L} = 10.4\,\mathrm{pb}^{-1}$), $\sqrt{s} = 161\,\mathrm{GeV}$ ($\int\mathcal{L} = 10.0\,\mathrm{pb}^{-1}$) and $\sqrt{s} = 130 - 136\,\mathrm{GeV}$ ($\int\mathcal{L} = 10.7\,\mathrm{pb}^{-1}$), taken in the years 1997, 1996 and 1995, were also included in the search for heavy stable charged particles.

For the combination of the results at different center–of–mass energies the expected cross–sections described in Sec. 7.1 were used. Limits were calculated for 60 slepton lifetimes between $10^{-12}\,\mathrm{s}$ and $10^{-6}\,\mathrm{s}$, and 60 slepton masses between $45\,\mathrm{GeV}/c^2$ and $105\,\mathrm{GeV}/c^2$ (i.e. $1\,\mathrm{GeV}/c^2$ steps).

The resulting cross–section limits at 95 % C.L. and for $\sqrt{s} = 208.1\,\mathrm{GeV}$ for selectrons, smuons and staus in the slepton co–NLSP scenario and staus in the stau NLSP scenario in the $\log(\tau) - M_{\tilde{\ell}}$ plane are shown in Fig. 9.2. For all slepton flavours the weakest exclusion is found in the very short lifetime region ($\tau = 10^{-12} - 10^{-11}\,\mathrm{s}$), due to the irreducible background from $\mathrm{W}^+\mathrm{W}^-$ production in the acoplanar lepton topology. Also, the smaller sensitivity for long lifetimes and masses around $60\,\mathrm{GeV}/c^2$, due to the effect described above, is clearly visible in all channels.

The best constraints are obtained for smuons (Fig 9.2 (b)), with an upper limit of at most 0.05 pb in the whole plane (apart from the region with a smuon mass above $100\,\mathrm{GeV}/c^2$, close to the kinematic limit), and at most 0.02 pb in a large part of the plane. For selectrons the constraints are slightly weaker: here cross–sections larger than 0.08 pb can be excluded in most of the selectron mass – lifetime plane. The difference between smuons and selectrons is explained by the fact that selectrons can be produced in the t–channel, which leads to a more forward production and thus to lower efficiencies. Finally, for staus cross–sections larger than 0.1 pb are excluded in most of the stau mass – lifetime plane, and cross–sections larger than 0.03 pb are excluded in a large part of the plane. The stau limits in the slepton co–NLSP scenario and the stau NLSP scenario are rather similar, with a small difference due to the slightly different theoretical cross–sections that are used for the combination of the results at various center–of–mass energies.

If the search for tracks with large impact parameters is not included in the combination, the cross–section limits are almost an order of magnitude worse for lifetimes around $10^{-10}\,\mathrm{s}$. This is shown in Fig. 9.3 for stau pair–production in the slepton co–NLSP scenario. For the calculation of the limits shown in this plot the searches for acoplanar leptons, for kinks and

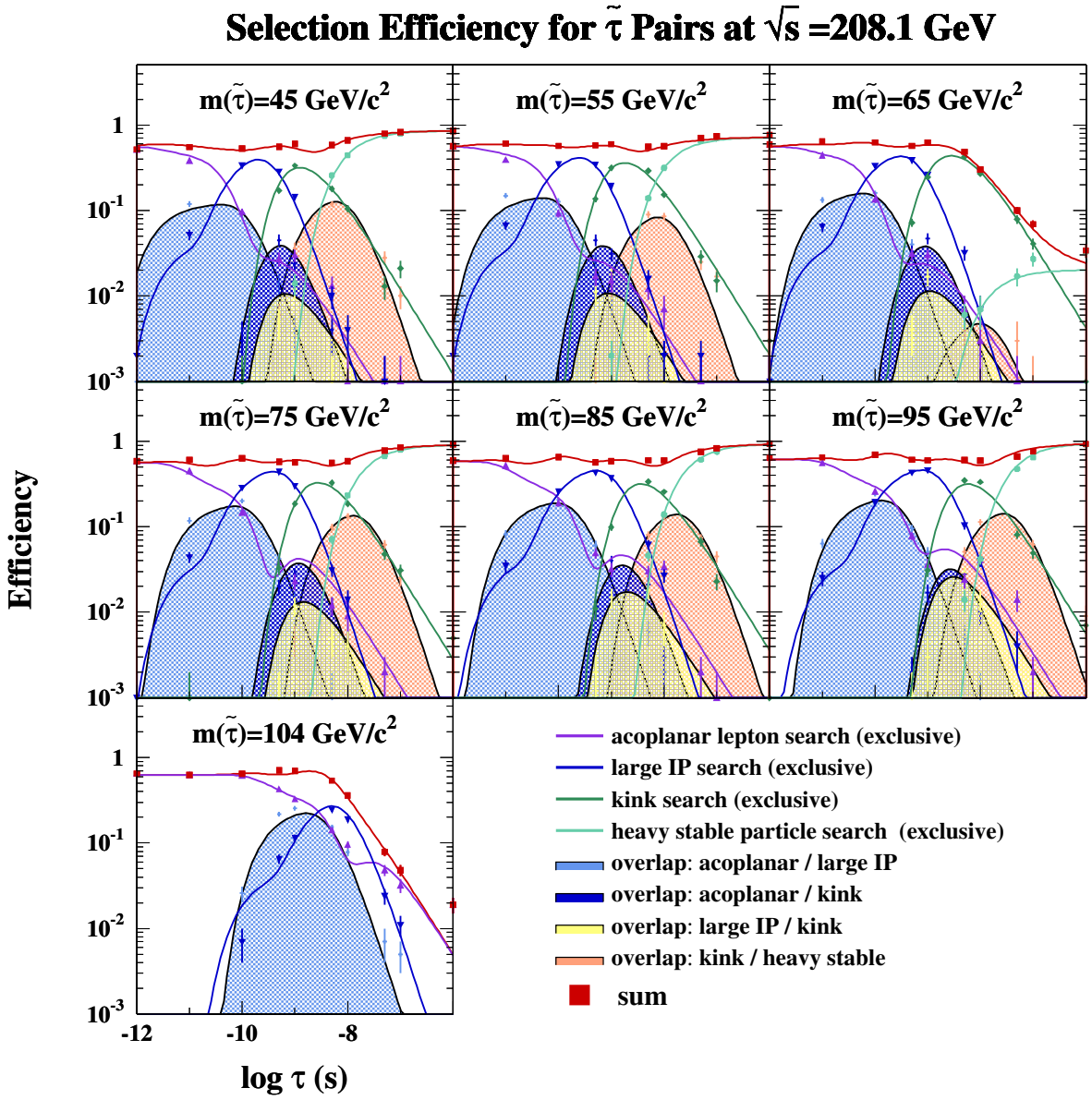


Figure 9.1: *Efficiencies for stau pair–production (both for the slepton co–NLSP scenario and the stau NLSP scenario) at $\sqrt{s} = 208.1$ GeV, as a function of the lifetime. In each plot the efficiencies are shown for a different stau mass between 45 GeV/c^2 and 104 GeV/c^2. The symbols represent the efficiencies for ten simulated lifetimes and the lines show the efficiency functions for events which are selected by the search for promptly decaying staus (violet), the search for large impact parameters (dark blue), the search for kinks (dark green) or the search for stable staus (light green) exclusively. The overlap efficiencies between these searches are shown as filled histograms if they exceed 0.1 %. The sum of all efficiencies, i.e. the four exclusive selection efficiencies and the four overlap efficiencies, is shown by the red squares and the corresponding red line.*

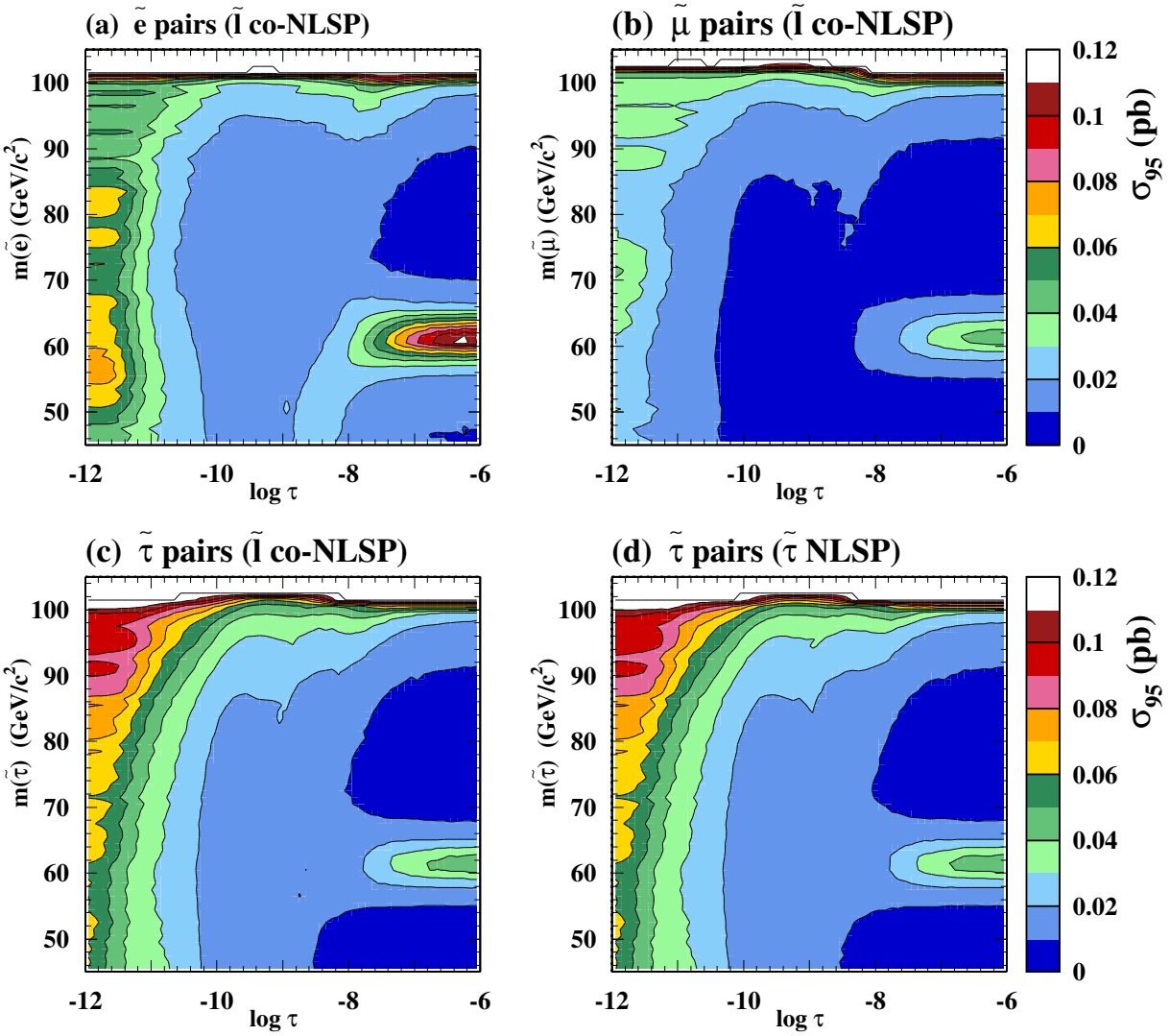


Figure 9.2: *Contours of the 95 % C.L. upper limits on the production cross–sections for slepton pair–production at $\sqrt{s}$ = 208 GeV in the slepton mass – lifetime plane. Shown are cross–section limits for (a) selectrons, (b) smuons and (c) staus in the slepton co–NLSP scenario and (d) staus in the stau NLSP scenario. The colours correspond to different ranges of the 95 % C.L. upper limit on the cross–section, as indicated by the colour map on the right side. For the calculation of these limits four analyses were combined: the searches for acoplanar leptons, for large impact parameters, for kinks and for heavy stable charged particles. The data taken in the years 1998–2000 (plus 1995–1997 for the search for heavy stable charged particles) are included.*

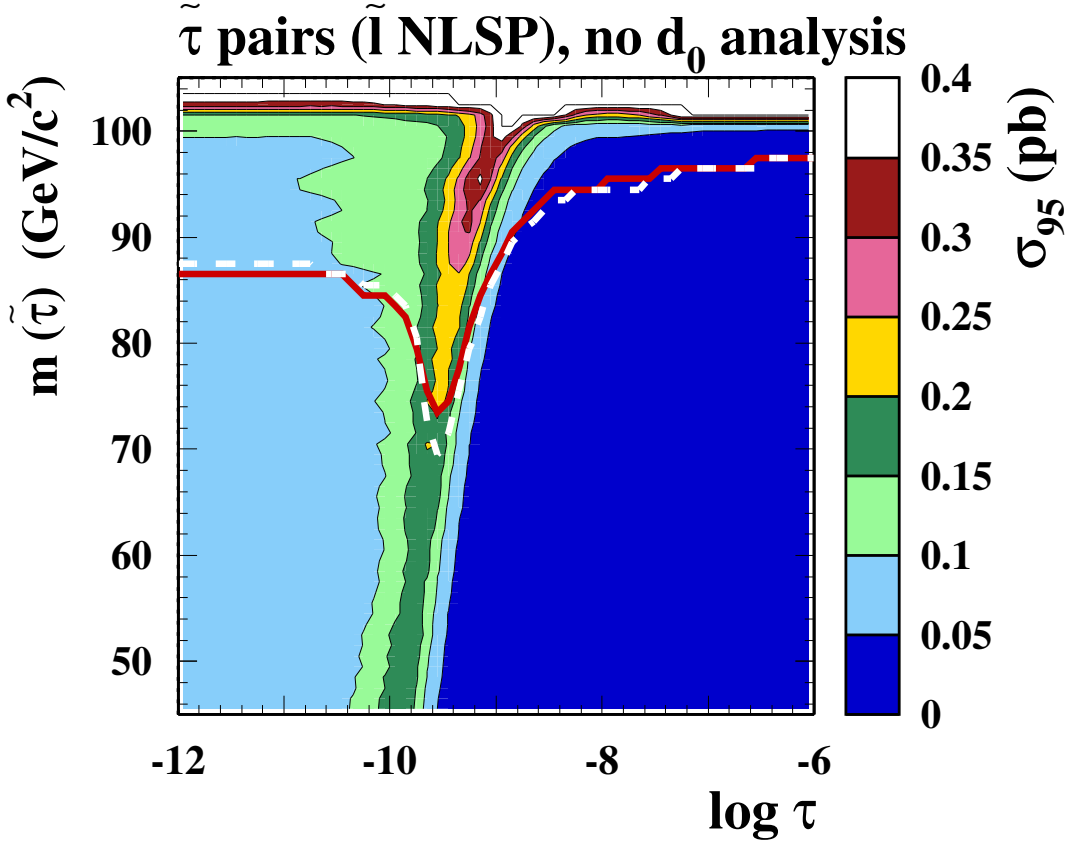


Figure 9.3: *Contours of the 95 % C.L. upper limits on the production cross–sections for stau pair–production in the slepton co–NLSP scenario at $\sqrt{s} = 208$ GeV in the stau mass – lifetime plane, without the search for tracks with large impact parameters. The colours correspond to different ranges of the 95 % C.L. upper limit on the cross–section, as indicated by the colour map on the right side. The scale for σ_{95} is different as in Fig. 9.2, to account for the now much weaker limits on the cross–section. The observed and expected mass limits are shown as solid red and dashed white lines, respectively. For the calculation of these limits three analyses were combined: the searches for acoplanar leptons, for kinks and for heavy stable charged particles.*

for heavy stable charged particles were combined. These weaker cross–section limits lead to much lower slepton mass limits, as discussed in the next section.

9.1.3 Constraints on the Slepton Masses

From the cross–section limits obtained for slepton pair–production in the slepton co–NLSP scenario and stau pair–production in the stau NLSP scenario, constraints on the slepton masses were determined . To obtain more precise mass limits than possible with the $1\,\mathrm{GeV}/c^2$ binning used for the calculation of the cross–section limits, the regions around the observed limits were re–scanned with a finer $200\,\mathrm{MeV}/c^2$ binning. The observed lower limits on the slepton masses at 95% C.L. in the $\log(\tau)-M_{\tilde{\ell}_R}$ and $\log(\tau)-M_{\tilde{\tau}_1}$ plane are shown as red lines in Fig. 9.4 for (a) selectrons, (b) smuons and (c) staus in the slepton co–NLSP scenario and (d) staus in the stau NLSP scenario. For each slepton flavour, the lowest mass constraints are found in the region with very short slepton lifetimes, with exception of the selectrons, where the region around $60\,\mathrm{GeV}/c^2$ cannot be excluded for long lifetimes. This is due to the effect of the crossing of the $\mathrm{d}E/\mathrm{d}x$ curves of heavy and Standard Model particles, described in detail in Sect. 9.1.2. For smuons and staus, though, this region can be excluded, because the expected cross–section is higher and the upper limit on the cross–section lower than for selectrons.

To obtain slepton mass limits that are valid for all slepton lifetimes, the cross–sections obtained by these "fine scans" were used to extract the most conservative limit by scanning over the lifetime. The resulting cross–section limits valid for all slepton lifetimes are shown in Fig. 9.5 as a function of the slepton mass for (a) selectrons, (b) smuons and (c) staus in the slepton co–NLSP scenario and (d) staus in the stau NLSP scenario. The expected cross–sections times branching ratio squared ($\sigma_{\mathrm{exp}}\cdot\mathrm{BR}^2$) at $\sqrt{s} = 208.1\,\mathrm{GeV}$, obtained from the minimisation in the GMSB parameter scan described in Sect. 7.1, are superimposed in these plots. The lower mass limits are given by the intersection points between $\sigma_{\mathrm{exp}}\cdot\mathrm{BR}^2$ and the observed upper cross–section limits.

The lower mass constraints at 95% C.L. for selectrons, smuons and staus in the slepton co–NLSP scenario are $m_{\tilde{\mathrm{e}}_\mathrm{R}} > 60.1\,\mathrm{GeV}/c^2$, $m_{\tilde{\mu}_\mathrm{R}} > 93.7\,\mathrm{GeV}/c^2$ and $m_{\tilde{\tau}_1} > 87.4\,\mathrm{GeV}/c^2$, respectively. In the stau NLSP scenario, staus with masses below $87.4\,\mathrm{GeV}/c^2$ are excluded at 95 % C.L.. The expected limits are $m_{\tilde{\mathrm{e}}_\mathrm{R}} > 60.0\,\mathrm{GeV}/c^2$, $m_{\tilde{\mu}_\mathrm{R}} > 93.6\,\mathrm{GeV}/c^2$, $m_{\tilde{\tau}_1} > 88.2\,\mathrm{GeV}/c^2$ (slepton co–NLSP scenario) and $m_{\tilde{\tau}_1} > 87.6\,\mathrm{GeV}/c^2$ (stau NLSP scenario). The slepton mass constraints are valid for all slepton lifetimes.

Without the search for tracks with large impact parameters presented in this work, a mass limit for the stau in the slepton co–NLSP scenario of $74.5\,\mathrm{GeV}/c^2$ would be observed, with an expected limit of $69.5\,\mathrm{GeV}/c^2$. The observed and expected limits are shown in Fig. 9.3.

Since the expected cross–sections are taken from a minimisation within the scanned GMSB parameter space (see Sec. 7.1), the mass limits are valid for all points within this scan. In particular, a messenger index $N \leq 5$ is assumed. For smuons and staus, where only s–channel production is possible, no strong dependence of the expected cross–sections on N was found. For selectrons, however, the cross–section in the t–channel depends on N, since the mass of the exchanged neutralino rises with N. This leads to a decrease of the minimal expected cross–section, and results in a lower mass limit for the selectron. However, as discussed in Chapter 7, very large values for N are theoretically disfavoured, if perturbativity of the gauge interactions up to the grand unification scale is required. E.g., for a messenger mass scale of $M = 100\,\mathrm{TeV}/c^2$, the relation $N \leq 5$ has to be fulfilled.

In the slepton co–NLSP scenario the sleptons are (by definition) degenerate within the stau mass, so that decays $\tilde{\ell} \to \ell\tilde{\chi}_1^0 \to \tilde{\tau}\tau\ell$ (with $\ell = \mu$, e) are forbidden. Therefore the smuon mass limit of $m_{\tilde{\mu}_\mathrm{R}} > 93.6\,\mathrm{GeV}/c^2$ can be used to deduce an indirect common mass limit on all sleptons of $m_{\tilde{\ell}} > 91.8\,\mathrm{GeV}/c^2$ within the slepton co–NLSP scenario.

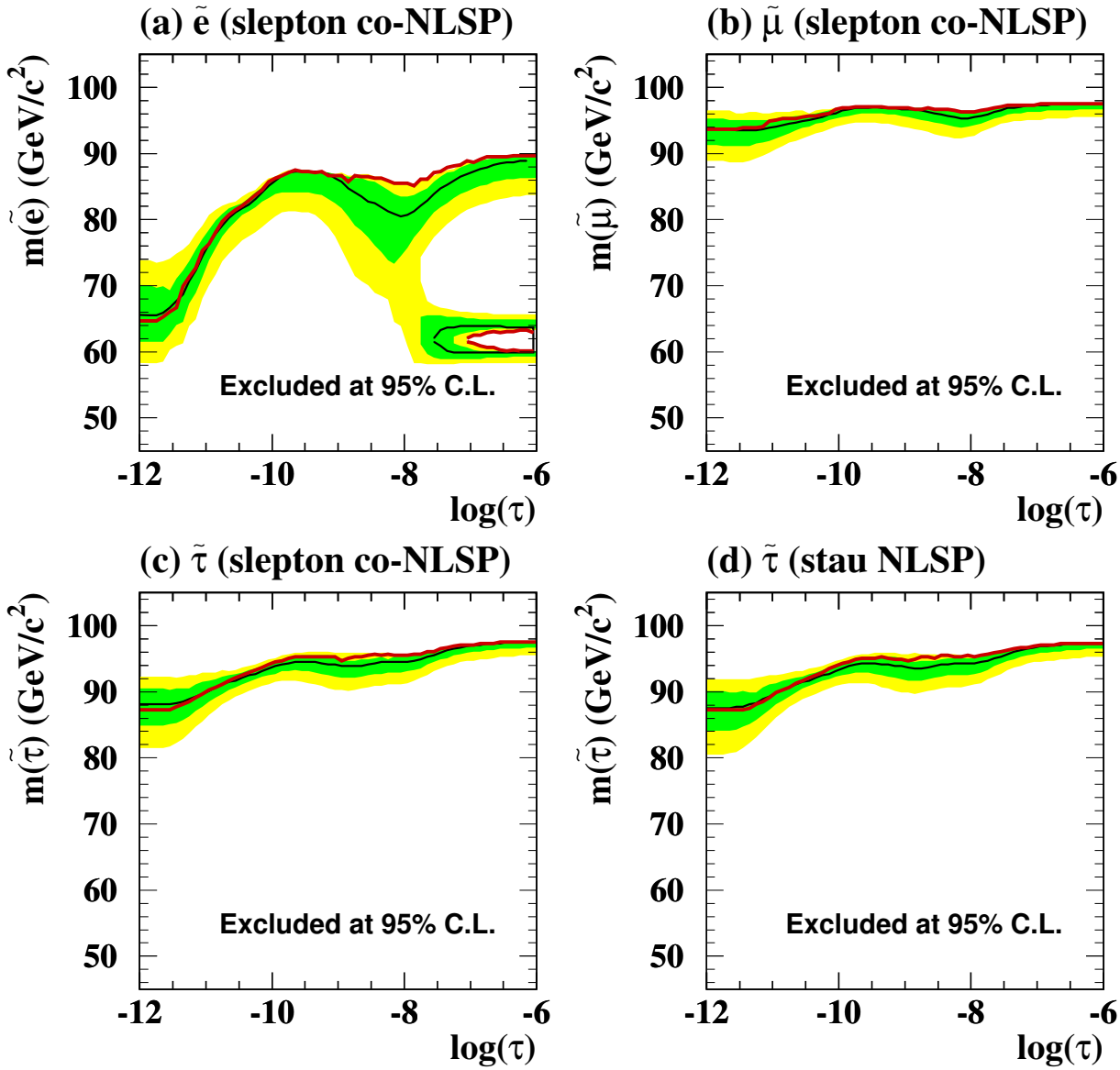


Figure 9.4: *The red lines represent the observed lower mass limits for $\sqrt{s} = 208$ GeV for (a) selectron, (b) smuon, and (c) stau pair–production in the slepton co–NLSP scenario and (d) stau pair–production in the stau NLSP scenario, as a function of the slepton lifetime. The region below this line is excluded at 95 % C.L.. The mass limits are valid for a messenger index $N \leq 5$. The data taken in the years 1998 to 2000 (plus 1995–1997 for the search for heavy stable charged particles) are included. The black lines represent the median expectations. The 68 % and 95 % probability intervals, centred on the median, are shown as green and yellow bands, respectively.*

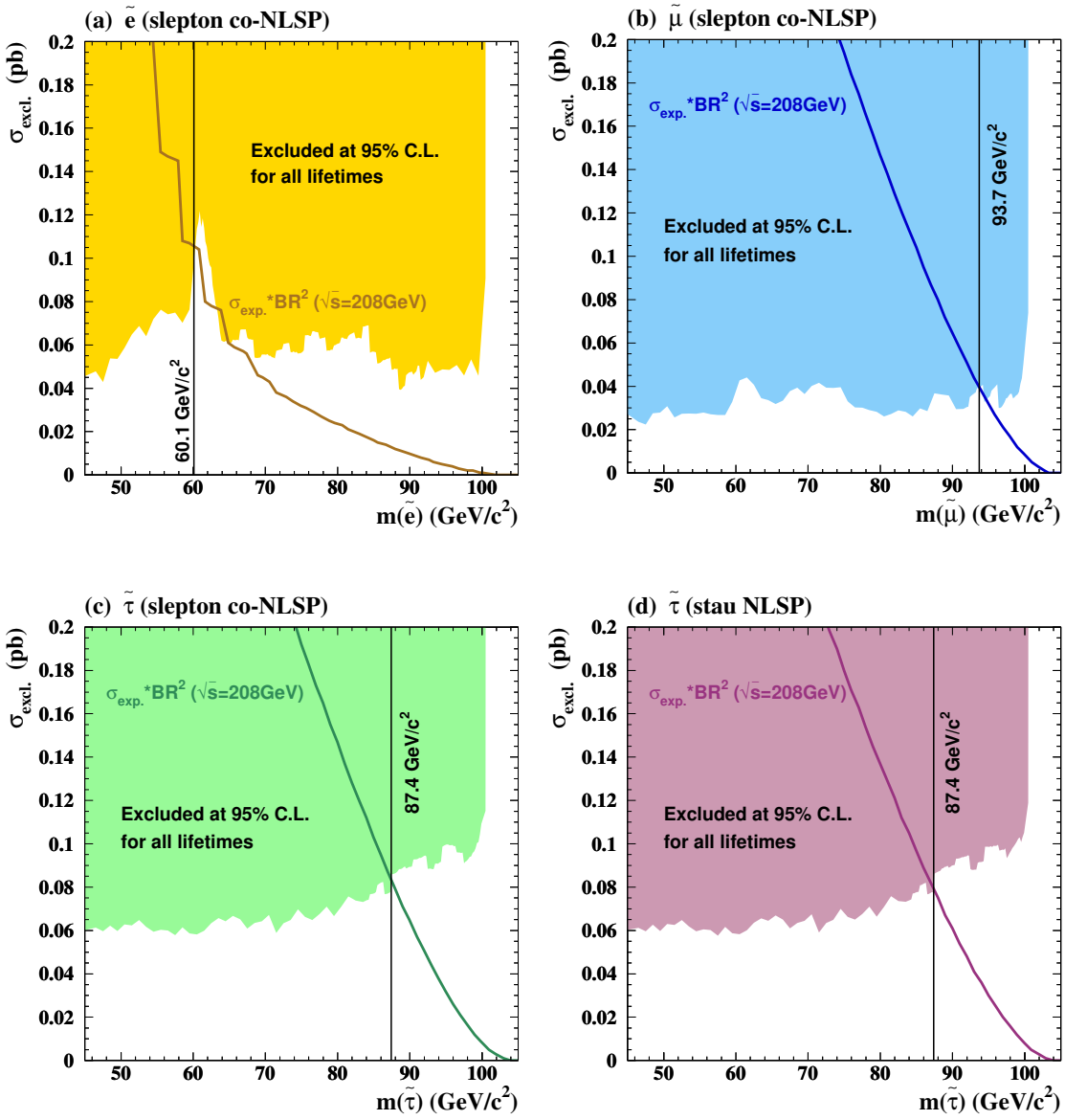


Figure 9.5: *The maximal excluded cross–sections at* 95 *% C.L. for* $\sqrt{s} = 208$ *GeV, valid for all lifetimes, are shown as filled histograms for (a) selectron, (b) smuon, (c) stau pair–production in the slepton co–NLSP scenario, and (d) stau pair–production in the stau NLSP scenario. These limits were obtained by a scan of the excluded cross–sections over all lifetimes for each slepton mass. The data taken in the years 1998 to 2000 (plus 1995–1997 for the search for heavy stable charged particles) are included. Superimposed as a solid coloured line is the minimum expected cross–section times branching ratio squared,* $\sigma_{\mathrm{exp}} \cdot BR^2$*, for each flavour. The expectations were obtained by the method described in Sect. 7.1. The intersection point of the expected and observed cross–sections gives the lower mass limit at 95 % C.L.. Mass limits of* $60.1\,GeV/c^2$ *for selectrons,* $93.7\,GeV/c^2$ *for smuons and* $87.4\,GeV/c^2$ *for staus in the slepton co–NLSP scenario and* $87.4\,GeV/c^2$ *for staus in the stau NLSP scenario are obtained. These mass limits are valid for all slepton lifetimes and for a messenger index* $N \leq 5$*.*

9.1.4 Cross–Section Limits for Neutralino Pair–Production

For neutralino pair–production with a slepton NLSP three analyses were combined: the search for events with ≥ 4 leptons plus missing energy, the large impact parameter search and the search for kinks. No selection is available yet for the case of very long slepton lifetimes, where acoplanar tracks with anomalous $\mathrm{d}E/\mathrm{d}x$ plus additional "normal" tracks are expected. A dedicated analysis is being prepared at OPAL and will be included in the future. Significant overlaps exist between the search for ≥ 4 leptons plus missing energy and the large impact parameter search ($\epsilon_{\max} \approx 22\,\%$), and between the large impact parameter and the kink search ($\epsilon_{\max} \approx 13\,\%$). For the background, an overlap of ≈ 0.01 events was found between the search for ≥ 4 leptons plus missing energy and the large impact parameter search at $\sqrt{s} = 189\,\mathrm{GeV}$. The data with $\sqrt{s} = 189 - 208\,\mathrm{GeV}$ were combined assuming a β/s dependence of the cross–sections.

Two scenarios exist in the theory: in the stau NLSP scenario the neutralino decays with 100 % branching ratio to $\tilde{\tau}_1\tau$, while in the slepton co–NLSP scenario it decays with equal branching fractions to all flavours. Both cases were studied.

For the slepton co–NLSP case the three exclusive selection efficiencies and the two significant overlap efficiencies are shown in Fig. 9.6 together with the total efficiency. As expected, due to the absence of a very long lifetime selection, the total efficiency decreases rather rapidly for lifetimes longer than $10^{-8}\,\mathrm{s}$. However, it does not vanish completely, since the search for ≥ 4 leptons plus missing energy also has some sensitivity for very long slepton lifetimes. This effect is even more pronounced in the stau NLSP scenario. In this case the tracks from the stable staus and the decay products from the primary taus are present in the detector, leading to the topology of at least four tracks from the vertex plus missing energy from the tau decays. For the smuons and selectrons, however, there is no missing energy, if the sleptons are stable.

For channels with cascade decays to sleptons the cross–sections depend on more than two variables: the mass and lifetime of the slepton (or NLSP in general) and the mass of the primary particle (plus eventually the masses of additional particles involved in the cascade decay). Therefore, for each mass of the primary particle (in steps of $1\,\mathrm{GeV}/c^2$), cross–section limits were calculated as a function of the NLSP mass and lifetime, with the same step sizes as for slepton pair–production. As an example, the cross—section limit in the $\log(\tau) - M_{\tilde{\ell}_R}$ plane, at $\sqrt{s} = 208.1\,\mathrm{GeV}$ and for a neutralino mass of $100\,\mathrm{GeV}/c^2$, is shown in Fig. 9.7 (a) for the slepton co–NLSP case. For this neutralino mass typically cross–sections larger than 0.05 pb can be excluded in the slepton co–NLSP scenario.

To obtain cross–section limits in the $M_{\tilde{\chi}_1^0} - M_{\tilde{\ell}_R}$ plane the lifetime dependence must be accounted for. For each neutralino mass the corresponding cross–section limits in the $\log(\tau) - M_{\tilde{\ell}}$ plane were used to obtain a lifetime–independent value for each slepton mass. For each slepton mass, a scan was performed over the lifetime to obtain the most conservative limit with the highest excluded cross–section. Since no dedicated search was available for the very long lifetimes, this was done in two ways: (1), including in the scan only lifetimes shorter than $10^{-8}\,\mathrm{s}$, corresponding to a proper decay length of 3 m; and, (2), including all lifetimes. In the first case the sensitivity is high for all considered lifetimes, while in the latter case the sensitivity is much reduced. However, since the search for ≥ 4 leptons plus missing energy maintains some efficiency also for very long lifetimes, particularly in the stau NLSP scenario, some sensitivity is achieved also in this case. Due to the relatively large theoretical cross–section for neutralino pair–production, even weak limits can later be used to exclude points in the GMSB parameter space (Section 9.3).

The limits at $\sqrt{s} = 208\,\mathrm{GeV}$, considering only lifetimes up to $10^{-8}\,\mathrm{s}$, for the slepton co–NLSP case are shown in Fig. 9.7 (b). Cross–sections larger than 0.08 pb can be excluded, except for very low mass differences ΔM between the neutralino and the sleptons, and for the region where both the neutralino and the sleptons are very heavy. Cross–sections larger

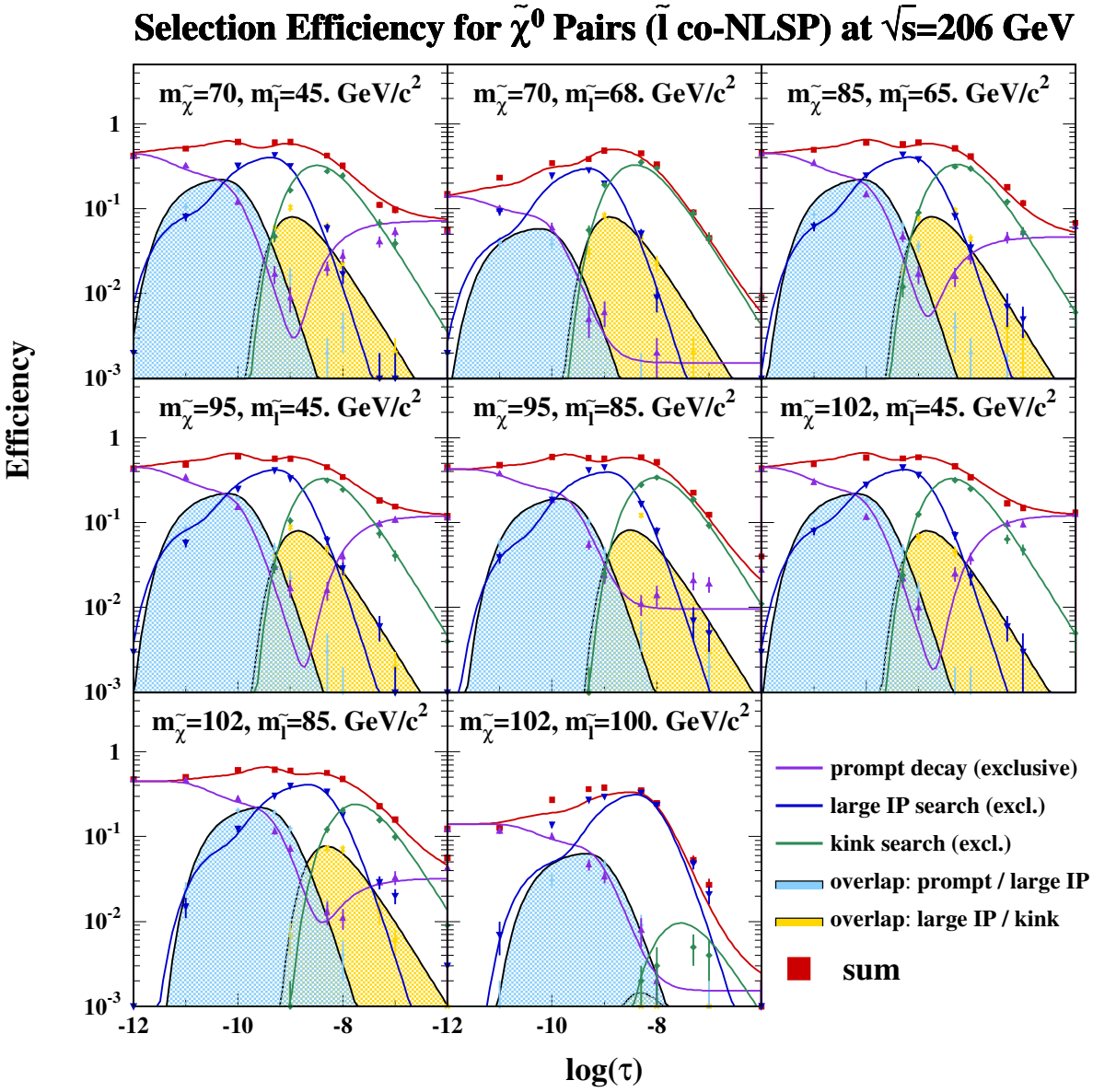


Figure 9.6: *Efficiencies for neutralino pair–production at $\sqrt{s} = 206$ GeV in the slepton co–NLSP scenario, as a function of the lifetime. In each plot the efficiencies are shown for a different neutralino – slepton mass combination. The symbols represent the efficiencies for ten simulated lifetimes and the lines show the efficiency functions for events which are selected by the search for ≥ 4 leptons plus missing energy (violet), the search for large impact parameters (blue) and the search for kinks (green) exclusively. The overlap efficiencies between these searches are shown as filled histograms if they exceed 0.1 %. The sum of all efficiencies, i.e. the three exclusive selection efficiencies and the two relevant overlap efficiencies, is shown by the red squares and the corresponding red line.*

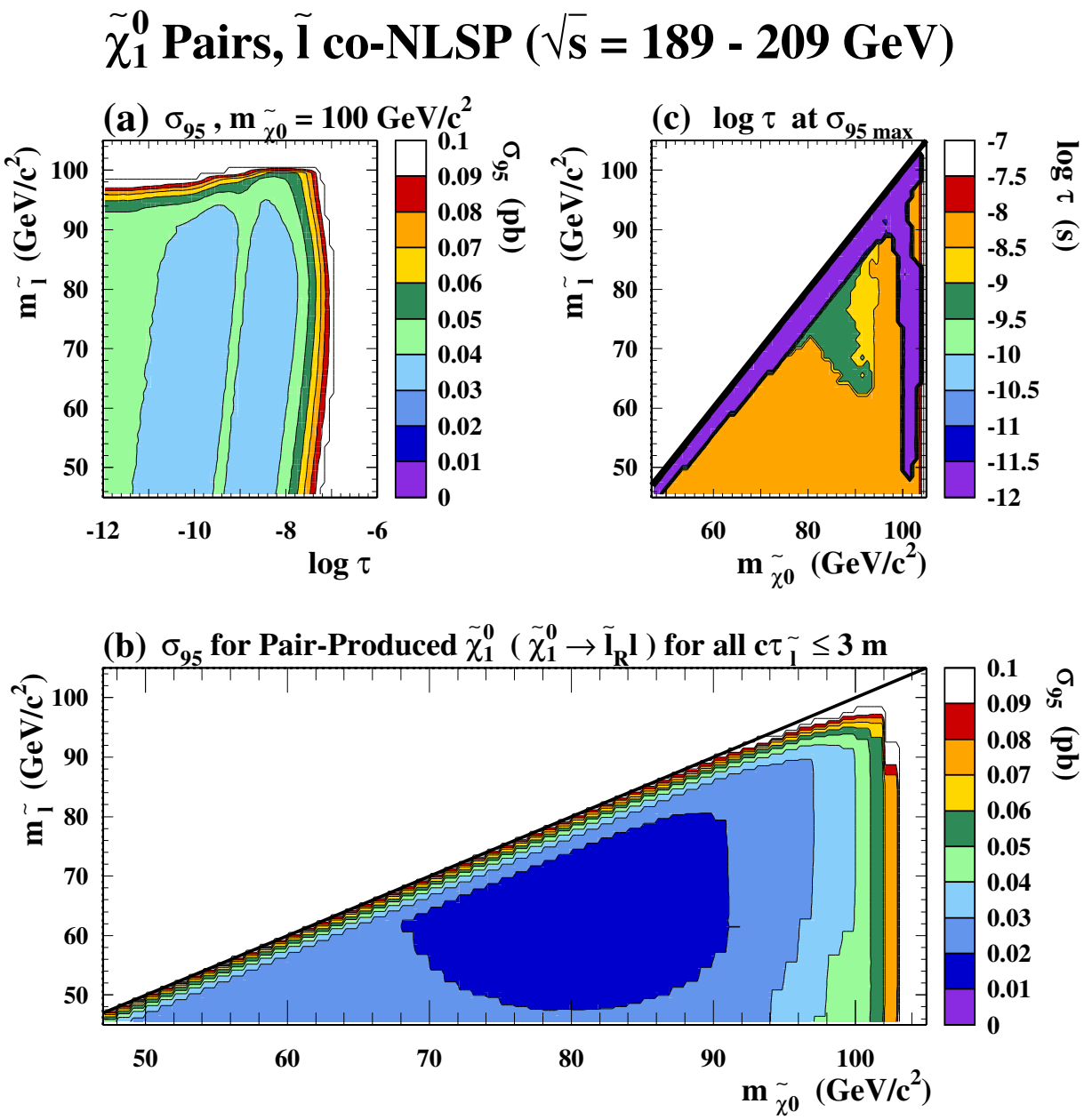


Figure 9.7: *Upper limits at 95 % C.L. on the production cross–section for neutralino pair–production in the slepton co–NLSP scenario at $\sqrt{s} = 208$ GeV. The data taken in the years 1998–2000 were combined assuming a β/s dependence of the cross–sections. Plot (a) shows contours of the excluded cross–section in the $m_{\tilde{\ell}_R}$ – lifetime plane, for a fixed neutralino mass of 100 GeV/c^2. The contours of the maximum excluded cross–section for each point in the $m_{\tilde{\chi}_1^0} - m_{\tilde{\ell}_R}$ plane, after elimination of the lifetime, is shown in (b). It is valid for proper decay lengths up to three metres. Plot (c) shows, for each point in the $m_{\tilde{\chi}_1^0} - m_{\tilde{\ell}_R}$ plane, the lifetimes corresponding to this cross–section limit.*

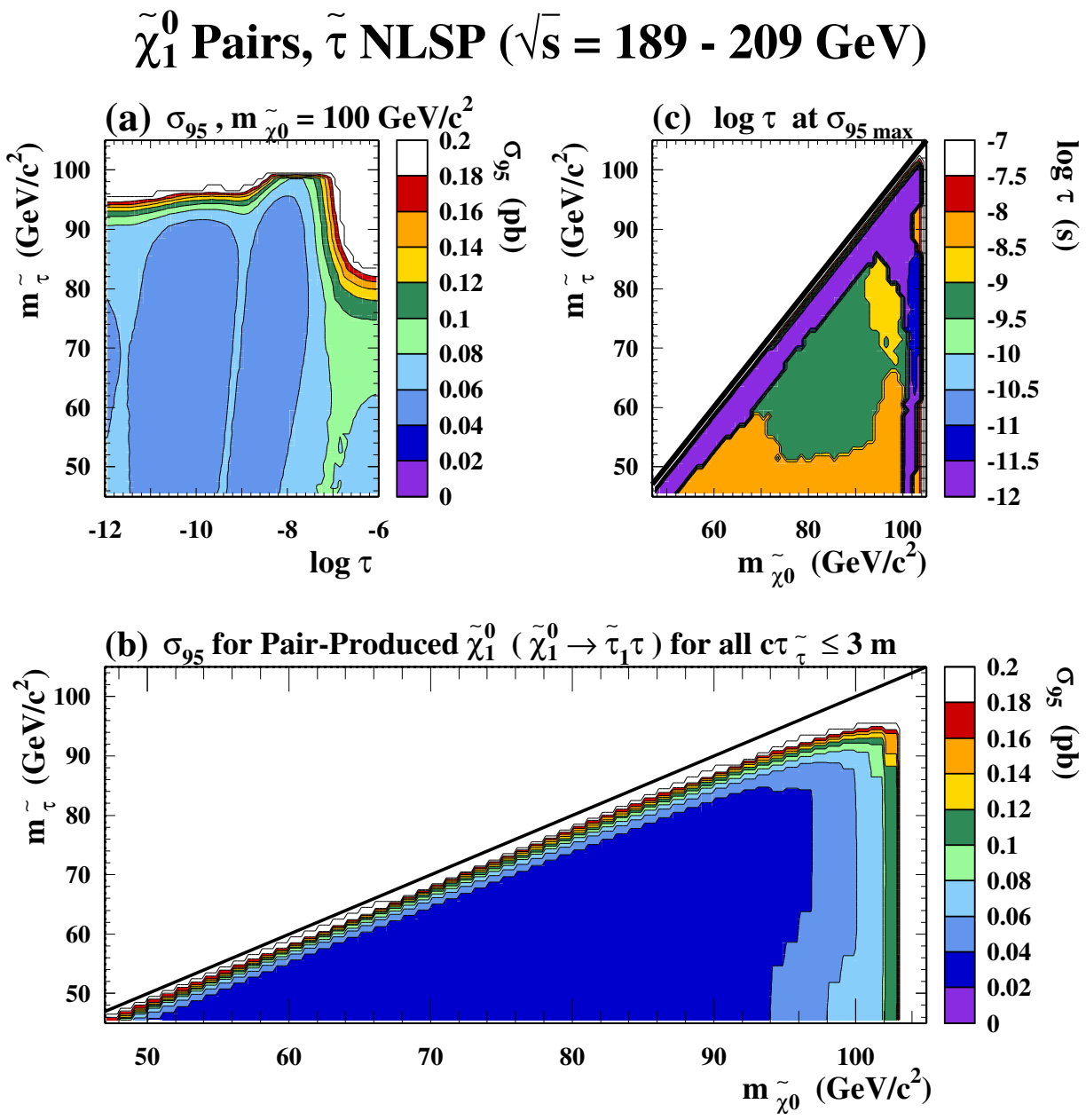


Figure 9.8: *Upper limits at 95 % C.L. on the production cross–section for neutralino pair–production in the stau NLSP scenario at $\sqrt{s} = 208$ GeV. The data taken in the years 1998–2000 were combined assuming a β/s dependence of the cross–sections. Plot (a) shows contours of the excluded cross–section in the $m_{\tilde{\tau}_1}$ – lifetime plane for a fixed neutralino mass of 100 GeV/c^2. The contours of the maximum excluded cross–section for each point in the $m_{\tilde{\chi}_1^0} - m_{\tilde{\tau}_1}$ plane, after elimination of the lifetime, is shown in (b). It is valid for proper decay lengths up to three metres. Plot (c) shows, for each point in the $m_{\tilde{\chi}_1^0} - m_{\tilde{\tau}_1}$ plane, the lifetimes corresponding to this cross–section limit.*

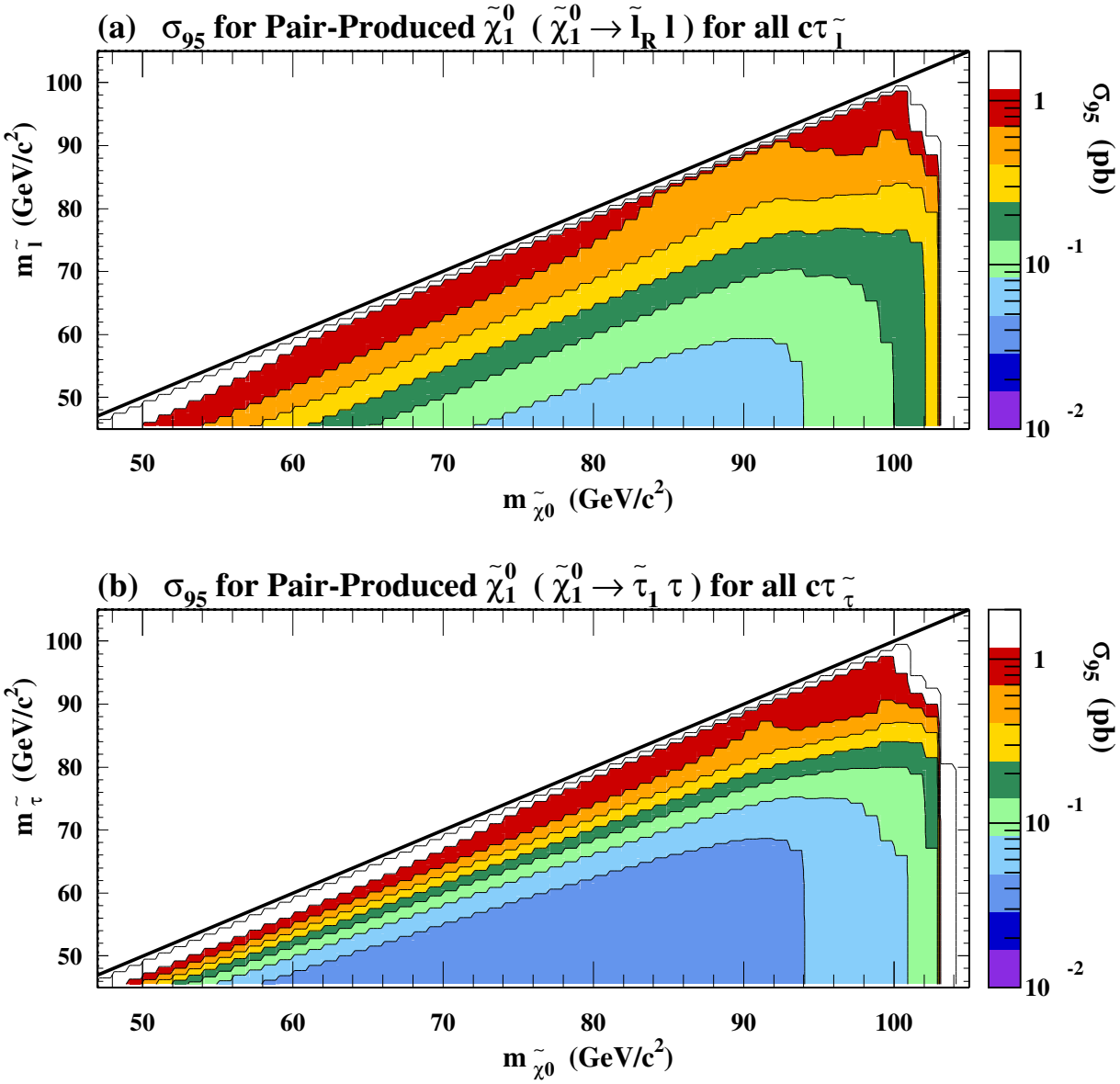


Figure 9.9: *Contours of the upper limits at 95 % C.L. on the production cross–section for neutralino pair–production in (a) the slepton co–NLSP scenario and (b) the stau NLSP scenario at $\sqrt{s} = 208$ GeV. The data taken in the years 1998–2000 were combined assuming a β/s dependence of the cross–sections. All NLSP lifetimes were taken into account.*

than 0.04 pb can be excluded in a large part of the $M_{\tilde{\chi}_1^0} - M_{\tilde{\ell}_R}$ plane.

In Fig. 9.7 (c) the lifetimes corresponding to these limits are shown. For the slepton co–NLSP case in most of the mass plane the weakest limit is found for a lifetime of 10^{-8} s, the longest lifetime considered for the limit calculation. For small ΔM, though, the zero lifetime analysis gives the weakest limit.

The cross–section limit for the stau NLSP case is shown in Fig 9.8. In (a) the cross—section limit in the $\log(\tau) - M_{\tilde{\tau}_1}$ plane, at $\sqrt{s} = 208.1\,\text{GeV}$ and for a neutralino mass of $100\,\text{GeV}/c^2$, is plotted. Typically, cross–sections above 0.08 pb are excluded. The limits at $\sqrt{s} = 208\,\text{GeV}$ in the $M_{\tilde{\chi}_1^0} - M_{\tilde{\tau}_1}$ plane, after elimination of the lifetime, are shown in Fig. 9.8 (b). In the stau NLSP scenario, with, in general, less energy deposited in the detector, the constraints are weaker than in the slepton co–NLSP scenario. Here in most of the mass plane cross–sections larger than 0.08 pb can be excluded, considering stau lifetimes up to 10^{-8} s. For the stau NLSP case, only in a minor part of the plane the highest limit is found for a lifetime of 10^{-8} s (Fig. 9.8 (c)).

The limits calculated including all lifetimes are shown in Fig. 9.9 for both scenarios. In the slepton co–NLSP case, shown in (a), an upper limit below 0.1 pb is found only in a small mass region, while for the stau NLSP case, shown in (b), this is the case in a significant part of the mass plane. In both cases cross–sections larger than 1 pb can be excluded in most of the $M_{\tilde{\chi}_1^0} - M_{\tilde{\ell}_R}$ plane.

9.1.5 Cross–Section Limits for Selectron and Smuon Pair–Production in the Stau NLSP Scenario

For smuon and selectron pair–production with a stau NLSP the same analyses as for neutralino pair–production (Sect 9.1.3) were used in the combination. No analysis covers very long lifetimes, thus the results in this channel are valid for lifetimes up to 10^{-8} s only.

Significant overlaps exist between the search for ≥ 4 leptons plus missing energy and the large impact parameter search ($\epsilon \approx 26\,\%$), between the search for ≥ 4 leptons plus missing energy and the kink search ($\epsilon \approx 10\,\%$) and between the large impact parameter and the kink search ($\epsilon \approx 7\,\%$). For the background, an overlap of ≈ 0.01 events was found between the search for ≥ 4 leptons plus missing energy and the large impact parameter search at $\sqrt{s} = 189\,\text{GeV}$.

Since in this channel the slepton undergoes a cascade decay, $\tilde{\ell}_R \rightarrow \tilde{\chi}_1^0 \ell \rightarrow \tilde{\tau}_1 \tau \ell$ (with $\ell = \mu$, e), the efficiencies depend on four parameters: the smuon mass, the neutralino mass and the stau mass, plus the stau lifetime. This is visible from Fig. 9.10, where the efficiencies of the three analysis and their overlaps are shown for different mass combinations. To eliminate one parameter without losing generality, the efficiency was minimised with respect to the neutralino mass. Then, with two masses and the lifetime left, the same method as for the neutralino pair–production was applied, i.e. for each smuon – stau mass combination the maximum excluded cross–section was extracted by scanning over all lifetimes. The zero lifetime search has some sensitivity also for long lifetimes, as in the neutralino pair–production channel. This sensitivity, however, is lost by the minimisation, and no limits were calculated for the "all lifetime" case.

The data with $\sqrt{s} = 189 - 208\,\text{GeV}$ were combined assuming a β^3/s dependence of the cross–sections.

Cross–section limits at 95 % C.L. and $\sqrt{s} = 208.1\,\text{GeV}$ for a fixed selectron or smuon mass of $100\,\text{GeV}/c^2$ are shown in Fig. 9.11 (a) and 9.12 (a) for selectron and smuon pair–production, respectively. In this example, both for selectron and smuon pair–production cross–sections larger than 0.25 pb are excluded in most of the stau mass – lifetime plane. The cross–section limits in the $M_{\tilde{\ell}_R} - M_{\tilde{\tau}_1}$ plane at $\sqrt{s} = 208.1\,\text{GeV}$, valid for decay lengths $\leq 3\,\text{m}$, are shown in Fig. 9.11 (b) for selectron and 9.12 (b) for smuon pair–production. For both slepton flavours, cross–sections above 0.25 pb are excluded in most

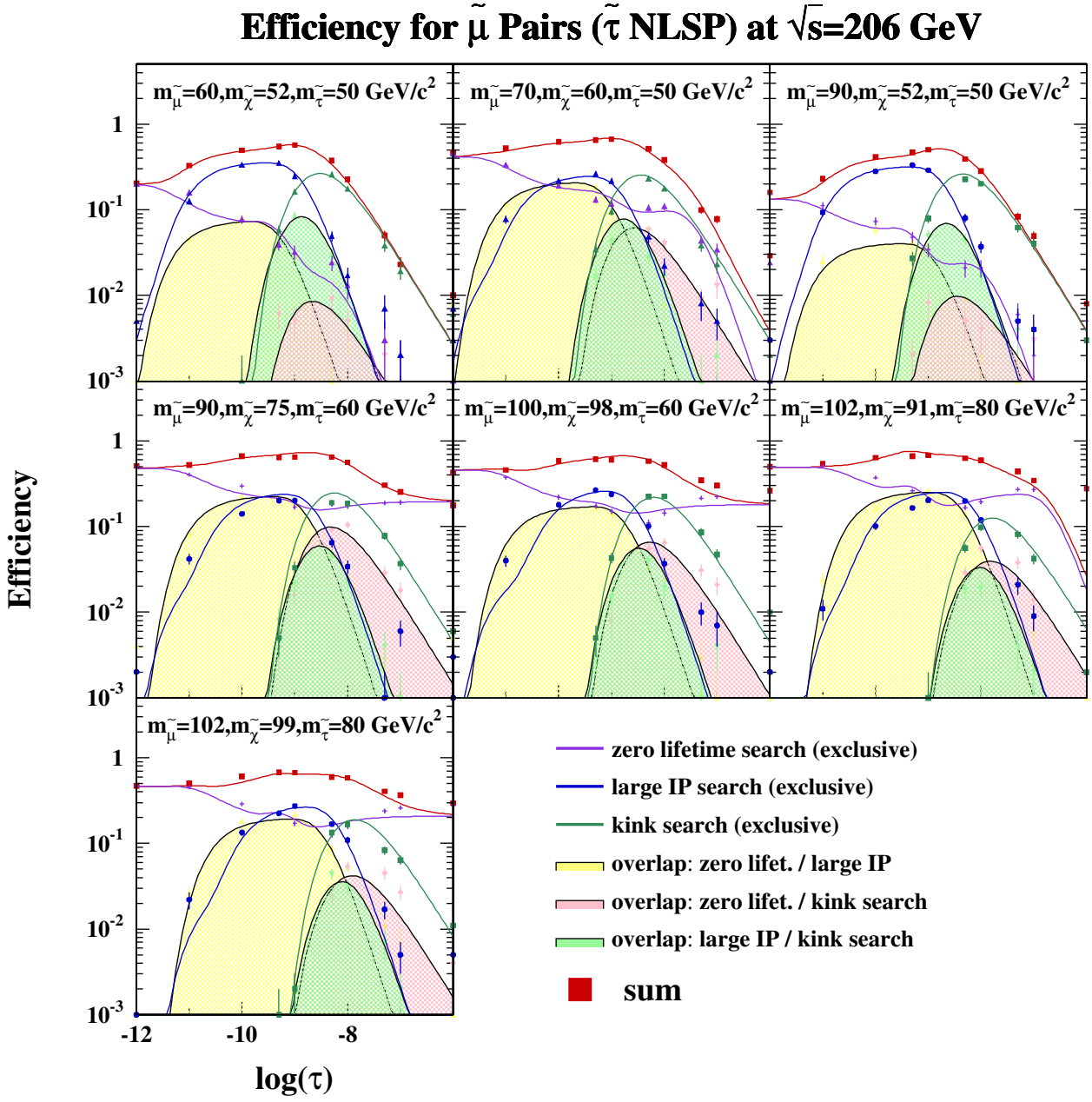


Figure 9.10: *Efficiencies for smuon pair–production at $\sqrt{s} = 206$ GeV in the stau NLSP scenario, as a function of the lifetime. In each plot the efficiencies are shown for a different combination of the smuon, neutralino and stau mass. The symbols represent the efficiencies for ten simulated lifetimes and the lines show the efficiency functions for events which are selected by the search for ≥ 4 leptons plus missing energy (violet), the search for large impact parameters (blue) and the search for kinks (green) exclusively. The overlap efficiencies between these searches are shown as filled histograms if they exceed 0.1 %. The sum of all efficiencies, i.e. the exclusive selection efficiencies and the overlap efficiencies, is shown by the red squares and the corresponding red line.*

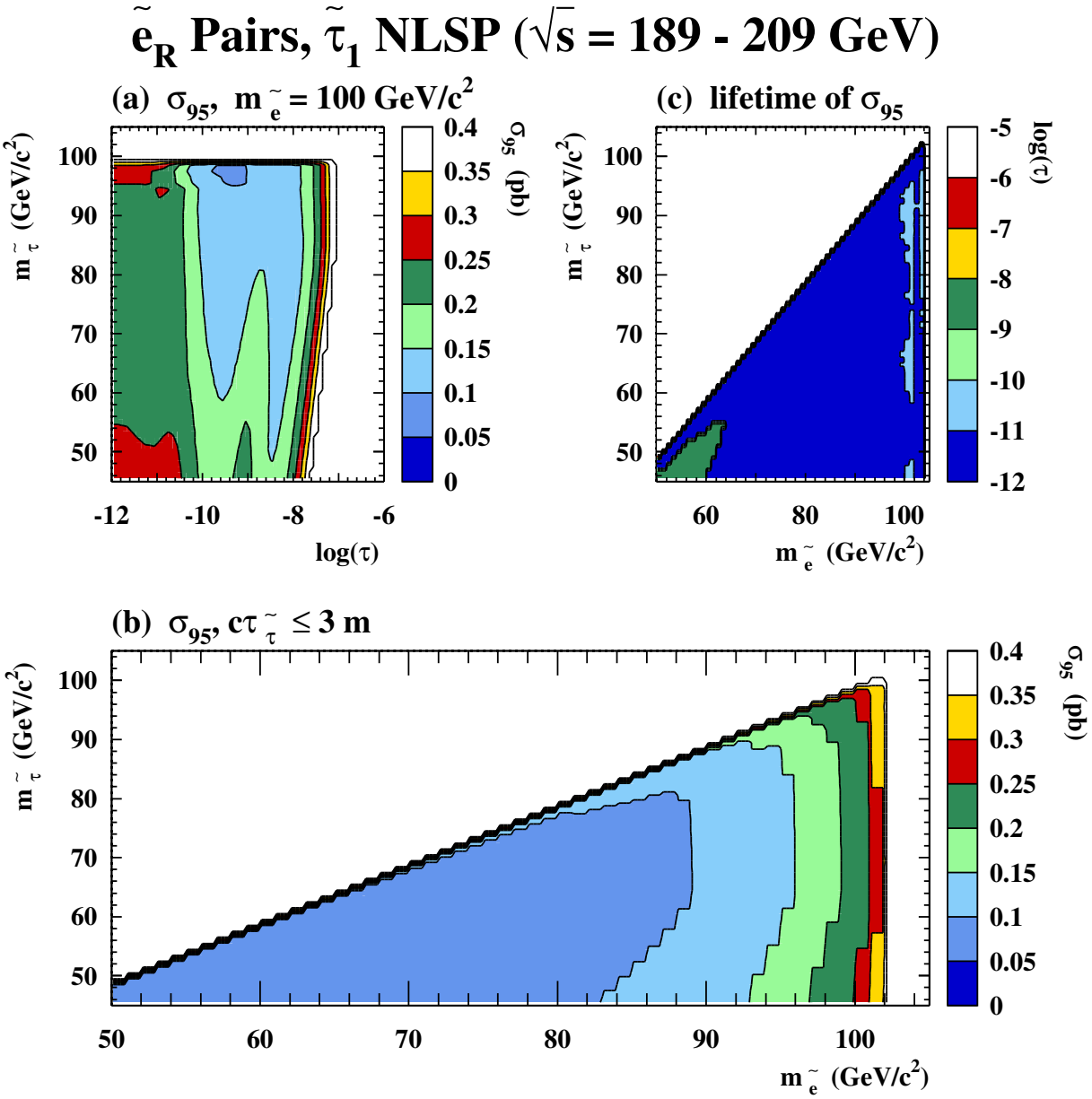


Figure 9.11: *Upper limits at 95 % C.L. on the production cross–section for selectron pair–production in the stau NLSP scenario at $\sqrt{s} = 208$ GeV. The data taken in the years 1998–2000 were combined assuming a β^3/s dependence of the cross–section. Plot (a) shows the contours of the excluded cross–section in the $m_{\tilde{\tau}_1}$ – lifetime plane for a fixed selectron mass of 100 GeV/c^2. Since the efficiency was minimised with respect to the neutralino mass, this plot is valid for all neutralino masses. The contours of the maximal excluded cross–section, after elimination of the lifetime, is shown in (b) as a function of $m_{\tilde{e}_R}$ and $m_{\tilde{\tau}_1}$. It is valid for proper decay lengths up to three metres. Plot (c) shows, for each point in the selectron – stau mass plane, the lifetimes corresponding to this cross–section limit.*

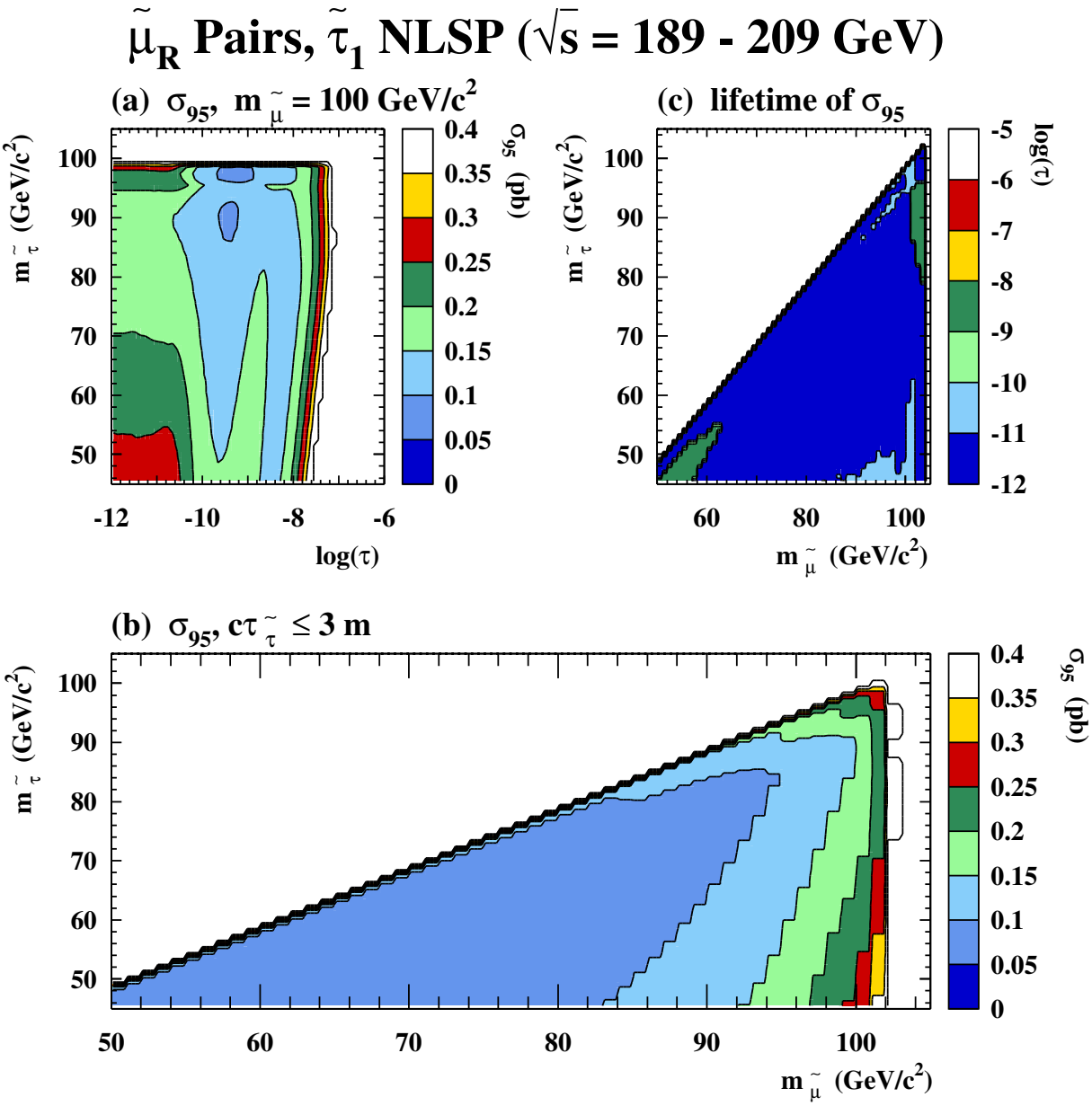


Figure 9.12: *Upper limits at 95 % C.L. on the production cross–section for smuon pair–production in the stau NLSP scenario at $\sqrt{s} = 208$ GeV. The data taken in the years 1998–2000 were combined assuming a β^3/s dependence of the cross–section. Plot (a) shows the contours of the excluded cross–section in the $m_{\tilde{\tau}_1}$ – lifetime plane for a fixed smuon mass of 100 GeV/c^2. Since the efficiency was minimised with respect to the neutralino mass, this plot is valid for all neutralino masses. The contours of the maximal excluded cross–section, after elimination of the lifetime, is shown in (b) as a function of $m_{\tilde{\mu}_R}$ and $m_{\tilde{\tau}_1}$. It is valid for proper decay lengths up to three metres. Plot (c) shows, for each point in the smuon – stau mass plane, the lifetimes corresponding to this cross–section limit.*

of the plane apart from the region where the stau is very heavy. For stau masses below $\approx 85\,\mathrm{GeV}/c^2$, cross–sections above 0.1 pb are excluded. For smuons slightly better results are obtained than for selectrons. Fig. 9.11 (c) and 9.12 (c) show the lifetimes corresponding to the highest excluded cross–sections at each point in the selectron/smuon – stau mass plane. In both cases the weakest limit is mostly found for very short lifetimes.

9.1.6 Cross–Section Limits for Chargino Pair–Production

The topology for chargino pair–production is similar to the topology of slepton pair–production with a slepton NLSP (Sect. 9.1.2), with the difference that a second invisible particle, the neutrino, carries away energy. Therefore the same analyses were used in the combination, i.e. the searches for acoplanar leptons, for tracks with large impact parameters and for tracks with kinks. The search for tracks with anomalous $\mathrm{d}E/\mathrm{d}x$ has no sensitivity for this channel, since it requires these tracks to be back–to–back, while here they are acoplanar. Thus, also in this channel only lifetimes up to 10^{-8} s, corresponding to a proper decay length of 3 m, were considered.

The efficiency function for slepton pair–production with a slepton NLSP was used, taking into account that here the slepton is a secondary particle. Thus, for the efficiency function, $\beta\gamma$ of the slepton was calculated from the chargino decay according to formulae (6.1) – (6.3). It was checked that the efficiency function so determined describes the efficiency well.

Cross–section limits were calculated both for the case of equal branching ratios for all flavours (slepton co–NLSP scenario) and 100 % branching ratio to $\tilde{\tau}_1\nu_\tau$ (stau NLSP scenario).

The data with $\sqrt{s} = 189 - 208\,\mathrm{GeV}$ were combined assuming a β/s dependence of the cross–sections.

To obtain cross–section limits that are valid for all lifetimes shorter than 10^{-8} s, the method described in Sect. 9.1.3 was used; i.e., for each chargino – slepton mass combination the maximum excluded cross–section was extracted by scanning over all lifetimes $< 10^{-8}$ s.

The cross–section limits at 95 % C.L. and $\sqrt{s} = 208.1\,\mathrm{GeV}$ for a fixed chargino mass of $99\,\mathrm{GeV}/c^2$ are shown in Fig. 9.13 (a) and 9.14 (a) for the slepton co–NLSP scenario and the stau NLSP scenario, respectively. In both cases cross–sections larger than 0.15 pb are excluded. The cross–section limits in the $M_{\tilde{\chi}_1^+} - M_{\tilde{\ell}_R}$ plane at $\sqrt{s} = 208.1\,\mathrm{GeV}$, valid for a proper slepton decay length $\leq 3\,\mathrm{m}$, are shown in Fig. 9.13 (b) for the slepton co–NLSP case and 9.14 (b) for the stau NLSP case. The obtained limits are similar and cross–sections larger than ≈ 0.2 pb are excluded. In a large part of the plane, cross–sections above 0.1 pb are excluded. Fig. 9.13 (c) and 9.14 (c) show the lifetimes corresponding to the highest excluded cross–sections at each point in the mass plane. In both cases the weakest limit is found for the very short lifetime, apart from the region with very large chargino masses. There the lowest limit is found at the edge of the considered lifetime range, since the kink search is not very efficient near the kinematic limit.

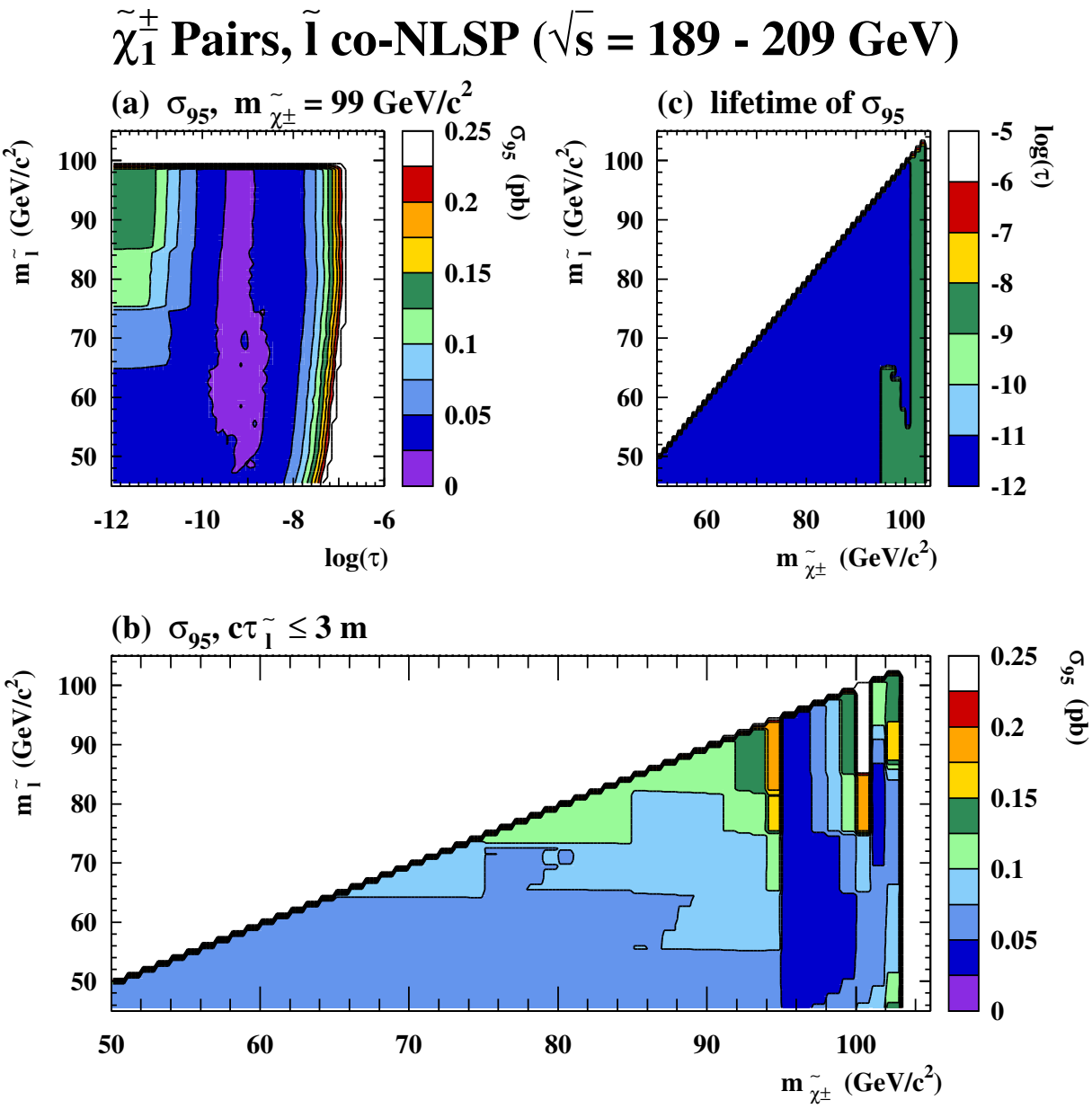


Figure 9.13: *Upper limits at 95 % C.L. on the production cross–section for chargino pair–production in the slepton co–NLSP scenario at $\sqrt{s} = 208$ GeV. The data taken in the years 1998–2000 were combined assuming a β/s dependence of the cross–sections. Plot (a) shows the contours of the excluded cross–section in the $m_{\tilde{\ell}_R}$ – lifetime plane for a fixed chargino mass of 99 GeV/c^2. The contours of the maximal excluded cross–section, after elimination of the lifetime, is shown in (b) as a function of $m_{\tilde{\chi}_1^+}$ and $m_{\tilde{\ell}_R}$. It is valid for proper decay lengths up to three metres. Plot (c) shows, for each point in the chargino – slepton mass plane, the lifetimes corresponding to this cross–section limit.*

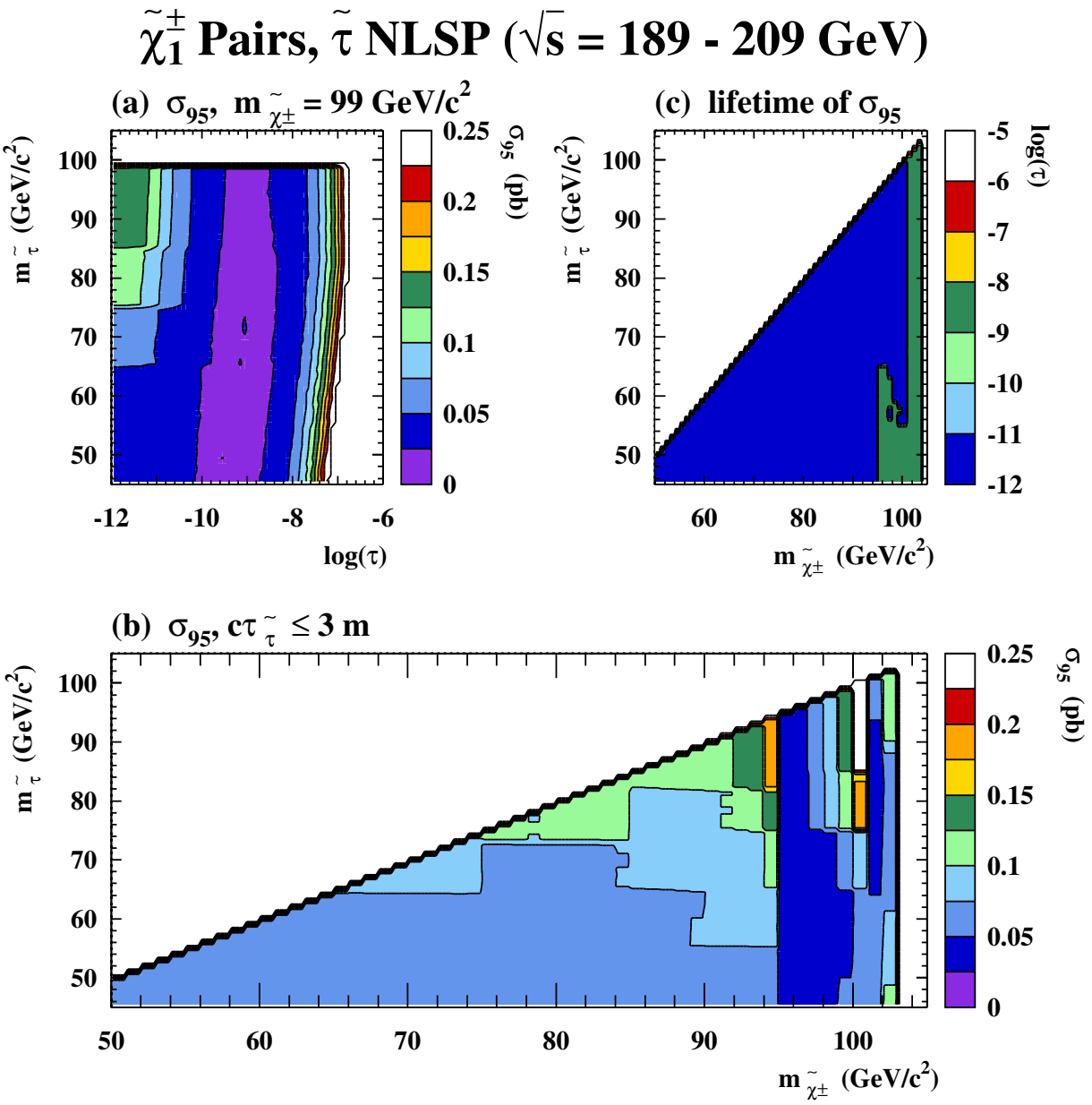


Figure 9.14: *Upper limits at 95 % C.L. on the production cross–section for chargino pair–production in the stau NLSP scenario at $\sqrt{s} = 208$ GeV. The data taken in the years 1998–2000 were combined assuming a β/s dependence of the cross–sections. Plot (a) shows the contours of the excluded cross–section in the $m_{\tilde{\tau}_1}$ – lifetime plane for a fixed chargino mass of 99 GeV/c^2. The contours of the maximal excluded cross–section, after elimination of the lifetime, is shown in (b) as a function of $m_{\tilde{\chi}_1^+}$ and $m_{\tilde{\tau}_1}$. It is valid for proper decay lengths up to three metres. Plot (c) shows, for each point in the chargino – stau mass plane, the lifetimes corresponding to this cross–section limit.*

9.2 The Neutralino as the NLSP

Up to this point only searches for topologies where the NLSP is a slepton were considered. However, in GMSB models also the neutralino can be the NLSP, as discussed in Chapter 2. The free parameters in the GMSB model are the overall mass scale of the SUSY particles, Λ, the ratio of the vacuum expectation values of the two Higgs doublets, $\tan\beta$, the mass scale of the messenger particles, M, the number of generations of messenger particles, N, and the sign of the Higgs sector mixing parameter, $sign(\mu)$. In Fig. 9.15 the regions in the $\Lambda - \tan\beta$ plane, where the neutralino, the stau or all sleptons are the NLSP, are shown in different colours, for $N = 1$ and different combinations of the parameters M and $sign(\mu)$. As visible from this plot, the neutralino is the NLSP in about half of the parameter space. For medium and high M it even dominates, while for low M the neutralino is the NLSP only for small Λ and $\tan\beta < 20$. The Figures 9.16 – 9.19 show the regions where the neutralino, the stau or all sleptons are the NLSP for the cases $N = 2 - 5$. For $N = 2$ the neutralino dominates for high M only, while for $N > 2$ the stau is the most important NLSP for all M, with the neutralino being the NLSP in the low Λ and low $\tan\beta$ region only. For positive μ the regions where the neutralino is the NLSP are identical to or slightly larger than for negative μ. The slepton co–NLSP scenario is realised in the region with $\tan\beta \lesssim 8$, only.

To constrain the GMSB parameter space for small N, it is therefore crucial to combine the searches for slepton NLSP signatures with searches that assume the neutralino to be the NLSP. This will be discussed in the following. Again, details about these analyses can be found in the references given below. In GMSB the neutralino decays as $\tilde{\chi}_1^0 \to \gamma\tilde{\mathrm{G}}$, resulting in final states with photons, missing energy and, depending on the channel, additional detector activity from leptons or hadrons. Just as for the slepton NLSP, the lifetime of the neutralino NLSP can have any value. The channels considered in the combination are:

- Neutralino pair–production: $\mathrm{e^+e^-} \to \tilde{\chi}_1^0\,\tilde{\chi}_1^0$
- Slepton pair–production: $\mathrm{e^+e^-} \to \tilde{\ell}^+\tilde{\ell}^- \to \tilde{\chi}_1^0\ell^+\,\tilde{\chi}_1^0\ell^-$
- Chargino pair–production: $\mathrm{e^+e^-} \to \tilde{\chi}_1^+\,\tilde{\chi}_1^- \to \tilde{\chi}_1^0\,\mathrm{W}^{+*}\,\tilde{\chi}_1^0\,\mathrm{W}^{-*}$, or, resulting in the same final state as the leptonic W decays, $\mathrm{e^+e^-} \to \tilde{\chi}_1^+\tilde{\chi}_1^- \to \ell^+\nu\,\tilde{\ell}^-\bar{\nu} \to \ell^+\nu\,\tilde{\chi}_1^0\,\ell^-\bar{\nu}\,\tilde{\chi}_1^0$

The following analyses were used for the combination (all results of these analyses are preliminary):

Zero Lifetime

- *Search for acoplanar photons:*
  If neutralinos are produced in pairs and both decay promptly, the topology is two photons along with missing energy. A search for such acoplanar photon pairs, which are predicted also in the context of many other models, was undertaken previously at OPAL. For details see [54].

- *Search for single photons:*
  If only one of the pair–produced neutralinos decays promptly or close to the interaction point, the topology is a single photon, along with a large amount of missing energy. The analysis that covers this topology is also described in [54].

- *Search for photon(s) and missing energy plus leptons/jets:*
  For the indirect production channels, if at least one of the neutralinos decays promptly or close to the event vertex, there will be at least one photon, missing energy and other activity from leptons or hadrons in the detector. A dedicated analysis for this topology was previously developed at OPAL. Details can be found in [55].

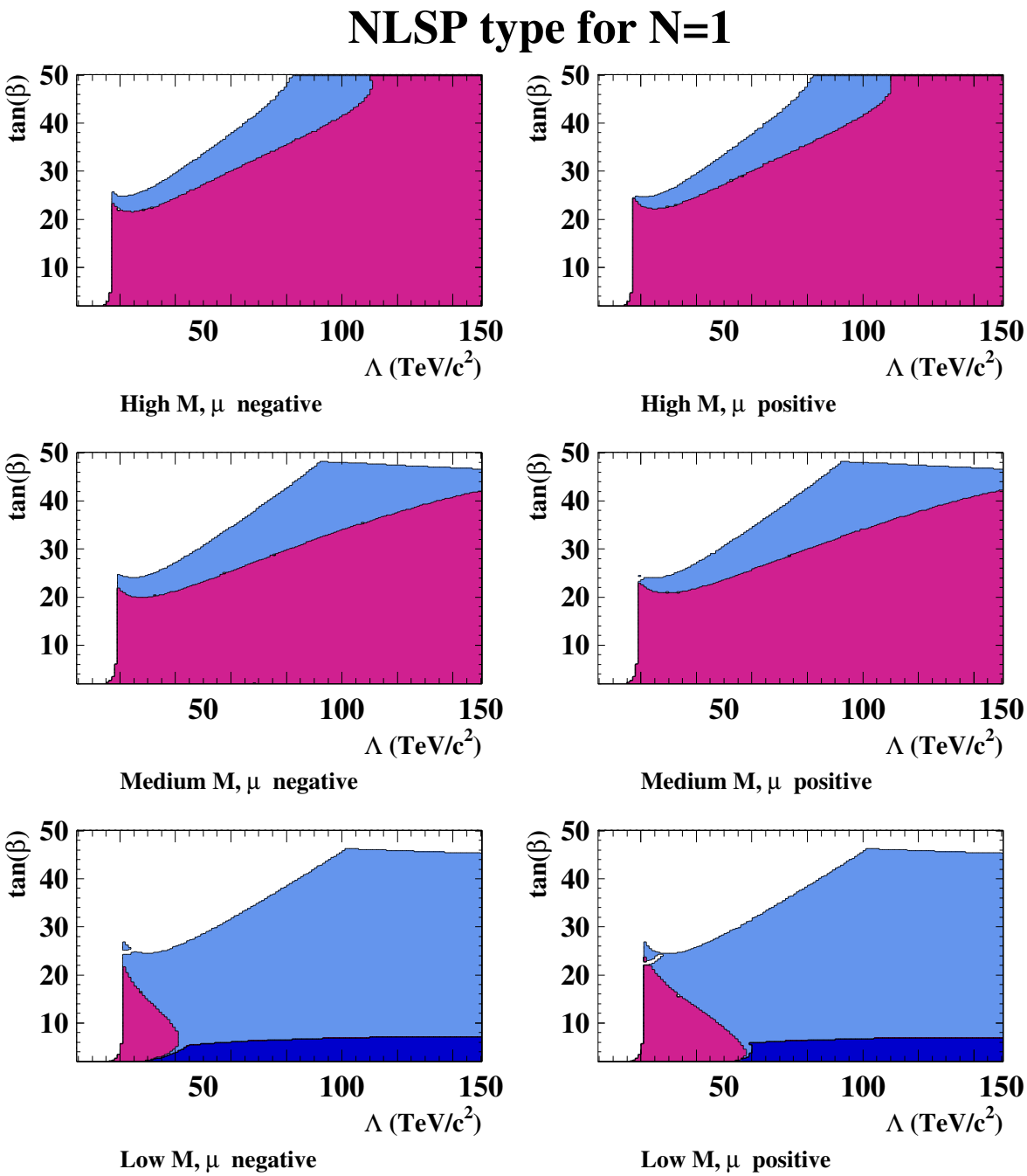


Figure 9.15: *The regions in the $\Lambda - \tan\beta$ plane, where either the neutralino, or the stau, or all sleptons (slepton co–NLSP scenario) are the NLSP, are shown in different colours, for the number of generations of messenger particles $N = 1$. Regions where the neutralino is the NLSP are coloured in magenta, regions where the stau is the NLSP are shown in light blue and regions where all sleptons are the NLSP are shown in dark blue. The six plots are for different combinations of the messenger mass M and sign(μ). From top to bottom: high M ($M = 10^6$ TeV/c^2), medium M ($M = 250$ TeV/c^2) and low M ($M = 1.01 \cdot \Lambda$), left: sign(μ) $= -1$, right: sign(μ) $= +1$.*

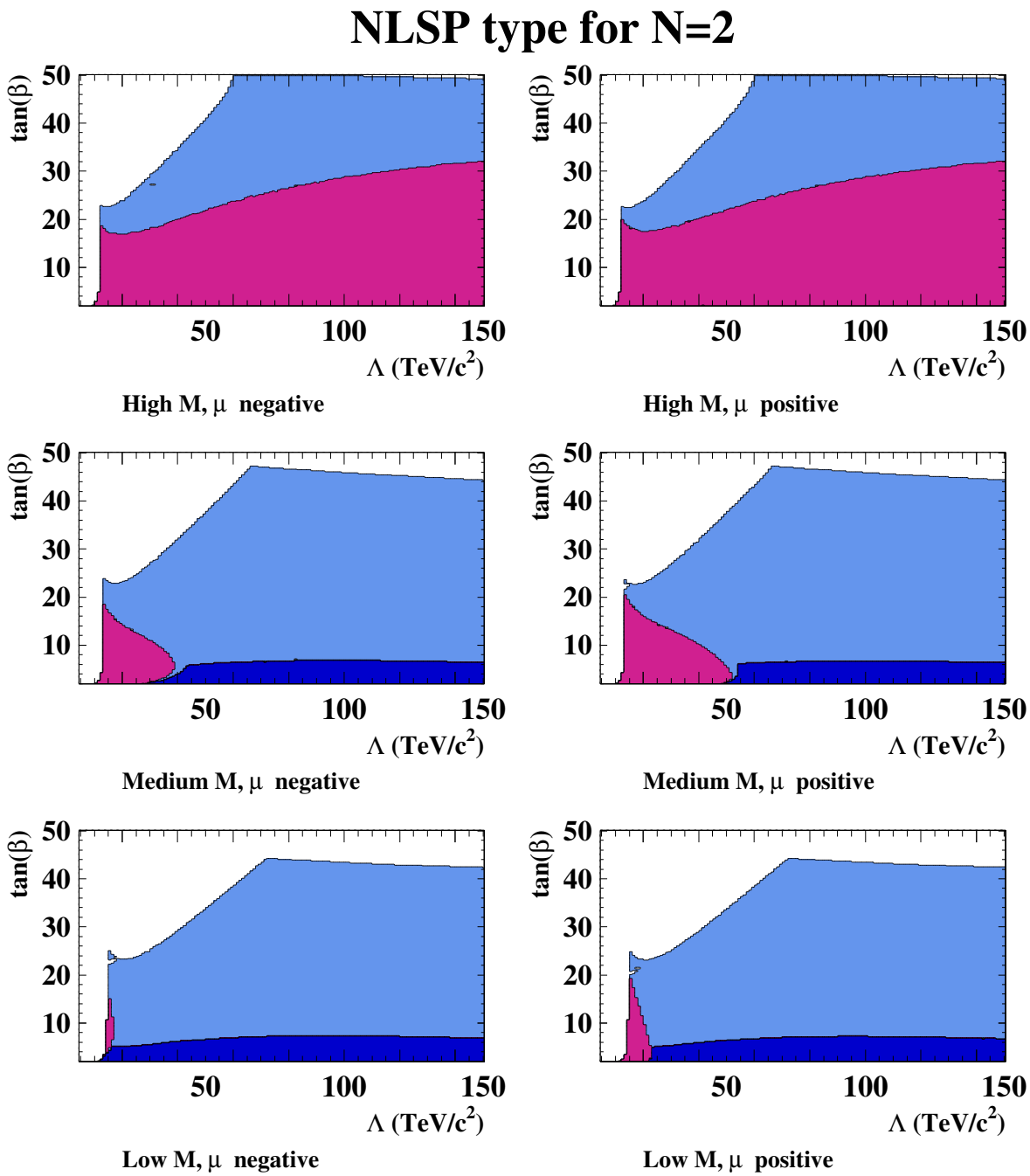


Figure 9.16: *The regions in the $\Lambda - \tan\beta$ plane, where either the neutralino, or the stau, or all sleptons (slepton co–NLSP scenario) are the NLSP, are shown in different colours, for the number of generations of messenger particles $N = 2$. Regions where the neutralino is the NLSP are coloured in magenta, regions where the stau is the NLSP are shown in light blue and regions where all sleptons are the NLSP are shown in dark blue. The six plots are for different combinations of the messenger mass M and sign(μ). From top to bottom: high M ($M = 10^6$ TeV/c^2), medium M ($M = 250$ TeV/c^2) and low M ($M = 1.01 \cdot \Lambda$), left: sign(μ) $= -1$, right: sign(μ) $= +1$.*

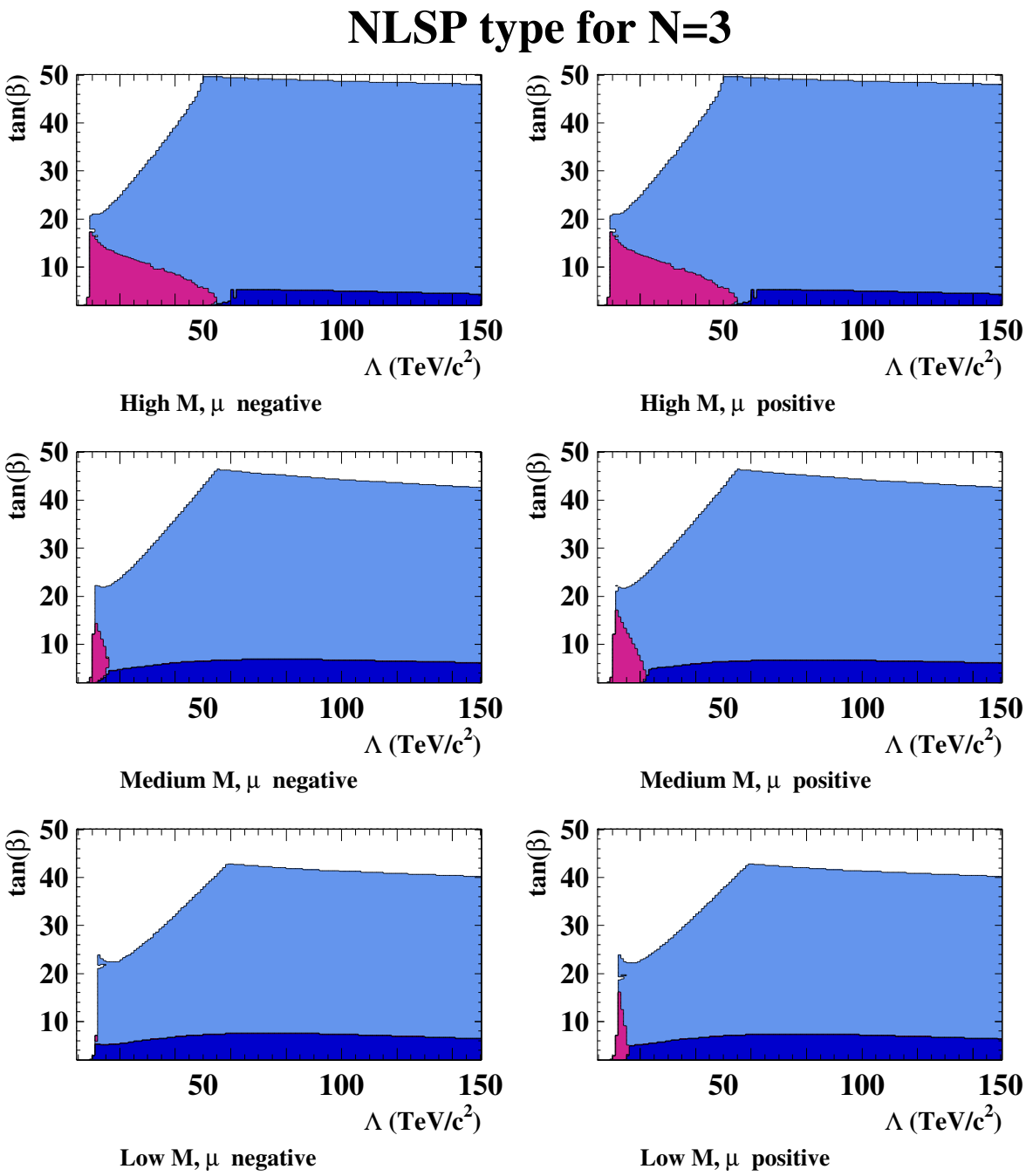


Figure 9.17: *The regions in the $\Lambda - \tan\beta$ plane, where either the neutralino, or the stau, or all sleptons (slepton co–NLSP scenario) are the NLSP, are shown in different colours, for the number of generations of messenger particles $N = 3$. Regions where the neutralino is the NLSP are coloured in magenta, regions where the stau is the NLSP are shown in light blue and regions where all sleptons are the NLSP are shown in dark blue. The six plots are for different combinations of the messenger mass M and sign(μ). From top to bottom: high M ($M = 10^6$ TeV/c^2), medium M ($M = 250$ TeV/c^2) and low M ($M = 1.01 \cdot \Lambda$), left: sign(μ) $= -1$, right: sign(μ) $= +1$.*

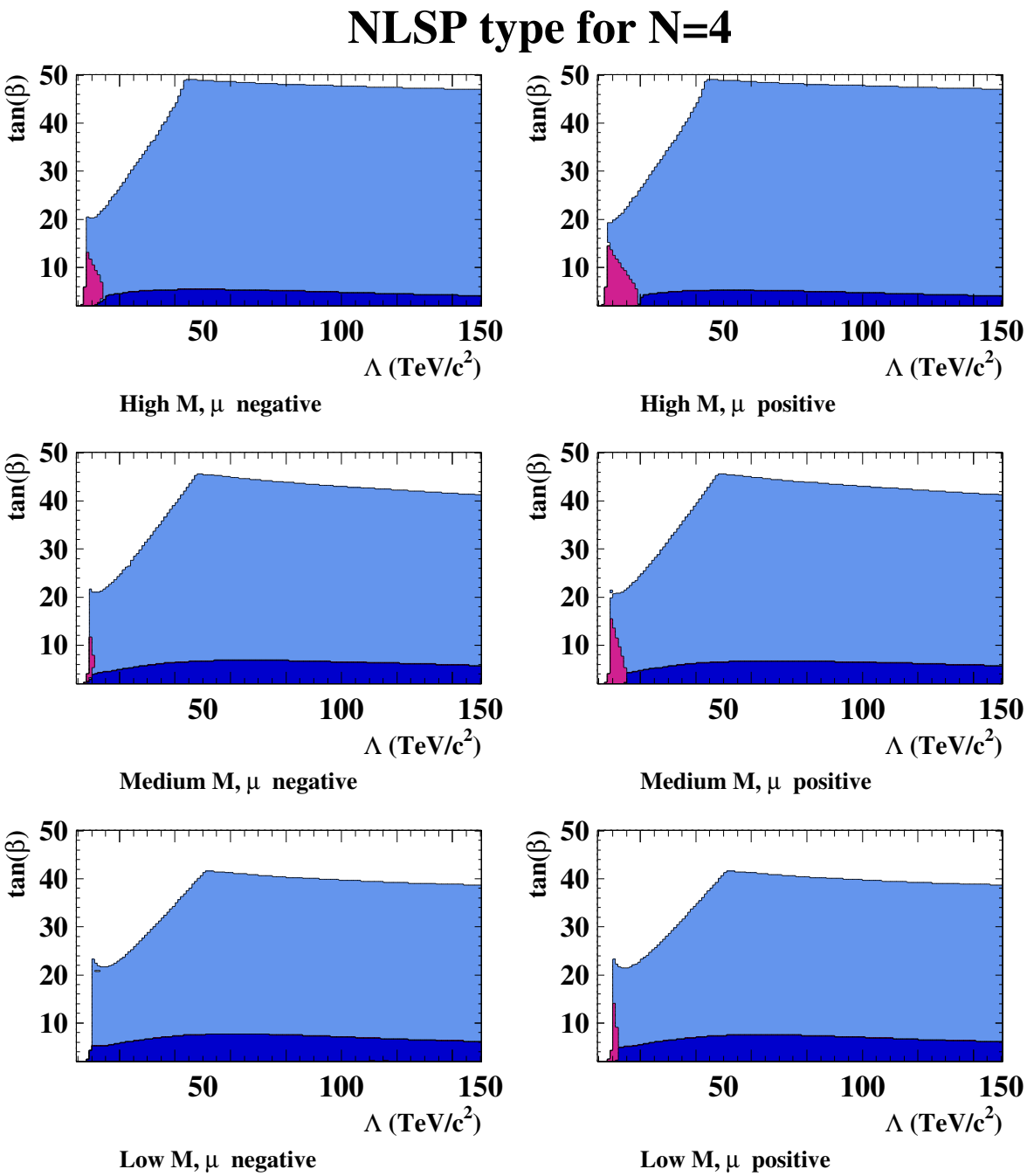


Figure 9.18: *The regions in the $\Lambda - \tan\beta$ plane, where either the neutralino, or the stau, or all sleptons (slepton co–NLSP scenario) are the NLSP, are shown in different colours, for the number of generations of messenger particles $N = 4$. Regions where the neutralino is the NLSP are coloured in magenta, regions where the stau is the NLSP are shown in light blue and regions where all sleptons are the NLSP are shown in dark blue. The six plots are for different combinations of the messenger mass M and $sign(\mu)$. From top to bottom: high M ($M = 10^6$ TeV/c^2), medium M ($M = 250$ TeV/c^2) and low M ($M = 1.01 \cdot \Lambda$), left: $sign(\mu) = -1$, right: $sign(\mu) = +1$.*

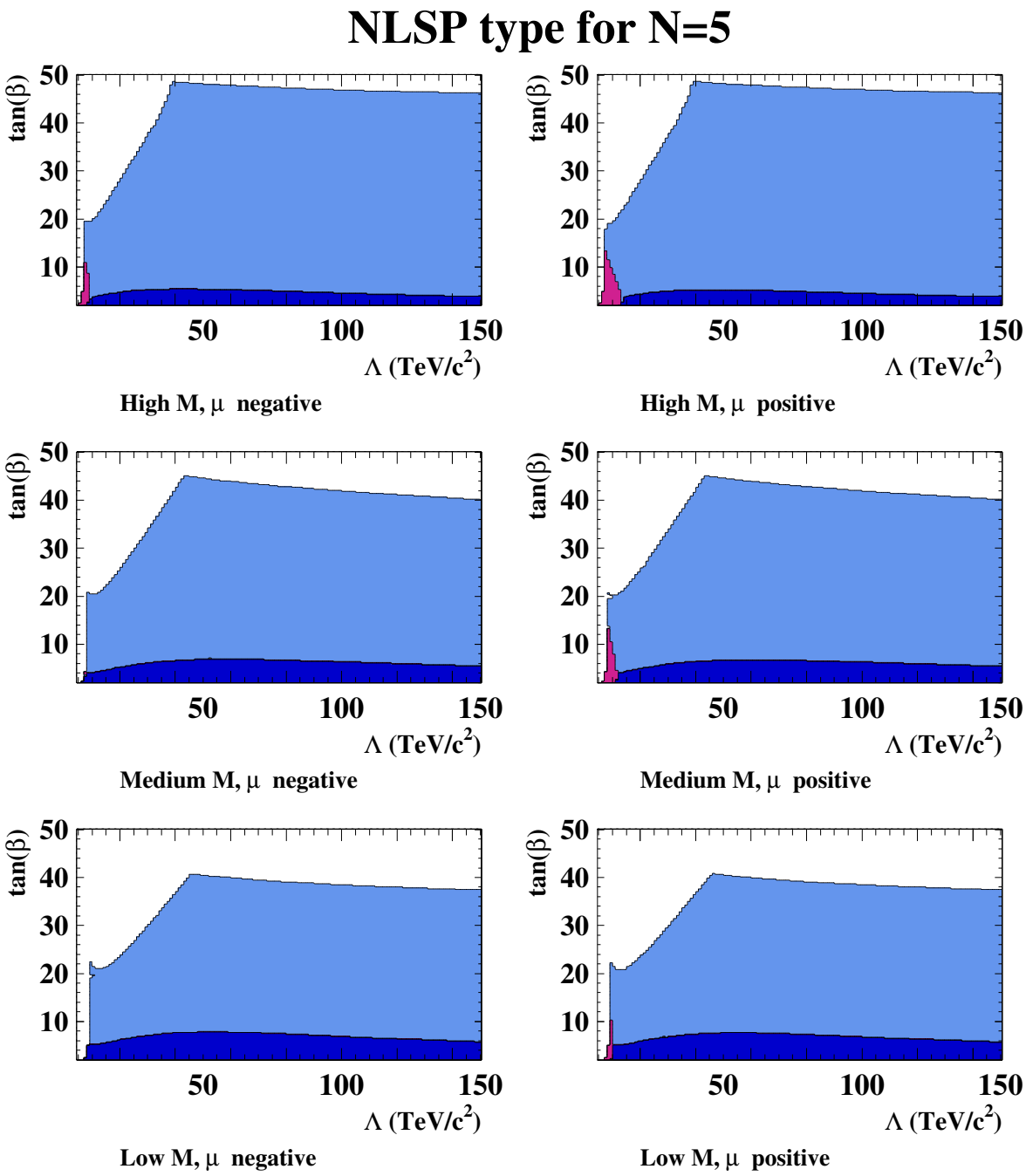


Figure 9.19: *The regions in the $\Lambda - \tan\beta$ plane, where either the neutralino, or the stau, or all sleptons (slepton co–NLSP scenario) are the NLSP, are shown in different colours, for the number of generations of messenger particles $N = 5$. Regions where the neutralino is the NLSP are coloured in magenta, regions where the stau is the NLSP are shown in light blue and regions where all sleptons are the NLSP are shown in dark blue. The six plots are for different combinations of the messenger mass M and sign(μ). From top to bottom: high M ($M = 10^6$ TeV/c^2), medium M ($M = 250$ TeV/c^2) and low M ($M = 1.01 \cdot \Lambda$), left: sign(μ) $= -1$, right: sign(μ) $= +1$.*

Intermediate Lifetimes

If the neutralinos decay in the detector, this leads to the topology of photons that do not point to the primary event vertex. No dedicated search was performed at OPAL for such non–pointing photons. Instead, the searches for promptly decaying neutralinos were used also for this lifetime range, since especially the search for single photons and the search for photons, missing energy plus leptons/jets maintain some ($> 10\,\%$) efficiency for lifetimes up to about $10^{-8}\,\mathrm{s}$. The searches do not require the photons to point to the primary vertex, thus the efficiency is limited by the probability of both photons decaying outside the electromagnetic calorimeter.

Infinite Lifetime

- *Search for acoplanar leptons:*
  For slepton pair–production and chargino pair–production with decays to sleptons or leptonic $\mathrm{W}^{\pm *}$ decays, a topology of acoplanar leptons is expected, if the neutralinos are stable. Therefore the analysis described in Sect. 9.1 and in [51] is suitable.

- *Search for charginos and neutralinos in the constrained MSSM:*
  For chargino pair–production with hadronic or semi–leptonic $\mathrm{W}^{\pm *}$ decays, in the case of stable neutralinos, the topology is identical to the corresponding channels in the constrained MSSM (cMSSM), where the neutralino is the LSP and therefore stable. Different analyses exist for final states with and without an identified lepton. These are described in [56].

9.2.1 Cross–Section and Mass Limits for Neutralino Pair–Production

For neutralino pair–production in the neutralino NLSP scenario, the searches for acoplanar and single photons were combined. If the neutralino is stable, or if both neutralinos decay outside the detector, the efficiency is zero. Since in this case no energy is deposited in the detector, such events are invisible and it is impossible to obtain results that are valid for all neutralino lifetimes.

In the selection for acoplanar photons the photons are not required to originate from the primary vertex, resulting in a relatively constant efficiency up to lifetimes of approximately $10^{-9}\,\mathrm{s}$, as visible from Fig. 9.20. For longer lifetimes, the efficiency decreases rapidly. The search for single photons has a sensitivity for events where one of the photons decayed outside the detector, extending the efficiency to lifetimes of approximately $10^{-7}\,\mathrm{s}$. However, the efficiency is small, and the analysis suffers from a high level of background. The overlap between the two selections is large ($\epsilon \approx 70\,\%$), as visible from Fig. 9.20, where the exclusive selection efficiencies and the overlap efficiency are shown. Since the single photon analysis requires *at least* one photon, it also selects most of the events of the acoplanar photon search. The overlap in data and background was evaluated by a comparison of the selected candidates and expected background events of the two analyses on an event–by–event basis, and was taken into account in the limit calculation.

The expected cross–section was taken from a minimisation in the GMSB parameter scan, as described in Sect. 7.1 .

The cross–section limit at 95 % C.L. and $\sqrt{s} = 208.1\,\mathrm{GeV}$ is shown in Fig. 9.21 (a). Up to lifetimes of approximately $10^{-9}\,\mathrm{s}$ cross–sections above 0.1 pb are excluded, apart from the region close to the kinematic limit. In most of the plane, the upper limit on the cross–section is below 0.03 pb. For longer lifetimes the sensitivity decreases rapidly, and for $\tau > 10^{-8}\,\mathrm{s}$ cross–sections above 1 pb cannot be excluded.

The corresponding limit on the neutralino mass at 95 % C.L. is shown in Fig. 9.21 (b). For prompt neutralino decays, a limit of $95.5\,\mathrm{GeV}/c^2$ is found (expected limit: $94.5\,\mathrm{GeV}/c^2$).

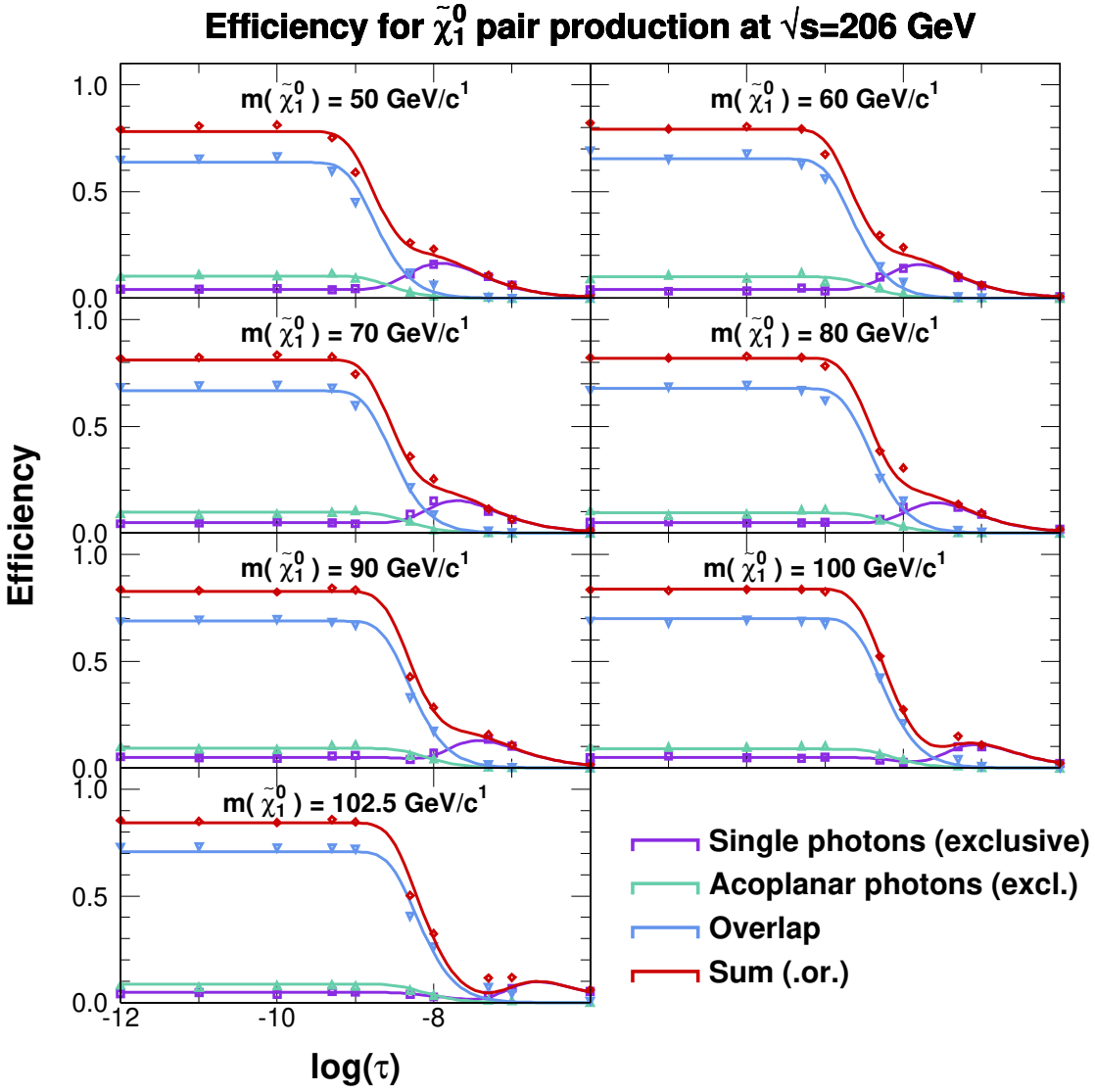


Figure 9.20: *Efficiencies for neutralino pair–production at $\sqrt{s} = 206$ GeV in the neutralino NLSP scenario, as a function of the lifetime. In each plot the efficiencies are shown for a different neutralino mass. The symbols represent the efficiencies for ten simulated lifetimes and the lines show the efficiency functions for events which are selected by the acoplanar photon search (green) and the search for single photons (violet) exclusively. The blue line gives the overlap efficiency between the two selections. The sum of all efficiencies, i.e. the two exclusive selection efficiencies and their overlap efficiency, is shown by the red symbols and the corresponding red line.*

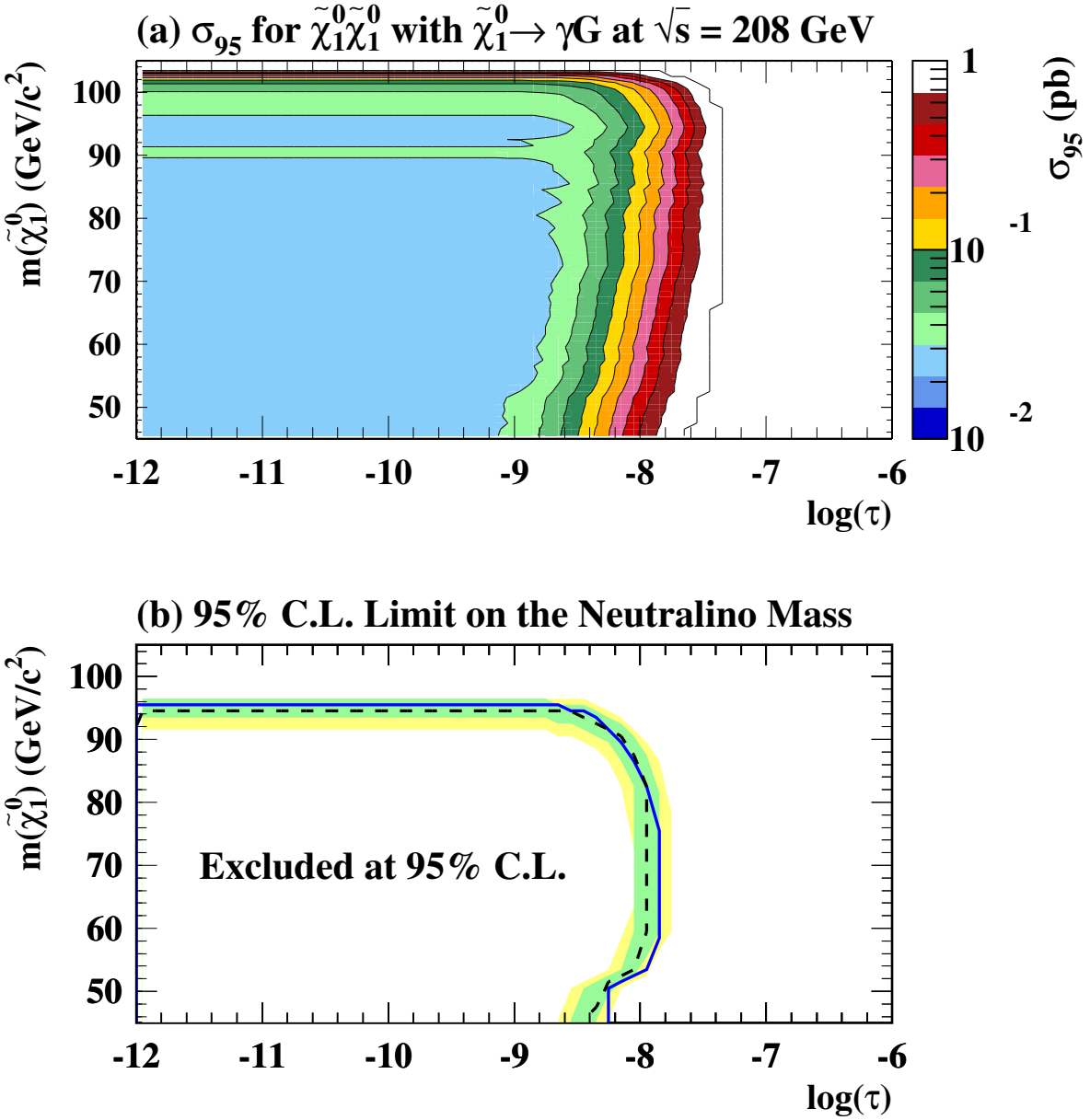


Figure 9.21: *(a) Contours of the cross–section limit at 95 % C.L. and $\sqrt{s}$ = 208 GeV for neutralino pair–production in the neutralino NLSP scenario, in the plane of the neutralino mass and lifetime. The data with $\sqrt{s}$ = 189 − 209 GeV are included. (b) Excluded region in the neutralino mass versus lifetime plane. The neutralino mass limit at 95 % C.L., as a function of the neutralino lifetime, is shown as a blue solid line. The dashed line represents the median expected limit, and the 68 % and 95 % probability intervals, centred on the median, are shown as green and yellow bands, respectively.*

This limit was calculated with a step size of $1\,\mathrm{GeV}/c^2$ for the neutralino mass, and is valid for a messenger index $N \leq 5$.

9.2.2 Cross–Section Limits for Slepton Pair–Production

For slepton pair–production with a neutralino NLSP two analyses were combined: the search for photons and missing energy plus leptons and/or jets for short lifetimes and the search for acoplanar leptons for long lifetimes. As can be seen from Fig. 9.22 for selectrons, the efficiency of the search for photons and missing energy plus leptons/jets is roughly constant up to lifetimes of $\approx 10^{-8}\,\mathrm{s}$. For this lifetime, the efficiency of the search for acoplanar leptons is already rising, thus the combined efficiency is fairly constant over the whole lifetime range. The overlap between the two analyses is of the order of 15 %. For the search for photons and missing energy plus leptons/jets only the results from the data of the year 2000 were included, while for the acoplanar lepton search data of 1998–2000 were used. The different datasets were combined assuming a β^3/s dependence of the cross–sections.

Cross–section limits were calculated using the same method as for the channels with cascade decays in the slepton NLSP case: first for each slepton mass and flavour limits in the $\log(\tau) - M_{\tilde{\chi}_1^0}$ plane were calculated. Then, for each slepton and neutralino mass, a scan over the lifetime was performed and the highest excluded cross–section was extracted. The resulting cross–section limits at 95 % C.L. and for $\sqrt{s} = 206.7\,\mathrm{GeV}$ in the $M_{\tilde{\ell}_R} - M_{\tilde{\chi}_1^0}$ plane are shown in Fig. 9.23 (a), 9.24 (a) and 9.25 (a) for selectrons, smuons and staus, respectively. The lifetimes at which the highest excluded cross–sections were found are shown in Fig. 9.23 (b), 9.24 (b) and 9.25 (b). Also shown are the cross–section limits for the case of promptly decaying neutralinos ($\tau = 10^{-12}\,\mathrm{s}$), where only the search for photons, missing energy plus leptons/jets contributes (Fig. 9.23 (c), 9.24 (c) and 9.25 (c)), and the case of very long–lived neutralinos ($\tau = 10^{-6}\,\mathrm{s}$), where only the search for acoplanar leptons contributes (Fig. 9.23 (d), 9.24 (d) and 9.25 (d)).

For selectrons the "all lifetime" limits for the cross–section (see Fig. 9.23 (a)) depend on the mass difference between the slepton and the neutralino, $\Delta M = M_{\tilde{\ell}_R} - M_{\tilde{\chi}_1^0}$, and vary between 0.03 pb for low ΔM and 0.1 pb for the case of large ΔM and light neutralinos. The lifetime giving the highest upper limit is mostly $\approx 10^{-8}\,\mathrm{s}$. For the zero lifetime case limits between 0.03 and 0.07 pb are obtained, while for long lifetime the limits are below 0.02 pb for small ΔM and below 0.07 pb in most of the plane.

The smuon limits look very similar and the "all lifetime" limits range from 0.03 pb for low ΔM to 0.09 pb for large ΔM and light neutralinos.

For staus the upper limits are higher. The "all lifetime" limits range from 0.04 pb for low ΔM to 0.16 pb for large ΔM and light neutralinos. The lifetime giving the highest upper limit is $10^{-6} - 10^{-7}\,\mathrm{s}$ in a large part of the mass plane, corresponding to the acoplanar lepton search. Correspondingly for the long lifetime case the limits in this channel range from 0.02 pb to 0.12 pb. For the zero lifetime case, though, limits are similar to the other channels and range from 0.02 to 0.08 pb.

9.2.3 Cross–Section Limits for Chargino Pair–Production

For chargino pair–production in the neutralino NLSP scenario again several analyses were combined. For short lifetimes, the search for photons and missing energy plus leptons/jets was used. This analysis is split into several selections, optimised for low and high–multiplicity and for three ΔM regions, with $\Delta M = M_{\tilde{\chi}_1^+} - M_{\tilde{\chi}_1^0}$. For long lifetimes, the search for acoplanar leptons was used for leptonic W decays, while for semi–leptonic and hadronic W decays the chargino/neutralino searches with and without an identified lepton were used. All long lifetime analyses were separately optimised for the eight different ΔM regions and eight different chargino masses used in the Monte Carlo simulation.

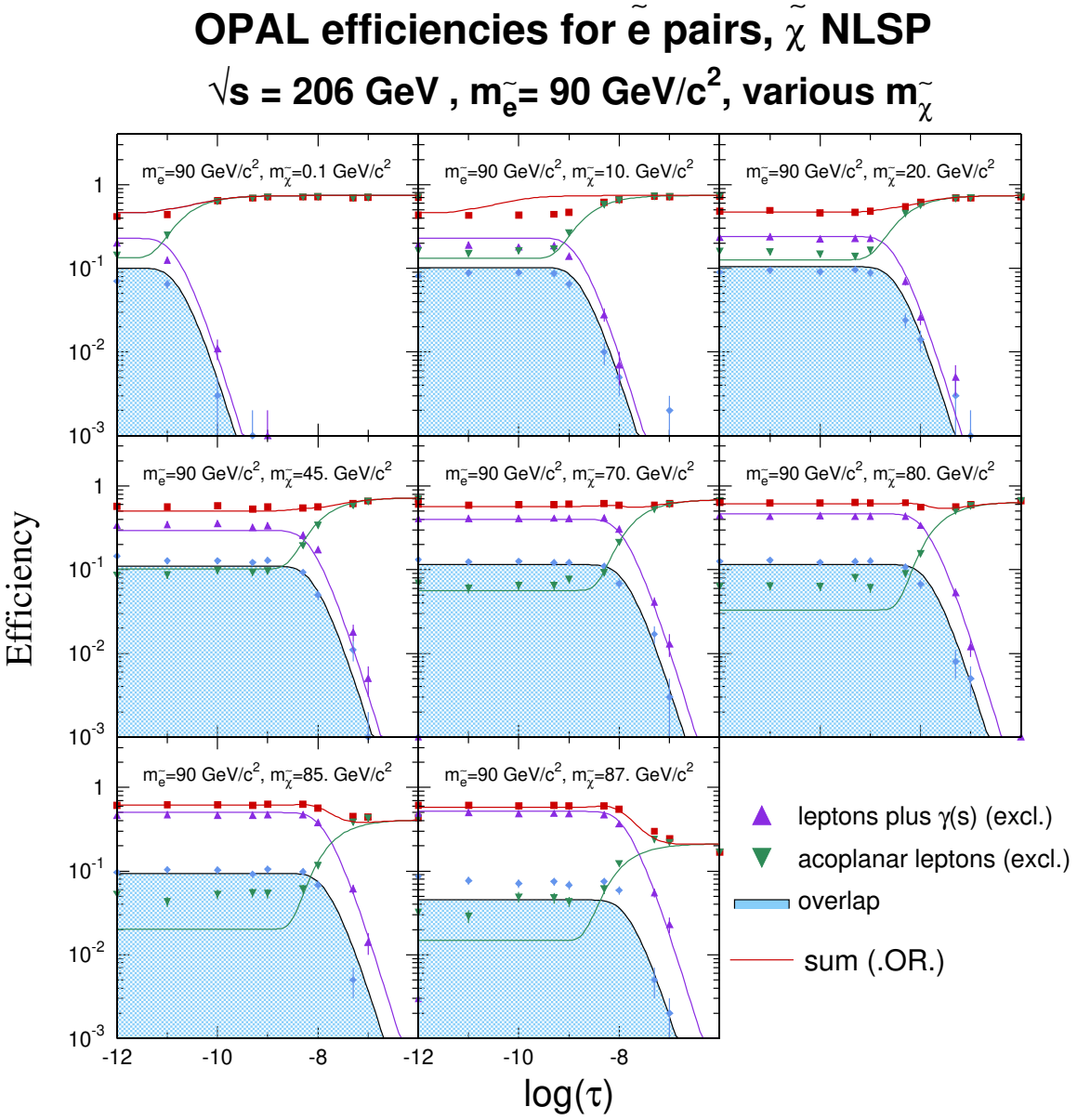


Figure 9.22: *Efficiencies for selectron pair–production with a neutralino NLSP for a selectron mass of 90 GeV/c^2 at $\sqrt{s}$ = 208.1 GeV, as a function of the lifetime. The plots show the efficiencies for neutralino masses of 0.1 GeV/c^2, 10.0 GeV/c^2, 20.0 GeV/c^2, 45.0 GeV/c^2, 70. GeV/c^2, 80.0 GeV/c^2, 85.0 GeV/c^2 and 87 GeV/c^2. The symbols represent the efficiencies for ten simulated lifetimes and the lines show the efficiency functions for events which are selected exclusively by the search for photons, missing energy plus leptons for short lifetimes (violet) and the search for acoplanar leptons for long lifetimes (green). The overlap efficiencies between these searches are shown as blue filled histograms. The sum of the efficiencies, i.e. the two exclusive selection efficiencies and their overlap, is shown by the red squares and the corresponding red line.*

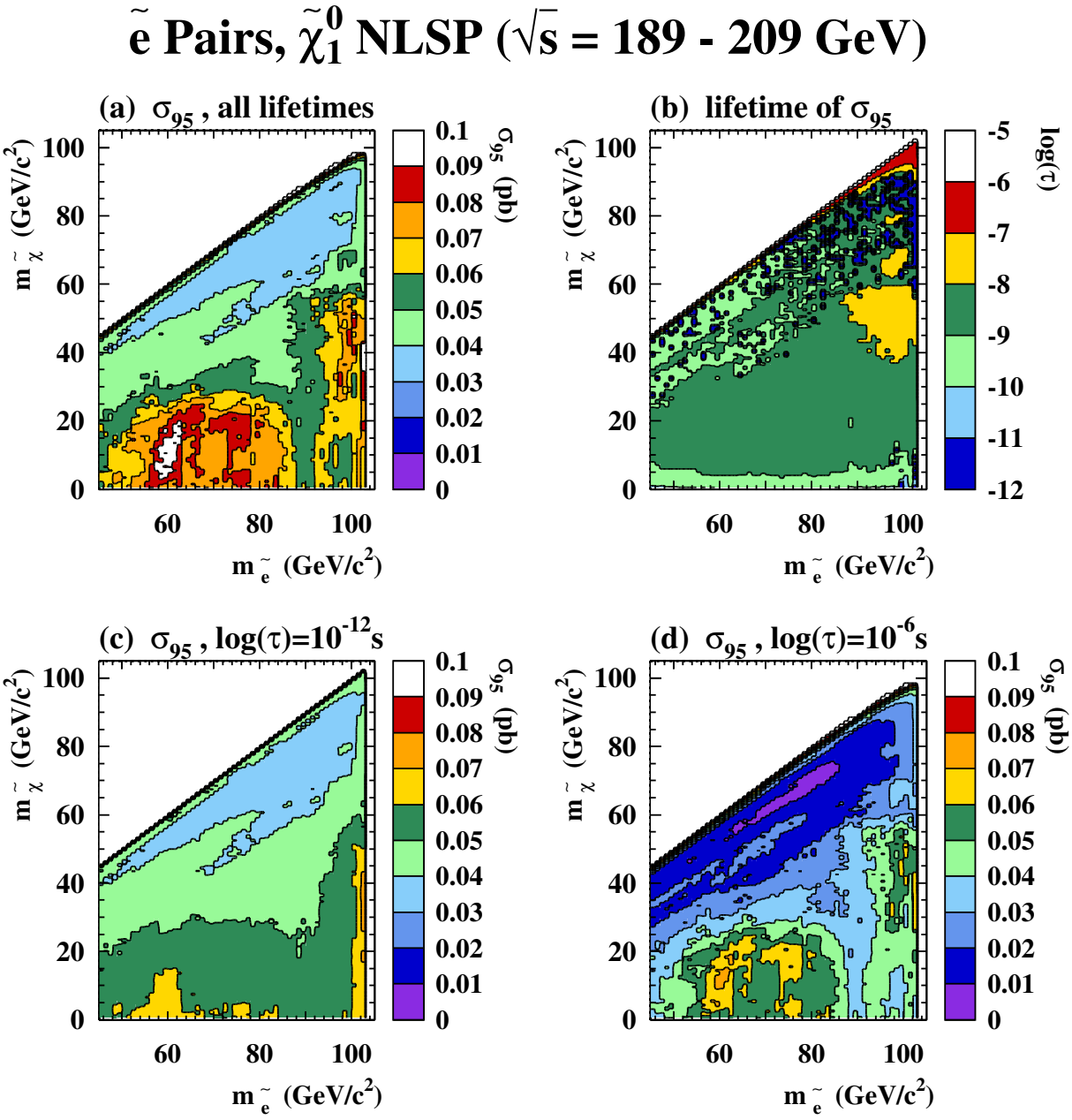


Figure 9.23: *Contours of the cross–section limits at 95 % C.L. and $\sqrt{s}$ = 207 GeV for selectron pair–production in the neutralino NLSP scenario. The cross–section limits in (a) are valid for all neutralino lifetimes. Plot (b) shows the lifetimes corresponding to these "all lifetimes" cross–section limits. The 95 % C.L. cross–section limits for prompt neutralino decays ($\tau = 10^{-12}$ s), where only the search for photons, missing energy plus leptons/jets contributes, are plotted in (c). In (d) the 95 % C.L. cross–section limits are shown for very long–lived neutralinos ($\tau = 10^{-6}$ s), where only the search for acoplanar leptons contributes.*

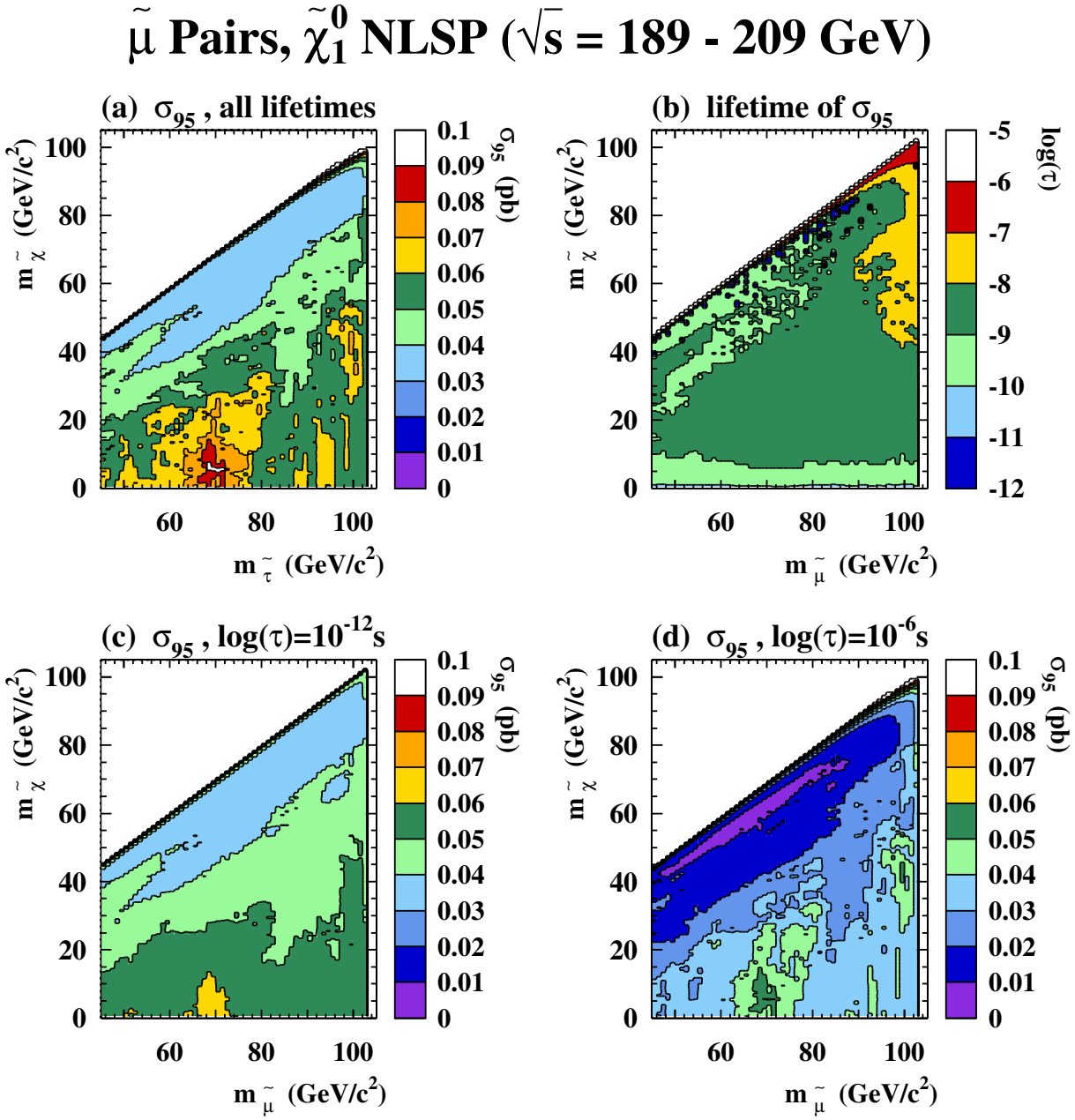


Figure 9.24: *Contours of the cross–section limits at 95 % C.L. and $\sqrt{s}$ = 207 GeV for smuon pair–production in the neutralino NLSP scenario. The cross–section limits in (a) are valid for all neutralino lifetimes. Plot (b) shows the lifetimes corresponding to these "all lifetimes" cross–section limits. The 95 % C.L. cross–section limits for prompt neutralino decays ($\tau = 10^{-12}$ s), where only the search for photons, missing energy plus leptons/jets contributes, are plotted in (c). In (d) the 95 % C.L. cross–section limits are shown for very long–lived neutralinos ($\tau = 10^{-6}$ s), where only the search for acoplanar leptons contributes.*

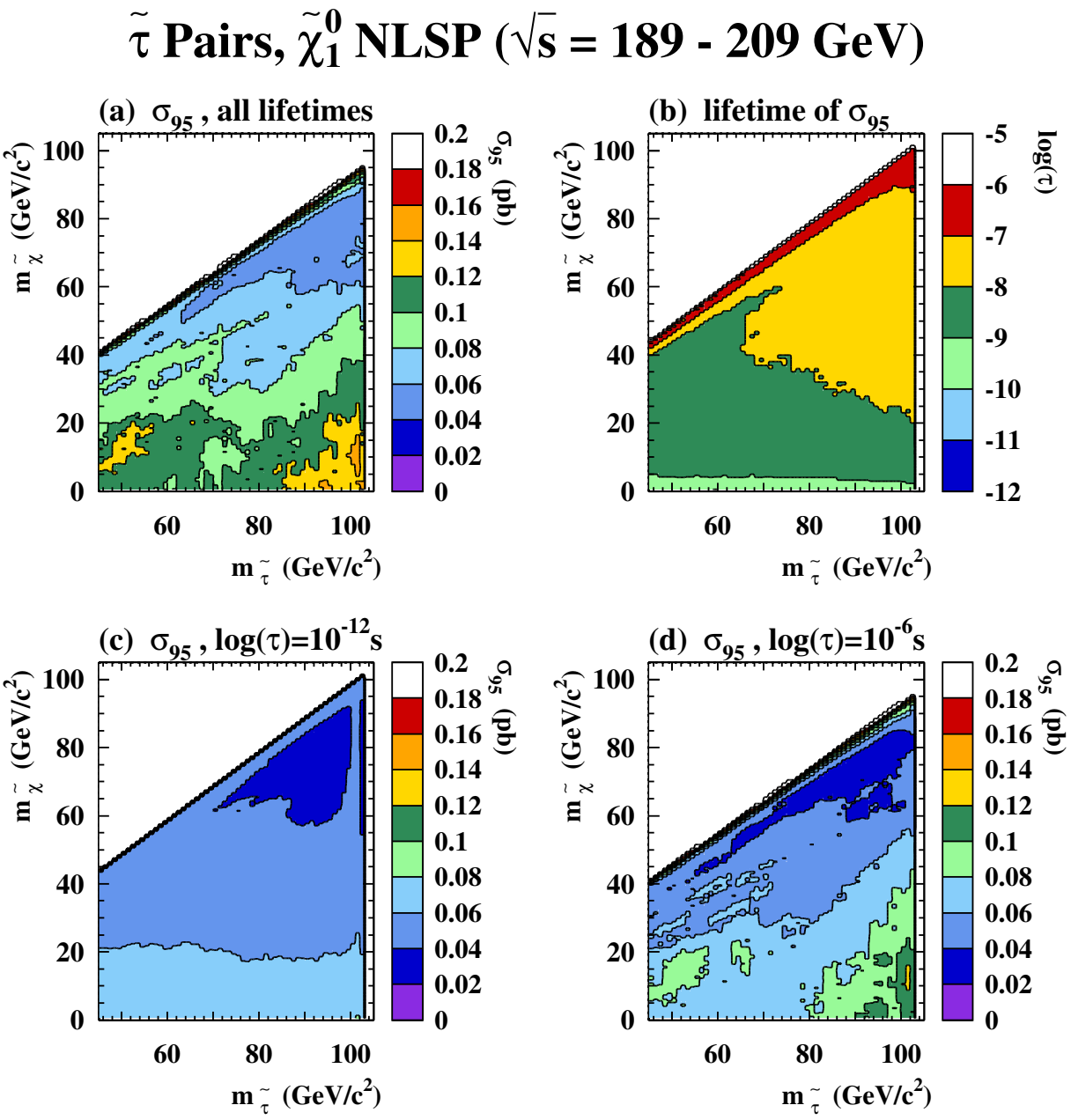


Figure 9.25: *Contours of the cross–section limits at 95 % C.L. and $\sqrt{s}$ = 207 GeV for stau pair–production in the neutralino NLSP scenario. The cross–section limits in (a) are valid for all neutralino lifetimes. Plot (b) shows the lifetimes corresponding to these "all lifetimes" cross–section limits. The 95 % C.L. cross–section limits for prompt neutralino decays ($\tau = 10^{-12}$ s), where only the search for photons, missing energy plus leptons/jets contributes, are plotted in (c). In (d) the 95 % C.L. cross–section limits are shown for very long–lived neutralinos ($\tau = 10^{-6}$ s), where only the search for acoplanar leptons contributes.*

In this channel the overlap had to be treated differently than before, since no information about the background and data events was available. Most of the analyses combined in this channel use a likelihood shape analysis, in which the information about the background is kept in form of histograms of the background likelihood distributions; information about individual events is not kept. Thus the overlaps were not treated as separate channels, but the overlap between two selections was counted for one of them only, and for the other selection the exclusive efficiency was used. Starting from the first analyses (photons plus missing energy plus leptons/jets, low multiplicity selection) with efficiency ϵ_1, the other analyses were added consecutively by taking only the efficiency for events that were not yet selected by previous analyses. To combine the second analysis with efficiency ϵ_2 with the first one, the "exclusive" efficiency for the second analysis, ϵ_2^*, was calculated from $\epsilon_2^* = \epsilon_2 - \epsilon_{12}$, where ϵ_{12} is the efficiency of the overlap between analyses 1 and 2. The exclusive efficiency of analysis 3 is then given by $\epsilon_3^* = \epsilon_3 - \epsilon_{13} - \epsilon_{32^*}$, where ϵ_{13} is the efficiency of the overlap between analyses 1 and 3, and ϵ_{32^*} is the overlap between the exclusive selection 2 (denoted as 2^*) and 3. In this way double counting of the efficiency is avoided. For the background of the analyses i with ϵ_i^* the background of the original analyses with ϵ_i was used, since the overlap in background was not known. Thus, if there was an overlap in background, it was counted for all affected analyses, which is not optimal but is conservative.

The resulting efficiencies are plotted in Fig. 9.26. The selections for photons and missing energy plus leptons/jets maintain a constant efficiency up to $\tau \approx 10^{-8}\,\mathrm{s}$, while dropping rapidly for longer lifetimes. The selections for leptonic and semi–leptonic W decays are efficient for $\tau > 10^{-8}\,\mathrm{s}$, and the search for hadronic W decays maintains some efficiency for all lifetimes. Overall, the total efficiency is much higher for short lifetimes, especially for low ΔM.

For the acoplanar lepton search the data from 1998–2000 were used. For the chargino and neutralino searches, results were available for the years 1999 and 2000, only. Finally, for the search for photons and missing energy plus leptons/jets only the data from the year 2000 were included. The results at different center–of–mass energies were combined assuming a β/s dependence of the cross–sections.

The cross–section limits were calculated with the same method as that used for the channels with cascade decays in the slepton NLSP case: first, for each chargino mass, cross–section limits in the $\log(\tau) - M_{\tilde{\chi}_1^0}$ plane were obtained. Then, for each chargino and neutralino mass, a scan over the lifetime was performed and the highest excluded cross–section was extracted. The resulting "all lifetime" cross–section limit at 95 % C.L., for $\sqrt{s} = 208.1\,\mathrm{GeV}$, in the $M_{\tilde{\chi}_1^+} - M_{\tilde{\chi}_1^0}$ plane is shown in Fig. 9.27 (a). Cross–sections above 0.25 pb are excluded in all of the mass plane, while in most of the plane cross–sections above 0.15 pb are excluded. The lifetime at which the highest cross–section limit was found is shown in Fig. 9.27 (b) for all mass points. The weakest limit is always found for long lifetimes, $\tau = 10^{-7} - 10^{-6}\,\mathrm{s}$. This is consistent with Fig. 9.27 (c), where the cross–section limits for the case of promptly decaying neutralinos ($\tau = 10^{-12}\,\mathrm{s}$), where mainly the search for photons, missing energy plus leptons/jets contributes, are plotted. Here the constraints are much stronger and cross–sections above 0.1 pb are excluded in the whole mass plane, although data are included from one year only. The case of very long–lived neutralinos ($\tau = 10^{-6}\,\mathrm{s}$) is plotted in Fig. 9.27 (d), with cross–section limits similar to (in some regions slightly better than) the "all lifetime" case.

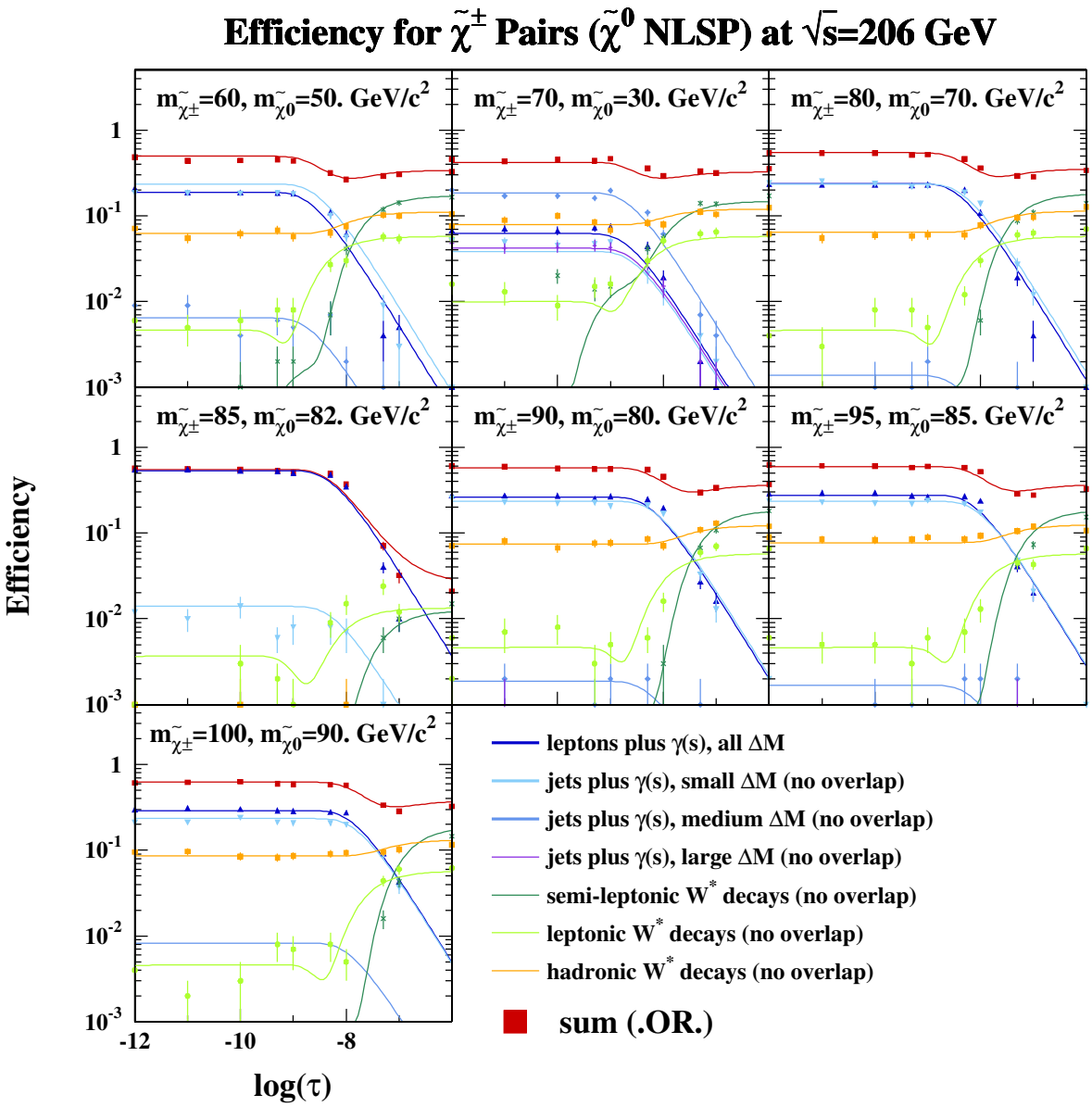


Figure 9.26: *Efficiencies as a function of the lifetime for chargino pair–production with a neutralino NLSP, for different combinations of the chargino and neutralino mass. The symbols represent the efficiencies for ten simulated lifetimes and the lines show the efficiency functions. The efficiencies for the three analyses for photons, missing energy plus leptons/jets for short lifetimes are shown in blue. The search for acoplanar leptons is shown in light green, and the searches for semi–leptonic and hadronic W* decays are shown in dark green and orange, respectively. The sum of the efficiencies is shown by the red squares and the corresponding red line.*

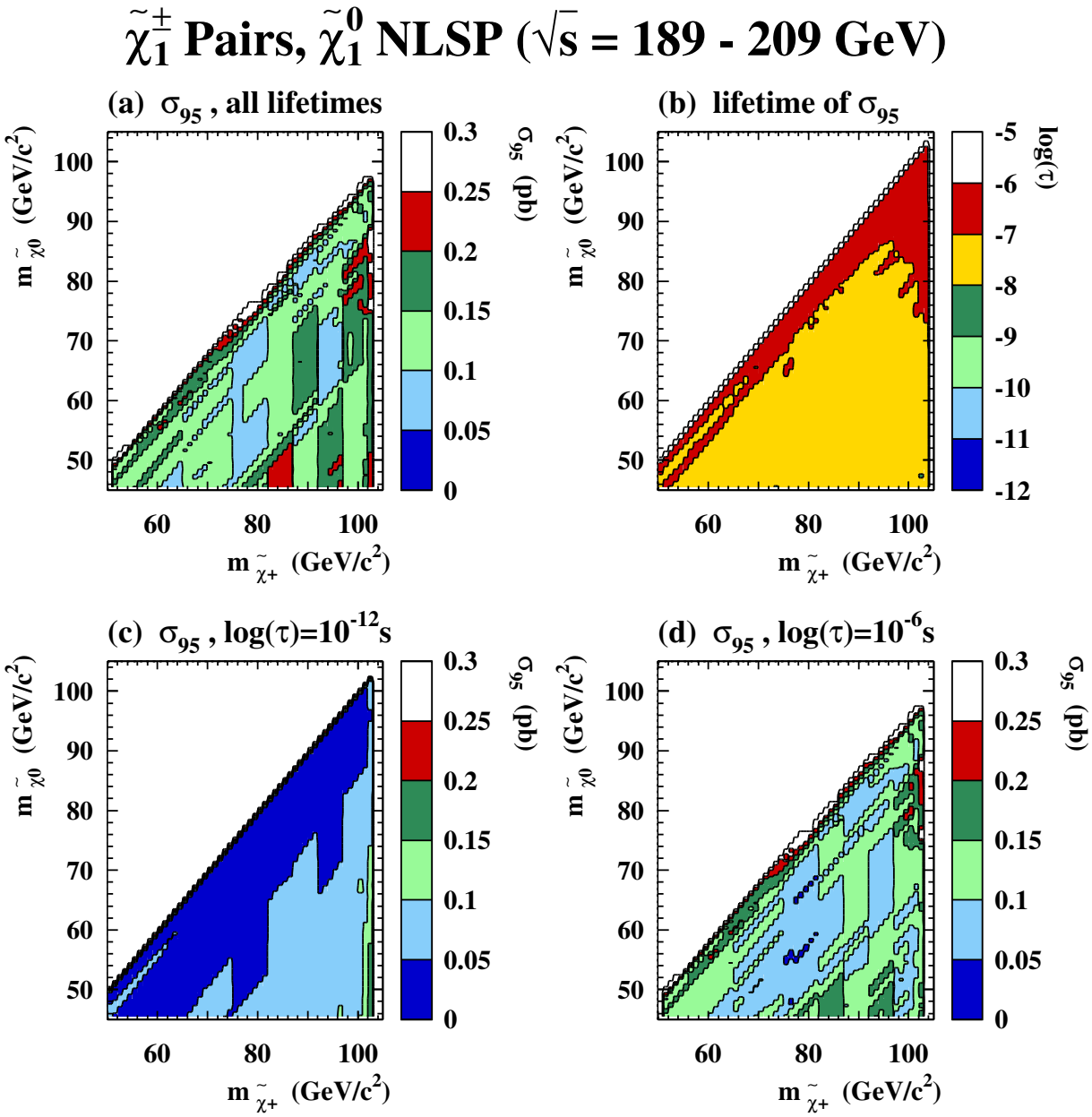


Figure 9.27: *Contours of the cross–section limits at 95 % C.L. and $\sqrt{s}$ = 208 GeV for chargino pair–production in the neutralino NLSP scenario. The cross–section limits in (a) are valid for all neutralino lifetimes. Plot (b) shows the lifetimes corresponding to these "all lifetimes" cross–section limits. The results for prompt neutralino decays ($\tau = 10^{-12}$ s), where mainly the search for photons, missing energy plus leptons/jets contributes, are plotted in (c). In (d) the limits are shown for very long–lived neutralinos ($\tau = 10^{-6}$ s).*

9.3 Interpretations in the Framework of the GMSB Model

9.3.1 Exlusions within the GMSB Parameter Space

Up to this point, cross–section and mass limits were presented. In addition, to interpret the experimental results in the framework of the GMSB model, the constraints on the production cross–sections were used to exclude points in the GMSB parameter space. For this interpretation, all channels described in Sect. 9.1 and 9.2 were included.

For each of the 30 sets of the GMSB parameters N, M and $sign(\mu)$ considered in the GMSB parameter scan (Chapter 7), the exclusion in the $\Lambda - \tan\beta$ plane was studied. At each point in this plane, the mass spectrum, the cross–sections for the various channels as well as their branching ratios are known. A point in the parameter space is excluded if it is kinematically accessible and the expected cross–section in at least one channel is lower than the experimental 95 % C.L. cross–section limit in this channel, taking into account the branching ratio(s). The regions where the NLSP is lighter than $45\,\mathrm{GeV}/c^2$ (LEP 1 search region) were not considered in this analysis.

Three cases were studied:

- all NLSP lifetimes ($10^{-12}\,\mathrm{s} \leq \tau \leq 10^{-6}\,\mathrm{s}$),
- negligible NLSP lifetime ($\tau = 10^{-12}\,\mathrm{s}$),
- NLSP lifetime $\tau < 10^{-8}\,\mathrm{s}$, corresponding to a proper decay length below three metres.

In addition to the most general case of all lifetimes, the two other cases were studied for the following reasons. For negligible lifetime, the best exclusion for the important case of $N = 1$ is found. This is due to the fact that for small lifetimes the search for neutralino pair–production in the neutralino NLSP scenario contributes, which improves the limit in the cases where the neutralino NLSP scenario is important, i.e. for low N. For the case $\tau < 10^{-8}\,\mathrm{s}$ the cross–section limits for neutralino pair–production in the neutralino NLSP scenario are much weaker than for negligible lifetimes, as described in Section 9.2.1, however they are still strong enough to exclude significant regions in the parameter space (while for the "all lifetime" case this analysis does not contribute at all). Although for lifetimes of $\tau < 10^{-8}\,\mathrm{s}$ smaller regions in the parameter space can be excluded compared to the case of negligible lifetime, for both cases rather similar constraints can be set on the parameter Λ, independent of $\tan\beta$ (the limits on Λ are discussed in the following section). Thus the constraints on Λ are relatively insensitive to lifetime for $\tau < 10^{-8}\,\mathrm{s}$, and the lifetime range where these limits are valid is extended by several orders of magnitude by studying the case $\tau < 10^{-8}\,\mathrm{s}$.

In Fig. 9.28 the excluded regions in the $\Lambda - \tan\beta$ plane, valid for all NLSP lifetimes, are shown for $N = 1$ and for the six combinations of M and sign(μ). The different colours correspond to different search channels, indicating the relevance of the various analyses in the parameter space. In general, for low M more points can be excluded than for high M, and slightly more points can be excluded for $\mu < 0$. The 2–tau and 2–lepton channels exclude a significant part of the parameter space where the slepton co–NLSP scenario or the stau NLSP scenario is realised, as visible from a comparison with Fig. 9.15. The importance of the slepton NLSP scenarios decreases with M: for small M, the sleptons can be the NLSP for all values of $\tan\beta$, with the slepton co–NLSP scenario being realised in the small $\tan\beta$ region. For large M the sleptons are the NLSP only for $\tan\beta \gtrsim 20$. The 4–lepton channel excludes points in a smaller part of the slepton NLSP parameter space, and these points are also excluded by the 2–tau or 2–lepton channels. In the neutralino NLSP channels, a large fraction of the neutralino NLSP points can be excluded by the searches for slepton pair–production. The chargino pair–production with a neutralino NLSP channel excludes mostly points that can also be excluded by the searches for sleptons, apart from the case of high M, where the charginos rule out additional points in the region with low $\tan\beta$. In this

channel a complication arises due to the fact that the chargino has two decay modes that can lead to the same final state:

(1) $\mathrm{e^+e^-} \to \tilde{\chi}_1^+ \, \tilde{\chi}_1^- \to \tilde{\chi}_1^0 \, \mathrm{W}^{+*} \, \tilde{\chi}_1^0 \, \mathrm{W}^{-*}$,

(2) $\mathrm{e^+e^-} \to \tilde{\chi}_1^+ \tilde{\chi}_1^- \to \tilde{\ell}^+ \nu \, \tilde{\ell}^- \bar{\nu} \to \ell^+ \nu \, \tilde{\chi}_1^0 \, \ell^- \bar{\nu} \, \tilde{\chi}_1^0$.

Since in the scan for the branching ratios of the different final states no information about the decay chain is available, it is impossible to decide if the branching ratio to the $\tilde{\ell}^- \bar{\nu} \, \tilde{\ell}^+ \nu$ final state is due to leptonic W decays (1), or due to the direct decay mode (2). Experimentally, only results from the decay channel (1) were used. The analyses sensitive to the leptonic final state are the search for acoplanar leptons for long lifetimes and the search for photons, missing energy plus leptons, for short lifetimes. It was checked that these analyses have a similar efficiency for both chargino decay modes that lead to the leptonic final state. The branching ratio to $\tilde{\ell}\nu$ was treated as if it was purely due to channel (1). Since the efficiency for (2) is roughly the same, even if this branching ratio was totally due to decay mode (2), the cross–section limits would essentially not be affected. Coming back to the regions excluded by this channel, in general, the production cross–section for charginos is larger than that for sleptons. Nevertheless, the sleptons give better exclusion limits than the charginos, because in GMSB models the charginos are mostly heavier than the (right–handed) sleptons. Thus, the charginos are kinematically limited and higher values of Λ can be reached by the sleptons.

The grey regions cannot be excluded. The light grey regions are not within the kinematic reach of LEP 2; i.e., the sleptons, the neutralino and the chargino are heavier than half the center–of–mass energy, at which the cross–section limits were calculated (206.7 GeV for slepton pair–production with a neutralino NLSP, 208.1 GeV for all other channels). In the dark grey regions at least one search channel presented here is kinematically allowed. Values of Λ of about $100\,\mathrm{TeV}/c^2$ for large and about $80\,\mathrm{TeV}/c^2$ for low $\tan\beta$ are reachable at LEP 2 for $N = 1$. For larger N the SUSY particles are in general heavier for the same value of Λ than for $N = 1$. For $N = 5$, Λ values of only about $25 - 35\,\mathrm{TeV}/c^2$, depending on $\tan\beta$, can be reached.

With increasing N, the slepton NLSP scenarios dominate more and more, and the neutralino is the NLSP only for small Λ and $\tan\beta$. This behaviour is particularly pronounced for low M. The exclusions for $N = 2 - 5$ are shown in Figures 9.29 – 9.32. As visible from these plots, for large N the most important channels are the 2–lepton and 2–tau channels. A significant part of the kinematically accessible parameter space is excluded.

For the case of negligible NLSP lifetime, the excluded regions, for messenger indices of $N = 1$ and $N = 3$, are shown in Fig. 9.33 and 9.34. One important difference with respect to the case of all lifetimes is that for negligible lifetimes the search for neutralino pair–production in the neutralino NLSP scenario excludes large parts of the neutralino NLSP regions. In addition, the search for chargino pair–production in the slepton NLSP scenarios contributes for short lifetimes and excludes points in a restricted part of the parameter space. Also the search for selectron or smuon pair–production in the stau NLSP scenario is now included and excludes, especially for low M, points in a significant region in the parameter space. However, these are also excluded by other channels. For slepton and chargino pair–production in the neutralino NLSP scenario, much stronger constraints on the cross–sections are obtained for very short lifetimes, as visible from Figures 9.23 – 9.25 and 9.27. This results in larger excluded regions for these channels. In the 4–lepton channel, where no dedicated analysis exists for long slepton lifetimes, the constraints for all lifetimes are particularly weak (Fig. 9.9). Therefore, in this channel more points can be excluded if only very short slepton lifetimes are considered. In the 2–lepton and 2–tau channel the "all lifetime" limits are almost identical to the limits for very short lifetimes, and no improvement is found.

Finally, the excluded regions for the case $\tau < 10^{-8}\,\mathrm{s}$ and $N = 1$ are shown in Fig. 9.35.

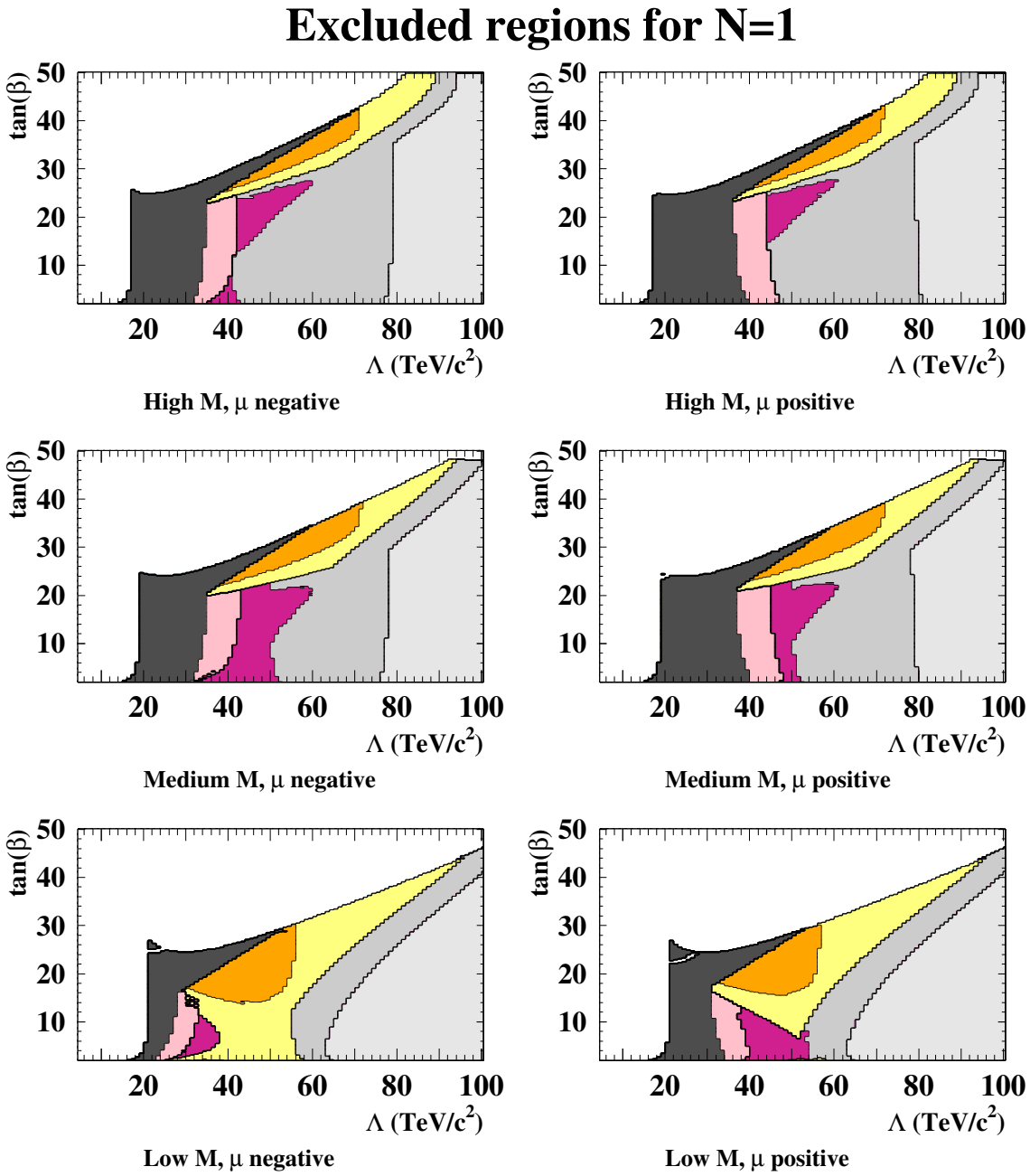


Figure 9.28: *Excluded regions in the $\Lambda - \tan\beta$ plane for $N = 1$ and different values of M and sign(μ), valid for all NLSP lifetimes. From top to bottom: high M ($M = 10^6$ TeV/c^2), medium M ($M = 250$ TeV/c^2) and low M ($M = 1.01 \cdot \Lambda$), left: sign(μ) $= -1$, right: sign(μ) $= +1$. The white regions are not allowed by theory. In the black regions the NLSP is lighter than 45 GeV/c^2. These regions were not considered in this analysis. The grey regions cannot be excluded, with the light grey region being beyond the kinematic reach of LEP 2. The coloured regions are excluded by:*

- *slepton pair–production in the slepton co–NLSP or stau NLSP scenario,*
- *neutralino pair–production in the slepton co–NLSP or stau NLSP scenario,*
- *selectron or smuon pair–production in the stau NLSP scenario,*
- *chargino pair–production in the slepton co–NLSP or stau NLSP scenario,*
- *neutralino pair–production in the neutralino NLSP scenario,*
- *slepton pair–production in the neutralino NLSP scenario,*
- *chargino pair–production in the neutralino NLSP scenario.*

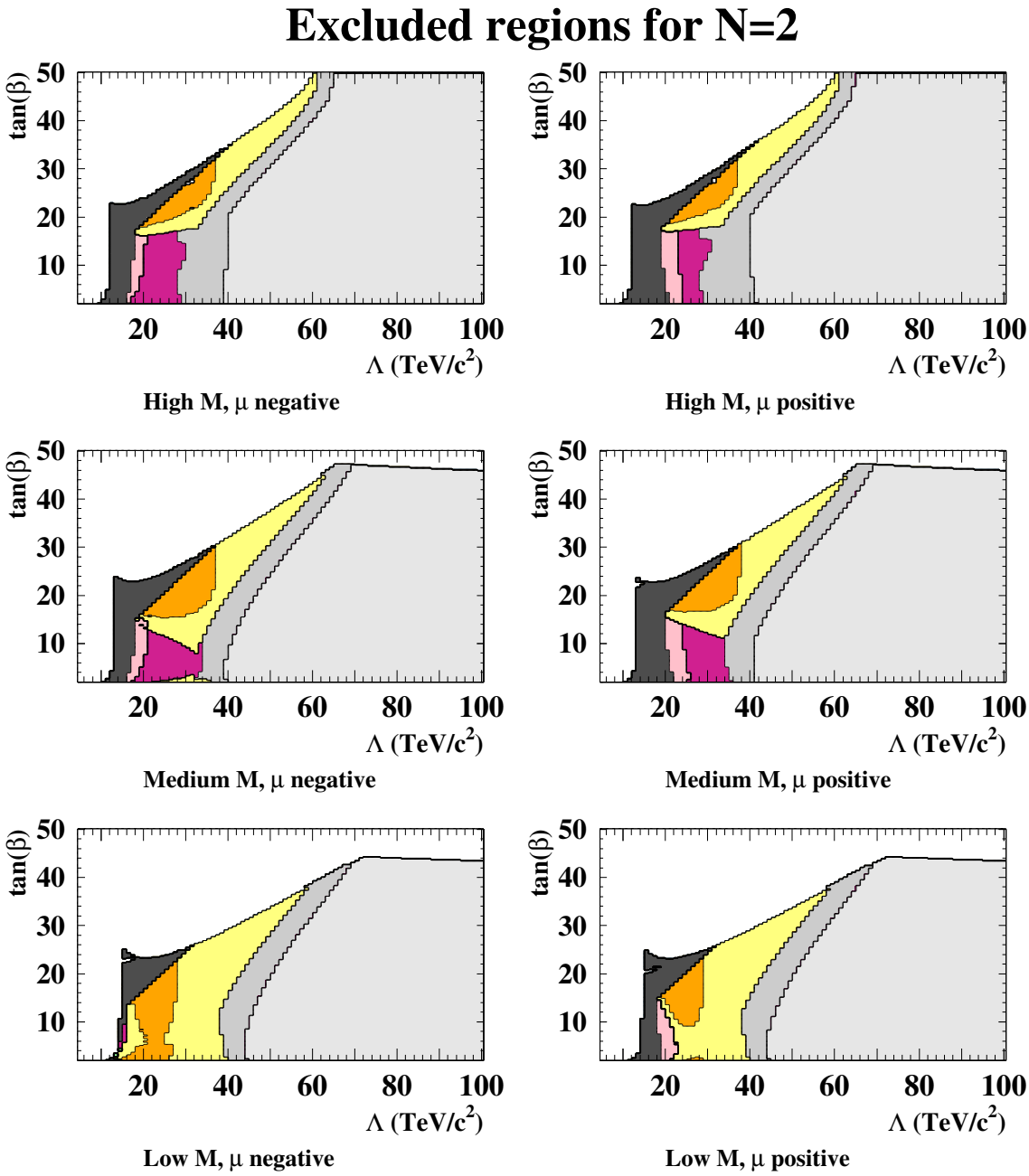


Figure 9.29: *Excluded regions in the $\Lambda - \tan\beta$ plane for $N = 2$ and different values of M and sign(μ), valid for all NLSP lifetimes. From top to bottom: high M ($M = 10^6$ TeV/c^2), medium M ($M = 250$ TeV/c^2) and low M ($M = 1.01 \cdot \Lambda$), left: sign(μ) $= -1$, right: sign(μ) $= +1$. The white regions are not allowed by theory. In the black regions the NLSP is lighter than 45 GeV/c^2. These regions were not considered in this analysis. The grey regions cannot be excluded, with the light grey region being beyond the kinematic reach of LEP 2. The coloured regions are excluded by:*

- *slepton pair–production in the slepton co–NLSP or stau NLSP scenario,*
- *neutralino pair–production in the slepton co–NLSP or stau NLSP scenario,*
- *selectron or smuon pair–production in the stau NLSP scenario,*
- *chargino pair–production in the slepton co–NLSP or stau NLSP scenario,*
- *neutralino pair–production in the neutralino NLSP scenario,*
- *slepton pair–production in the neutralino NLSP scenario,*
- *chargino pair–production in the neutralino NLSP scenario.*

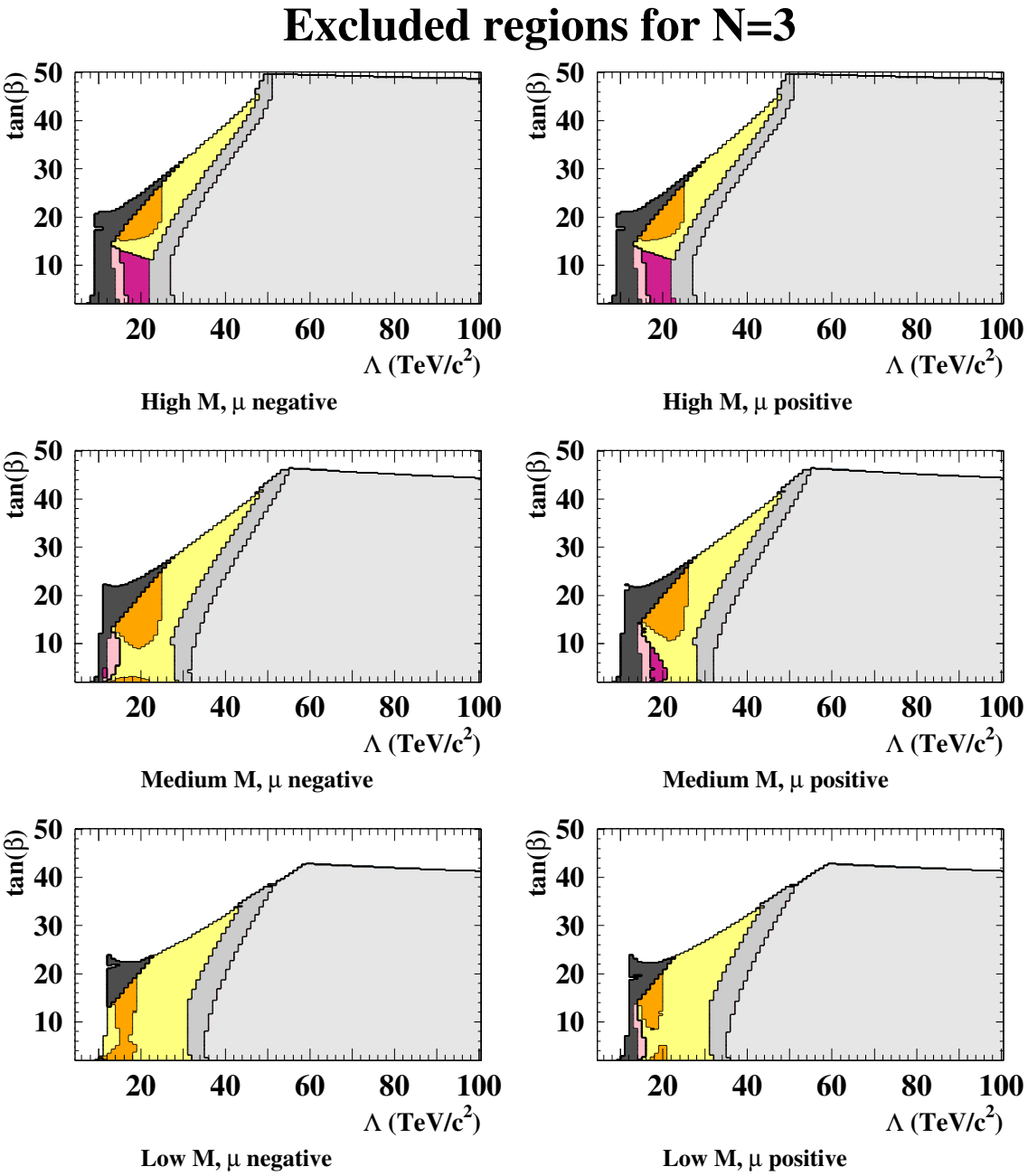


Figure 9.30: *Excluded regions in the $\Lambda - \tan\beta$ plane for $N = 3$ and different values of M and sign(μ), valid for all NLSP lifetimes. From top to bottom: high M ($M = 10^6$ TeV/c^2), medium M ($M = 250$ TeV/c^2) and low M ($M = 1.01 \cdot \Lambda$), left: sign(μ) $= -1$, right: sign(μ) $= +1$. The white regions are not allowed by theory. In the black regions the NLSP is lighter than 45 GeV/c^2. These regions were not considered in this analysis. The grey regions cannot be excluded, with the light grey region being beyond the kinematic reach of LEP 2. The coloured regions are excluded by:*

- *slepton pair–production in the slepton co–NLSP or stau NLSP scenario,*
- *neutralino pair–production in the slepton co–NLSP or stau NLSP scenario,*
- *selectron or smuon pair–production in the stau NLSP scenario,*
- *chargino pair–production in the slepton co–NLSP or stau NLSP scenario,*
- *neutralino pair–production in the neutralino NLSP scenario,*
- *slepton pair–production in the neutralino NLSP scenario,*
- *chargino pair–production in the neutralino NLSP scenario.*

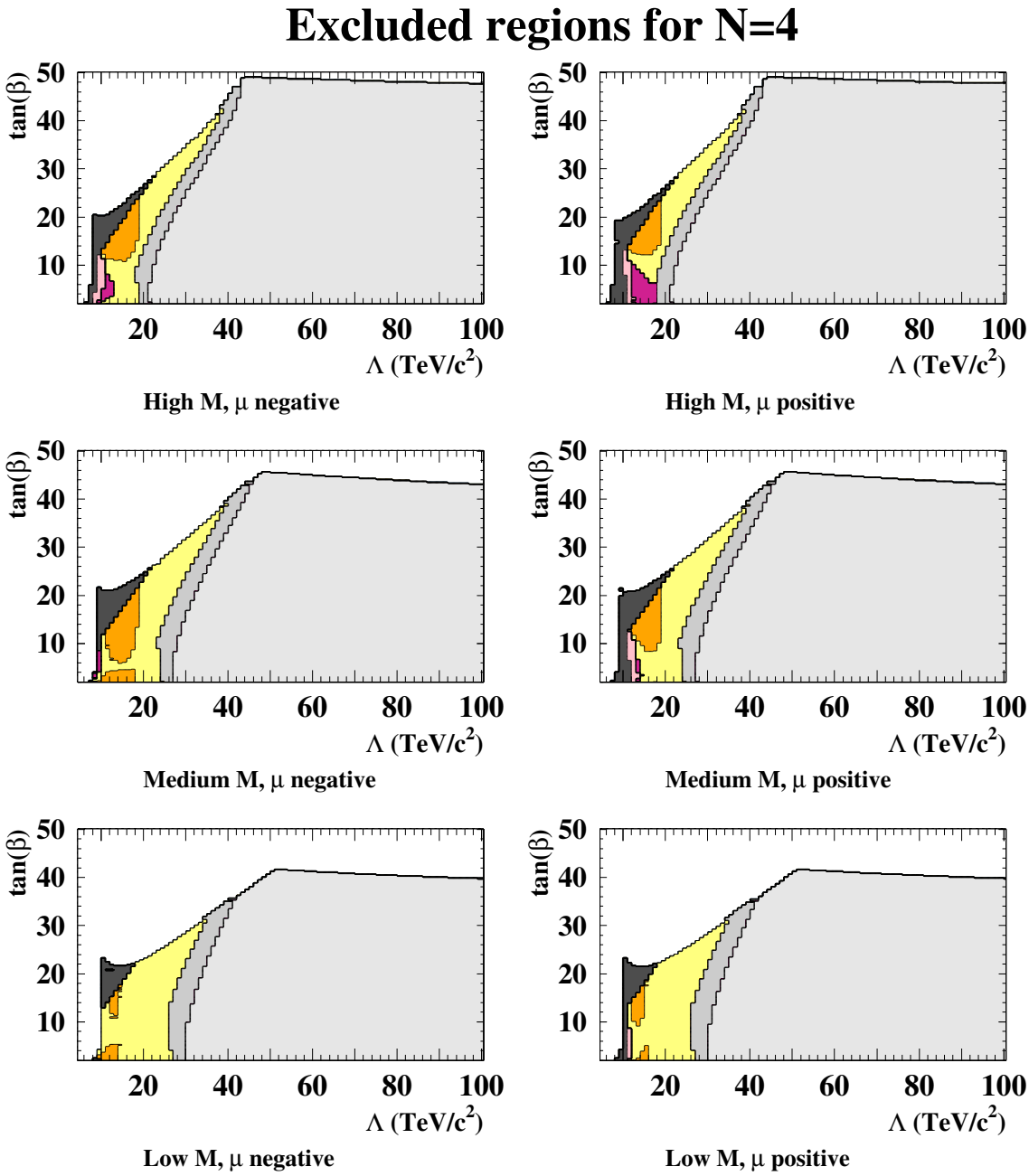


Figure 9.31: *Excluded regions in the $\Lambda - \tan\beta$ plane for $N = 4$ and different values of M and sign(μ), valid for all NLSP lifetimes. From top to bottom: high M ($M = 10^6$ TeV/c^2), medium M ($M = 250$ TeV/c^2) and low M ($M = 1.01 \cdot \Lambda$), left: sign(μ) $= -1$, right: sign(μ) $= +1$. The white regions are not allowed by theory. In the black regions the NLSP is lighter than 45 GeV/c^2. These regions were not considered in this analysis. The grey regions cannot be excluded, with the light grey region being beyond the kinematic reach of LEP 2. The coloured regions are excluded by:*

- *slepton pair–production in the slepton co–NLSP or stau NLSP scenario,*
- *neutralino pair–production in the slepton co–NLSP or stau NLSP scenario,*
- *selectron or smuon pair–production in the stau NLSP scenario,*
- *chargino pair–production in the slepton co–NLSP or stau NLSP scenario,*
- *neutralino pair–production in the neutralino NLSP scenario,*
- *slepton pair–production in the neutralino NLSP scenario,*
- *chargino pair–production in the neutralino NLSP scenario.*

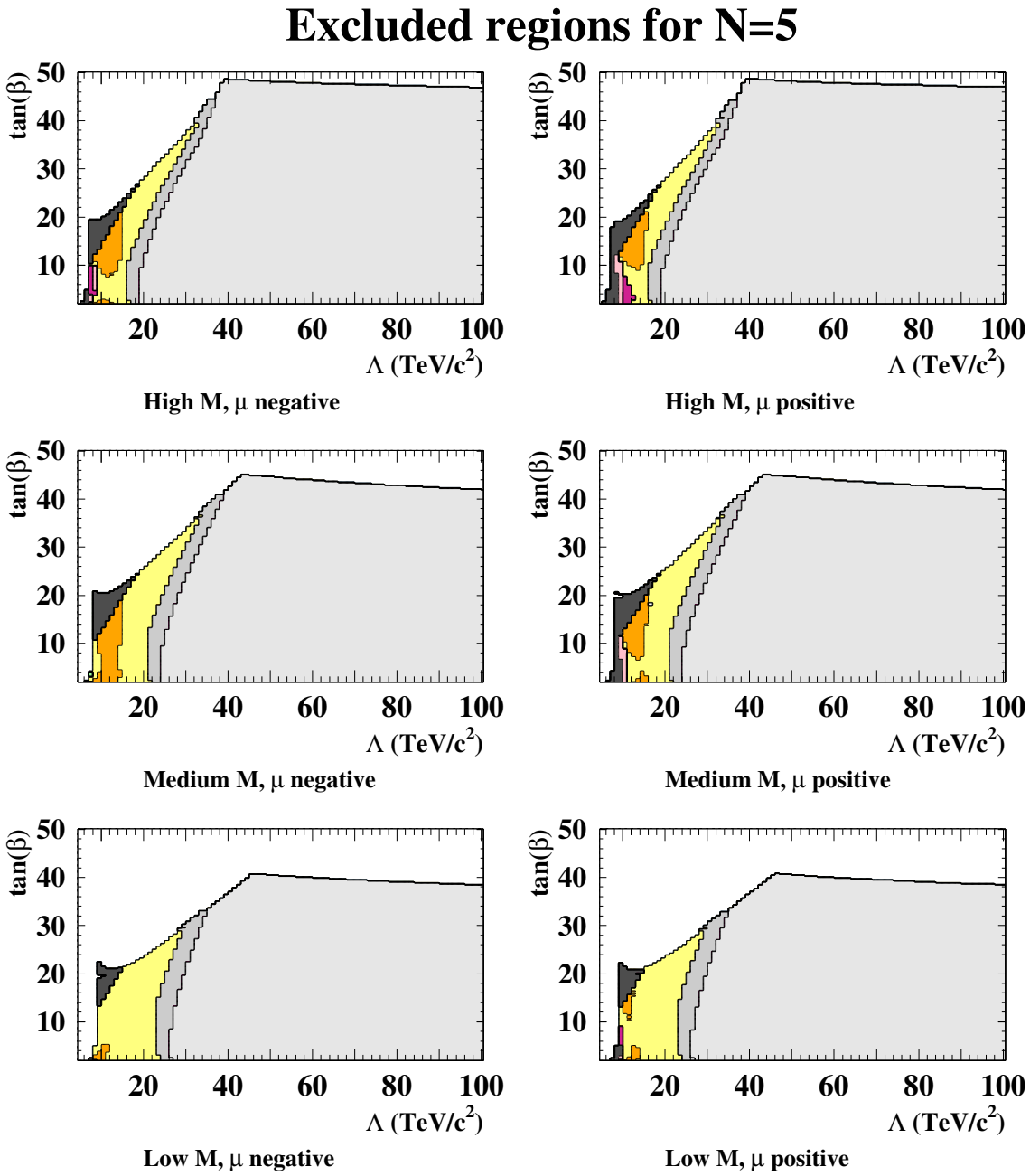


Figure 9.32: *Excluded regions in the $\Lambda - \tan\beta$ plane for $N = 5$ and different values of M and sign(μ), valid for all NLSP lifetimes. From top to bottom: high M ($M = 10^6$ TeV/c^2), medium M ($M = 250$ TeV/c^2) and low M ($M = 1.01 \cdot \Lambda$), left: sign(μ) $= -1$, right: sign(μ) $= +1$. The white regions are not allowed by theory. In the black regions the NLSP is lighter than 45 GeV/c^2. These regions were not considered in this analysis. The grey regions cannot be excluded, with the light grey region being beyond the kinematic reach of LEP 2. The coloured regions are excluded by:*

- *slepton pair–production in the slepton co–NLSP or stau NLSP scenario,*
- *neutralino pair–production in the slepton co–NLSP or stau NLSP scenario,*
- *selectron or smuon pair–production in the stau NLSP scenario,*
- *chargino pair–production in the slepton co–NLSP or stau NLSP scenario,*
- *neutralino pair–production in the neutralino NLSP scenario,*
- *slepton pair–production in the neutralino NLSP scenario,*
- *chargino pair–production in the neutralino NLSP scenario.*

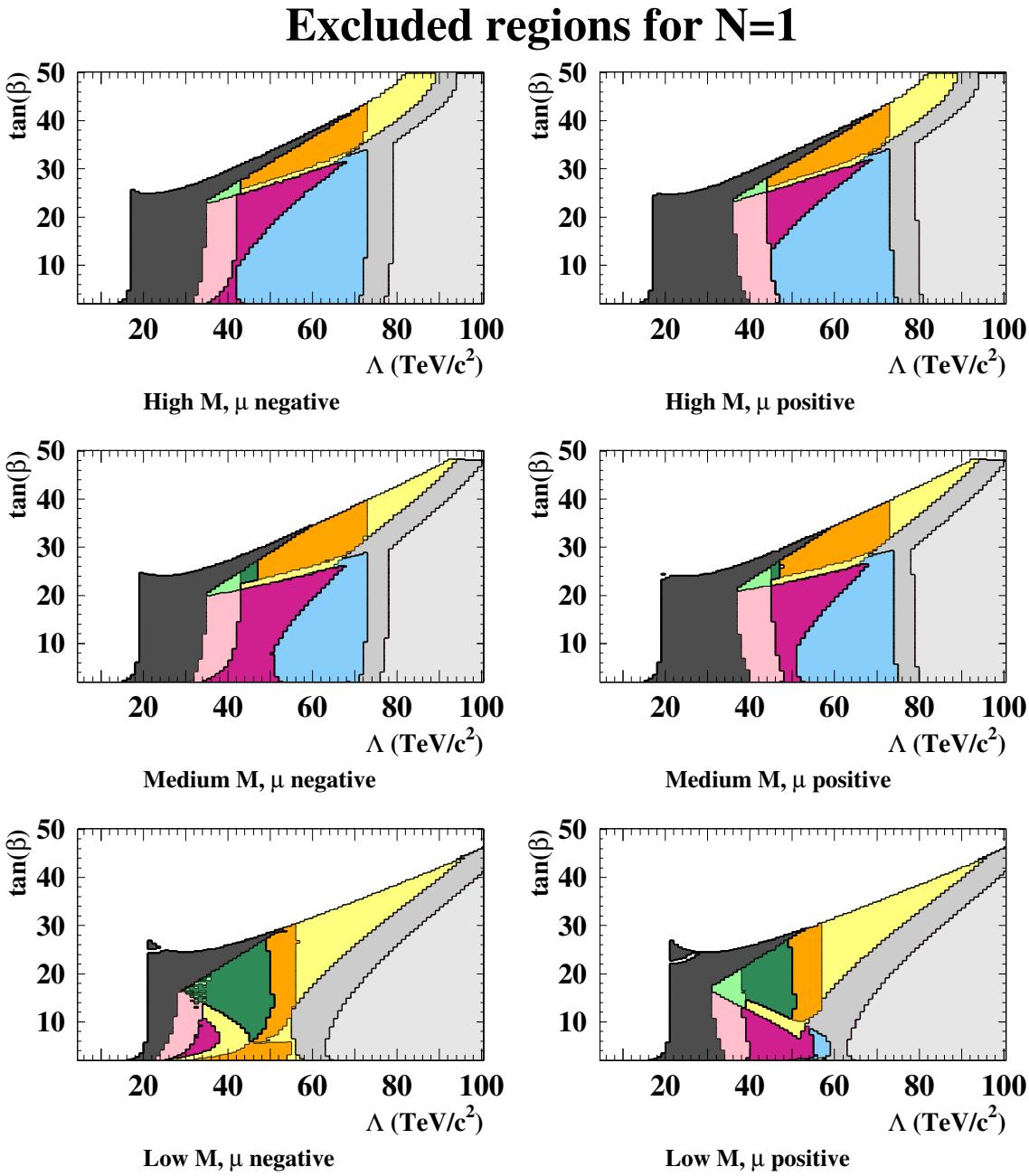


Figure 9.33: *Excluded regions in the $\Lambda - \tan\beta$ plane for $N = 1$ and different values of M and sign(μ), for negligible NLSP lifetimes ($\tau = 10^{-12}$ s). From top to bottom: high M ($M = 10^6$ TeV/c^2), medium M ($M = 250$ TeV/c^2) and low M ($M = 1.01 \cdot \Lambda$), left: sign(μ) $= -1$, right: sign(μ) $= +1$. The white regions are not allowed by theory. In the black regions the NLSP is lighter than 45 GeV/c^2. These regions were not considered in this analysis. The grey regions cannot be excluded, with the light grey region being beyond the kinematic reach of LEP 2. The coloured regions are excluded by:*

- *slepton pair–production in the slepton co–NLSP or stau NLSP scenario,*
- *neutralino pair–production in the slepton co–NLSP or stau NLSP scenario,*
- *selectron or smuon pair–production in the stau NLSP scenario,*
- *chargino pair–production in the slepton co–NLSP or stau NLSP scenario,*
- *neutralino pair–production in the neutralino NLSP scenario,*
- *slepton pair–production in the neutralino NLSP scenario,*
- *chargino pair–production in the neutralino NLSP scenario.*

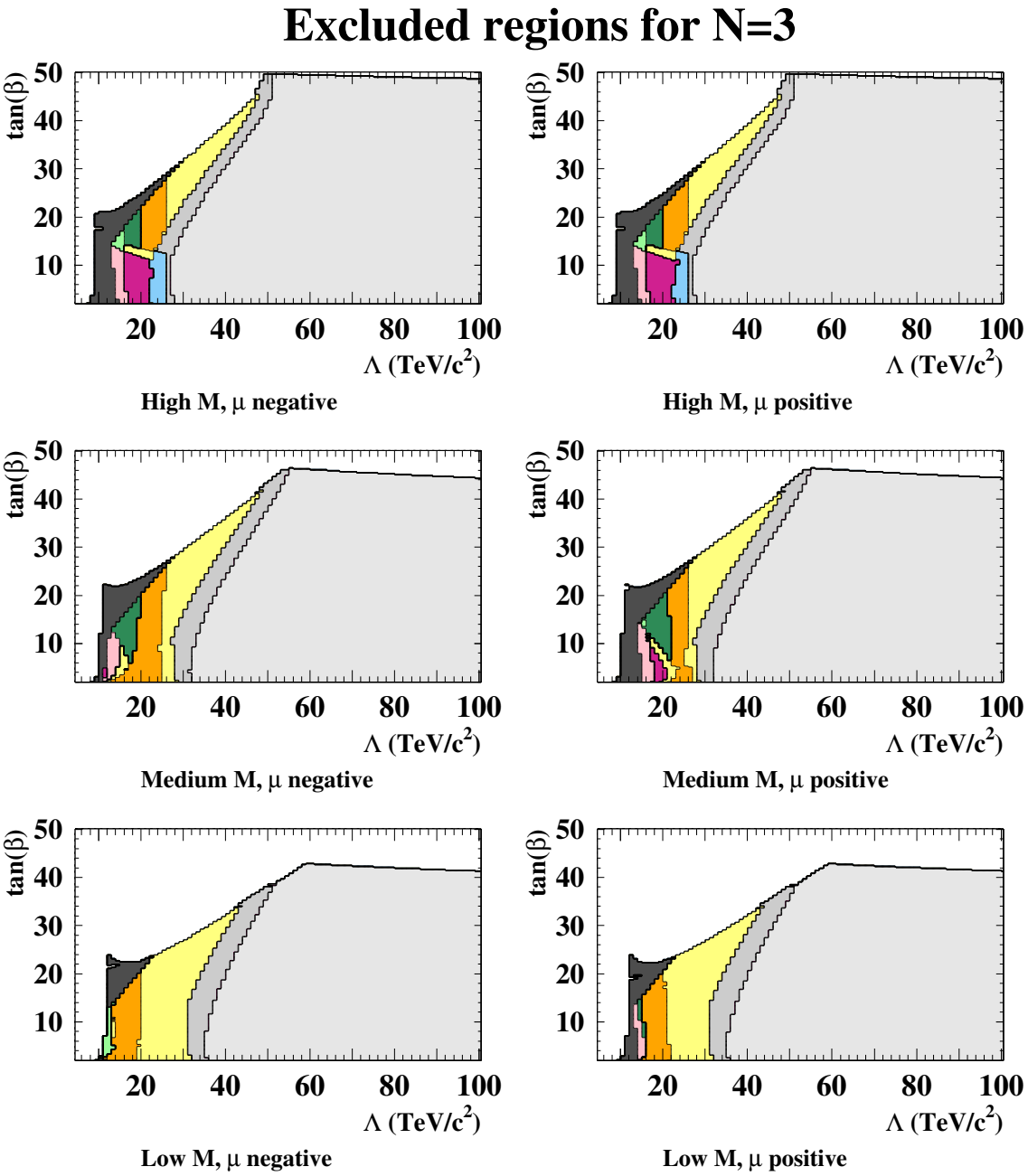


Figure 9.34: *Excluded regions in the $\Lambda - \tan\beta$ plane for $N = 3$ and different values of M and sign(μ), for negligible NLSP lifetimes ($\tau = 10^{-12}$ s). From top to bottom: high M ($M = 10^6$ TeV/c^2), medium M ($M = 250$ TeV/c^2) and low M ($M = 1.01 \cdot \Lambda$), left: sign(μ) $= -1$, right: sign(μ) $= +1$. The white regions are not allowed by theory. In the black regions the NLSP is lighter than 45 GeV/c^2. These regions were not considered in this analysis. The grey regions cannot be excluded, with the light grey region being beyond the kinematic reach of LEP 2. The coloured regions are excluded by:*

- *slepton pair–production in the slepton co–NLSP or stau NLSP scenario,*
- *neutralino pair–production in the slepton co–NLSP or stau NLSP scenario,*
- *selectron or smuon pair–production in the stau NLSP scenario,*
- *chargino pair–production in the slepton co–NLSP or stau NLSP scenario,*
- *neutralino pair–production in the neutralino NLSP scenario,*
- *slepton pair–production in the neutralino NLSP scenario,*
- *chargino pair–production in the neutralino NLSP scenario.*

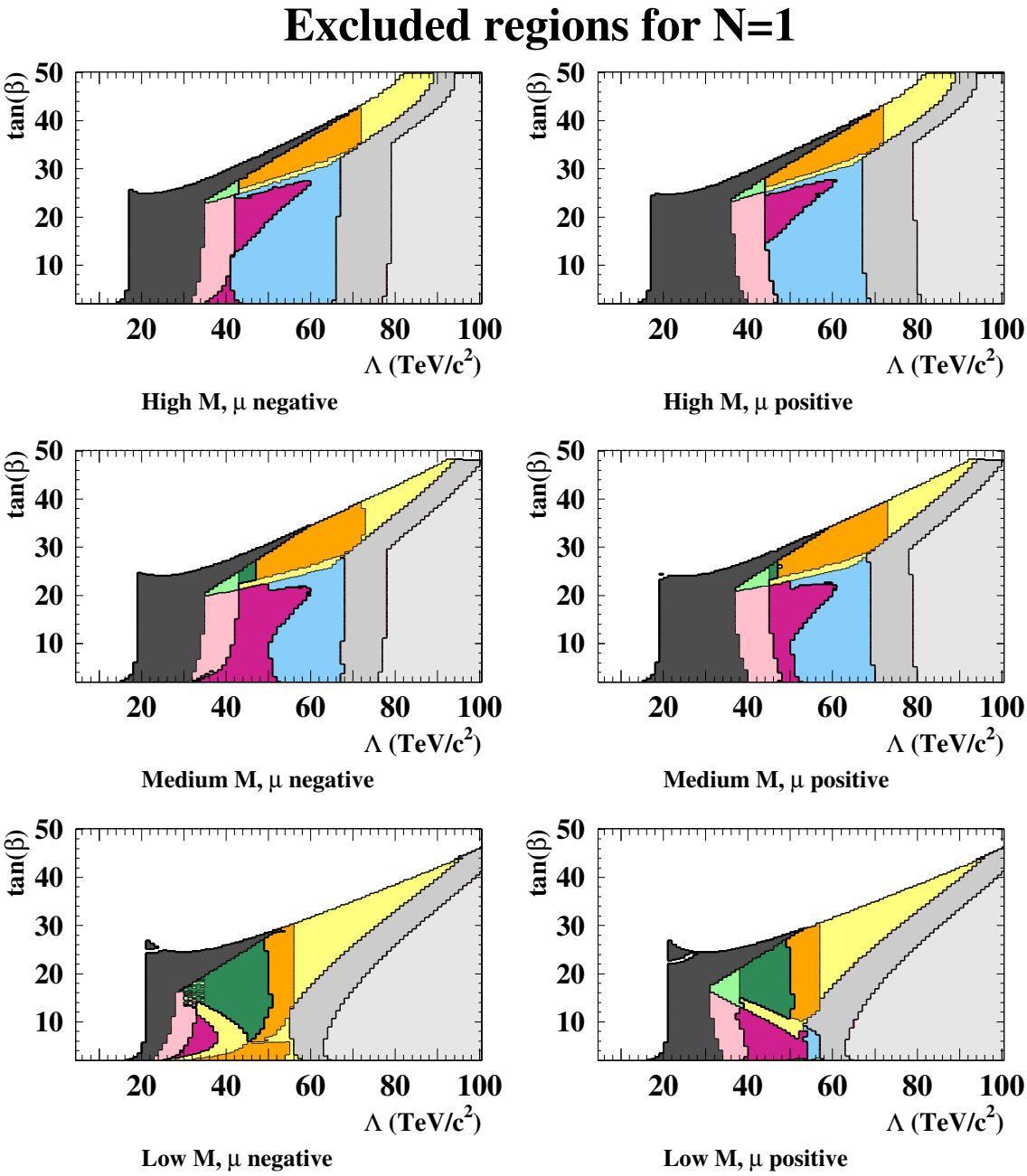


Figure 9.35: *Excluded regions in the $\Lambda - \tan\beta$ plane for $N = 1$ and different values of M and $sign(\mu)$, for lifetimes $< 10^{-8}$ s, corresponding to a proper decay length < 3 m. From top to bottom: high M ($M = 10^6$ TeV/c^2), medium M ($M = 250$ TeV/c^2) and low M ($M = 1.01 \cdot \Lambda$), left: $sign(\mu) = -1$, right: $sign(\mu) = +1$. The white regions are not allowed by theory. In the black regions the NLSP is lighter than 45 GeV/c^2. These regions were not considered in this analysis. The grey regions cannot be excluded, with the light grey region being beyond the kinematic reach of LEP 2. The coloured regions are excluded by:*

- *slepton pair–production in the slepton co–NLSP or stau NLSP scenario,*
- *neutralino pair–production in the slepton co–NLSP or stau NLSP scenario,*
- *selectron or smuon pair–production in the stau NLSP scenario,*
- *chargino pair–production in the slepton co–NLSP or stau NLSP scenario,*
- *neutralino pair–production in the neutralino NLSP scenario,*
- *slepton pair–production in the neutralino NLSP scenario,*
- *chargino pair–production in the neutralino NLSP scenario.*

9.3.2 Constraints on the SUSY Particle Mass Scale Λ

From the exclusions in the $\Lambda - \tan\beta$ plane presented in the previous section, lower limits on the SUSY particle mass scale Λ, independent of $\tan\beta$, were inferred. This parameter determines, for fixed N, the GMSB particle spectrum at the messenger scale, since the gaugino masses are given by

$$m_{\lambda_i}(M) \sim N \cdot \Lambda \frac{\alpha_i(M)}{4\pi},$$

where λ_i are the gaugino fields of gauge group i and the α_i are the GUT normalised coupling constants of these gauge groups. Also the messenger scale scalar masses are determined by Λ:

$$m^2(M) \sim 2N \cdot \Lambda^2 \sum_{i=1}^{3} k_i \left(\frac{\alpha_i(M)}{4\pi}\right)^2.$$

The sum is over the gauge groups $SU(3)_C \times SU(2)_L \times U(1)_Y$ (details are discussed in Chapter 2).

Constraints on Λ were again obtained for three cases: all NLSP lifetimes ($10^{-12}\,\mathrm{s} \leq \tau \leq 10^{-6}\,\mathrm{s}$), negligible NLSP lifetimes ($\tau = 10^{-12}\,\mathrm{s}$), and for NLSP lifetimes $\tau < 10^{-8}\,\mathrm{s}$. The results for these lifetimes and the 30 parameter sets included in the scan are summarised in Table 9.2. As visible from this table, the constraints on Λ decrease with larger N, with typical lower limits of $50\,\mathrm{TeV}/c^2$ for $N = 1$ and $15\,\mathrm{TeV}/c^2$ for $N = 5$. The constraints depend slightly on M, and are almost independent of the sign of the parameter μ.

For $N \leq 3$, the constraints are lower for the case of all lifetimes than for negligible NLSP lifetimes, while for larger N the same limits are found. As already mentioned, for small lifetimes the search for neutralino pair–production in the neutralino NLSP scenario contributes and improves the limits in the cases of small N, where the neutralino NLSP scenario is important.

For $\tau < 10^{-8}\,\mathrm{s}$, the Λ limits are, apart from two parameter combinations, identical to the case of negligible lifetimes. The validity in lifetime of the strong Λ constraints obtained for negligible lifetimes can thus be extended by several orders of magnitude, with slightly lower limits obtained only for two of the parameter combinations studied.

In conclusion, constraints on Λ of $\Lambda > 40$, 27, 21, 17, $15\,\mathrm{TeV}/c^2$ were derived for $N =$ 1, 2, 3, 4, 5, respectively, for all NLSP lifetimes.

The constraints on Λ imply lower limits on the masses of all SUSY particles and Higgs bosons, including those that are kinematically not accessible at LEP 2. Such lower limits were calculated for all N, for the cases of all NLSP lifetimes and $\tau < 10^{-8}\,\mathrm{s}$. The results are shown in Fig. 9.36 for all particles for which no mass limits could be derived directly, i.e. the $\tilde{\chi}_1^\pm$, $\tilde{\chi}_2^\pm$, $\tilde{\chi}_2^0$, $\tilde{\chi}_3^0$, $\tilde{\chi}_4^0$, $\tilde{\tau}_2$, $\tilde{\mu}_L$, $\tilde{\mathrm{e}}_L$, and the Higgs bosons. It has to be stressed, however, that the program used for the parameter scan (SUSYGEN) is not recommended by the authors for detailed studies of the Higgs sector [18]. For the case $\tau < 10^{-8}\,\mathrm{s}$, stronger mass constraints are found especially for the lighter chargino.

Without any Λ constraint, the sleptons, the $\tilde{\chi}_2^0$ and the light Higgs h^0 can be rather light ($< 100\,\mathrm{GeV}/c^2$), while for the other particles masses of typically $100 - 150\,\mathrm{GeV}/c^2$ are allowed in the GMSB models considered in the scan. The indirect constraint on the light Higgs h^0 is below experimental bounds, while for all other particles severe constraints are implied by the lower limits on Λ obtained in this work.

Lower limit at 95 % C.L. on Λ [TeV/c^2] for all NLSP lifetimes						
		$N=1$	$N=2$	$N=3$	$N=4$	$N=5$
High M	$\mu<0$	40	27	21	17	15
	$\mu>0$	43	27	21	17	15
Medium M	$\mu<0$	49	31	26	22	20
	$\mu>0$	49	33	26	22	20
Low M	$\mu<0$	54	37	30	25	22
	$\mu>0$	52	37	30	25	22
Lower limit at 95 % C.L. on Λ [TeV/c^2] for $\tau = 10^{-12}$ s						
		$N=1$	$N=2$	$N=3$	$N=4$	$N=5$
High M	$\mu<0$	67	33	22	17	15
	$\mu>0$	67	34	22	17	15
Medium M	$\mu<0$	66	33	26	22	20
	$\mu>0$	67	34	26	22	20
Low M	$\mu<0$	54	37	30	25	22
	$\mu>0$	52	37	30	25	22
Lower limit at 95 % C.L. on Λ [TeV/c^2] for $\tau < 10^{-8}$ s						
		$N=1$	$N=2$	$N=3$	$N=4$	$N=5$
High M	$\mu<0$	64	33	22	17	15
	$\mu>0$	66	34	22	17	15
Medium M	$\mu<0$	66	33	26	22	20
	$\mu>0$	67	34	26	22	20
Low M	$\mu<0$	54	37	30	25	22
	$\mu>0$	52	37	30	25	22

Table 9.2: *Lower limits at 95 % C.L. on the SUSY particle mass scale Λ, for various sets of the GMSB parameters M, N and sign(μ). Three cases were considered: all NLSP lifetimes (10^{-12} s$\leq \tau \leq 10^{-6}$ s), negligible NLSP lifetimes ($\tau = 10^{-12}$ s), and $\tau < 10^{-8}$ s.*

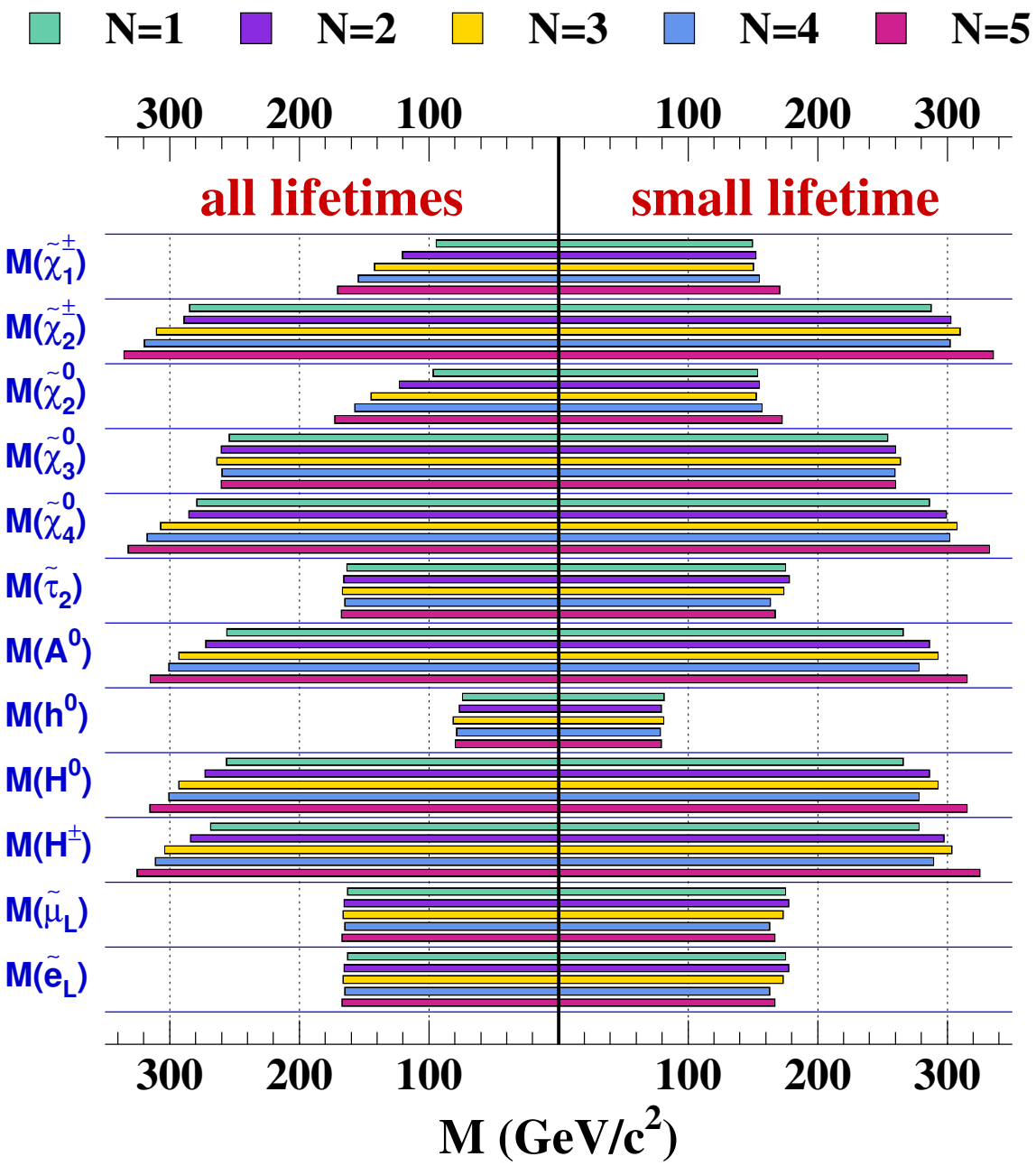


Figure 9.36: *Indirect constraints on the masses of various particles, implied by the limits on the parameter Λ, for different values of the messenger index N and within the framework of the GMSB parameter scan used in this work. Left: mass constraints valid for all NLSP lifetimes, right: mass constraints valid for small NLSP lifetimes $< 10^{-8}$ s.*

Chapter 10

Summary and Discussion

In the Gauge Mediated Supersymmetry Breaking model the next–to–lightest supersymmetric particle (NLSP) is the lightest slepton in a large part of the parameter space, and its lifetime is a free parameter. For intermediate slepton lifetimes of about $10^{-11} - 10^{-9}$ s, corresponding to proper decay lengths of the order of millimetres to several tens of centimetres, the decay of the slepton to a lepton and an invisible gravitino leads to the experimental topology of tracks with large impact parameters. In this work a search for sleptons with intermediate lifetimes was performed, using data from e^+e^- collisions recorded with the OPAL detector at LEP 2. The results of this search for sleptons with intermediate lifetimes were combined with other OPAL analyses for promptly decaying, long–lived and stable sleptons.

A program was developed that allows for proper simulation of supersymmetric particles with arbitrary lifetimes and their decays. This program is used by all OPAL GMSB searches as well as searches for other supersymmetric processes with long–lived particles.

Efficient selections, exploiting the topology of tracks with large impact parameters, were developed for all production channels possible in GMSB models with a slepton NLSP at LEP 2 energies: slepton pair–production, neutralino pair–production and chargino pair–production. Unmodeled background, which gives a serious contribution to the total expected background for this topology, was successfully removed. No evidence for sleptons with intermediate lifetimes was found in the data set taken at $\sqrt{s} = 189 - 209\,\mathrm{GeV}$ with an integrated luminosity of approximately $600\,\mathrm{pb}^{-1}$. Instead, for all channels the number of selected candidates is in good agreement with the number of events expected from Standard Model sources. For selectron and smuon pair–production in the scenario where the sleptons are degenerate in mass (slepton co–NLSP scenario), which is the channel with the lowest level of remaining background, no candidate was selected, while 0.09 events are expected from Standard Model processes.

To obtain limits on cross–sections and masses that are independent of the slepton lifetime, a combination was performed that includes also other OPAL searches covering negligible, long and infinite slepton lifetimes. In all channels studied, cross–section limits were presented. For slepton pair–production in the slepton co–NLSP scenario, stau pair–production in the stau NLSP scenario and for neutralino pair–production, these cross–section limits are valid for all slepton lifetimes. The cross–section limits for slepton pair–production in the stau NLSP scenario and chargino pair–production are valid for proper slepton decay lengths up to 3 m.

Mass limits were derived for selectrons, smuons and staus. To reach as much generality as possible within the framework of the GMSB model, a scan of the GMSB parameters was performed, and the expected cross–section was calculated from a minimisation within this scan. Slepton mass limits of $m_{\tilde{e}_R} > 60.1\,\mathrm{GeV}/c^2$ for the right–handed selectron (expected limit: $m_{\tilde{e}_R} > 60.0\,\mathrm{GeV}/c^2$), $m_{\tilde{\mu}_R} > 93.7\,\mathrm{GeV}/c^2$ for the right–handed smuon (expected limit: $m_{\tilde{\mu}_R} > 93.6\,\mathrm{GeV}/c^2$) and $m_{\tilde{\tau}_1} > 87.4\,\mathrm{GeV}/c^2$ for the lighter stau (expected limit: $m_{\tilde{\tau}_1} > 88.2\,\mathrm{GeV}/c^2$ in the slepton co–NLSP scenario and $m_{\tilde{\tau}_1} > 87.6\,\mathrm{GeV}/c^2$ in the stau

NLSP scenario) were derived, for a messenger index $N \leq 5$ and independent of the slepton lifetime. These limits significantly improve and generalise previous OPAL results: in [55], based on the data set taken at $\sqrt{s} = 189\,\mathrm{GeV}$, slepton mass limits of $M_{\tilde{\tau}_1} = 69\,\mathrm{GeV}/c^2$ and $M_{\tilde{\mu}_R,\tilde{\mathrm{e}}_R} = 88\,\mathrm{GeV}/c^2$ (assuming a mass degeneracy between the smuon and the selectron) were established for $\tan\beta = 20$. For the case of $\tan\beta = 2$, a mass limit of $M_{\tilde{\ell}} = 83\,\mathrm{GeV}/c^2$ (assuming a mass degeneracy among the sleptons) was reported. These numbers are valid for $N \leq 4$ and prompt slepton decays. Previously, with the large impact parameter topology uncovered, a smuon mass limit of approximately $50\,\mathrm{GeV}/c^2$ was quoted for all slepton lifetimes [57].

The results of the studies presented here can be compared with results from the other LEP collaborations, ALEPH, DELPHI and L3. The slepton mass limits of the ALEPH [58], DELPHI [59] and L3 [60] collaborations, together with the results from OPAL presented in this work, are summarised in Table 10.1, and the stau mass limits are shown in Fig. 10.1. As visible, the results presented in this thesis surpass previous LEP results, both for the observed and expected limit. It has to be stressed that the ALEPH selectron limit was calculated by neglecting the t–channel contribution and its destructive interference with the s–channel to the expected cross–section. Considering the interference would reduce the ALEPH limit significantly.

	$M(\tilde{\mathrm{e}}_R)$ [GeV/c^2]	$M(\tilde{\mu}_R)$ [GeV/c^2]	$M(\tilde{\tau}_1)$ [GeV/c^2]	$\sqrt{s}$ [GeV]
ALEPH	83 (s–channel only)	88	77 (82)	189–209
DELPHI	–	88	82.5	130–209
L3	–	–	63.5 (67)	200
OPAL	60.1 (60.0)	93.7 (93.6)	87.4 (88.2/87.6)	189–209

Table 10.1: *Compilation of selectron, smuon and stau mass limits at 95 % C.L. within the GMSB model from ALEPH, DELPHI, L3 and OPAL, as presented in this thesis. The expected limits are given in parentheses, when available from the experiment (for OPAL, the two numbers for staus correspond to the slepton co– and the stau NLSP scenario). The OPAL search for heavy stable charged particles uses, in addition, the data with* $\sqrt{s} = 130 - 183$ *GeV.*

To interpret the experimental results in terms of the GMSB model, the constraints on the production cross–sections were used to exclude regions within the GMSB parameter space. Significant parts of the kinematically accessible parameter space with a slepton NLSP can be excluded by the presented combination. For a messenger index $N = 1$, or larger N but a small SUSY particle mass scale Λ, the neutralino rather than the slepton is the NLSP. Thus, to establish constraints on Λ, searches for topologies with a neutralino NLSP had to be included. This combination yields constraints on Λ of $\Lambda > 40$, 27, 21, 17, $15\,\mathrm{TeV}/c^2$ for $N = 1$, 2, 3, 4, 5, respectively, independent of the NLSP lifetime. For prompt NLSP decays, the limits are $\Lambda > 52$, 33, 22, 17, $15\,\mathrm{TeV}/c^2$ for $N = 1$, 2, 3, 4, 5, respectively. This surpasses previous OPAL limits of $\Lambda > 48$, 31, 22, $19\,\mathrm{TeV}/c^2$ for $N = 1$, 2, 3, 4, respectively, valid for the special case of zero NLSP lifetime [55].

The ALEPH collaboration quotes constraints on Λ of $\Lambda > 36\,\mathrm{TeV}/c^2$ for $N = 1$ and $\Lambda > 10\,\mathrm{TeV}/c^2$ for $N = 5$, valid for all NLSP lifetimes. The DELPHI collaboration reports a limit of $\Lambda > 17.5\,\mathrm{TeV}/c^2$ for $N \leq 4$ and negligible NLSP lifetimes.

No hint for any SUSY particles was found at LEP. For the near future, the best chance to discover supersymmetry will be at the Tevatron, where protons and antiprotons collide at $\sqrt{s} = 1.96\,\mathrm{TeV}$. At this center–of–mass energy, the main production channels in GMSB models are $\tilde{\chi}_1^+\tilde{\chi}_1^-$ and $\tilde{\chi}_1^\pm\tilde{\chi}_2^0$. The primary particles decay and the cascades terminate with the lightest slepton, if it is the NLSP. In the stau NLSP scenario the D0 experiment, for

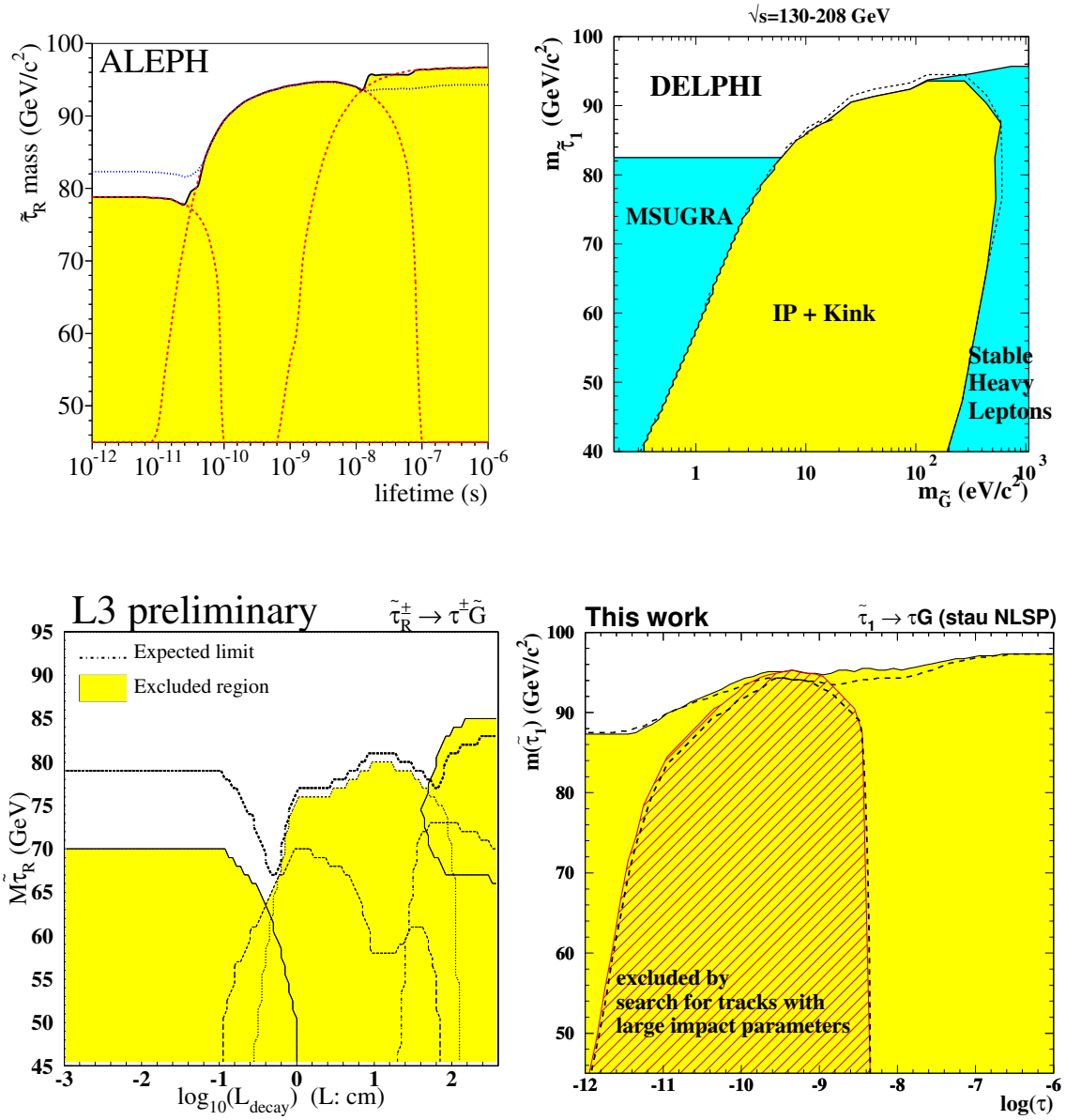


Figure 10.1: *Overview of stau mass limits obtained at LEP. Top left: stau mass limit at 95 % C.L. from ALEPH, as a function of the lifetime [58]. The expected limit is shown as a blue line. The red lines indicate the regions excluded by the searches for acoplanar leptons, for large impact parameters and kinks, and for heavy stable charged particles. Top right: stau mass limit at 95 % C.L. from DELPHI, as a function of the gravitino mass [59]. The blue region is excluded by the searches for large impact parameters and tracks with kinks, and the yellow regions are excluded by the search for sleptons in gravity mediated models (MSUGRA) and the search for stable heavy leptons. The dotted line gives the expected limit for the large impact parameter and kink searches. Bottom left: stau mass limit at 95 % C.L. from L3, as a function of the stau decay length [60]. The thick line represents the expected limit. The thin lines indicate, from left to right, the regions excluded by the searches for sleptons with zero lifetime, tracks with large impact parameters, tracks with kinks, and heavy stable charged particles (top: with, bottom: without using dE/dx). Bottom right: the stau mass limit, as a function of the lifetime, as presented in this work (Sect. 9.1.3), is shown as yellow histogram. The hatched region is excluded at 95 % C.L. by the search for tracks with large impact parameters. The dashed lines indicate the expected limits for the combination and the large impact parameter search.*

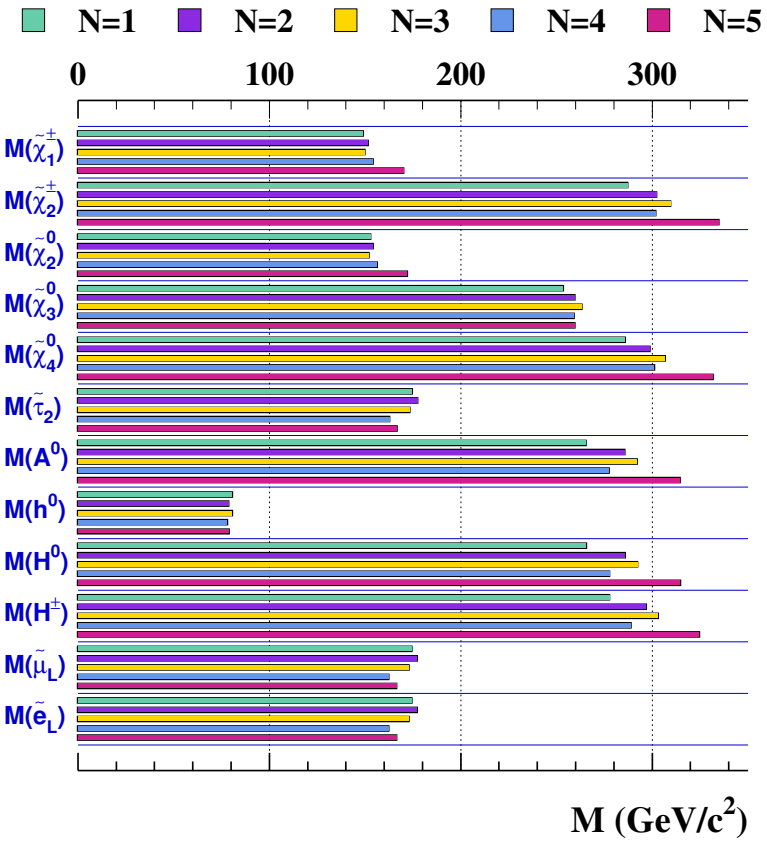


Figure 10.2: *Indirect constraints on the masses of various particles, implied by the limits on the parameter* Λ*. These constraints are valid for NLSP lifetimes* $< 10^{-8}$ *s, corresponding to a proper decay length below three metres, and within the framework of the GMSB parameter scan used in this work.*

example, will be able to discover a chargino with a mass up to 160 GeV/c^2 for negligible stau lifetime, assuming an integrated luminosity of 2 fb^{-1} [61]. If the stau is stable, a chargino with a mass up to 340 GeV/c^2 and a stau with a mass up to 160 GeV/c^2 can be discovered. In Figure 10.2 indirect constraints on the masses of various particles, implied by the lower constraints on the parameter Λ obtained in this work, are shown. For a short–lived stau and a messenger index $N = 2$, as used by D0, a mass of the lighter chargino below approximately 150 GeV/c^2 is indirectly excluded by this work.

At the LHC (Large Hadron Collider), with a center–of–mass energy of 14 TeV, squarks and gluinos will be produced copiously, if SUSY exists at the electroweak scale. Other supersymmetric processes will form the main background, and the issue will be to decide between different SUSY models. If GMSB exists and complete decay chains can be kinematically reconstructed, most GMSB parameters can be determined. This was studied for several scenarios and it was found that typically relative errors of 10–20 % will be achieved for most parameters, for an integrated luminosity of 10 fb^{-1} [62].

The results of a preliminary version of the analysis presented in this thesis are publicly available as a conference contribution [40], and entered into a preliminary LEP combination released for Moriond Electroweak 2002. A publication of the results presented here is planned for summer 2002. This will be the final OPAL publication on GMSB searches. In addition, a combination of the final results from all LEP collaborations is planned.

Appendix A

The OPAL Track Parameters

Charged particles cause hits in the jet chamber from which tracks are reconstructed. Each track is parametrised by the five parameters ϕ_0, κ, d_0, $\tan\lambda$ and z_0. The first three parameters describe the track in the plane transverse to the beam axes ($x-y$ or $r-\phi$ plane), while the last two parameters parametrise the track in the plane defined by z and the path–integral s along the track in the $r-\phi$ plane. The definition of the track parameters is given below. For illustration the track parameters are depicted in Fig. A.1.

- The parameter ϕ_0 is the azimuthal angle of the track tangent at the point of closest approach (p.c.a.). The p.c.a. is the point on the extrapolated track with the smallest distance to the origin, i.e. it is not necessarily a point between the first and last recorded hit of the track.

- The curvature κ of the track is given by:

$$|\kappa| = \frac{1}{2\rho}\,,$$

  where ρ is the radius of the curvature of the track. The sign of κ is defined such that for positive κ the angle ϕ increases if one moves along the track starting from the p.c.a. into the direction with decreasing $|x|$. For the magnetic field pointing in the $+z$ direction, as in OPAL, the tracks of negatively charged particles have a positive curvature. Consequently, the charge of the particle can be calculated by

$$q = -sign\left(\frac{B_z}{\kappa}\right)\,.$$

- The parameter d_0 is the impact parameter of the track, i.e. $|d_0|$ is the distance from the p.c.a. to the origin in the transverse plane, and the sign is derived from the formula:

$$d_0 = q\cdot(\rho - r_c).$$

  Here r_c is the radial distance of the centre of the track circle.

- The parameter $\tan\lambda$ describes the slope of the track in the $s-z$ plane. The angle λ is complementary to the polar angle θ: $\lambda = 90^\circ - \theta$, thus $\tan\lambda = \cot\theta$.

- Finally z_0 is the z coordinate of the point of closest approach.

The momentum components of the particle are then given by:

$$p_T\,(\mathrm{GeV/c}) \;=\; \frac{1}{2}\left|\frac{B_z\,(\mathrm{kG})}{\kappa\,(\mathrm{cm}^{-1})}\right| c\,(\mathrm{cm}\cdot\mathrm{s}^{-1})\cdot 10^{-14}$$

$$
\begin{aligned}
p_x &= p_T \cos\phi_0 \\
p_y &= p_T \sin\phi_0 \\
p_z &= p_T \tan\lambda \\
p &= p_T \sqrt{1+\tan^2\lambda}\,.
\end{aligned}
$$

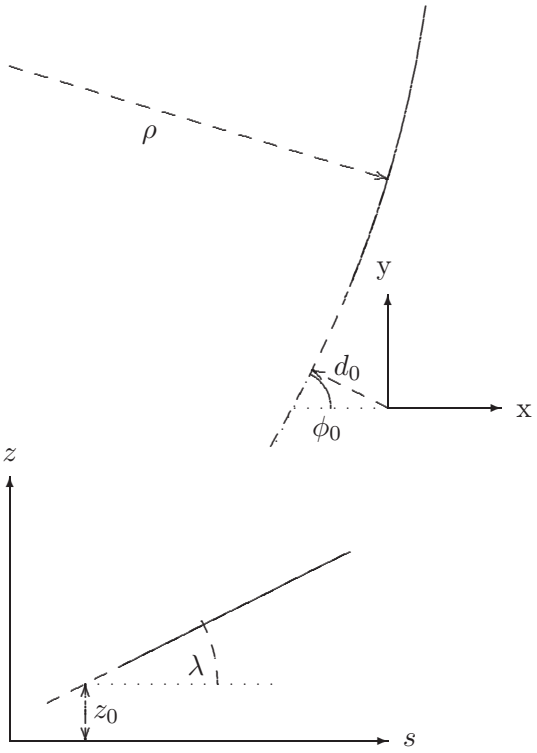


Figure A.1: *The track parameters in the $x-y$ (top) and $z-s$ plane (bottom). The solid lines depict the measured part of the track, the dashed line its interpolation.*

Appendix B

The Signal Monte Carlo Grid

In this appendix a complete list of the simulated signal Monte Carlo points for the slepton NLSP channels is given. For all channels the following ten NLSP lifetimes were simulated: $\tau = 10^{-12}$, 10^{-11}, 10^{-10}, $5 \cdot 10^{-10}$, 10^{-9}, $5 \cdot 10^{-9}$, 10^{-8}, $5 \cdot 10^{-8}$, 10^{-7}, 10^{-6} s.

- Selectron and smuon pair–production in the slepton co–NLSP scenario:
  $\sqrt{s} = 208.1\,\text{GeV}$.
  $M_{\tilde{\ell}_R} = 45,\ 50,\ 55,\ 60,\ 65,\ 70,\ 75,\ 80,\ 85,\ 90,\ 95,\ 100,\ 104\,\text{GeV}/c^2$.

- Stau pair–production: $\sqrt{s} = 208.1\,\text{GeV}$.
  $M_{\tilde{\tau}_1} = 45,\ 50,\ 55,\ 60,\ 65,\ 70,\ 75,\ 80,\ 85,\ 90,\ 95,\ 100,\ 101,\ 102,\ 103,\ 104\,\text{GeV}/c^2$.

- Neutralino pair–production with a slepton NLSP: $\sqrt{s} = 206.0\,\text{GeV}$.
  For both the stau NLSP scenario and the slepton co–NLSP scenario 17 combinations of neutralino and slepton masses were generated:
  $M_{\tilde{\chi}_1^0} = 50\,\text{GeV}/c^2$: $M_{\tilde{\ell}} = 45,\ 48\,\text{GeV}/c^2$
  $M_{\tilde{\chi}_1^0} = 70\,\text{GeV}/c^2$: $M_{\tilde{\ell}} = 45,\ 65,\ 68\,\text{GeV}/c^2$
  $M_{\tilde{\chi}_1^0} = 85\,\text{GeV}/c^2$: $M_{\tilde{\ell}} = 45,\ 65,\ 83\,\text{GeV}/c^2$
  $M_{\tilde{\chi}_1^0} = 95\,\text{GeV}/c^2$: $M_{\tilde{\ell}} = 45,\ 65,\ 85,\ 93\,\text{GeV}/c^2$
  $M_{\tilde{\chi}_1^0} = 102\,\text{GeV}/c^2$: $M_{\tilde{\ell}} = 45,\ 65,\ 85,\ 95,\ 100\,\text{GeV}/c^2$

- Chargino pair–production with a slepton NLSP: $\sqrt{s} = 206.0\,\text{GeV}$.
  For both the stau NLSP scenario and the slepton co–NLSP scenario 24 combinations of chargino and slepton masses were generated:
  $M_{\tilde{\chi}_1^+} = 60\,\text{GeV}/c^2$: $M_{\tilde{\ell}} = 50,\ 57\,\text{GeV}/c^2$
  $M_{\tilde{\chi}_1^+} = 70\,\text{GeV}/c^2$: $M_{\tilde{\ell}} = 50,\ 60,\ 67\,\text{GeV}/c^2$
  $M_{\tilde{\chi}_1^+} = 80\,\text{GeV}/c^2$: $M_{\tilde{\ell}} = 50,\ 60,\ 70,\ 75\,\text{GeV}/c^2$
  $M_{\tilde{\chi}_1^+} = 90\,\text{GeV}/c^2$: $M_{\tilde{\ell}} = 50,\ 60,\ 70,\ 80,\ 83\,\text{GeV}/c^2$
  $M_{\tilde{\chi}_1^+} = 100\,\text{GeV}/c^2$: $M_{\tilde{\ell}} = 50,\ 60,\ 70,\ 80,\ 89\,\text{GeV}/c^2$
  $M_{\tilde{\chi}_1^+} = 102.5\,\text{GeV}/c^2$: $M_{\tilde{\ell}} = 50,\ 60,\ 70,\ 80,\ 90\,\text{GeV}/c^2$

- Slepton pair–production in the stau NLSP scenario: $\sqrt{s} = 206.0\,\text{GeV}$.
  61 combinations of slepton, neutralino and stau masses were generated:
  $M_{\tilde{\ell}_R} = 60\,\text{GeV}/c^2$: $M_{\tilde{\tau}_1} = 50\,\text{GeV}/c^2$: $M_{\tilde{\chi}_1^0} = 52,\ 58\,\text{GeV}/c^2$
  $M_{\tilde{\tau}_1} = 56\,\text{GeV}/c^2$: $M_{\tilde{\chi}_1^0} = 58\,\text{GeV}/c^2$
  $M_{\tilde{\ell}_R} = 70\,\text{GeV}/c^2$: $M_{\tilde{\tau}_1} = 50\,\text{GeV}/c^2$: $M_{\tilde{\chi}_1^0} = 52,\ 60,\ 68\,\text{GeV}/c^2$
  $M_{\tilde{\tau}_1} = 60\,\text{GeV}/c^2$: $M_{\tilde{\chi}_1^0} = 62,\ 68\,\text{GeV}/c^2$
  $M_{\tilde{\tau}_1} = 66\,\text{GeV}/c^2$: $M_{\tilde{\chi}_1^0} = 68\,\text{GeV}/c^2$
  $M_{\tilde{\ell}_R} = 80\,\text{GeV}/c^2$: $M_{\tilde{\tau}_1} = 50\,\text{GeV}/c^2$: $M_{\tilde{\chi}_1^0} = 52,\ 65,\ 78\,\text{GeV}/c^2$
  $M_{\tilde{\tau}_1} = 60\,\text{GeV}/c^2$: $M_{\tilde{\chi}_1^0} = 62,\ 70,\ 78\,\text{GeV}/c^2$

$$
\begin{aligned}
& & M_{\tilde{\tau}_1} &= 70\,\mathrm{GeV}/c^2\colon\ M_{\tilde{\chi}_1^0} = 72,\ 78\,\mathrm{GeV}/c^2 \\
& & M_{\tilde{\tau}_1} &= 76\,\mathrm{GeV}/c^2\colon\ M_{\tilde{\chi}_1^0} = 78\,\mathrm{GeV}/c^2 \\
M_{\tilde{\ell}_R} &= 90\,\mathrm{GeV}/c^2\colon & M_{\tilde{\tau}_1} &= 50\,\mathrm{GeV}/c^2\colon\ M_{\tilde{\chi}_1^0} = 52,\ 70,\ 88\,\mathrm{GeV}/c^2 \\
& & M_{\tilde{\tau}_1} &= 60\,\mathrm{GeV}/c^2\colon\ M_{\tilde{\chi}_1^0} = 62,\ 75,\ 88\,\mathrm{GeV}/c^2 \\
& & M_{\tilde{\tau}_1} &= 70\,\mathrm{GeV}/c^2\colon\ M_{\tilde{\chi}_1^0} = 72,\ 80,\ 88\,\mathrm{GeV}/c^2 \\
& & M_{\tilde{\tau}_1} &= 80\,\mathrm{GeV}/c^2\colon\ M_{\tilde{\chi}_1^0} = 82,\ 88\,\mathrm{GeV}/c^2 \\
& & M_{\tilde{\tau}_1} &= 86\,\mathrm{GeV}/c^2\colon\ M_{\tilde{\chi}_1^0} = 88\,\mathrm{GeV}/c^2 \\
M_{\tilde{\ell}_R} &= 100\,\mathrm{GeV}/c^2\colon & M_{\tilde{\tau}_1} &= 50\,\mathrm{GeV}/c^2\colon\ M_{\tilde{\chi}_1^0} = 52,\ 75,\ 98\,\mathrm{GeV}/c^2 \\
& & M_{\tilde{\tau}_1} &= 60\,\mathrm{GeV}/c^2\colon\ M_{\tilde{\chi}_1^0} = 62,\ 80,\ 98\,\mathrm{GeV}/c^2 \\
& & M_{\tilde{\tau}_1} &= 70\,\mathrm{GeV}/c^2\colon\ M_{\tilde{\chi}_1^0} = 72,\ 85,\ 98\,\mathrm{GeV}/c^2 \\
& & M_{\tilde{\tau}_1} &= 80\,\mathrm{GeV}/c^2\colon\ M_{\tilde{\chi}_1^0} = 82,\ 90,\ 98\,\mathrm{GeV}/c^2 \\
& & M_{\tilde{\tau}_1} &= 90\,\mathrm{GeV}/c^2\colon\ M_{\tilde{\chi}_1^0} = 92,\ 98\,\mathrm{GeV}/c^2 \\
& & M_{\tilde{\tau}_1} &= 96\,\mathrm{GeV}/c^2\colon\ M_{\tilde{\chi}_1^0} = 98\,\mathrm{GeV}/c^2 \\
M_{\tilde{\ell}_R} &= 102.5\,\mathrm{GeV}/c^2\colon & M_{\tilde{\tau}_1} &= 50\,\mathrm{GeV}/c^2\colon\ M_{\tilde{\chi}_1^0} = 52,\ 76.2,\ 99.9\,\mathrm{GeV}/c^2 \\
& & M_{\tilde{\tau}_1} &= 60\,\mathrm{GeV}/c^2\colon\ M_{\tilde{\chi}_1^0} = 62,\ 81.3,\ 99.9\,\mathrm{GeV}/c^2 \\
& & M_{\tilde{\tau}_1} &= 70\,\mathrm{GeV}/c^2\colon\ M_{\tilde{\chi}_1^0} = 72,\ 86.2,\ 99.9\,\mathrm{GeV}/c^2 \\
& & M_{\tilde{\tau}_1} &= 80\,\mathrm{GeV}/c^2\colon\ M_{\tilde{\chi}_1^0} = 82,\ 91.2,\ 99.9\,\mathrm{GeV}/c^2 \\
& & M_{\tilde{\tau}_1} &= 90\,\mathrm{GeV}/c^2\colon\ M_{\tilde{\chi}_1^0} = 92,\ 96.2,\ 99.9\,\mathrm{GeV}/c^2 \\
& & M_{\tilde{\tau}_1} &= 98\,\mathrm{GeV}/c^2\colon\ M_{\tilde{\chi}_1^0} = 99.9\,\mathrm{GeV}/c^2
\end{aligned}
$$

In all cases 1000 events were generated for each point of the mass grid.

Bibliography

[1] H.P. Nilles, Phys. Rept. **110** (1984) 1.

[2] J. Ellis, "Beyond the Standard Model for Hillwalkers", hep–ph/9812235 (1998).

[3] S.P. Martin, "A Supersymmetry Primer", hep–ph/9709356 v3, April 1999.

[4] L. Alvarez–Gaume, J. Polchinski and M.B. Wise, Nucl. Phys. B **221** (1983) 495.

[5] G.F. Giudice and R. Rattazzi, Phys. Rept. **322** (1999) 419.

[6] S. Ambrosanio, G.D. Kribs and S.P. Martin, Phys. Rev. D **56** (1997) 1761.

[7] S. Dimopoulos, S. Thomas and J.D. Wells, Nucl. Phys. B **488** (1997) 39.

[8] Z. Chacko, M.A. Luty, I. Maksymyk and E. Ponton, JHEP **04** (2000) 1.

[9] W. Beenakker, M. Klasen, M. Kramer, T. Plehn, M. Spira and P.M. Zerwas, Phys. Rev. Lett. **83** (1999) 3780.

[10] OPAL Collaboration, K. Ahmet *et al.*, Nucl. Instrum. Meth. A **305** (1991) 275.

[11] S. Anderson *et al.*, Nucl. Instrum. Meth. A **403** (1998) 326.

[12] Michael Hauschild, private communication (2002).

[13] S. Kluth and D. Ward,"A Study of the Performance of the OPAL Electromagnetic Calorimeter using $e^+e^-\gamma$ Events", OPAL Technical Note TN108, July 1992.

[14] B.E. Anderson *et al.*, IEEE Trans. Nucl. Sci. **41** (1994) 845.

[15] J. Allison *et al.*, Nucl. Instrum. Meth. A **317** (1992) 47.

[16] R. Brun *et al.*, GEANT3, CERN–DD/EE/84–1 (1987) 175.

[17] C. Hawkes, D. Lellouch, M. Redmond, O. Schaile and M. Schröder, "ROPE Users' Guide", OPAL–Offline Note 16/OFFL–0487, last update March 2002.

[18] S. Katsanevas and P. Morawitz, Comput. Phys. Commun. **112** (1998) 227.

[19] N. Ghodbane, "SUSYGEN3, an Event Generator for Linear Colliders", hep–ph/9909499 (1999).

[20] T. Sjöstrand, Comput. Phys. Commun. **82** (1994) 74.

[21] W. Beenakker *et al.*, "WW Cross–Sections and Distributions", in "Physics at LEP2", Vol.1, eds. G. Altarelli, T. Sjöstrand and F. Zwirner, CERN 96–01 (1996) 127.

[22] E. Barberio and Z. Wąs, Comput. Phys. Commun. **79** (1994) 291.

[23] E. Boudinov *et al.*, "$\gamma\gamma$ Event Generators", hep–ph/9512371 (1995).

[24] G. Marchesini *et al.*, Comput. Phys. Commun. **67** (1992) 465.

[25] J.A.M. Vermaseren, Nucl. Phys. B **229** (1983) 347.

[26] F.A. Berends, P.H. Daverveldt and R. Kleiss, Comput. Phys. Commun. **40** (1986) 271, 285, 309; Nucl. Phys. B **253** (1985) 421.

[27] F.A. Berends and R. Kleiss, Nucl. Phys. B **186** (1981) 22.

[28] S. Jadach, B.F.L. Ward and Z. Wąs, Comput. Phys. Commun. **130** (2000) 260.

[29] T. Sjöstrand, Comput. Phys. Commun. **82** (1994) 74; Comput. Phys. Commun. **112** (1998) 227.

[30] S. Jadach, J.H. Kuhn and Z. Wąs, Comput. Phys. Commun. **64** (1990) 275; S. Jadach *et al.*, Comput. Phys. Commun. **76** (1993) 361.

[31] S. Jadach, W. Placzek and B.F.L. Ward, Phys. Lett. B **390** (1997) 298.

[32] D. Karlen, Nucl. Phys. B **289** (1987) 23.

[33] G. Montagna, O. Nicrosini and F. Piccinini, Comput. Phys. Commun. **98** (1996) 206.

[34] J. Fujimoto *et al.*, Comput. Phys. Commun. **100** (1997) 128.

[35] S. Jadach *et al.*, Comput. Phys. Commun. **119** (1999) 272.

[36] K. Cheung, D.A. Dicus, B. Dutta and S. Nandi, Phys. Rev. D **58** (1998) 15008.

[37] C. Hawkes, "Luminosity Counting in ROPE", OPAL Technical Note TN003, October 1990.

[38] T. Behnke, M. Jimack, R. Van Kooten and R. Kowalewski, "Constrained Track Refitting from DST", OPAL Technical Note TN029, February 1991.

[39] Particle Data Group, D.E. Groom *et al.*, Eur. Phys. J. C **15** (2000) 1.

[40] OPAL Collaboration, "Searches for Intermediate Lifetime Signatures in GMSB Models with a Slepton NLSP in e^+e^- Collisions at $\sqrt{s} = 189 - 209\,\mathrm{GeV}$", OPAL Physics Note PN478, July 2001.

[41] OPAL Collaboration, G. Abbiendi *et al.*, Eur. Phys. J. C **14** (2000) 199.

[42] OPAL Collaboration, K. Ackerstaff *et al.*, Eur. Phys. J. C **6** (1999) 253.

[43] C. Rembser and B. List, "Description of Selection Efficiencies in Searches for Heavy Particles with Finite Lifetime", OPAL Technical Note TN643, February 2000.

[44] E. Duchovni, J. Ihmels, J. Kraskiewicz and A. Wodecki, "Decay State Signatures at LEP2 for the Supersymmetric Theories with Gauge Mediated Supersymmetry Breaking", Weizmann Institute preprint WIS/09/00–June–DPP.

[45] LEP Higgs Working Group, ALEPH Collaboration, DELPHI Collaboration, L3 Collaboration and OPAL Collaboration, "Searches for the Neutral Higgs Bosons of the MSSM: Preliminary Combined Results Using LEP Data Collected at Energies up to 209 GeV", hep–ex/0107030, July 2001.

[46] OPAL Collaboration, Eur. Phys J. C **13** (2000) 553;
OPAL Collaboration, "Tests of the Standard Model and Contraints on New Physics from Measurements of Fermion–pair Production at 192–202 GeV at LEP", OPAL Physics Note PN424, March 2000;
OPAL Collaboration, "Measurements of Standard Model Processes in e^+e^- Collisions at $\sqrt{s} \sim 203 - 209$ GeV", OPAL Physics Note PN469, February 2001;
http://opalinfo.cern.ch/opal/group/smproc/swlumi_1999.txt;
http://opalinfo.cern.ch/opal/group/smproc/swlumi_2000.txt.

[47] R. Batley, R. Hawkings, M. Hildreth and T. Junk, "ODSIZL 2.11, DST–Level Tracking Adjustments and Refit with Silicon Hits", OPAL Technical Note TN520, September 2000.

[48] http://opalinfo.cern.ch/opal/group/cj/cj.html.

[49] T. Junk, Nucl. Instrum. Meth. A **434** (1999) 435.

[50] R.D. Cousins and V.L. Highland, Nucl. Instrum. Meth. A **320** (1992) 331.

[51] A general outline of the analysis can be found in OPAL Collaboration, G. Abbiendi *et al.*, Eur. Phys. J. C **14** (2000) 51;
details of the most recent version of the analysis, used in this work, can be found in T.E. Marchant, "Search for New Physics Using Acoplanar Lepton Pair Events in e^+e^- Collisions at $\sqrt{s} = 183 - 208\,\mathrm{GeV}$", March 2002, Thesis, University of Manchester, accessible from http://home.cern.ch/marchant/; (publication in preparation).

[52] R. McPherson, "A Selection of Events with ≥ 4 Charged Leptons and Missing Energy in e^+e^- Collisions with $\sqrt{s} = 189 - 209\,\mathrm{GeV}$", OPAL Technical Note TN712, February 2002.

[53] OPAL Collaboration, K. Ackerstaff *et al.*, Phys. Lett. B **433** (1998) 195;
S. Braibant, M. Fanti and P. Giacomelli, "Search for Stable and Long–lived Massive Charged Particles in e^+e^- Collisions at $\sqrt{s} = 130 - 189\,\mathrm{GeV}$", OPAL Physics Note PN395, July 1999;
an updated publication, including the data of 1999 and 2000, is in preparation (Phu Tran, private communication).

[54] OPAL Collaboration, G. Abbiendi *et al.*, Eur. Phys. J. C **18** (2000) 253;
an updated publication, including the data of 1999 and 2000, is in preparation (Peter Krieger, private communication).

[55] OPAL Collaboration, G. Abbiendi *et al.*, Phys. Lett. B **501** (2001) 12.

[56] An old version of the analysis is described in OPAL Collaboration, G. Abbiendi *et al.*, Eur. Phys. J. C **14** (2000) 187;
a publication of an optimised analysis, used in this work, is in preparation (Isabel Trigger, private communication).

[57] OPAL Collaboration, G. Abbiendi *et al.*, "Searches for Light Gravitino Signatures in e^+e^- Collisions at $\sqrt{s} = 189\,\mathrm{GeV}$", OPAL Physics Note PN397, July 1999.

[58] ALEPH Collaboration, "Search for Gauge Mediated SUSY Breaking Topologies in e^+e^- Collisions at Center–of–Mass Energies up to 209 GeV", hep–ex/0203024, March 2002.

[59] DELPHI Collaboration, P. Abreu *et al.*, Phys. Lett. B **503** (2001) 34;
DELPHI Collaboration, T. Alderweireld *et al.*, "Update of the Search for Supersymmetric Particles in Light Gravitino Scenarios", DELPHI 2002–011 CONF 552, March 2002.

[60] L3 Collaboration, "Search for Supersymmetry in e^+e^- Collisions at $\sqrt{s} = 202 - 208\,\mathrm{GeV}$", L3 Note 2707, July 2001.

[61] J. Qian (D0 Collaboration), "Sensitivity to Gauge Mediated Supersymmetry Breaking Models of the Fermilab Upgraded Tevatron Collider", hep–ph/9903548, Oct. 1998.

[62] I. Hinchliffe and F. E. Paige, Phys. Rev. D **60** (95002) 1999.

Acknowledgements

At this stage I would like to express my gratitude to the people who supported me.

I thank my supervisor Prof. Jürgen von Krogh for giving me the opportunity to work on this interesting subject and for his continous support. I also thank him and Prof. Peter Bock for making it possible for me to attend the Lake Louise Winter Institute 2001, the XXXVIIth Rencontres de Moriond (EW) and the Herbstschule für Hochenergiephysik in Maria Laach and for the wonderful three years at CERN.

I would like to thank Prof. Michael G. Schmidt for the second expertise for this thesis and for his participation in the examination commitee.

Thanks very much to all the co–authors of the OPAL Physics Note for their patient collaboration. Thanks also to the members of the editorial board, Silvia Arcelli, Michael Hauschild, Naoko Kanaya and Oliver Pooth, for their critical feedback and useful suggestions.

I thank all the members of the OPAL GMSB working group for many fruitful discussions, especially Rob McPherson and Naoko Kanaya.

I am grateful to the conveners of the OPAL searches working group, Rob McPherson, Paolo Giacomelli, Sylvie Braibant–Giacomelli, Christoph Rembser and Isabel Trigger, for their support of this work.

Thanks to the CJ–DAQ team, namely my Heidelberg colleages Anna Okpara and Dirk Wetterling plus Michael Hauschild, for the exciting times in the OPAL pit.

For careful proof–reading of this thesis I thank Rob McPherson, Thomas Kress, Klaus Rabbertz and Christoph Rembser.

Finally a special thanks goes to my colleage Christoph Rembser, for all his assistance, support, advice, encouragement and patience, and for borrowing me his car for several weeks when mine was stolen. It was great fun to work with you!